European Commission

The High Temperature Gas-cooled Reactor

Safety considerations of the (V)HTR-Modul

Kugeler, K., Nabielek, H.,
Buckthorpe, D.
Editors: Scheuermann, W., Haneklaus, N., Fütterer, M.

2017

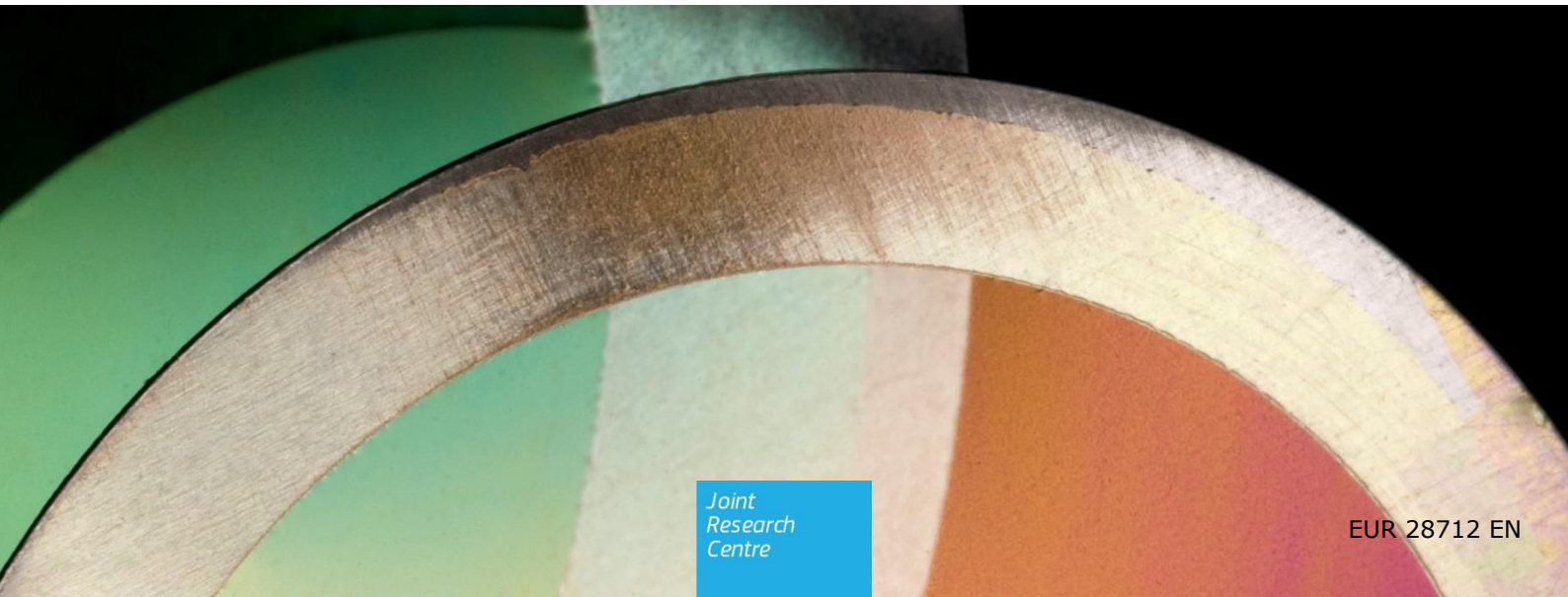

Joint Research Centre

EUR 28712 EN

Contact information
Name: Fütterer, M.
Address: European Commission, DG Joint Research Centre – JRC, Directorate G, Unit G.I.4 – Nuclear Reactor Safety & Emergency Preparedness; P.O. Box 2, NL-1755 ZG Petten, Netherlands
Email: Michael.FUETTERER@ec.europa.eu
Tel.: +31 22456-5158

JRC Science Hub
https://ec.europa.eu/jrc

JRC107642

EUR 28712 EN

PDF	ISBN 978-92-79-71311-8	ISSN 1831-9424	doi:10.2760/270321
Print	ISBN 978-92-79-71312-5	ISSN 1018-5593	doi:10.2760/970340

Luxembourg: Publications Office of the European Union, 2017

How to cite this report: Scheuermann, W., Haneklaus, N. and Fütterer, M., editor(s), Kugeler, K., Nabielek, H. and Buckthorpe, D., *The High Temperature Gas-cooled Reactor: Safety considerations of the (V)HTR-Modul*, EUR 28712 EN, Publications Office of the European Union, Luxembourg, 2017, ISBN 978-92-79-71311-8, doi:10.2760/270321, JRC107642.

Acknowledgement

European researchers and engineers gained considerable experience with the High Temperature Gas-cooled Reactor (HTR or HTGR). After the successful operation of experimental and commercial HTRs, the Three Mile Island accident in 1978 led to a reorientation of HTR designs towards reduced power (200-600 MWth) and inherent decay-heat removal features based on the demonstrated fission-product retention capability of coated-particle fuel up to about 1 600 °C.

The concept of such a reactor was developed by Siemens/Interatom in the 1980s: the so-called HTR Module. Based on a reduced thermal power of 200 MW and construction details, the release of radioactivity in accident conditions can be avoided. However, the Chernobyl accident in 1986 marked the end of the HTR Module development in Germany. In particular, the licensing process was stopped due to political decisions. However, after a decade of interruption, the European and international effort on the development of an inherently safe nuclear reactor picked up speed again with the creation of the European High Temperature Reactor Technology Network (HTR-TN). HTR-TN has proposed and executed several European R & D projects and launched international collaboration initiatives. One of these, the Generation IV International Forum (GIF), founded in May 2001, selected this concept for the very high temperature reactor (VHTR). At that time, the VHTR was primarily seen as a candidate for a Generation IV reactor with the particular mission of electricity and large-scale bulk hydrogen production via thermochemical processes. Today, and due to the large market sector in industrial heat demand, more emphasis is given to the cogeneration of heat (mostly steam) and power with HTRs.

In Europe, along with several smaller projects, two large projects specifically related to HTR technology were put in place. Raphael (reactor for process heat, hydrogen and electricity generation), a 4-year project with 37 partners, started in 2005. Archer (advanced high-temperature reactors for cogeneration of heat and electricity R & D), again a 4-year project, with 33 partners, started in 2010. Both projects successfully performed the R & D required with a view to confirming the high technology readiness level for the design, demonstration and deployment of such a reactor, in particular for their use as highly efficient plants for cogeneration of heat and power.

The Raphael project focused on (V)HTR technology developments needed for industrial reference designs in the areas of reactor physics, safety, fuel and fuel-cycle back end, materials and components. Moreover system integration with the reference designs was carefully checked and documented.

The Archer project then extended the current state of knowledge of the European (V)HTR technology basis with R & D to support the demonstration of nuclear cogeneration with HTR. One of the deliverables of Archer was to document the current state of knowledge in the form of an HTR handbook with a specific focus on safety. It was meant to provide the basis for future research and development. The present book is composed of chapters recalling the concept of the HTR Module, fuel and fuel performance, components, materials and safety. The appendix summarises the most important experiments concerning safety.

As editors we thank the authors of the book, Professor emeritus Dr Kurt Kugeler, from the RWTH Aachen, Germany, who contributed to chapters of the HTR concepts, components and safety, Dr Heinz Nabielek, from Forschungszentrum Jülich, Germany, who provided the chapter on fuel and fuel

performance, and Mr Derek Buckthorpe from AMEC Foster Wheeler, who wrote the chapter on materials.

We are grateful to the colleagues who did the hard job of digitising drawings and plots from printed paper of older reports to be included in this book, namely Janis Lapins, Dustin Sanchristobal and Nicolai Kaufmann from the Institute of Nuclear Technology and Energy systems (IKE), University of Stuttgart, Germany.

Last but not least our acknowledgements are addressed to the European Commission, especially to Dr Georges van Goethem for his encouragements to produce and publish this book.

The editors

Walter Scheuermann (University of Stuttgart, Germany)

Nils Haneklaus (University of Berkeley, United States)

Michael Fütterer (European Commission — Joint Research Centre, Petten, the Netherlands)

Contents

List of figures 1
List of tables 8
1. Introduction 11
2. The concept of the HTR Module 15
2.1. Concept of the plant 16
3. Core layout parameter for the HTR Module 20
3.1. Overview 20
3.2. Core power density 21
3.3. H/D ratio of the core 23
3.4. Layout of the core of the HTR Module 25
3.5. Helium pressure 26
3.6. Helium temperatures in the primary circuit 26
3.7. Heavy metal and burnup 27
3.8. Feeding principles 28
3.9. Questions concerning the plant layout 28
4. Fuel and fuel performance 30
4.1. Fuel manufacturing 32
4.1.1. UO_2 fuel kernels 32
4.1.2. TRISO coating 32
4.1.3. Spherical fuel element 34
4.1.4. As-manufactured fuel quality 38
4.2. HTGR fuel performance under accident conditions 40
4.2.1. Simulation testing of core heat-up depressurisation under dry conditions 40
4.2.2. Fission-product release from UO_2 kernels at 1 600 °C 41
4.2.3. Comparison of fuel quality at 1 600 °C 42
4.2.4. KÜFA tests in Jülich 1985-1995 and in Karlsruhe 2005-2010 43
4.3. Accident simulation testing under oxidising conditions 47
4.3.1. Simulation of water ingress accident 47
4.3.2. Simulation of air ingress accident 48
4.4. Fuel performance limits 49
4.5. Summary 51
5. Components 52

5.1. Primary system 52
5.2. Core structures 55
5.3. Shutdown systems 60
5.4. The fuel-handling system 63
5.5. Primary enclosure 64
5.6. Surface cooler 67
5.7. Hot gas duct 67
5.8. Steam generator 69
5.9. The intermediate heat exchanger 72
5.10. Helium circulator 79
5.11. Helium purification plant 83
5.12. Depressurisation systems 84
5.13. Decay heat removal installations 86
5.14. Reactor protection system 89
5.15. Steam turbine plant 92
5.16. Cooling system 94
5.17. Handling of radioactivity 95
5.18. Status of development of components and the concept of the HTR Module for cogeneration 98
6. Materials 102
6.1. Primary system and primary enclosure 102
6.2. Reactor core 111
6.3. Shutdown system 115
6.4. Hot gas duct 116
6.5. Circulator 117
6.6. Steam generator 119
6.7. Intermediate heat exchanger 121
6.8. Turbine for direct cycle and turbine plant 124
7. Safety 127
7.1. Relevant accident scenarios 127
7.1.1. Accident case A: reactor under full pressure, loss of forced cooling ... 131
7.1.2. Accident case B: reactor at normal pressure, surface cooler working. 133
7.1.3. Accident case C: reactor under normal pressure, surface cooler fails 136
7.1.4. Water ingress into the primary circuit 137

7.1.5. Air ingress into the primary circuit 145
7.1.6. Accident case D: concrete structures of the reactor system are destroyed; the reactor is covered with rubble 152
7.2. Self-acting decay heat removal 154
7.2.1. Overview of the concept 154
7.2.2. Valuation of parameters influencing the decay heat removal concept 156
7.2.3. Influence of uncertainties relating to the different steps of the transport chain for decay heat removal on the maximum fuel temperature 165
8. Appendix A 171
8.1. Irradiation tests in MTRs and in AVR 171
8.2. Irradiation envelope 172
8.3. MTR irradiation analysis 176
8.4. HTR Module proof test analysis 178
8.5. AVR real-time irradiation testing 180
9. Appendix B 187
9.1. Experiments regarding self-acting decay heat removal in modular high-temperature gas-cooled reactors 187
9.1.1. Overview 187
9.2. Heat transport in the reactor core $\boldsymbol{\lambda eff T}$ 191
9.2.1. Laboratory experiments 191
9.2.2. SANA experiment 193
9.2.3. LUNA experiments 197
9.3. Heat transport through the shield of the core 201
9.3.1. Heat transport of the graphite reflector including the influence of irradiation ($\boldsymbol{\lambda G(T, D)}$) 201
9.4. Heat transport in gaps between reactor internal structures by radiation and free convection — general experiences from laboratory experiments 205
9.4.1. General experiences from laboratory experiments 205
9.4.2. PASCO experiment to measure $\boldsymbol{\alpha conv(T)}$ and $\boldsymbol{\alpha rad(T)}$ 208
9.5. Heat transfer from the surface of the reactor pressure vessel by free convection and radiation 211
9.5.1. INWA experiment 211
9.5.2. JAERI experiment (Japan) 216
9.5.3. Heat release from the surface of the CASTOR vessel 221
9.6. Heat transport in the outer structures around the reactor pressure vessel 223

9.6.1. Overview of different design options 223
9.6.2. Behaviour of the surface cooling system 225
9.6.3. Heat storage and transport in the concrete structures of the inner reactor cell 226
9.6.4. Behaviour of large concrete structures at high temperatures..... 228
9.6.5. Cooling of the surface of the reactor pressure vessel by interventions 232
9.7. Heat transport inside the reactor building — integral experiments 233
9.8. Heat release from the reactor building to the environment..... 235
9.9. Integral experiments on the AVR reactor, demonstration of the concept of self-acting decay heat removal 237
9.9.1. Loss of active cooling (reactor under full pressure)..... 237
9.9.2. Loss of active cooling (reactor under normal helium pressure of 1 bar) 240
10. References 246

List of figures

Figure 1: Goals and criteria (U.S. DOE Nuclear Energy Research Advisory Committee and the Gen. IV International Forum, 2002) 12
Figure 2: Fuel element of a pebble-bed reactor 13
Figure 3: Fuel element of a block type reactor 14
Figure 4: Arrangement of the buildings of an HTR plant with two modular units 17
Figure 5: Vertical cross section of the reactor building (How to obtain an inherently safe power reactor, 2007) 18
Figure 6: Horizontal cross section of the reactor building (How to obtain an inherently safe power reactor, 2007) 19
Figure 7: Principle of the secondary steam cycle of a cogeneration plant containing a heat source (module unit as nuclear heat source) 20
Figure 8: Influences to be considered in view of core power density 21
Figure 9: Qualitative relationships for optimisation of core power density 23
Figure 10: Scanning electron microscope photograph of a purposely cracked TRISO-coated particle showing the fuel kernel and the coating layers (*source:* Forschungszentrum Jülich) 30
Figure 11: High-magnification scanning electron microscope photomicrograph of the TRISO coating (Rooyen, 2010) (*source:* Nelson Mandela Metropolitan University) . 31
Figure 12: Schematic of high-temperature fluidised-bed CVD coating furnace (*source:* NUKEM Technologies) 34
Figure 13: Cross section of German reference 60 mm-diameter spherical fuel element showing TRISO particles randomly distributed in the 50 mm-diameter fuel zone (*source:* NUKEM Technologies) 35
Figure 14: Process steps in manufacturing the German reference 60 mm-diameter HTGR spheres (*source:* NUKEM Technologies) 36
Figure 15: Number of UO_2 TRISO particle defects in sphere manufacture as a function of the number of particles in the spherical fuel element 39
Figure 16: Temperature evolution during depressurisation and core heat-up in small modular HTGRs in comparison to the temperature profiles used in KÜFA tests 41
Figure 17: Fission-product release from exposed UO_2 kernels during 1 600 °C heating test 42
Figure 18: Iodine-131 release from various fuel configurations during 1 600 °C heating tests 43
Figure 19: Krypton-85 release during heating tests with irradiated LEU UO_2 TRISO spherical fuel elements irradiated in MTRs (HFR, FRJ2) and in AVR 44
Figure 20: Caesium-137 release during heating tests with irradiated LEU UO_2 TRISO spherical fuel elements irradiated in MTRs (HFR, FRJ2) and in AVR 45
Figure 21: Krypton-85 release at 1 600 °C from compacts with 11 % to 14 % FIMA burnup in comparison to spherical fuel elements (FE) with 4 % to 9 % FIMA..... 46
Figure 22: Enhanced ^{85}Kr release from irradiated spherical fuel element AVR 89/30 under intermittent steam injections 48

Figure 23: Statistical evaluation of defective and failed LEU UO_2 TRISO particle fractions in reference 60 mm-diameter spherical fuel elements 52
Figure 24: Primary system of an HTR Module (200 MWth) 53
Figure 25: Bottom reflector of the THTR 55
Figure 26: Side reflector of the THTR (left: vertical cross section; right: horizontal cross section) 56
Figure 27: Bottom reflector of the Chinese HTR-10 57
Figure 28: Some details of core structures: connection between ceramic structures and core barrel 58
Figure 29: Concept of connection of the hot gas duct to the core internals in HTR .. 59
Figure 30: Ducting of the helium in the reactor internals 60
Figure 31: Positions of the borings in the side reflector (six reflector rods, 18 KLAK positions) 61
Figure 32: Principle of the second shutdown system (KLAK) of the HTR Module 62
Figure 33: Concept of fuel handling in pebble-bed HTR (MEDUL cycle for a two-module plant) 63
Figure 34: Arrangement of the primary enclosure 65
Figure 35: Concept of the surface cooler of the HTR Module 67
Figure 36: Hot gas duct 68
Figure 37: Steam generator of the HTR Module — overview of the component 70
Figure 38: Depressurisation system for the steam generator 71
Figure 39: Primary circuit of a modular HTR with IHX (left: principal flow diagram; right: T-Q diagram for use of nuclear heat 72
Figure 40: Arrangement of HTR Module (a) with helix IHX (b) or U tube IHX (c) (Nuclear Energy for Hydrogen Production) 74
Figure 41: Intermediate heat exchanger for nuclear applications (Technical and Safety Aspects of Processes of Hydrogen Production using Nuclear Energy, 2005) (left: helical tube bundle; right: details of hot gas collector tube and support structures) 75
Figure 42: Flow sheet of 10 MW KVK facility for testing nuclear process-heat components 76
Figure 43: 10MW KVK facility for testing nuclear process-heat components 77
Figure 44: Two IHX components tested in KVK (left: Helical tube bundle by SteinmOIIer; right: U tube bundle by Balcke-Durr) 77
Figure 45: Correlation between specific diameter and specific rotation speed for HTR blower 81
Figure 46: Helium circulator of the HTR Module 82
Figure 47: Concept of gas purification of the HTR Module consisting of three tracks 83
Figure 48: Flow sheets of THTR gas purification plant 84
Figure 49: System for the depressurisation of the primary system 85
Figure 50: Decay heat removal in a modular HTR 86
Figure 51: Concept of surface cooler 87
Figure 52: Results for a ‘total loss of active cooling’ accident; failure of the surface cooler; storage and transport of heat in the concrete cell (HTR Module, 200 MWth) 89

Figure 53: Connections in the reactor protection system of the HTR Module 91
Figure 54: Steam turbine system for process-steam delivery from a power plant with two modular HTRs and two turbines 93
Figure 55: Overview of cooling systems of the HTR Module 95
Figure 56: Flow of activity which is envisaged for the HTR Module 96
Figure 57: Vessel steels — comparison of allowable strengths 104
Figure 58: Phase diagram for Fe at 350 °C 106
Figure 59: PWR and WWER regulatory guides — shift in DBTT with dpa dose 107
Figure 60: Effect of irradiation on dimensional change 111
Figure 61: Schematic overview of the graphite irradiation experiments 113
Figure 62: Change in E/Eo with irradiation dose for graphite 114
Figure 63: An arrangement for a carbon-fibre composite control rod 116
Figure 64: HTR cooler THTR 300 119
Figure 65: Plate heat exchanger (flow direction and mock-up) 123
Figure 66: Examples of welding involved in joining the plates 123
Figure 67: Overview of possible impacts and events in nuclear power plants: proposal for classification 128
Figure 68: Aspects of earthquakes: (a) estimated annular probability that an earthquakes (as large as the value on the X-axis) could occur (e.g. THTR 300, Germany (20)); (b) probability of damaging components depending on the acceleration 129
Figure 69: Probability of damaging components depending on the acceleration 129
Figure 70: Forces of an aeroplane crashing into the containment (different DBA, BDBA and EAA events) 130
Figure 71: Temperatures (right) in the core in case of loss of forced convection in a modular HTR core, here HTR Module, 200 MWth (illustrated at left), at full helium pressure 131
Figure 72: Results of calculations for the THTR 300 (750 MWth) in case of ‘loss of active cooling’ accident 132
Figure 73: Results for the total loss of coolant and active cooling; failure of the surface cooler; storage and transport of heat in the concrete cell accident (HTR Module 200 Mth) 133
Figure 74: Neutron multiplication in the core of a modular HTR without active shutdown (examples: HTR Module, 200 MWth) 135
Figure 75: Results for the accident: total loss of active cooling; failure of the surface cooler; storage and transport of heat in the concrete cell (HTR Module, 200 MWth) 136
Figure 76: Pressure as function of time in the THTR primary circuit due to water penetration from a defective steam generator tube (operating pressure 40 bar) 140
Figure 77: Corrosion rate of A3 graphite in water vapour as a function of temperature 142
Figure 78: Corrosion rate of A3 graphite in water vapour as a function of total pressure p 142
Figure 79: Corrosion rate of A3 graphite in water vapour as a function of burnup 143

Figure 80: Decrease in the strength of the fuel due to corrosion in steam (6:42) ... 143
Figure 81: Integral corrosion rate in water vapour as a function of burnup for standard conditions. Reflector graphite ATR-2E and ASR 1RS and fuel element graphite A3-3 and A3-27 (6:37) ... 144
Figure 82: Flammability of water-gas helium-air mixtures at different temperatures 145
Figure 83: equilibrium and ration of CO/CO_2 ... 148
Figure 84: Measured reaction rates of corrosion of graphite pebble beds by air ... 148
Figure 85: Decrease of the maximum load before rupture of the fuel elements depending on the corrosion time at variable temperatures (corrosion in air) ... 149
Figure 86: Flammability limits for the air/carbon monoxide/helium system ... 149
Figure 87: Schematic diagram of the chimney effect during air ingress into the HTR core ... 150
Figure 88: Mass flow depending on the leakage cross section and on the temperature in the core (measured from the reactor module) ... 152
Figure 89: Accident case D — concrete structures are destroyed, reactor is covered with rubble: (a) model for calculations; (b) results of calculations for the time dependence of relevant temperatures ... 153
Figure 90: Stationary radial temperature profile in case of self-acting decay heat removal in a modular HTR (Tmax in the hottest part of the core) ... 154
Figure 91: Release fraction of fission products from pebble bed fuel elements containing TRISO-coated particles ... 156
Figure 92: Schematic system for balancing decay heat production and dissipation from the core ... 157
Figure 93: Qualitative picture of the above-derived solution ... 158
Figure 94: Qualitative dependence of a radial temperature profile in the core (at $\boldsymbol{t = t*}$ with $\boldsymbol{fDt*}$) ... 160
Figure 95: Heat transport across gaps in the core ... 161
Figure 96: Simplified model to evaluate the system in a very extreme accident ... 163
Figure 97: Qualitative values of temperature of reactor pressure vessel and fuel dependent on time ... 164
Figure 98: Uncertainties relating to measured parameters for the heat transport in the reactor system in case of a ‘total loss of active cooling’ accident: ... 167
Figure 99: Spheres for temperature measurements in the core of the AVR (with melt-wires — the X-ray below shows the molten wires) ... 168
Figure 100: Aspects of temperature measurements in the AVR: (a) temperatures obtained from melt-wire experiments; (b) calculated maximum temperature in core ... 169
Figure 101: Irradiation envelope of fuel burnup versus mean operating temperature for LEU UO_2 TRISO particles in accelerated irradiation tests in European MTRs and in AVR prior to 2000 ... 174
Figure 102: Measured 85mKr release rates during the irradiation of tests HFR-K5 and HFR-K6 ... 178
Figure 103: Detailed comparison of measured and calculated ^{88}Kr release rates for fuel elements HFR-K6/2 and 3 throughout the 634 full-power days of irradiation. Also

shown are the measured temperatures at the spheres' surface. Release source terms are from contamination 180
Figure 104: Distribution of spherical fuel element types in the AVR core as a function of operating history (Verfondern, 2007) 181
Figure 105: Distribution of AVR inner core maximum fuel element surface temperatures and outer core maximum fuel element surface temperatures as obtained from the 1986 melt-wire tests 182
Figure 106: Release of ^{85}Kr measured during accident simulation testing of GLE-3 spherical fuel elements irradiated to various burnups in the AVR. The first part of the two-digit number refers to the consecutive AVR sampling event, and the second is a sequential s 183
Figure 107: Post-irradiation fission gas release fractions at 1 250 °C measured during heat-up prior to accident simulation tests with GLE-3 fuel elements containing LEU UO_2 TRISO particles of various burnups. The horizontal lines show predicted krypton release fractions 185
Figure 108: Stationary radial temperature profile in case of self-acting decay heat removal in a modular HTR (Tmax in the hottest part of the core) 187
Figure 109: Parameters which influence the chain of the self-acting transport of decay heat in a modular HTGR 188
Figure 110: Overview of experiments to evaluate the concept of self-acting decay heat removal of a modular HTR 191
Figure 111: Measurement of ($\boldsymbol{\lambda eff}(\boldsymbol{T})$) in a laboratory experiment with 6 cm graphite balls: (a) arrangement for measurement of ($\boldsymbol{\lambda eff}(\boldsymbol{T})$ in a pebble bed; (b) result for the effective heat conductivity in a pebble bed ($\boldsymbol{\lambda eff}(\boldsymbol{T})$) 192
Figure 112: Dependencies of $\boldsymbol{\lambda eff}$ from temperature and irradiation status 193
Figure 113: SANA-test facility: (a) cross section; (b) picture 193
Figure 114: Characteristic results of measurements of stationary temperature profiles in the SANA facility (heating power 50 KW; N2 as filling gas; no radial insulation). 195
Figure 115: Comparison between measured and calculated values in the SANA facility (power 30 KW; helium as filling gas; without insulation) 196
Figure 116: Results of free-convection measurements: transport of heat by natural convection; difference between nitrogen and helium 196
Figure 117: Experimental facility LUNA: (a) overview; (b) view into the pebble bed 198
Figure 118: Measurements and calculations — results of the LUNA facility: (a) mass flow dependent on time; (b) temperature dependent on time (air at 36 bar); (c) temperature dependent on time (helium at 37 bar); (d) mass flow in circuit in case of different positions of the heat sink 200
Figure 119: Aspects of heat transport in the side reflector of a modular HTR in case of self-acting decay heat removal 201
Figure 120: Behaviour of irradiated graphite relevant for the description of 'loss of active cooling' accidents and action of self-acting decay heat removal: heat conductivity dependent on fast neutron dose and temperature (irradiation at 950 °C) 202

Figure 121: Aspects of heat transport through the graphite reflector in case of 'loss of cooling' accidents: (a) radial dependence of neutron flux (e.g. AVR; 1.85 m under core upper surface); (b) axial dependence of neutron flux (e.g. AVR; on core axis); (c) positions of the reflector 204
Figure 122: Positions where natural convection plays a role 205
Figure 123: Heat transport mainly by free convection and radiation — three important situations in the chain of heat transport of a modular HTR: (a) between two surfaces in the reactor internals; (b) from hot surfaces to the atmosphere of the reactor containment building to concrete structures 206
Figure 124: Dependence of the function $\boldsymbol{\beta TT1, T2, \varepsilon 1\ \varepsilon 1, \varepsilon 2 = 1}$ 207
Figure 125: PASCO test facility to measure the release of heat from hot surfaces by radiation and free convection and to determine flow velocities 209
Figure 126: Heat-transfer coefficients and possible heat fluxes 210
Figure 127: Internals of the INWA-test facility 212
Figure 128: Time dependence of heat flux on the liner surface of the INWA test facility (a power of 4 kW corresponds to a heat flux of/4 kW/m^2) 213
Figure 129: Radial dependence in the reactor pressure vessel and concrete cell structures (at the time when the highest temperature of the vessel occurs) 214
Figure 130: Time dependence of the temperatures during experiments in the liner-surface of the INWA-test facility (a power of 4 kW corresponds to a heat flux of 4 kW/m2). 214
Figure 131: Heat-transfer numbers by natural convection measured in INWA test facility dependent on the height for the cases of normal operation and of 'loss of active cooling' accidents 215
Figure 132: Some important results of tests carried out at the INWA test facility (a) time dependence of temperatures of liner and concrete (heat flux: 4 KW/m^2); (b) heat flux dependent on the temperature of the outer wall (here: 50 °C) and the surface of the cast-iron vessel 216
Figure 133: Schematic diagram of the JAERI test facility for the measurement of heat fluxes and temperature distributions 217
Figure 134: Schematic flow sheet of the JAERI-test facility 218
Figure 135: Case A: 94 KW; nitrogen; 1.1 MPa; cooling water in cooling system .. 219
Figure 136: Case B: 77.5 KW; helium; 0.47 MPa; cooling water in cooling system 219
Figure 137: Cooling panel operated with air (8 KW; helium; 1 MPa; air coolant) ... 220
Figure 138:Principle of heat transport in storage vessels for spent fuel elements: (a) the principle of a storage vessel with surface cooling; (b) the radial temperature profile; (c) the axial temperature profile; (d) some data and relations for temperature differences 222
Figure 139: Results of measurement of heat transfer by free convection on the surface of storage vessels 223
Figure 140: Possibilities to set up reactor vessel and outer cell systems with good heat-transfer and heat-storage capabilities 224
Figure 141: Heat transfer if the surface cooler fails 226
Figure 142: Heating of the inner concrete cell after failure of the surface cooler 227

Figure 143: Strength of concrete at higher temperatures 228
Figure 144: Changes to important parameters of concrete at high temperatures: (a) heat conductivity; (b) modulus of elasticity 228
Figure 145: Time dependence of temperatures supporting concrete structures of modular HTRs ('total loss of active cooling' and 'failure of surface cooler' accidents) 229
Figure 146: Experimental facility to test large concrete blocks at high temperatures 230
Figure 147: Some results of tests on large concrete blocks 231
Figure 148: Results of experiments reflooding a liner cooling system 232
Figure 149: Different situations of heat transfer by free convection in the containment building 233
Figure 150: Concepts to remove the decay heat from the reactor containment building 235
Figure 151: Alternative cooling concepts for reactor containment buildings 236
Figure 152: Loss of active cooling + loss of all shutdown rods (blocked..... 239
Figure 153: Calculated temperature distribution inside the AVR during loss of decay heat removal accident (calculations for the assumption 'loss of control and loss of active decay heat removal', reactor under full helium pressure)..... 240
Figure 154: Decay heat production in the AVR during total loss of active cooling with a depressurised core 241
Figure 155: Positions of thermocouples to measure temperatures in the internal structures of the AVR: (a) vertical section; (b) horizontal section 241
Figure 156: Results of a 'loss of coolant and loss of pressure in primary system' experiment in the AVR (46 MW; T_{He} = 950 °C)..... 243
Figure 157: Temperature distribution inside the AVR reactor system in a 'loss of coolant' accident (calculations for the assumption: total loss of coolant and loss of active decay heal removal)..... 244
Figure 158: Time-dependent temperature distribution in the AVR during 'total loss of active decay heat removal' accident, depressurisation of primary circuit: temperature (maximum values at centre line) depending on time 245

List of tables

Table 1: Overview of high temperature reactors 13
Table 2: Thermodynamic design aspects of pebble-bed reactors 20
Table 3: Some data on the core layout (AVR and THTR data for comparison) 25
Table 4: German reference coated particle: LEU UO_2 with an LTI TRISO coating ... 31
Table 5: Design functions of the ceramic coating layers of the TRISO-coated fuel particle 32
Table 6: Typical parameters for CVD processes employed to deposit ceramic coating layers on dense LEU UO_2 fuel kernels to produce TRISO-coated particles (Huschka, 1977; Nothnagel, 2010) 34
Table 7: Production-scale manufacturing details for high-quality spherical elements containing LEU UO_2 TRISO-coated fuel particles during period 1980 to 1988 37
Table 8: Failure statistics for LEU UO_2 TRISO-coated fuels based on burn-leach results 40
Table 9: Heating tests in KORA with irradiated unbonded particles and irradiated fuel spheres in air (Schenk, 1995) 49
Table 10: Final statistical evaluation of the performance data collected during manufacture, irradiation testing and accident testing of reference 50
Table 11: Some data on the primary system of the HTR Module (1 unit) 54
Table 12: Data on the ceramic core structures of the THTR 55
Table 13: Data on the core structure of the HTR Module (AVR and THTR data for comparison) 59
Table 14: Data on the vessels of the primary enclosure 65
Table 15: Data on the surface cooling system 67
Table 16: Data on the hot gas duct of the HTR Module (some data on the EVO plant are added for comparison) 68
Table 17: Steam generator data 70
Table 18: Comparison of IHX data tested in a KVK facility with data on IHX for nuclear application 73
Table 19: Data on the helium circulator of the HTR Module (THTR circulator data for comparison) 82
Table 20: Some data on the steam turbine plant for the production of process heat by cogeneration 93
Table 21: Pre-calculated and measured values of THTR 94
Table 22: Estimate of yearly releases of radioactive isotopes from an HTR Module plant 97
Table 23: Values of release of radioactivity during AVR operation: (a) release of radioactive substances into the atmosphere; (b) transfer of radioactive water from the AVR In the KFA 98
Table 24: Safety concept of HTR Module compared to that of AVR 100
Table 25: Evaluation of components of the HTR Module 101
Table 26: Qualification issues for HTR/VHTR reactor pressure vessel 104
Table 27: Qualification issues for HTR/VHTR reactor pressure vessel 109
Table 28: Codes and standards issues for HTR/VHTR reactor pressure vessel 110

Table 29: Typical range of graphite grades in an irradiation experiment 112
Table 30: Graphite core material issues and requirements 114
Table 31: Control rod material issues and requirements for the HTR and VHTR ... 116
Table 32: Hot gas duct material issues and requirements for the HTR and VHTR. 117
Table 33: Circulator material issues and requirements for the HTR and VHTR..... 118
Table 34: Steam Generator material issues and requirements for the HTR and VHTR 120
Table 35: Main characteristics for direct and indirect from hydraulic and thermal consideration 122
Table 36: IHX material issues and requirements for the HTR and VHTR..... 124
Table 37: Chemical composition of IN 792 DS and CM 247 LC DS blade materials (weight %)..... 126
Table 38: Turbine material issues and requirements for the HTR and VHTR..... 126
Table 39: Regarded severe accidents and their probability (P) 128
Table 40: Comparison of some data on aeroplanes for DBA, BDBA and EAA events 130
Table 41: Accidents relevant for self-acting decay heat removal..... 130
Table 42: Heat transport mechanism and temperature limits: (a) heat transport mechanism in different structures; (b) limiting parameters for the concept (e.g. HTR Module, 200 MWth) 154
Table 43: Characteristics of the wires shown in Figure 99..... 168
Table 44: Estimates of the influence of uncertainties on the fuel temperature in case of a ‘total loss of cooling’ accident 170
Table 45: Historical overview of German irradiation tests in the development of coated particles from 1972 to 2010 (IAEA 2012) 171
Table 46: The nominal maximum HTGR design operating conditions, for which the MTR irradiation tests were patterned..... 173
Table 47: In-reactor operating parameters for the MTR irradiation tests conducted on modern high-quality LEU UO_2 TRISO fuel particles irradiated in the German fuel development programme..... 175
Table 48: LEU UO_2 TRISO-coated particle fuel performance in accelerated MTR irradiation tests based on EOL Kr R/B values and the temperature-dependent fractional release values for an exposed oxide fuel kernel 177
Table 49: ^{85}Kr fractional release measurements made during the 1 250 °C+ hold temperature on AVR type GLE-3 fuel elements prior to accident simulation tests at higher temperatures 184
Table 50: Data on the experiment 194
Table 51: Characteristic of fast neutron dose at different positions of reflector (e.g. HTR Module; after 30 years of operation)..... 204
Table 52: Some relations for the natural convection of air..... 208
Table 53: Important data on the test facility..... 218
Table 54: Values of emissivity of some different materials in the self-acting decay heat removal chain 221

Table 55: Comparison of some data on the surface cooler of the modular HTR and the surface cooler of a coal-fired boiler 225
Table 56: Temperature dependence of factor C 234
Table 57: Temperature dependence of the factor $C*$ in the equation for free convection around a body of diameter da 235

1. Introduction

Nuclear energy production is a recent technology. The first nuclear reactor demonstrating the feasibility of a sustained and controlled chain reaction was built in Chicago in 1942. In 1957 a nuclear reactor produced electricity for the first time. In the 60 years since then significant technological progress has been achieved.

Three generations of nuclear reactors have been successively developed and a fourth is currently being developed, demonstrating the constant progress and technical and industrial vitality of nuclear energy. The technology is mature, with approximately 450 nuclear reactors currently providing 17 % of the world's electricity, without greenhouse gas emissions.

It must also be stressed that the technological progress and innovations achieved or currently being developed are all based on the same fundamental physical principles of nuclear fission, the feasibility of which was demonstrated some 70 years ago.

Heavy nuclides, like uranium, plutonium and thorium, are fissioned by neutrons and release heat within the fuel material confining the radioactivity. This heat is extracted while simultaneously cooling the fuel by circulating a coolant (water in current European light-water reactors). The heat recovered is used to run a turbine and a generator, which produces electricity.

A lot of effort has been invested in international cooperation to define goals for the nuclear energy systems of the future, and also to select the key technologies for achieving them. The effort has been made primarily through the Generation IV International Forum (GIF), which the American Department of Energy initiated in 2000.

The technology roadmap developed by GIF is the starting point to identify and organise research and development of the new generation of reactors to be built around 2030 to 2040. To do so, four goals have been defined. Each of the systems comprises a nuclear reactor, an energy conversion system and the necessary fuel cycle, fuel manufacturing, spent fuel and final waste-management equipment.

The four major goals have been separated out into 15 criteria and 24 performance indicators or metrics (Figure 1). These goals are:

- sustainability
- economics
- safety and reliability
- proliferation resistance and physical protection.

4 goal areas	8 goals	15 criteria	24 metrics
Sustainability	SU1 Resource utilisation	SU1-1 Fuel Utilisation	• Use of fuel resources
	SU2 Waste minimization and management	SU2-1 Waste minimization	• Waste mass • Volume • Heat load • Radiotoxicity
		SU2-2 Environmental impact of waste management and disposal	• Environmental impact
Economics	EC1 Life cycle cost	EC1-1 Overnight construction costs EC1-2Production costs EC2-1 Construction duration	• Overnight construction costs • Production costs • Construction duration
	EC2 Risk to capital	EC1-1 Overnight construction costs EC2-1 Construction duration	• Overnight construction costs • Construction duration
Safety and reliability	SR1 Operational safety and reliability	SR1-1 Reliability SR1-2 Work/public routine exposure SR1-3 Work/public accident exposure	• Forced outage rate • Routine exposures • Accident exposures
	SR2 Core damage	SR2-1 Robust safety features	• Reliable reactivity control • Reliable decay heat removal
		SR2-2 Well characterized models	• Dominant phenomena uncertainty • Long fuel thermal response time • Integral experiments scalability
	SR3 Offsite emergency response	SR3-1 Well characterized source term /energy	• Source term • Mechanisms for energy release
		SR3-2 Robust mitigation features	• Long system time constants • Long effective holdup
Proliferation resistance and physical protection	PR1 Proliferation resistance and physical protection	PR1-1 Susceptibility to diversion or undeclared production	• Separated materials • Spent fuel characteristics

Figure 1: Goals and criteria (U.S. DOE Nuclear Energy Research Advisory Committee and the Gen. IV International Forum, 2002)

A final selection criterion was the degree of technological innovation in the candidate systems — which provides excellent grounds for wide-reaching international cooperation — and the possible spin-offs for other nuclear systems or for the current or next generation of nuclear reactors.

The following six systems deemed the most promising at the end of this evaluation exercise were called on to rally forum cooperation on development work starting from 2004:

- VHTR — very high-temperature reactor system, over 1 000 °C, helium-cooled, dedicated to hydrogen production or hydrogen/electricity cogeneration;
- GFR — gas-cooled fast reactor system — Helium-cooled fast reactor;
- SFR — sodium-cooled fast reactor system;
- SCWR — supercritical water-cooled reactor system;
- LFR — lead-cooled fast reactor system — lead or Pb-Bi alloy-cooled fast reactor;
- MSR — molten salt reactor.

VHTR scored very well with the exception of sustainability because of its open fuel cycle, which requires reprocessing to increase sustainability. From a technological point of view the VHTR is a further development of the high temperature reactor (HTR), which was developed in the years from 1960 to 2001 (Table 1).

Table 1: Overview of high temperature reactors

	Dragon	Pech-Bottom	AVR	Fort St-Vrain	THTR300	HTTR	HTR10
Site	Winfrith (United Kingdom)	Pennsylvania (United States)	Jülich (Germany)	Colorado (United States)	Schmehausen (Germany	Oarai (Japan)	HT10 (China)
Criticality	1964	1966	1966	1974	1983	1998	2001
Shutdown	1975	1974	1988	1989	1989	-	-
MWth	20	115.5	46	842	750	30	10
MWel	-	40	15	330	300	-	-
He pressure (bar)	20	24.6	10	48	40	40	30
Inlet temperature (℃)	335	343	175	406	262	395	250-300
Outlet temperature (℃)	835	715	850	785	750	850-950	700-900
Power density (MW/m^3)	14	8.3	2.3	6.3	6	2.5	2
Fuel elements	Prisms	Prisms	Pebbles	Prisms	Pebbles	Prisms	Pebbles
Cycle	Varied	U/Th	U235/Th	U235/Th	U235/Th	Enriched U	Enriched U

Two basic fuel element designs of the HTR have been developed and implemented, one in Germany and the other in the United States.

The main characteristic of the German design is the conditioning of compacted microparticles in a graphite matrix in the form of spheres with a diameter of 60 mm (Figure 2). They are continuously inserted in and extracted from the reactor at a rate of one pebble approximately every 20 seconds. When a pebble reaches its maximum depletion rate it is replaced with a new one.

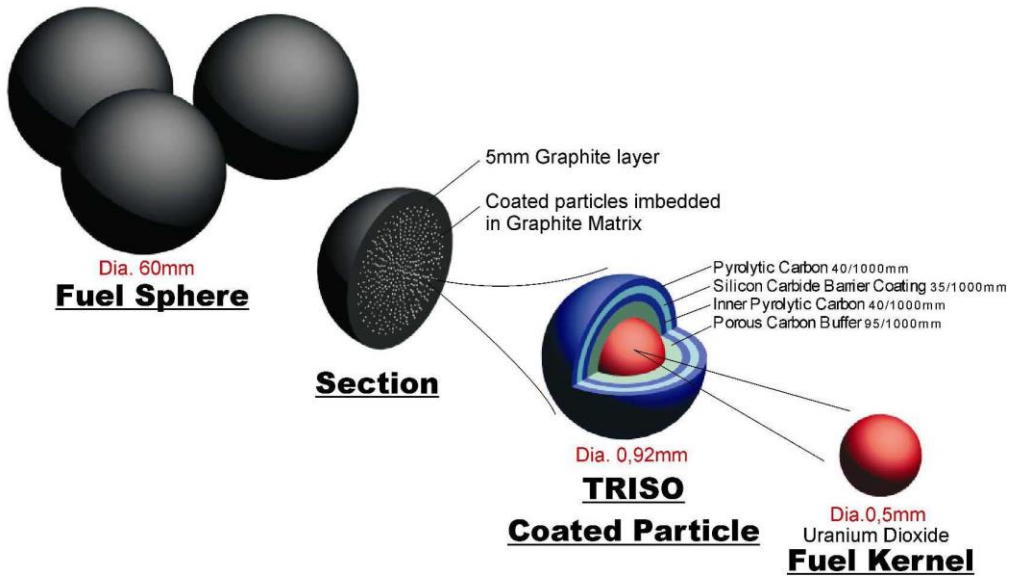

Figure 2: Fuel element of a pebble-bed reactor

The first German HTR was the *Arbeitsgemeinschaft Versuchsreaktor* (AVR) built at the Jülich Research Centre. This centre has maintained very high competence in this technology. The AVR set new records (for HTRs) in terms of performance and operating duration. Its construction began in 1961. It was connected to the electric power network in 1966 (15 MWel) and shut down in 1988. It served as an experimental platform for fuel technology development within the scope of cooperation between the Jülich Research Centre and NUKEM, the fuel industrial manufacturer still considered to be a reference today. The core temperature of 850 °C at the start of operation was increased to 950 °C. The steel pressure vessel design served to achieve design transients (e.g. core cooling loss) that contributed to validating the safety concepts applied in this type of reactor.

The AVR showed the viability of the pebble bed concept and demonstrated its reliability through physical tests for which the plant was not initially designed. A loss of coolant flow without scram was simulated in 1970, and a loss of coolant transient was also achieved prior to final shutdown.

The fuel has undergone significant developments and improvements at the Jülich Research Centre, in partnership with NUKEM (manufacturer).

The second HTR built in Germany was the THTR-300 (thorium high-temperature reactor), which went critical in 1983. This was a 300 MWel commercial reactor with a concrete vessel, built by Brown Boveri. The operation of the THTR was marked by a number of technical problems that did not seem impossible to overcome. In particular, a planned inspection in 1988 revealed the rupture of a number of bolts securing hot duct insulation plates, which, combined with an unfavourable political context, led to the decision to permanently decommission the facility in 1989 after only 423 equivalent full-power days

The American family differs from the German family mainly in terms of core and fuel organisation. The core is composed of prismatic graphite blocks containing the fuel compacts (Figure 3).

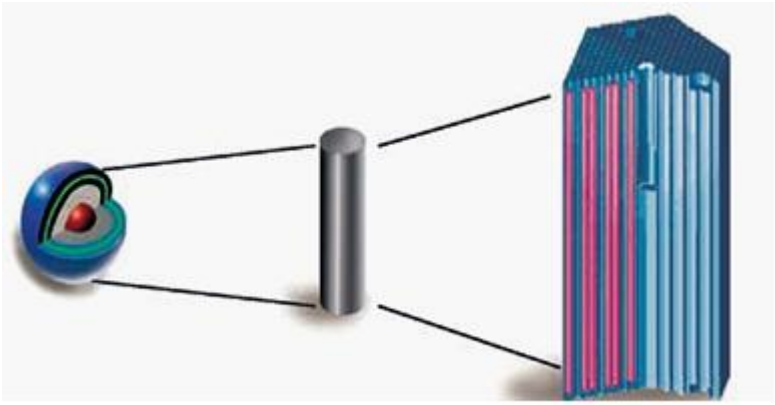

Figure 3: Fuel element of a block type reactor

The first commercial implementation was Peach Bottom (40 MWel), which went critical in early 1966 and was shut down in 1974. After the discovery of an increasing number of fuel cladding ruptures, a second core was fabricated using more advanced technology, improving the quality of the first porous graphite layer and the characteristics of successive layers. 93 % availability was achieved during irradiation of this second core, and reactor coolant system activity remained extremely low,

indicating the excellent quality of the new fuel. The reactor subsequently operated without major problems and was shut down for economic reasons.

The second implementation was Fort Saint-Vrain (330 MWel), construction of which began in 1968 and which went critical in 1974. Its operation was marked by technical problems (namely accidental water ingress in the reactor coolant system causing accelerated corrosion of steel components and poor availability) and it was finally decommissioned in 1989. Despite the negative functional aspects of its operation, the excellent leak-tightness of the fuel elements led to very positive radiological results for operation and maintenance activities, with the exception of tritium releases due to water leaks.

On the whole, the operating experience from German and American prototypes has largely confirmed the technical expectations regarding HTRs, i.e.:

- very good behaviour of the particle fuel under irradiation, even at high temperatures, and low release of fission products in the coolant gas providing very clean reactors;
- possibility of using high-temperature helium as coolant gas;
- easy control, high thermal inertia and significant operating safety margins (demonstrated at real scale with the AVR).

The impact of the Three Mile Island accident and the excellent safety characteristics of HTRs (thermal inertia, good apparent core conductivity, low power density) have led to research on configurations allowing completely passive residual power evacuation. Low-power HTRs are particularly well suited to satisfying this new passive safety requirement, like the concept of the German HTR Modular reactor which has been developed by Siemens-Interatom. This 80 MWel reactor uses the radiating capacity of a metal vessel to ensure passive cooling of the fuel, the temperature of which remains below 1 600 °C regardless of accident conditions. This reactor was never built, but a detailed design has been completed and some licensing issues have been solved.

HTR reactors like the HTR Module with an electric power of 100 to 300 MWel set the trend for current design, while in current European research projects cogeneration is in favour of electricity generation.

2. The concept of the HTR Module

The concept of the HTR Module has been developed by Interatom/Siemens as a nuclear heat source to deliver not only electricity but also process heat. In the first stage the process-heat production should produce process steam with a wide area of applications. In the next stage the process heat should be used to supply high temperature processes with the necessary process energy.

Through a specific core design it becomes possible that, on the one hand, only reflector elements are required to shut down the system and, on the other hand, and perhaps more importantly, the decay heat after a depressurisation accident and the outage of all active decay heat-removal systems can be removed from the core through natural processes, and that as a consequence the fuel temperature does not exceed a temperature at which fission products are released to the environment. Experiments in the past have shown that the critical temperature is 1 600 °C. New research indicates that 1 800 °C could be possible.

The particles containing the fission material are so called TRISO particles loaded with 7g of uranium per fuel sphere and an enrichment of 8.6 % of fissile material. The fuel elements are spheres with a diameter of 60 mm, consisting of a spherical fuel zone approximately 50 mm in diameter, in which the TRISO-coated particles are randomly distributed in graphitic matrix material (see Figure 2).

The technology of the HTR Module and its components is based on the experiences of AVR, THTR and the general development of HTR in different countries in the world.

2.1. Concept of the plant

The overall arrangement of the HTR Module power plant is shown in Figure 4. The central part is the reactor building, which contains the two modular units. In this central building some auxiliary systems are also installed (fuel-handling system, gas purifications, helium storage, helium supply systems).

It consists of two HTR Module units, along with some auxiliary and supporting systems.

The HTR Module units are separated from each other by a maintenance hall. An external concrete building is the enclosure for the inner building. The function of the concrete building is to protect the reactor building against external events such as an aeroplane crash, gas-cloud explosion or earthquake.

The reactor auxiliary building, positioned directly beside the reactor building, contains some important systems such as circuits for the start-up or shutdown of the reactor, intermediate cooling systems and the system provided to depressurise the primary circuit and to condensate the water after a strong water ingress accident.

Between the two modules there is a central channel to separate the two reactor units in the common reactor building.

The reactor building fulfils all current requirements in the nuclear licensing process (e.g. Germany) regarding impacts from the outside:

- aeroplane crash (phantom military machine),
- gas-cloud explosion (Δp_{max} = 0.3 bar),
- earthquake (acceleration: 0.3 g).

A very important building is used for the intermediate storage of spent fuel elements. Here the vessels filled with spent fuel elements are set up and cooled by radiation, conduction and free convection. Eventually the operation time of this storage system could be much longer than that of the reactor itself.

The question of how long the intermediate storage time will be is a topic of optimisation between the aspects of final storage and intermediate storage. Currently, time schedules of more than five decades seem to be advantageous.

The control room, installations for control and regulation, reactor protection system, emergency electrical supply systems and further components (computers, climate and air conditioning plants) are located in the switchgear building.

The energy conversion takes place in the turbine building. It houses the turbine and the electrical generator, all heat exchangers, pipes and pumps of the water/steam circuit and components to decouple process steam for process-heat applications.

A cooling installation, consisting of wet cooling towers operated by forced convection from blowers, is also part of the plant.

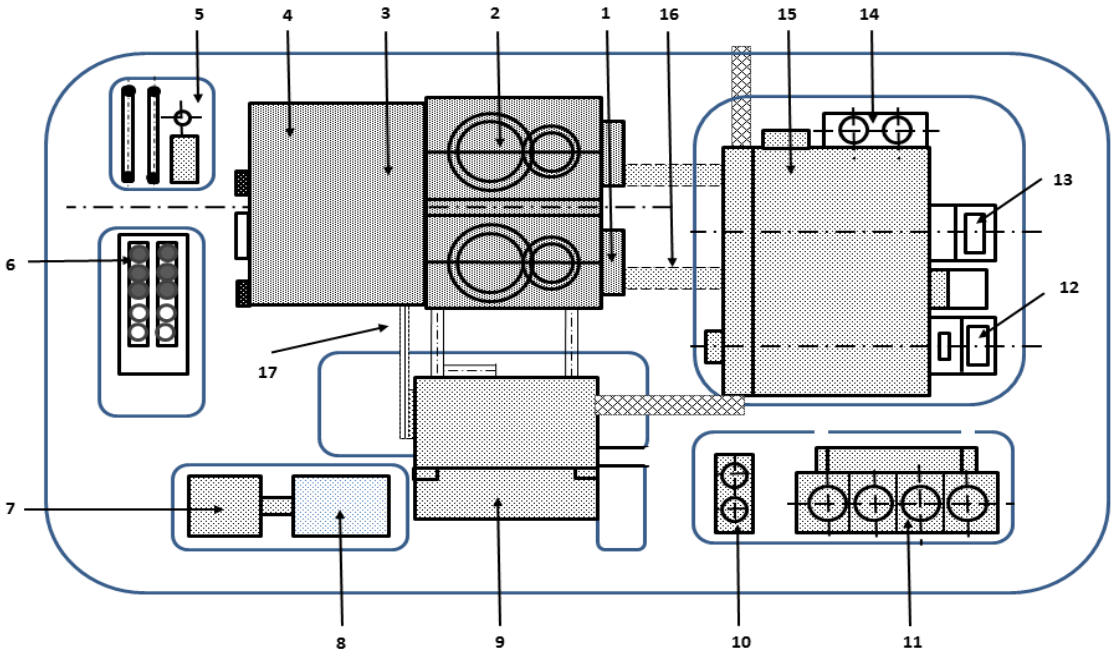

Figure 4: Arrangement of the buildings of an HTR plant with two modular units

The numbers denoted in Figure 4 describe the different parts of the plant:

1. annex to reactor building
2. reactor building
3. stack
4. reactor auxiliary building
5. central gas supply
6. intermediate storage for spent fuel elements
7. control/entrance building
8. offices
9. switchgear building
10. cooling towers
11. cooling towers
12. switchgear building
13. transformers
14. deionised water storage
15. turbine hall
16. connection bridge
17. channels for cables.

Figure 5 and Figure 6 show the vertical and horizontal cross sections of the reactor building.

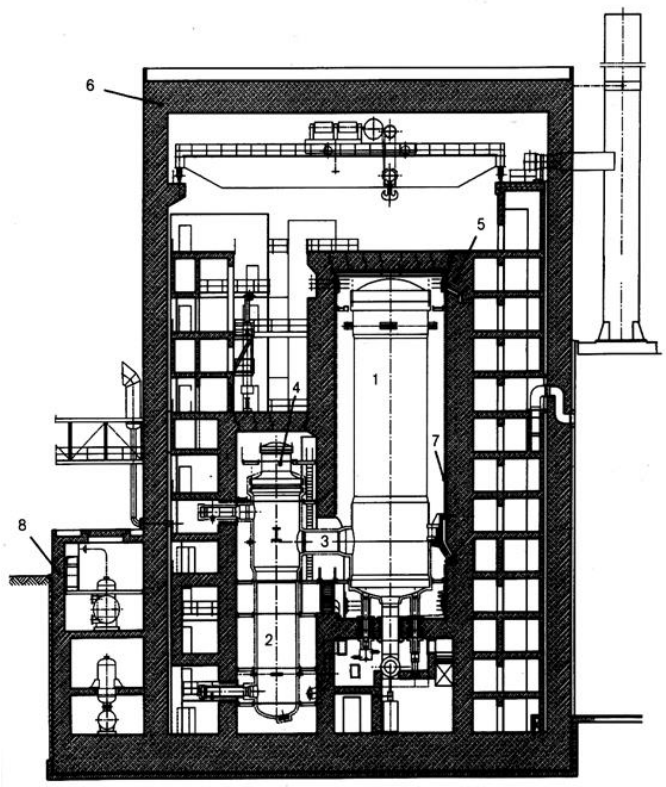

Figure 5: Vertical cross section of the reactor building (How to obtain an inherently safe power reactor, 2007)

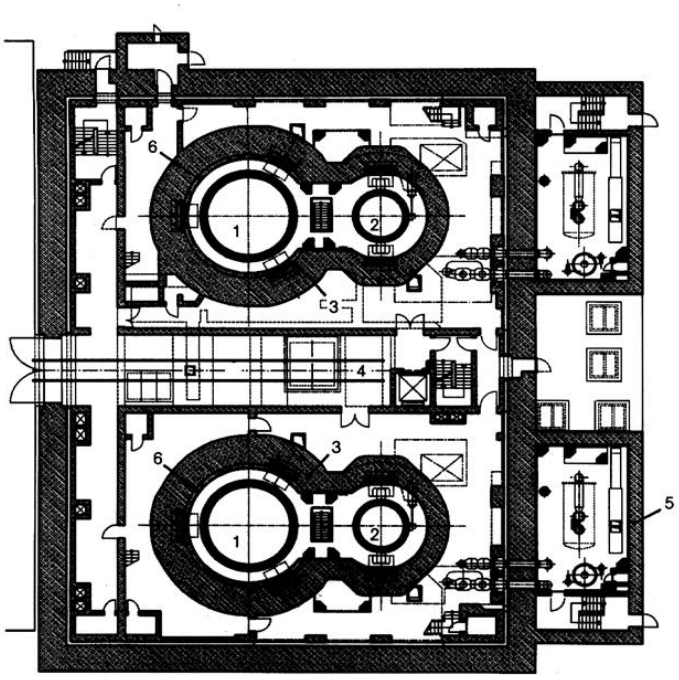

Figure 6: Horizontal cross section of the reactor building (How to obtain an inherently safe power reactor, 2007)

The turbine building basically contains the components of the water/steam cycle (Figure 7), with the steam turbine and electric power generator and the components for the process-steam system. The cooling tower structure (hybrid concept) is placed within a short distance of the turbine building.

Further auxiliary buildings contain the intermediate fuel elements storage facilities , the gas treatment station, the office and general purpose building and the security building.

As far as protection against strong impacts from the outside is concerned, the following buildings in particular need special protection and require an adequate design:

- the reactor containment building,
- the intermediate storage building for spent fuel elements,
- the auxiliary building containing radioactive materials.

The question of impacts from outside and the measures to govern these undergo a dynamic process during the long-time schedule of a nuclear project. The changes of assumptions on aeroplane crashes are a characteristic example of these conditions.

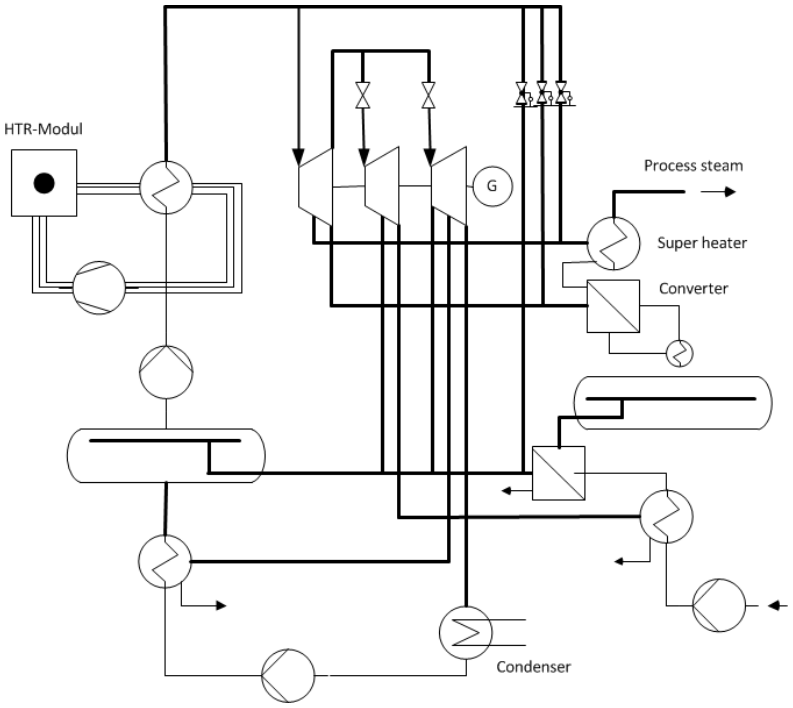

Figure 7: Principle of the secondary steam cycle of a cogeneration plant containing a heat source (module unit as nuclear heat source)

3. Core layout parameter for the HTR Module

3.1. Overview

The layout of an HTR core is influenced by a multitude of data. Here qualitative arguments will be specified for a few of them to enable assessment of layout data for plants. Important parameters are the mean power density of the core, the helium inlet temperature (T_{in}), the helium outlet temperature (T_{out}), the helium pressure (p_{He}), the H/D ratio of the core (height/diameter), the burnup of fuel, the heavy-metal content in the fuel elements, the particle concept and the manner of fuel element handling — the so called OTTO and MEDUL cycle. OTTO is the abbreviation of 'once through then out' and MEDUL is the German abbreviation of *Mehrfachdurchlauf* where the fuel elements are reloaded in the core until defined burnup is reached. In Table 2 layout data for already operational and planned plants are represented. In the following, important aspects to be considered in the layout process will be discussed.

Table 2: Thermodynamic design aspects of pebble-bed reactors

Parameter	AVR	THTR	HTR Module reactor	HTR100	HTR500
Fuel element handling	MEDUL	MEDUL	MEDUL	MEDUL	OTTO
Streaming direction cooling gas fuel elements	Cocurrent	Cocurrent	Cocurrent	Counter current	Cocurrent
Average core power density	2.2 MW/m^3	6 MW/m^3	3 MW/m^3	4.2 MW/m^3	5.5 MW/m^3

Cooling gas heating	270 °C -> 950 °C	250 °C -> 750 °C	250 °C -> 700 °C	250 °C -> 730 °C	250 °C -> 730 °C

3.2. Core power density

The power density of the core in particular is one of the most important layout parameters, influencing many plant characteristics. As shown in Figure 8 the power density influences important reactor components as well as characteristic properties of HTR plants.

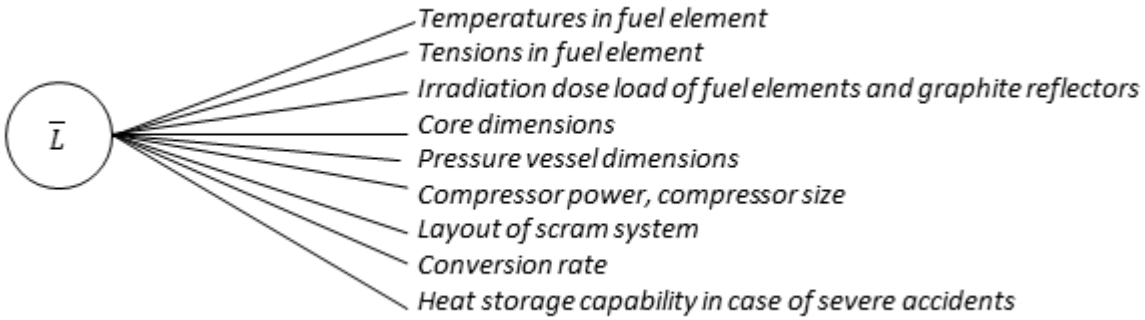

Figure 8: Influences to be considered in view of core power density

The appropriate choice of core power density should consider the following aspects:

- The core power density should not be too high to prevent the fuel and surface temperatures of the elements from being too high and to keep the thermal stresses of these components within reasonable limits. The acceptable boundary for HTR fuel elements is relatively high — a mean power density of ~ 10 MW/m³ was shown to be reasonable in radiation tests.
- The core dimensions and the core power density should be chosen in such a way that in extreme accidents ('total loss of active cooling') the decay heat could be removed from the core to the outside of the reactor just by heat radiation, heat conduction and natural convection of air or air/helium mixtures. During this process a maximum fuel temperature of 1 600 °C should not be exceeded. In this case just a very small amount of fission products would be released.
- The loads on fuel elements and reflectors due to irradiation increase with increasing power density and limit the mean value to < 8 MW/m³ with a view to a plant lifetime of 30 years, which is normally taken as the basis of a general layout.
- The choice of high power density in the core and therefore of high pressure losses in the cooling loop may eventually prevent the use of a single-stage radial blower. Due to this the technical costs would be increased. A boundary for the use of single-stage radial blowers is a pressure loss greater than 1.3 bar.
- In order to ensure an economical plant layout the ratio of the blower power and electric power (N_{blower}/N_{el}) should be bounded. Values of 3-5 % are believed to be acceptable.

- The core dimension, and therefore containment dimension, increases with decreasing core power density. Through this the costs of investment are increased. Optimisation considerations in this context will be described below.
- The requirements for the shutdown system increase with increasing core power density due to increased provision for reactivity reserve and xenon compensation.
- The conversion rate is very advantageous in core constellations with low power densities due to comparable low parasitic absorptions of neutrons in protactinium.
- The choice of core power density has a special meaning with regard to heat retention in the reactor core as a consequence of severe accidents characterised by the depressurisation of the cooling loop and the failure of all residual heat removal systems. In this case cores with low power density behave very inertly and are characterised by a limitation of the temperatures during the accident to non-critical values below 1 600 °C.

Considering the abovementioned aspects, mean core power densities between 3 and 6 MW/m³ are reasonable and can be the base for the design of further plans. The importance of the core power density with regard to the economical optimisation of an HTR plant can be seen in the following qualitative examination.

The costs of investment for a complete plant in view of the influence of core power density can be approximated from:

$$K_{inv} = K_{inv}^{0} + \frac{a_1}{\bar{L}} \quad (1)$$

The costs of operation, which are mainly due to the power consumption of the blower, are low:

$$K_{op} = K_{op}^{0} + N_{blow} \cdot x \cdot T = K_{op}^{0} + a_2 \bar{L}^2 \cdot x \cdot T \quad (2)$$

Here, T is the full load operating duration in hours and x is the electricity rate. The total annual cost for the plant will be:

$$K_{tot} = K_{op} + K_{inv} \cdot \bar{a} \quad (3)$$

with $\bar{a}$ as a factor covering interest payments, taxes, insurance and maintenance. The dependency of the total annual cost from core power density is therefore:

$$K_{tot}(\bar{L}) = C_1 + \frac{C_2}{\bar{L}} + C_3 \cdot \bar{L}^2 \quad (4)$$

and with $C_1 = K_{inv}^{0} \cdot \bar{a} + K_{op}^{0}$, $C_2 = a_1 \cdot \bar{a}$, $C_3 = a_2 \cdot T \cdot x$. The conditions to minimise the total annual costs are:

$$\frac{\partial K_{tot}}{\partial \bar{L}} = 0, \frac{\partial^2 K_{tot}}{\partial \bar{L}^2} > 0 \quad (5)$$

From an economic view the optimum of core power density depending on the parameters discussed is:

$$\bar{L}_{opt} \sim \sqrt[3]{\frac{a_1 \cdot \bar{a}}{2\, a_2\, T\, x}} \quad (6)$$

One should choose a low power density if the value $\bar{a}$ is low (essentially given at low rates of interest and long recovery periods). In particular, with a high degree of capacity utilisation and a high electricity rate one should also prefer low power densities. Safety considerations especially advocate the choice of low power densities. The relationship with regard to the costs, discussed above, is shown qualitatively in Figure 9.

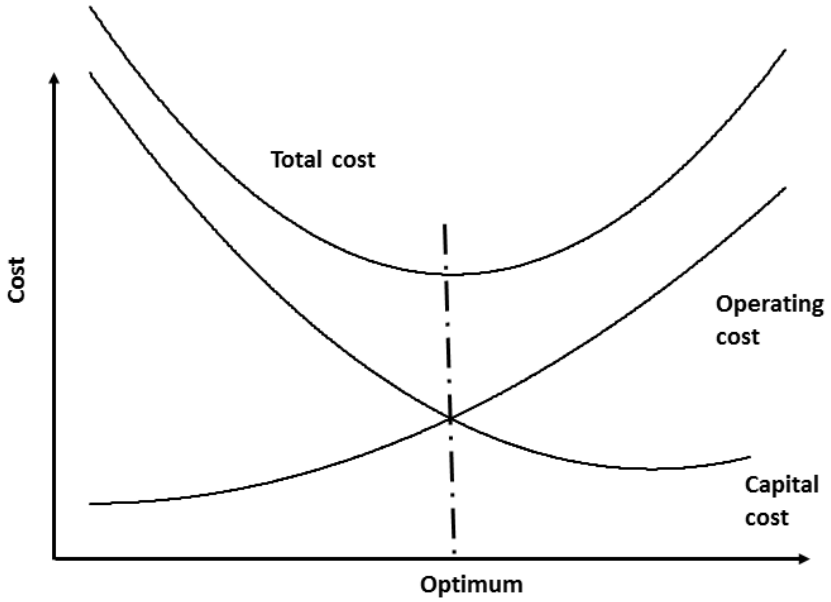

Figure 9: Qualitative relationships for optimisation of core power density

3.3. H/D ratio of the core

The choice of the height to diameter ratio (H/D) of a reactor core is of primarily importance in relation to neutron economics. Practically all reactors built so far aim for an H/D ratio near 1 to keep the critical mass and therefore the mass of fissile heavy metal as low as possible. Neutron losses due to leakage are minimised using this layout principle. In future HTR plants the principle of inherent safety through the removal of residual heat through the reactor vessel surface will gain additional importance, and from this a completely different ratio for H/D results. First of all, some remarks on optimisation on the base of neutron physics. Based on the criticality condition of a cylindrical core:

$$B^2 = \left(\frac{\pi}{H}\right)^2 + \left(\frac{2.405}{R}\right)^2 \qquad (7)$$

and the relation:

$$V = \pi R^2 H \qquad (8)$$

in which:

B = buckling

R = core radius

H = core height

V = volume of the core

the volume of the core can be formulated as:

$$V(H) = \pi \cdot (2.405)^2 \cdot \frac{H}{B^2 - \left(\frac{\pi}{H}\right)^2} \quad (9)$$

The demand for a minimised core size and a minimised mass of fissile heavy metal leads to an optimisation condition of the kind:

$$\frac{\partial V}{\partial H} = 0, \frac{\partial^2 V}{\partial H^2} > 0 \quad (10)$$

In detail, the condition for a minimised core size leads to:

$$H = \frac{\sqrt{3} \cdot \pi}{B}, = \sqrt{\frac{3}{2}} \cdot \frac{2.405}{B}, V = \frac{148}{B^2} \quad (11)$$

which yields the ratio:

$$\frac{R}{H} = \frac{2.405}{\sqrt{2} \cdot \pi} = 0.55 \quad (12)$$

From this consideration, the theoretical optimum for the H/D ratio is 0.9 with regard to the condition for minimised mass of fissionable fuel. To reach passive removal of heat via the surface of the reactor vessel, the heat transport lengths inside the reactor have to be as short as possible, to keep maximum fuel temperatures for a given core power density under a certain level in the case of a hypothetical severe accident with depressurisation and loss of all cooling systems. Detailed considerations concerning this issue yield a ratio for H/D of between 2.5 and 3 for low-power HTR plants. Furthermore, the core height should not be too large because, according to the relations:

$$\Delta p \sim H^3 \quad (13)$$

$$N_p \sim H^3 \quad (14)$$

Pressure loss (Δp) and pump power (N_p) increase cubically with increasing core height. For these reasons, reactor core heights of greater than 10 m are not efficient. A very important requirement for new reactor concepts in the future will be the possibility to construct simple shutdown systems for the operation of regulation and shutdown processes from the outer lateral sides of the core. Considerations on neutron physics yield an upper limit for the core radius of cylindrical systems of about 1.5 m. By using graphite noses, which may contain shutdown elements and extend into the core, the core radius could be enlarged to 1.75 m. Apart from that the transition to core geometries other than cylinders is possible so as to fulfil the requirement to influence reactivity from the sides. High cores, i.e. large H/D ratios, have a positive effect in terms of a uniform sphere flow. If vessel steel containers are used to incorporate the reactor core, the limitation of the containment diameter < 6 m and the need for a reflector thickness of 1 m lead to core diameters of around 3 m.

3.4. Layout of the core of the HTR Module

Some major requirements had to be fulfilled during the laying out of the core of the HTR Module. In part they were very different from those, which until that time were usual in HTR technology. These new aspects were mainly introduced to improve the safety of the concept.

- All control and shutdown procedures are carried out from the side reflector. The penetration of rods into the pebble bed is totally avoided. Interactions between shutdown elements and fuel elements are excluded.
- The strong negative temperature coefficient should be sufficient to shut down the reactor (hot status); this includes the stopping of the helium circulator, as this has been used in the AVR as a normal procedure.
- The fuel elements pass the reactor often enough (MEDUL cycle) to provide relatively flat power density distribution in the axial direction. In the HTR Module this includes 15 runs through the core.
- The uranium content of single fuel elements was limited to small values (7 g/fuel element) to provide a large moderation ratio in the core. In this case, during water ingress accidents the reactivity gain is relatively small and unimportant.
- As far as the dimensions of the core of the HTR Module are concerned, the possibility to remove the self-acting decay heat and to limit the maximum temperature to a value of 1 600 °C and the requirement to shut down the system (1st and 2nd system) leads to a core diameter of 3 m and an average power density of 3 MW/m^3. The fuel management causes a peak factor in the power density of 1.7. The core height has some limitations because the pressure drop in the core depends cubic from the height of the core. The technical requirement to use single stage helium circulators and therefore to limit the total pressure drop in the primary helium circuit limits the allowable pressure drop in the core. Together with the planned thermal power of 200 MW for one unit, these conditions result in an average core height of 9.4 m for the HTR Module.

Some important data on the core of the HTR Module are given in Table 3. For comparison the data on the AVR core and the THTR core are included. This table demonstrates that the main data on the core layout of the HTR Module can be evaluated as being fully proven.

Large differences result from changes to the control and shutdown system. The avoidance of graphite noses allows equalisation of the flow of pebbles in the core. The arrangement of all absorber elements in borings in the side reflector reduces the forces on fuel elements drastically.

Table 3: Some data on the core layout (AVR and THTR data for comparison)

Parameter	Dimension	HTR Module	AVR	THTR
Thermal power	MW	200	46	750
Average core power density	MW/m^3	3	2.2	6
Fuel cycle		MEDUL	MEDUL	MEDUL
Flow of helium		Downwards	Upwards	Downwards
Helium pressure	bar	60	10	40
Helium inlet temperature	Celsius	250	220	220

Average helium outlet temperature	Celsius	700	950	750
Max. helium outlet temperature	Celsius	750	1 050	850
Mass flow of helium	kg/s	85.5	15	280
Core diameter	M	3	3	5.2
Core height (average)	M	9.43	3	5.2
Shutdown elements		Inside reflector	In graphite noses	Inside reflector + pebble bed
Max. temperature in LOCA	Celsius	< 1 600	< 1 300	< 2 400

3.5. Helium pressure

Determining the helium pressure in the primary system (p_{He}), the following aspect has to be considered: increasing pressure increases the efficiency of the plant due to decreasing expenses relating to pumping power. The ratio of blower power to reactor power is:

$$\frac{N_{blower}}{N_R} \approx \frac{1}{p_{He}} \tag{15}$$

Or for the approximate total efficiency of the power plant:

$$\eta_{tot} \approx \eta_{cp} - \frac{const}{p_{He}} \tag{16}$$

where η_{cp} denotes the efficiency of the thermodynamic cycle process. Heat-transfer processes in heat exchangers are increased with increasing pressure, i.e. increase the heat flux through pipe walls and by this decrease the heat exchange surface. With increasing pressure, flow cross sections or pressure losses may be reduced in all parts of HTR plants. However, increasing the system pressure will increase the stresses in the primary system due to higher mechanical loads. This would make a proportional increase in the thickness of the vessel wall necessary. An increase in system pressure would also lead to an increase in helium inventory. The reactor building has to be designed to withstand depressurisation due to an accident. Extensive analyses showed pressures in the range between 40 and 60 bar to be the best compromise for HTR plants in view of the use of vessel steel containers as well as containers from reinforced concrete.

3.6. Helium temperatures in the primary circuit

The choice of helium inlet temperature (T_{in}) into the reactor core influences the layout of an HTR plant in the following way: depending on the flow path, the inlet temperature determines the temperature of the top and bottom reflectors respectively and should always be higher than 200 °C to avoid problems connected with the Wigner effect. Specific amounts of energy from irradiation are stored in the graphite lattice; these amounts of energy can escape the lattice continuously only at temperatures > 200 °C. For a constant helium loop layout the helium mass flux increases with increasing T_{in}. As a consequence, a blower with a higher level of power has to be installed. A simple estimate for the dependency reads as follows:

$$N_{blower} \sim \dot{m}^3 \quad (17)$$

The layout of the primary circuit becomes more complicated with increasing inlet temperature of the cooling gas. The material properties of the steel in the reactor pressure vessel (RPV) get worse; in the case of a reinforced concrete container the expenses for liner insulation would increase. With increasing helium inlet temperature the areas of the heater surfaces are reduced, particularly in the cooling water pre-heater. In particular, the effect of increasing helium mass flux with increasing helium inlet temperature has a disadvantageous impact on all gas-conducting systems, especially on the hot gas channels. Either the dimensions increase or increased pressure losses have to be accepted. A certain limit for the construction of sensitive reactor structures can be found approximately at $T_{in} \sim 400$ °C. Considering all of the aspects mentioned above, a reactor inlet temperature in a range between 220 and 300 °C is a good compromise for HTR systems.

In determining the helium outlet temperature (T_{out}) of the reactor core, the following aspects have to be considered: with increasing T_{out} the mass flux decreases while all other parameters are fixed, and we get the already-discussed advantages such as reductions in pressure losses, blower power, increase in system effectiveness and advantages for the layout of gas-conducting structures. On the other hand, steam generators without helium heated pre-heaters in particular need a helium temperature < 750 °C to avoid problems for the layout of the superheater systems due to tube wall temperatures being too high. Specific process-heat applications need temperatures as high as 1 000 °C in the helium loop.

Especially, in case core rods are to be used, the helium outlet temperature must be examined thoroughly. The strength values of highly heat-resistant construction materials considerably decrease at temperatures > 700 °C. Complete ceramic materials as fuel elements and structural graphite are in the first instance insensitive in view of the temperature choice, however impurities inside the helium loop will react faster with graphite surfaces at increased temperatures. Experiences with AVR showed that the level of fission-product release depended on the hot gas temperature during normal operation. The heating surfaces in steam generators or process-heat exchangers become smaller with increasing T_{out}. Hot gas-conducting pipes can be made of metal; at higher temperatures ceramic materials should be used. For electrical power generating plants temperatures of between 700 and 750 °C and for process-heat-generating systems temperatures of between 900 and 950 °C are reasonable compromises.

3.7. Heavy metal and burnup

The heavy-metal content per fuel element (FE) is in a wide range between 5 g/FE and 15 g/FE and has been used successfully for a long time in the AVR reactor. The following aspects are to be considered when choosing these parameters: the cost of the production of the fuel elements decreases with increasing heavy-metal load; the same aspect is valid for the cost of radioactive waste management, due to the proportionality of the cost to the volume of the fuel elements. The heavy-metal load has an important role, inversely proportional to the moderation ratio for neutron physics of an HTR core. Moderation ratios of between 300 and 500 lead to acceptable core layouts and fuel costs. For water ingress incidents, the heavy-metal load plays a role to such a degree that the moderator ratio is increased by the penetrating water and therefore an increase in reactivity may be possible. Fuel elements with low heavy-metal loads have a positive characteristic with regard to the latter aspect. It

is in principal possible to assemble an HTR core from a mixture of pure graphite spheres ('blind spheres') and fuel element spheres and, by so doing, to lower manufacturing and waste-management costs. Decades of experience with the AVR reactor and analyses of irradiation programmes led to a technologically and economically reasonable compromise for values of approximately 100 000 MWd/t of heavy metal for the fuel burnup. Certain shifts result from different heavy-metal loads of the fuel elements or from different fuel cycles. In particular, if in future an increase in the conversion rate or even fuel breeding systems should be required, the tendency will go in the direction of a lower burnup, to keep the influence of parasitic neutron capture in protactinium-233 as low as possible while using a thorium cycle. The available particle types today are mainly TRISO particles. From an operational point of view, the initially developed BISO-coated particles are completely sufficient concerning fission-product release, however they are outperformed by the behaviour of TRISO-coated particles in case of hypothetical accident conditions, for example with core heat-up to temperatures > 1 500 °C. Advantages seen in nuclear fuel processing of BISO particles should not play a role in the next several decades. There are no big differences in the production costs for fuel experiments with different particle types. Today, fuel elements with BISO and TRISO particles can be seen to be fully tested and commercially deployable due to the long-term tests in AVR reactors.

3.8. Feeding principles

Today, two different feeding systems are available for pebble-bed reactors. The multi-cycle feeding process (MEDUL) tested in AVR and THTR reactors, where the fuel elements pass multiple times through the reactor core until they reach their final burnup stage, allows the partially burned-up fuel elements to be controlled and measured from time to time. As a consequence of this operational mode, relatively uniform power generation is reached in the axial direction. The peak factors of the power density distribution are low. On the other hand, considerable effort is needed for burnup determination, distribution and re-feed of the fuel elements. One of the reasons for developing the OTTO mode was to considerably reduce the number of components in the fuel feeding system. At the same time it is possible with the OTTO cycle fuel feeding system to keep the temperature difference between the cooling gas and the fuel at the core outlet very low, therefore with regard to fuel element stresses, a cooling gas temperature > 1 000 °C can be realised technically. On the other hand, the OTTO mode increases the effective dose stresses of the top reflector and the upper lateral reflectors due to the large increase in fast neutron flux in the upper core region. If core rods are used in reactors with an OTTO fuel cycle, attention has to be paid to compacting effects after repeated core penetrations of the rods to greater depths, due to the missing possibility of loosening up of the pebble bed by recirculation of the spheres. The use of OTTO cycles is not favoured at core heights > 6 m due to a very high peak factor in the power density, with negative consequences on, for example, core heat-up in case of a hypothetical accident.

3.9. Questions concerning the plant layout

In addition, it should be mentioned here that, unlike in reactor lines that have been established in the long-term such as pressurised or boiling-water reactors, for the technical design of the plant layout different ways have been realised. Here only some important aspects are mentioned. Details

of individual components linked to design questions can be found in the ‘Components’ section . Out of the multitude of possibilities, only a few variants are briefly explained here.

Vessel concept: Initially applicable here are, as a first principle, a steel RPV, reinforced concrete containment or prestressed containers latter made of spheroidal cast iron or cast steel may be used. In case of a reinforced concrete vessel, the components of the primary circuit may be incorporated in a big cavern, as was the case in the THTR. Or the so-called pod boiler principle may be used, in which the reactor core in a central cavity and the heat exchangers in the container wall are located in different cavities. Layouts for the primary loop oriented at concepts used for pressurised water reactors were developed for the HTR. At this point the layout principles of the modular reactor are referred to, in which the reactor and heat exchanger are located in separate steel containers, connected via a coaxial pipe. Instead of vessel steel containers, at least for the housing of the reactor, prestressed pressure vessels made of spheroidal cast iron, cast steel or even concrete may be used in the future.

Hot gas pipes: These components can consist of coaxial pipes with inner insulation or simple pipes with corresponding inner insulation. Also, the flow through ceramic structures as flow conducting principle may be beneficially used. This principle was successfully used for two decades in the AVR and the concept was also used for the HTR-100 reactor.

Residual heat removal: For the removal of residual heat, production loops or separate residual heat removal loops are under consideration. After a certain time, the liner cooling system can take over the removal of residual heat in reinforced concrete vessels. For reactor systems with — to a large extent — inherent safety features concrete cell coolers outside the RPV are envisaged, or, after failure of the concrete cell coolers, the concrete structures themselves will work as heat sinks.

Number of loops: Depending on the total power of the plant, and partly also corresponding to the intended use of the nuclear heat source loop, between 1 and 8 loops are planned or were put in place, respectively.

Arrangement of blowers: Every loop has its own primary loop blower. These blowers may be placed either above or below the steam generator or, as in the case of the THTR, laterally (inside the reinforced concrete wall).

Shutdown elements: In some designs, the use of core rods and reflector rods are provided. Particularly for plants in the mid-power range, this diverse implementation of the shutdown system was carried out or is planned for new plants, respectively. For plants in the low-power range, all shutdown and control processes should be carried out from the core boundary. To achieve this goal, reflector rods and absorber systems for small shutdown spheres falling into reflector rod holes will be used.

Reactor safety building: Depending on the layout principle, with regard to severe accidents this building can be equipped with or without inner liners. In addition it is possible to construct the building above or below the surface, or partly below.

The above listing of layout principles is given only in a very incomplete manner. These principles allow different technical solutions for HTR plants depending on the type of application, installation

size and requirements imposed. Optimisation is always possible under consideration of safety features and equipment, cost-effectiveness and current state of technology.

4. Fuel and fuel performance

Originally developed to provide oxidation resistance for carbide fuel kernels, the coated particle has advanced into a sophisticated fission product containment system that can operate at the high temperatures of a high-temperature gas-cooled reactor (HTGR). Each coated particle is a miniature fuel element with a ceramic kernel that contains fissile or fertile fuel material protected by a sequence of ceramic coating layers that perform specific design functions. The fuel kernel is commonly an oxide or carbide compound of uranium (with various enrichments), thorium or plutonium. The ceramic coatings in most general use are pyrolytic PyC and SiC, although a variety of other materials like ZrC continue to be developed. The TRISO-coated fuel particle, shown in Figure 10, has a dense SiC layer sandwiched between two dense PyC layers. Figure 11 is generally accepted worldwide as the reference particle concept for HTGRs. Research and development continues worldwide to further improve and extend the TRISO particles' fuel performance envelope.

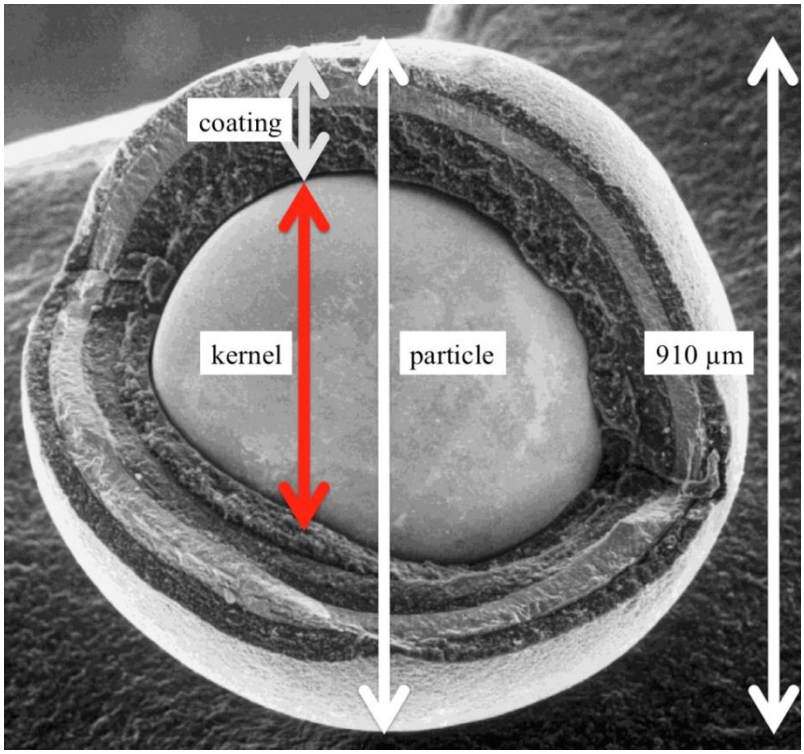

Figure 10: Scanning electron microscope photograph of a purposely cracked TRISO-coated particle showing the fuel kernel and the coating layers (*source:* Forschungszentrum Jülich)

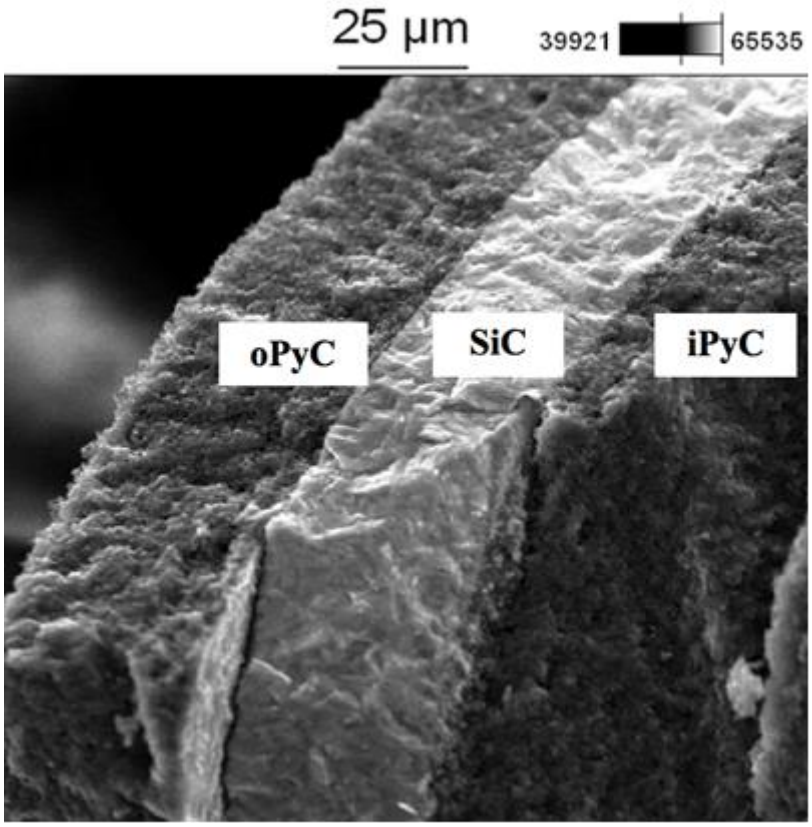

Figure 11: High-magnification scanning electron microscope photomicrograph of the TRISO coating (Rooyen, 2010) (*source:* Nelson Mandela Metropolitan University)

The low-enriched uranium (LEU) UO_2 LTI TRISO particle is often referred to as 'modern HTGR fuel'. Table 4 describes the general characteristics of the reference fuel particle design.

Table 4: German reference coated particle: LEU UO_2 with an LTI TRISO coating

Component	Material	Dimensions (µm)	Density (Mg/m^3) (as-fabricated)
Fuel kernel	Uranium dioxide (UO_x, $x \leq 2.015$)	Diameter: 500	≥ 10.4
TRISO coating			
Buffer layer	Porous	Thickness: 95	~ 1.0
Inner PyC layer	Dense PyC	Thickness: 40	1.85
Fission product barrier	Dense SiC	Thickness: 35	3.20
Outer PyC layer	Dense PyC	Thickness: 40	1.85

4.1. Fuel manufacturing

Fuel elements contain near defect-free UO_2 TRISO-coated particles, homogeneously distributed within a graphite matrix with very low levels of uranium contamination. The processes used to manufacture this fuel are now being used worldwide (China, France, Korea, South Africa, United States) to reproduce the German high-quality fuel of the 1980s.

4.1.1. UO_2 fuel kernels

The spherical fuel kernel consists of stoichiometric uranium dioxide (UO_2) of near theoretical density. The kernel is the primary power source and generates almost all the fission products. The fuel kernel also serves as a significant barrier to radionuclide release by immobilising many of the fission products as stable oxide compounds and delaying the diffusive release of others, allowing them to decay into more stable isotopes. These processes substantially reduce fission-product release from particles employing oxide fuel compounds.

Modern fuel kernels are produced from aqueous heavy-metal solutions. The LEU UO_2 fuel kernels manufactured for the high-quality fuel particles in the German fuel development programme were based on a modified sol-gel external gelation microsphere fabrication process, developed by NUKEM and known as the gel precipitation process. Other HTGR fuel-kernel manufacturing processes may utilise the internal gelation technique for microsphere fabrication (Vaidya, 2008) (Hunt, 2010).

LEU UO_2 fuel-kernel production was found to be relatively simple, with few process steps and small volumes of effluent and waste, and well suited to automated manufacturing (Kadner, 1977) (Venter, 2004). Similar kernel-fabrication processes are employed to make the LEU UO_2 fuel kernels used in spherical elements for the HTR-10 and the HTR-PM in China (Fu X., 2004) and as the reference kernel-making process for the PBMR project in South Africa (Mueller, 2006).

4.1.2. TRISO coating

The TRISO coating is composed of four successive ceramic layers and fabricated over a dense heavy metal spherical fuel kernel. Each of the layers has one or more design functions as outlined in Table 5.

Table 5: Design functions of the ceramic coating layers of the TRISO-coated fuel particle

TRISO particle coating layer	Design function
Buffer (50 % dense)	- Provides void volume for gaseous fission products and reaction products (CO, CO_2) released from fuel kernel. - Accommodates fuel-kernel swelling. - Protects PyC and SiC layers from fission product recoil.
Inner PyC (density ≥ 1.85 Mg/m^3)	- Diffusion barrier to fission products, retains gaseous fission products. - Impermeable layer prevents Cl_2 from reaching kernel during SiC deposition and prevents CO from interacting with SiC during irradiation. - Provides mechanical substrate for deposition of SiC layer.

	- Induces compressive stresses in SiC due to irradiation induced shrinkage.
SiC (density ≥ 3.20 Mg/m^3)	- Primary barrier to fission products, retains all gaseous and solid fission products (except Ag) at normal operating temperatures < 1 250 °C and in accidents up to1 600 °C. - Load bearing layer for particle.
Outer PyC (density > 1.85 Mg/m^3)	- Creates compressive stress on SiC due to irradiation-induced shrinkage. - Retains gaseous fission products. - Provides bonding layer with carbonaceous fuel element matrix.

The first coating is a low-density porous carbonaceous layer called the buffer and it is deposited directly over the fuel kernel. The buffer layer provides the necessary void volume for the accumulation of gaseous fission products released from the fuel kernel, accommodates fuel-kernel swelling and serves as a sacrificial layer for fission fragments.

The second layer is a high-density, isotropic carbon layer, called the inner pyrocarbon (iPyC). Porosity in the iPyC is strictly controlled since the SiC layer deposited on its surface partially extends into the surface pores, tightly adhering to this layer. The iPyC is a gas-tight coating that protects the kernel from hot gaseous chlorine compounds during SiC deposition and provides a smooth substrate for SiC deposition. The iPyC retains the fission gases Xe and Kr and serves as a diffusion barrier to metallic fission products. During irradiation, this layer shrinks and the contraction helps to reduce tensile stresses on the SiC.

The third layer is a near theoretical density SiC layer. The SiC layer is sandwiched between two PyC layers and serves as the pressure-bearing component of the particle as well as the primary metallic fission product diffusion barrier.

The fourth layer is another high-density, isotropic carbon layer, called the outer pyrocarbon (oPyC). This layer serves as a further diffusion barrier for gaseous and metallic fission products, and like the iPyC layer it also contracts during irradiation, helping to reduce tensile stress on the SiC. The oPyC also protects the SiC during particle handling and sphere/compact formation, and provides a bonding surface for the overcoating process.

The four ceramic coating layers in the TRISO design are prepared by chemical vapour deposition (CVD) processes in high-temperature fluidised-bed furnaces. The schematic in Figure 12 shows the primary components of a high-temperature fluidised-bed furnace. Deposition conditions such as temperatures and rates are shown in Table 6 for each of the constituent layers, along with the carrier and deposition gases employed (Brähler, 2008) (Brähler, 2010). They are representative for the TRISO-coated LEU UO_2 fuel particles produced in the 1980s within the German fuel development programme and are similar in recent fuel programmes.

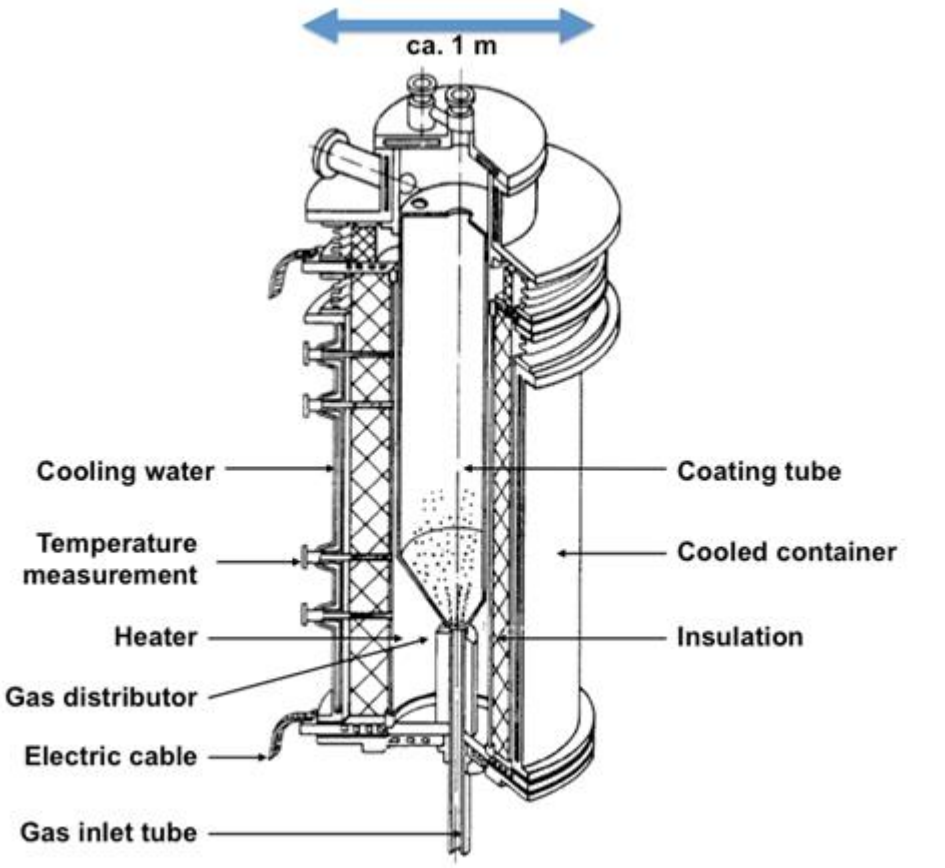

Figure 12: Schematic of high-temperature fluidised-bed CVD coating furnace (*source:* NUKEM Technologies)

Table 6: Typical parameters for CVD processes employed to deposit ceramic coating layers on dense LEU UO_2 fuel kernels to produce TRISO-coated particles (Huschka, 1977; Nothnagel, 2010)

Layer	Source gas/ carrier gas	Deposition temperature (°C)	Coating reactions	Deposition rate (µm/min)
Buffer	C_2H_2/Ar	1 300–1 450	$C_2H_2 \rightarrow 2C + H_2$	15-25
IPyC	C_3H_6+C_2H_2/Ar	1 250–1 400	$C_3H_6 \rightarrow 3C + 3H_2$ $C_2H_2 \rightarrow 2C + H_2$	3-7
SiC	CH_3SiCl_3/H_2	1 500–1 600	$CH_3SiCl_3 + H_2 \rightarrow$ $SiC + 3HCl + 3H_2$	0.2
OPyC	C_3H_6+C_2H_2/Ar	1 250–1 400	$C_3H_6 \rightarrow 3C + 3H_2$ $C_2H_2 \rightarrow 2C + H_2$	3-7

4.1.3. Spherical fuel element

The fuel element for a pebble-bed HTGR (Nabielek, 1984) (Nabielek, et al., 1990) (Tang C.H., 2002) (Vaidya, 2008) is a sphere with a diameter of 60 mm consisting of a spherical fuel zone with a diameter of ~ 50 mm, in which the TRISO-coated particles are randomly distributed in graphitic matrix material. A fuel-free shell of graphite matrix ~ 5 mm thick is then moulded to the fuel zone (Figure 13). The matrix material consists of a carbonised organic binder and nuclear-grade graphite

material that acts as a fission neutron moderator, heat-transfer medium and protection against external forces. The graphitic matrix material exhibits high density, high thermal conductivity, high mechanical strength, low thermal expansion, low anisotropy, low Young's modulus, good corrosion resistance, good dimensional stability under neutron irradiation and a very low concentration of impurities (Schulze, 1982).

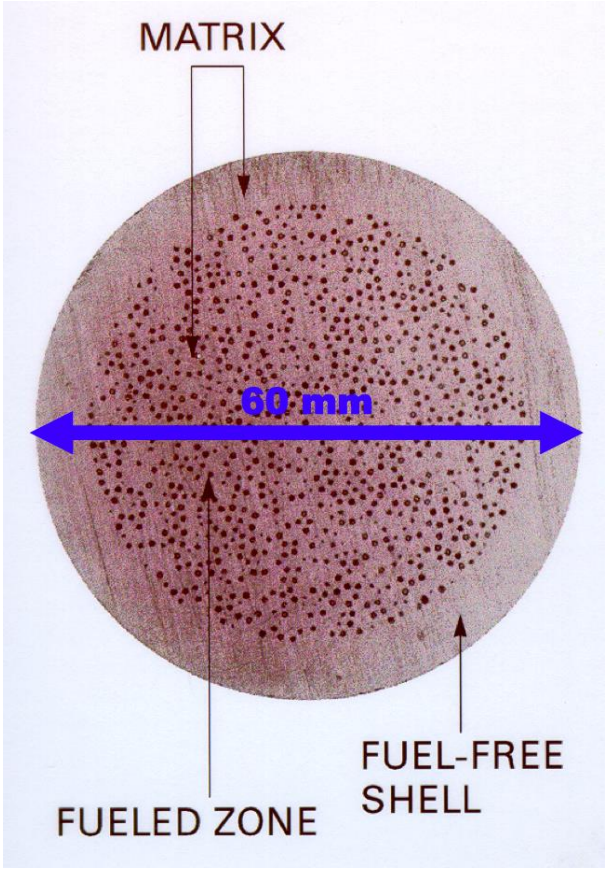

Figure 13: Cross section of German reference 60 mm-diameter spherical fuel element showing TRISO particles randomly distributed in the 50 mm-diameter fuel zone (*source:* NUKEM Technologies)

Spherical fuel elements are used in the core of a pebble-bed reactor that is cylindrical or annular in shape and filled with several hundred thousand spherical elements. Fresh fuel elements and graphite elements are inserted from the top and slowly sink down through the core under the influence of gravity. On-load refuelling during full-power operation is a matter of course. When the fuel elements reach the bottom of the core they are funnelled through a mechanical unloading system where the irradiated spheres can be withdrawn or recirculated. In recirculating systems like AVR, THTR and HTR Module each fuel sphere is tested for mechanical and chemical integrity and a burnup measurement is made. Those fuel elements identified for further operations are recirculated and reinserted at the top of the core. In once-through systems the fuel spheres are withdrawn completely.

The fabrication process for spherical elements as developed by NUKEM in Germany, shown in Figure 14, consists of the following steps: (1) resinated graphitic matrix powder preparation (kneading, drying, milling); (2) overcoating of particles; (3) pre-moulding of fuel zone and high-pressure cold isostatic pressing of the complete fuel element; (4) machining; and (5) carbonisation at 800 °C and final heat treatment at 1950 °C.

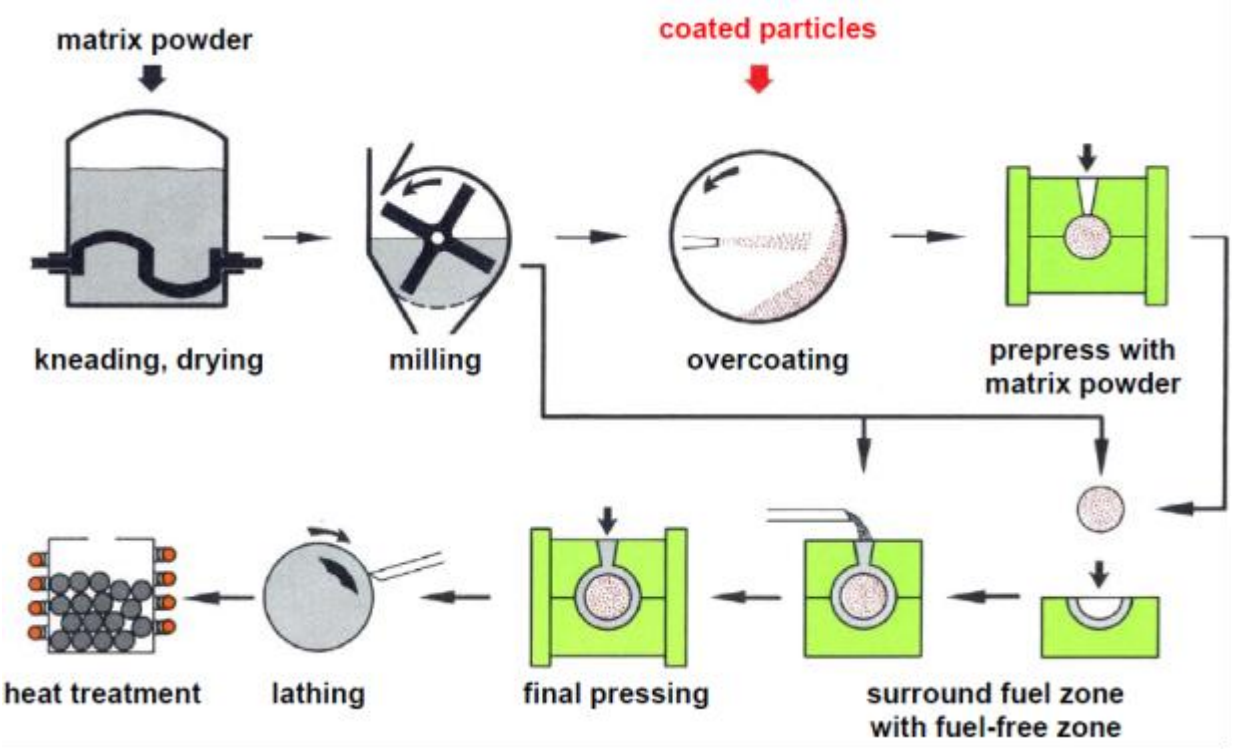

Figure 14: Process steps in manufacturing the German reference 60 mm-diameter HTGR spheres (*source:* NUKEM Technologies)

Following Germany's selection of LEU UO_2 with a TRISO coating as its reference HTGR particle system in 1980, NUKEM Technologies manufactured large numbers of high-quality spherical elements in production-scale facilities. In total, 59 400 spherical elements were produced and destined for real-time irradiation in the AVR and accelerated irradiation performance tests in European MTRs. Table 7 provides the fuel manufacturing and characterisation details for this massive effort (Hrovat, et al., 1988) (Schulze, 1982) (IAEA, 1997).

In 1981 NUKEM fabricated 24 600 spherical fuel elements for AVR Reload 19, with the designation GLE-3. These elements were fabricated from fuel particle production sets comprising multiple LEU UO_2 kernel production runs and TRISO-coated particle batches. The enrichment of the GLE-3 elements was 9.82 wt % ^{235}U and each spherical element contained 16 400 coated particles. The GLE-3 elements were all fabricated with A3-27 matrix material with a measured as-manufactured free uranium fraction, as designated by the U_{free}/U_{total} value of $< 50.7 \times 10^{-6}$.

Approximately 100 test elements, including 60 mm-diameter spherical elements along with non-reference test elements (20 mm-diameter spheres and cylindrical compacts), were also produced for accelerated irradiation testing in 1981 in the LEU Phase 1 effort. The test specimens selected for accelerated testing in the first series of MTR experiments (SL P1, HFR-K3, HFR-P4, FRJ2-K13 and FRJ2-P27) contained fuel particles with an enrichment of 9.82 wt % ^{235}U.

Two additional large-scale fuel element production campaigns were manufactured in 1983 and 1985. They were AVR Reload 21, consisting of 20 500 elements designated as type GLE-4/1, and AVR Reload 21-2, consisting of 14 000 elements designated as type GLE 4/2. Three GLE-4/1 fuel elements were included in accelerated MTR irradiation test FRJ2-K15. The GLE-4 elements were also fabricated from particle production sets comprising multiple LEU UO_2 fuel-kernel production runs and TRISO-coated particle batches. The enrichment of the GLE-4 elements was 16.76 wt % ^{235}U and each spherical element contained 9 560 coated particles. The GLE-4/1 elements were fabricated with A3 27 matrix material with a measured as-manufactured free uranium fraction of < 43 × 10 6. The GLE-4/2 elements utilised A3-3 matrix material. More GLE-4/2 elements were fabricated for AVR than actually inserted for AVR refuelling purposes. The remaining elements were made available to European test facilities and HTGR research/development in other countries (China), and for future irradiation tests (HFR-EUbis (Fütterer M., 2008) in 2004 and HFR-EU1 (Laurie M, 2010) (Tang C.H., 2010) in 2006) and out-of-reactor testing (HFR Petten and PBMR, South Africa).

Table 7: Production-scale manufacturing details for high-quality spherical elements containing LEU UO_2 TRISO-coated fuel particles during period 1980 to 1988

	Pre-1985 production			Post-1985 production	
Characteristic	GLE-3	Phase 1	GLE-4/1	GLE-4/2	Proof Test
Kernel diameter (µm)	500	497	501	502.2	508
Kernel density (Mg/m^3)	10.80	10.81	10.85	10.86	10.72
Coating layer thickness (µm)					
Buffer	93	94	92	92.3	102
Inner PyC	38	41	38	40.6	39
SiC	35	36	33	35.9	36
Outer PyC	40	40	41	39.6	38
Coating density (Mg/m^3)					
Buffer	1.01	1.00	1.013	1.012	1.02
Inner PyC	1.86	~ 1.9	~ 1.9	1.87	1.92
SiC	3.19	3.20	3.20	3.2	3.20
Outer PyC	1.89	1.88	1.88	1.87	1.92
Fuel loading					
Heavy metal (g/FE)	10	10	6	6	9.4
^{235}U (g/FE)	1	1	1	1	1
Enrichm. (wt % ^{235}U)	9.82	9.82	16.76	16.76	10.6
No CP/FE	16 400	16 400	9560	9560	14 600
Matrix material	A3-27	A3-27	A3-27	A3-3	A3-3
Free uranium fraction U_{free}/U_{total} (× 10^{-6})	50.7	35	43.2	7.8	13.5
Kernel sets	5	1	2	5	1
Coating batches	65	1	54	29	8
Coating batch size (kg)	5	5	3	3	5
CP batch designation	HT232-245	EUO 2308	HT354-383	HT385-393 HT395-404 HT406-423	EUO 2358-2365
FE production lots	14	-	11	8	-
FE produced	24 600	100	20 500	14 000	200

The fuel production processes employed to produce the AVR Reload 21-2 resulted in the highest-quality fuel ever produced in the German fuel development programme. The as-manufactured free uranium fraction value for the GLE-4/2 spherical elements was $< 8 \times 10^{-6}$.

A final fuel production campaign was conducted by NUKEM in 1988 to produce spherical elements for a proof test of the HTR Module concept. Approximately 200 reference spheres were fabricated from particle production sets comprising TRISO-coated particle batches. The proof test fuel particles had an enrichment of 10.6 wt % ^{235}U. Each proof test spherical element contained 14 600 particles and utilised A3-3 matrix material. A total of eight spherical elements were selected for irradiation in the HTR Module proof test rigs HFR-K5 and HFR-K6 (four elements in each test, HFR — Petten). The as-manufactured free uranium fraction value for the proof test spherical elements was $< 13.5 \times 10^{-6}$. After irradiation in Petten, these eight spheres were sent to the Jülich Research Centre for PIE and later to ITU Karlsruhe for accident condition testing. Since then, fabrication processes based on those developed by NUKEM have been used to manufacture spherical HTGR fuel elements in China (Huschka H., 1977) and in South Africa (Nabielek, et al., 2010).

4.1.4. As-manufactured fuel quality

In HTGR coated fuel particles, the SiC layer represents the most important barrier to retain fission products. Its material properties and its mechanical and structural integrity are essential during fuel element manufacture, irradiation, throughout accidents and in long-term fuel storage at a disposal site. The burn-leach test has been established as the safest method to ascertain SiC integrity in oxide TRISO-coated particles.

During the burn-leach test, the graphitic or carbonaceous components of the sample (oPyC in loose coated particles, complete spherical fuel elements, compact, coupons) are burnt in a muffle furnace at ~ 800 °C under air convection. The residue is treated with nitric acid and the amount of dissolved uranium analysed. Since SiC is corrosion resistant, it will withstand the attack. However, a particle with an imperfect or weak SiC coating layer will lead to a near quantitative kernel uranium inventory in the nitric acid solution. In addition, the uranium content of incompletely coated particles (PyC only) will be dissolved and measured in the solution.

The burn-leach test results are presented as a ratio of the measured uranium (in acid solution) to the total uranium content of the original sample (U_{free}/U_{total}). The detection limit of burn-leach testing on unbonded particles and fuel elements is of the order 1×10^{-6} or 0.0001 wt %.

The quality of the spherical fuel elements manufactured in production-scale facilities by NUKEM were characterised using the burn-leach technique. The results are provided in Table 7 and Table 8 and shown in Figure 15. Blue circles represent measured burn-leach results obtained by NUKEM demonstrating the post-1985 improvement in manufacturing quality. The improvements in quality these data represent were due to the improved and perfected tabling of kernels and particles and the introduction of an automated process for overcoating of particles. The quality level of the German fuel produced in the 1980s set a worldwide standard that was later followed by other countries active in HTGR fuel development.

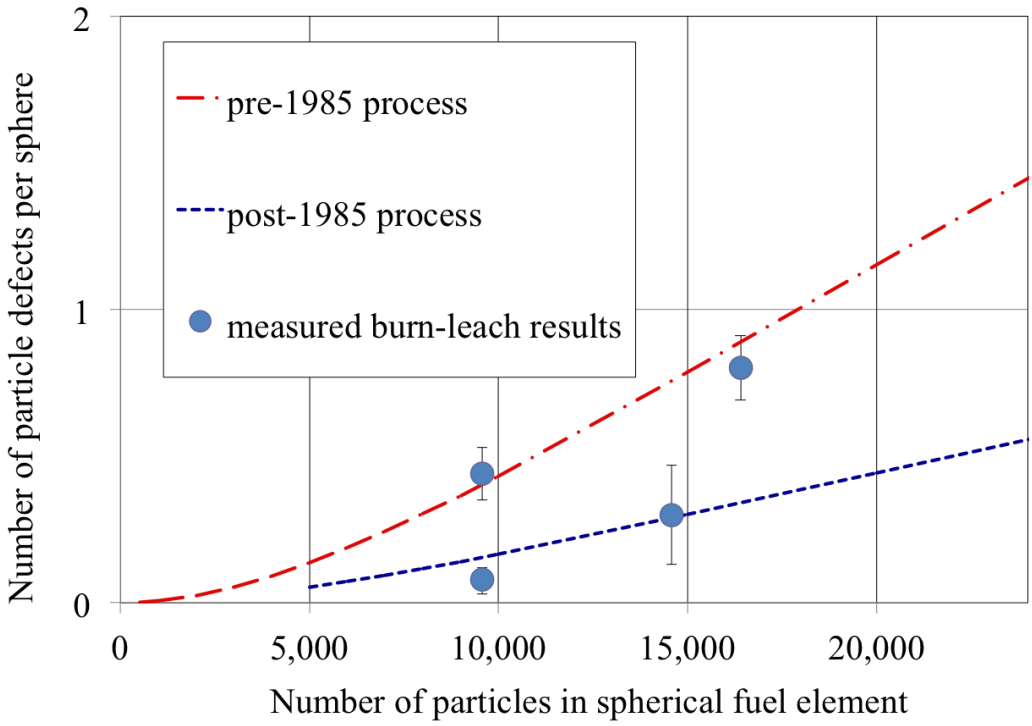

Figure 15: Number of UO_2 TRISO particle defects in sphere manufacture as a function of the number of particles in the spherical fuel element

However, for fuel quality, the limitations of failure statistics (Audebeau, 1971) must be considered. With the observation of n defects in a sample of N particles, the expected failure fraction x is given by the ratio n/N. The quality of this result is strongly dependent on the sample size, N. When the true failure fraction is ζ, then the probability of observing n failures in a sample of N particles is proportional to $\zeta^n \cdot (1-\zeta)^{N-n}$ and this represents the binomial distribution (Abramowitz, et al., 1965). Given that in a random sample of size N, there are n failures observed, the probability C that the true failure fraction will be in the range $0 \le \zeta \le \zeta_{max}$ is given by the incomplete beta function (Abramowitz M., 1965b).

$$C = \frac{\int_o^{\zeta_{max}} \zeta^n (1-\zeta)^{N-n} d\zeta}{\int_o^1 \zeta^n (1-\zeta)^{N-n} d\zeta} = B_{\zeta_{max}}(n+1, N+1-n) \qquad (18)$$

Therefore, evaluating the one-sided upper 95 % limit of the expected failure fraction n/N can be accomplished by computing the inverse, viz.:

$$\zeta_{max} = B_{0.95}^{-1}(n+1, N+1-n) \qquad (19)$$

The results for the LEU UO_2 TRISO fuel burn-leach data are listed in Table 8. In terms of free uranium, these are better by an order of magnitude than the earlier BISO fuels (Kania M.J., 1980) for AVR and THTR with U_{free} /U_{total} between 3 and 9 × 10^{-4}.

Table 8: Failure statistics for LEU UO_2 TRISO-coated fuels based on burn-leach results

	Pre-1985 production		Post-1985 production	
Fuel element type	AVR 19	AVR 21-1	AVR 21-2	Proof test fuel
Year of production	1981	1983	1985	1988
Particles per sphere	16 400	9 560	9 560	14 600
Spheres tested	70	55	40	10
Particles tested (= N)	1 148 000	525 800	382 400	146 000
Defects found (= n)	56	24	3	3
Defect particle fraction expected (= n/N) upper 95 %	 49 × 10^{-6} 61 × 10^{-6}	 46 × 10^{-6} 64 × 10^{-6}	 8 × 10^{-6} 20 × 10^{-6}	 21 × 10^{-6} 53 × 10^{-6}

4.2. HTGR fuel performance under accident conditions

Demonstrating the capability of spherical fuel elements to withstand a severe depressurisation accident with no measurable loss of fission product was a primary objective of the German fuel development programme. Since the 1970s, irradiated fuel elements retrieved from AVR and from MTR tests have been investigated in accident simulation tests. Prior to the mid 1980s, the temperature margins explored were up to 2500 °C where fission-product release was massive.

In response to the reactor designer's requirement for a passively safe HTGR, the KÜFA (Kühlfinger Apparatur, i.e. cold finger device) furnace was designed and installed in the hot cells of the Jülich Research Centre for high precision, online fission-product release measurements under simulated accident conditions (Gottaut H., 1990). This facility made it possible to demonstrate that modern LEU UO_2 TRISO-coated fuel particles retain all safety-relevant fission products up to 1 600 °C at a level not exceeding release under normal operating conditions, which in itself is very low.

4.2.1. Simulation testing of core heat-up depressurisation under dry conditions

The maximum expected fuel element temperature evolution in a 'depressurised loss of forced coolant' (DLOFC) accident in a small modular HTGR is shown in Figure 15 (Reutler, et al., 1984). The maximum fuel temperature limit is set at 1 600 °C based upon the estimated maximum core temperature of ~ 1 500 °C plus a reasonable estimate of the effect thermal property uncertainties have on this maximum temperature estimate. For testing purposes, the temperature range 1 600-1 700-1 800 °C is of interest for the core heat-up simulation testing programme as illustrated in Figure 15. The most relevant fission and activation products include the long-lived strontium (^{90}Sr), silver (^{110m}Ag), caesium (^{134}Cs, ^{137}Cs) and krypton (^{85}Kr) and the short-lived iodine (^{131}I) and xenon (^{133}Xe) fission products.

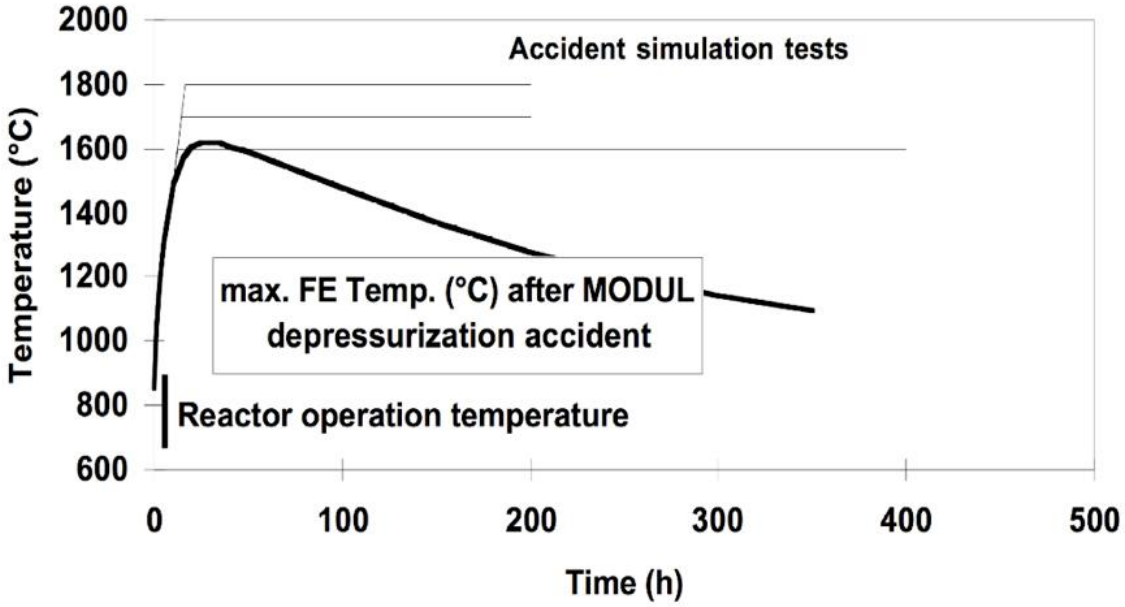

Figure 16: Temperature evolution during depressurisation and core heat-up in small modular HTGRs in comparison to the temperature profiles used in KÜFA tests

4.2.2. Fission-product release from UO_2 kernels at 1 600 °C

Little fission product retention can be expected in exposed UO_2 fuel kernels at elevated temperatures. Figure 17 shows that the release of silver, xenon, iodine and caesium from an exposed UO_2 fuel kernel quickly approaches 100 % during a 1 600 °C heating test. Early, within the 30-hour heat-up phase to the test temperature, significant release has already occurred for ^{131}I, ^{133}Xe and ^{137}Cs. After 50 to 100 h at 1 600 °C, nearly 100 % of the inventories of these fission products have been released. Only the fission product ^{90}Sr is strongly retained in the oxide kernels at this temperature, but this is not the case for carbide kernels. The primary barriers to the volatile fission products like iodine, xenon and caesium are the coating layers of the TRISO-coated particle, especially the SiC layer.

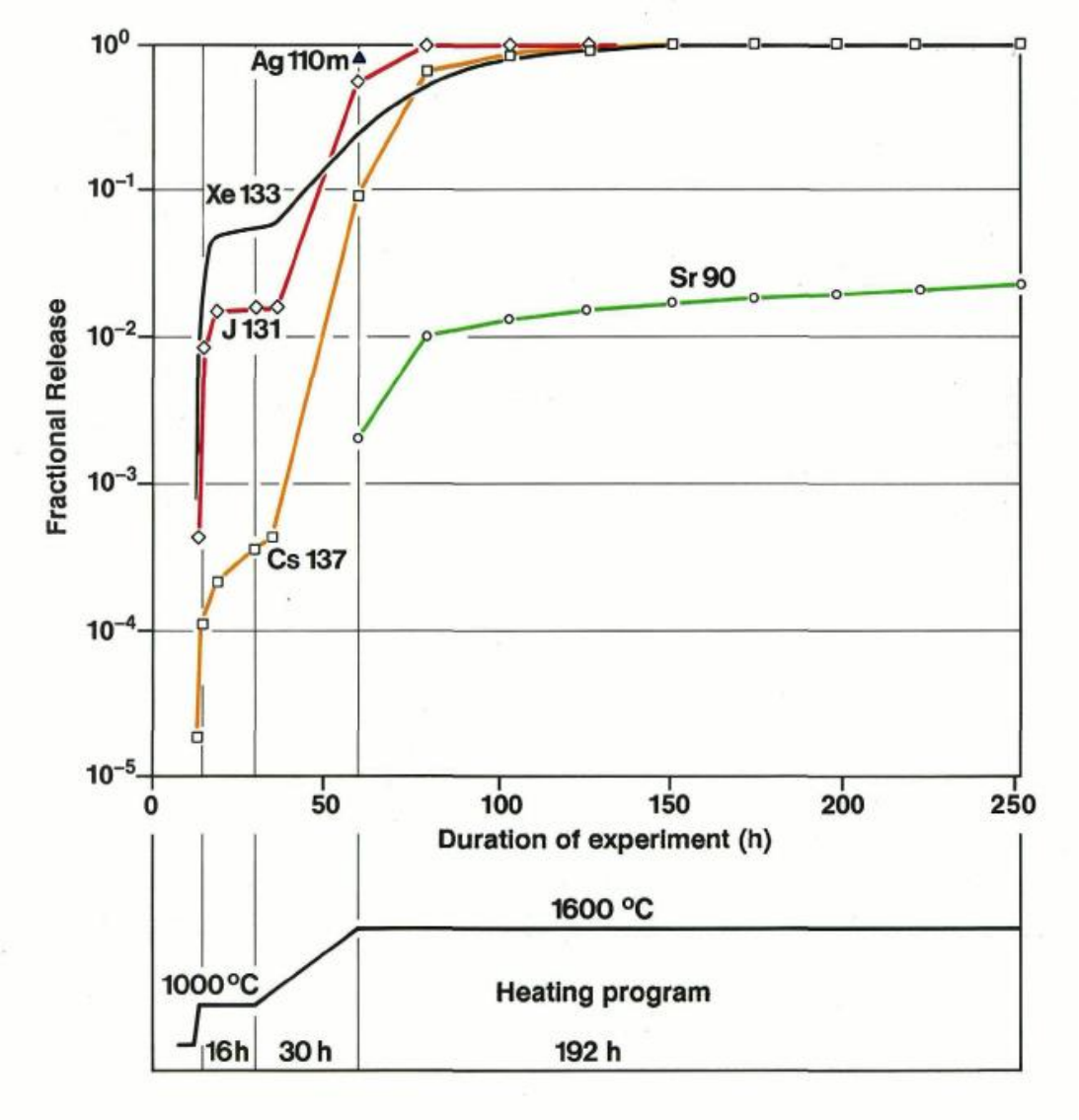

Figure 17: Fission-product release from exposed UO_2 kernels during 1 600 °C heating test

4.2.3. Comparison of fuel quality at 1 600 °C

With regard to the measurement of ^{131}I (half-life = 8.02 d) release from various fuel configurations during heating at 1 600 °C, Figure 18 illustrates three different release behaviours (Schenk, et al., 1991):

- exposed UO_2 fuel kernels, ~ 100 % ^{131}I release;
- irradiated fuel elements with TRISO-coated fuel particles (cross-contaminated in the AVR by older lower-performance BISO fuel from the 1960s and 1970s), ^{131}I release behaviour at 10^{-5} level; and
- irradiated fuel elements with modern TRISO-coated fuel particles, ^{131}I release behaviour at the 10^{-9} to 10^{-8} level.

The experimental results represent iodine release from a UO_2 fuel kernel, from a contaminated HTGR fuel element and from modern HTGR fuel elements irradiated in a clean environment, and in between these are nine orders of magnitude in release.

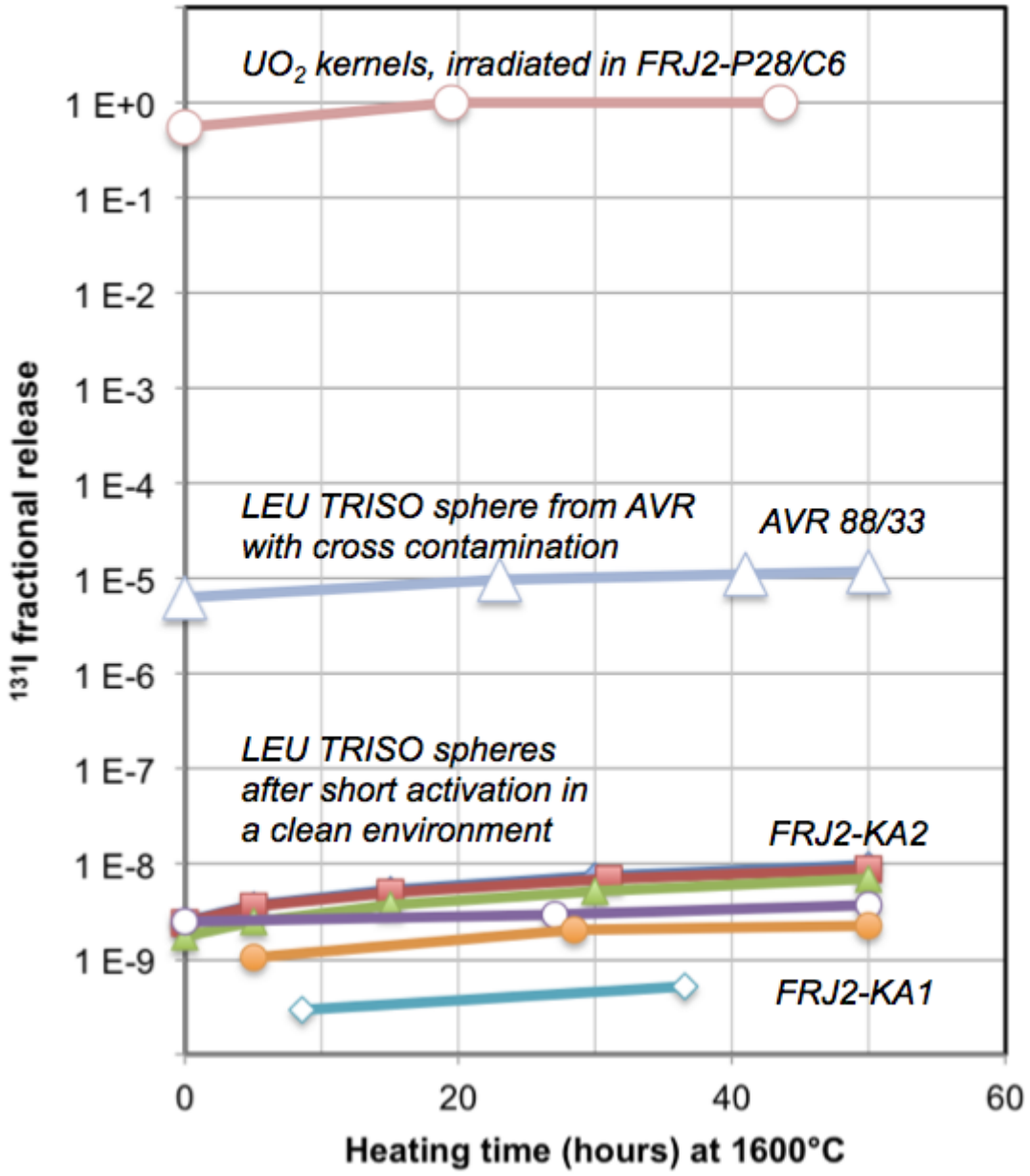

Figure 18: Iodine-131 release from various fuel configurations during 1 600 °C heating tests

4.2.4. KÜFA tests in Jülich 1985-1995 and in Karlsruhe 2005-2010

In the unrestricted core heat-up simulation tests performed on irradiated spherical fuel elements containing LEU UO_2 TRISO particles, no single particle failures, nor any noticeable caesium or strontium releases, were observed during the first few hundred hours in any of the 1 600 °C heating tests. The number of particle failures and the fission-product release inventories do however increase as the accident simulation temperature rises to 1 700 °C and 1 800 °C. Figure 19 and Figure

20 show the measured time-dependent krypton and caesium release profiles during isothermal heating tests conducted at 1 600 °C to 2 100 °C. The krypton and caesium releases are representative of a whole series of fission products. The heating tests demonstrate near 100 % retention at 1 600 °C for the accident-specific first hundred hours or more.

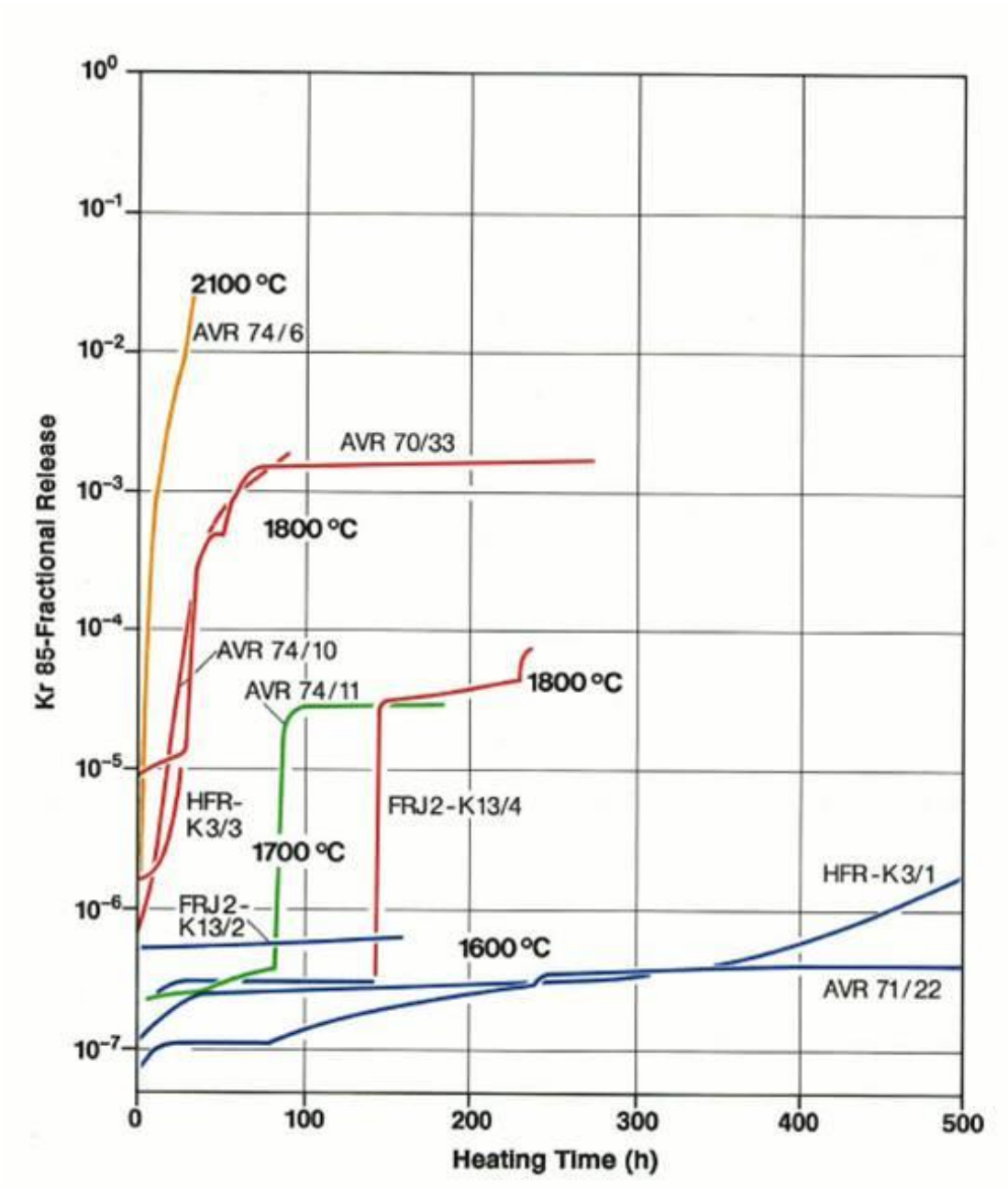

Figure 19: Krypton-85 release during heating tests with irradiated LEU UO_2 TRISO spherical fuel elements irradiated in MTRs (HFR, FRJ2) and in AVR

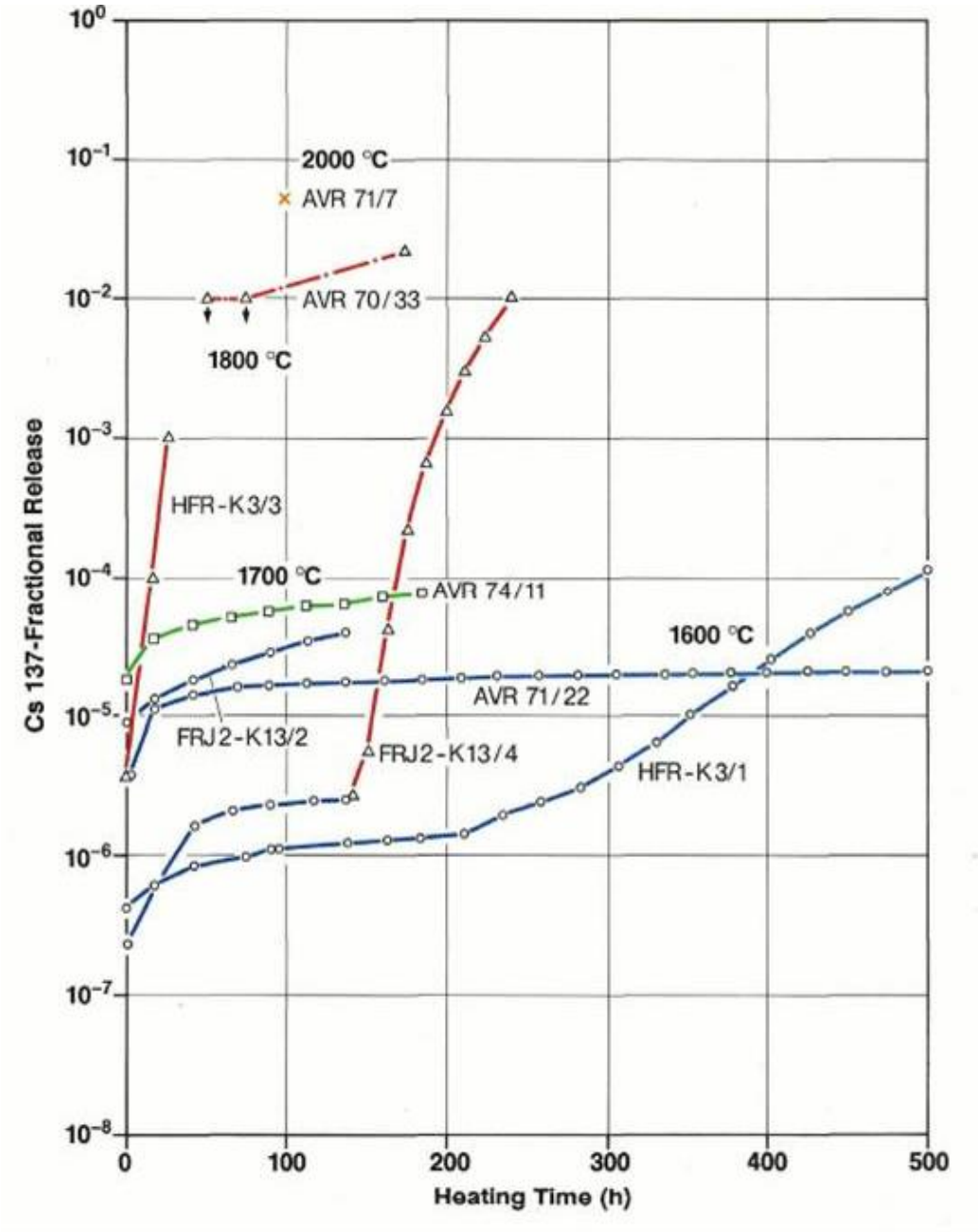

Figure 20: Caesium-137 release during heating tests with irradiated LEU UO_2 TRISO spherical fuel elements irradiated in MTRs (HFR, FRJ2) and in AVR

In particular:

- Caesium is retained at 1 600 °C in the fuel kernel, by the SiC and by the A3 matrix of the fuel element with SiC providing for the strongest retention. This retention, however, can only be guaranteed by modern high-quality TRISO coatings. At 1 800 °C there is no delay in caesium release by the kernel and the matrix, and SiC also becomes permeable to most fission products.
- Krypton is always released later than caesium due to the additional retention provided by the dense, intact pyrocarbon layers. However, if the PyC layers are not intact krypton is released as readily as caesium.

- Strontium is retained much better in oxide kernels and the sphere matrix than caesium. Therefore, strontium release generally occurs later than caesium.

More recently, accident simulation testing with irradiated LEU UO_2 TRISO spherical fuel elements have been performed in Karlsruhe, Germany (Freis, 2010) (Seeger, 2012) in a recently installed KÜFA facility. These tests are still under evaluation, but results show clearly that there was not a single particle failure in all these additional heating tests.

If the maximum burnup in the fuel element is kept strictly below 11 % FIMA, as is typical for current pebble-bed concept HTGR designs, the allowable fuel temperature limit may be higher than 1 600 °C. However, this remains to be established with new experiments. If the burnup of UO_2 TRISO-coated particle fuel is pushed to ~ 15 % FIMA, fuel temperature must be rigorously limited to ≤ 1 600 °C (Figure 21). High burnup (14 % FIMA) LEU UO_2 TRISO fuels show particle failure during the first 300 hours at 1 600 °C. No particle failure was observed in lower burnup compact (11 % FIMA) at 1 600 °C.

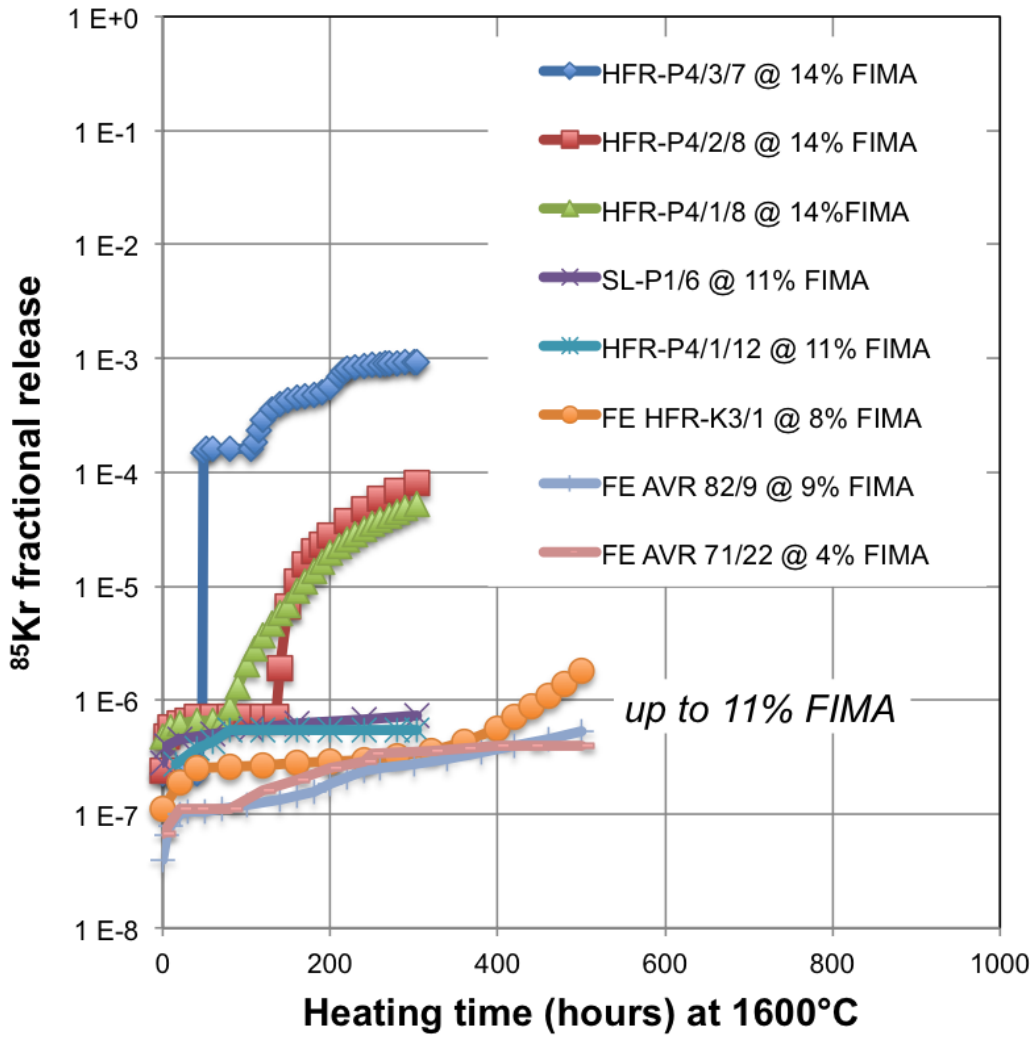

Figure 21: Krypton-85 release at 1 600 °C from compacts with 11 % to 14 % FIMA burnup in comparison to spherical fuel elements (FE) with 4 % to 9 % FIMA

4.3. Accident simulation testing under oxidising conditions

To assess fuel behaviour and fission-product release in accidents under oxidising conditions, the KORA furnace facility was designed and installed in the Jülich hot cells. This facility enables the simulation of (i) steam ingress, typically at 800 °C, and (ii) air ingress effects on TRISO-coated particles in the range from 1 300 °C to 1 500 °C.

Steam ingress can lead to the additional release of fission gases and iodine from defective (manufacture-induced) and failed (irradiation-induced) fuel particles. Data are available from in-reactor and out-of-reactor testing programmes.

During unimpeded air ingress, early assumptions predicted complete particle failure at 1 100 °C. However, the available experimental evidence shows that it takes several days at 1 100 °C to oxidise the graphite in a spherical fuel element still leaving the TRISO particles intact. Only prolonged air ingress at 1 300 °C or at higher temperatures initiates failure of the TRISO-coated particles.

4.3.1. Simulation of water ingress accident

In the accident simulation tests for a water ingress accident with heated irradiated fuel spheres, water vapour is intermittently added to the helium purge gas. An enhanced release of fission gas was found to occur in the presence of exposed UO_2 from failed fuel particles in the irradiated sphere. Figure 22 illustrates this enhanced release of ^{85}Kr from the irradiated fuel element AVR 89/30 that contained two fabrication-related defective particles; 57 % of the stored krypton inventory was released during the steam injection. This release behaviour is similar to that observed after an increase in temperature. Intact TRISO-coated particles are not affected by water vapour over a wide range of temperatures.

Irradiated UO_2 fuel kernels obtained by cracking particles deconsolidated from spherical fuel elements, simulating irradiation-induced failures, exhibited a strong burnup dependence of the enhanced fission gas release (^{85}Kr) after repeated water vapour injections at 800 °C. Only ~ 2 % of the ^{85}Kr inventory was released from kernels with a burnup of 5 % FIMA due to water vapour. In contrast, more than 17 % was released from kernels with a burnup of 9 % FIMA.

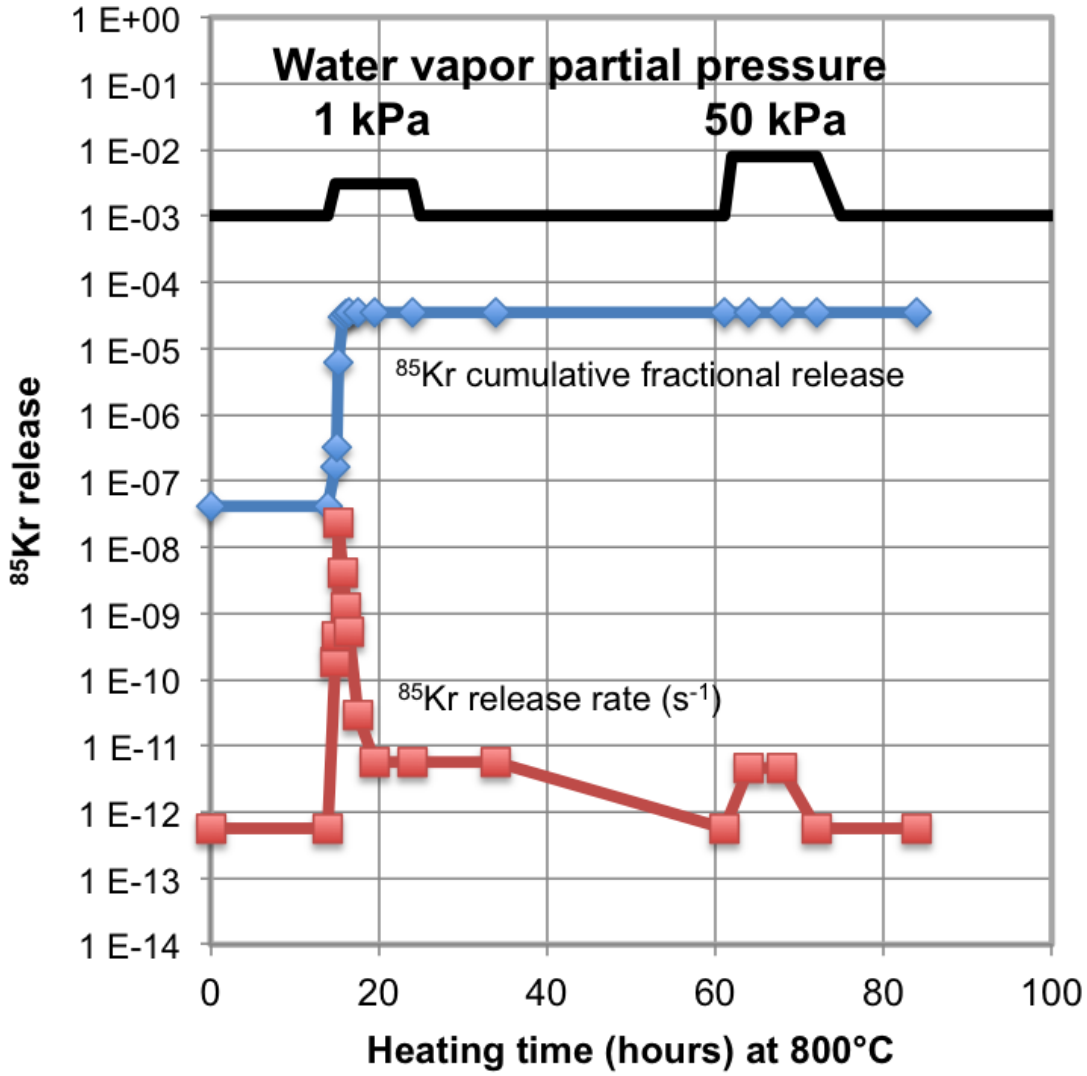

Figure 22: Enhanced ^{85}Kr release from irradiated spherical fuel element AVR 89/30 under intermittent steam injections

4.3.2. Simulation of air ingress accident

The prerequisite for air ingress in an HTGR is a very large leak, such as a rupture of the connecting vessel between the reactor core and the steam generator. Only then can excessively high graphite corrosion occur because of sufficient oxygen supply. Under extreme circumstances (open cell, open reactor building) it will still take 1 to 2 days for corrosion of the spherical fuel element fuel-free zone to progress to the point where the first fuel particles are exposed. At this point it is important how long the SiC coatings of the particles remain intact.

Samples of 10 irradiated particles, each deconsolidated from an irradiated AVR spherical element, along with individual AVR fuel spheres were heated in an air stream of 30 litres per hour to investigate the air oxidation of the ceramic particle coatings and fuel element materials. The results of these investigations in terms of ^{85}Kr release and particle failure in KORA (*Korrosionsapparatur*, i.e. corrosion device) furnace simulation tests are shown in Table 9.

Table 9: Heating tests in KORA with irradiated unbonded particles and irradiated fuel spheres in air (Schenk, 1995)

			Test conditions			^{85}Kr release		
Fuel sample	No of particles	Burnup (% FIMA)	Heat-up (h)	Max. temperature (°C)	Time (h)	First failed particle after/at	No of failed particles	Fraction of failed particles
AVR 92/29.12	10	9.2	14	1 400	400	397 h	1	0.1
AVR 73/8, 11	10	4.7	15	1 500	25	8 h	10	1.0
AVR 92/29.13	10	9.2	15	1 500	25	3 h	10	1.0
AVR 92/29.11	10	9.2	28	1 620	1	1613 °C	10	1.0
AVR 89/12	16 400	9.4	13	1 300	410	258 h	4	2.4×10^{-4}
AVR 92/22	16 400	8.8	14	1 400	140	1 h	20	1.2×10^{-3}
AVR 89/14	16 400	9.0	14	1 400	70	2 h	12	7.3×10^{-4}

In air ingress simulation tests conducted at 1 100 °C, complete oxidation of the graphite matrix in spherical elements takes 70 to 100 hours. However, the TRISO-coated UO_2 fuel particle remained intact over this period. During subsequent testing at elevated temperatures, the first SiC layers of particles were damaged at 1 300 °C, although only after more than 10 days of air ingress exposure. As the temperature increases during air ingress the time to SiC failure and fission-product release decreases. The first particle failures were observed after 1 or 2 hours at 1 400 °C and these may have been as-manufactured defective particles. In the 10 TRISO particle samples the first particle failure was observed after ~ 400 hours of exposure to air ingress at 1 400 °C. After 3 to 8 hours of exposure to air ingress at 1 500 °C the first particle failures were observed. In exposure to air ingress conditions at ~ 1 600 °C the first particle failures occurred at the end of the heat-up phase of the test when 1 600 °C was reached.

4.4. Fuel performance limits

With modern HTGR fuels, the German LEU UO_2 TRISO fuel performance is characterised by:

- near complete retention of fission products in intact particles during normal operating conditions at temperatures < 1 250 °C and in accident conditions at temperatures ≤ 1 600 °C;
- very low levels of contamination present in the outer coating layer of the TRISO particle and in the graphitic matrix of the fuel element.

In this manner, the source term is dominated by defects during manufacture and by failures during irradiation and in accidents. Many tests conducted between 1981 and 2010 demonstrated excellent behaviour and the final performance assessment is limited only by sampling statistics. Therefore, in a

conservative way, the performance data collected during manufacture, irradiation testing and accident testing of reference 60 mm-diameter spherical fuel elements are presented in Table 10.

Table 10: Final statistical evaluation of the performance data collected during manufacture, irradiation testing and accident testing of reference

HTGR fuel spheres and fuel bodies with UO_2 TRISO particles		No of fuel bodies (60 mm-diameter spheres)	No of coated particles N	No of defective/failed coated particles n	Expected failure fraction = n/N	One-sided upper 95 % confidence limit
Manufacture	pre-1985	125	1 673 800	80		
	post-1985	50	528 400	6		
	total	175	2 202 200	86	3.9×10^{-5}	4.7×10^{-5}
Irradiation testing	MTRs	19	276 680	0		
	AVR	24	393 600	0		
	total	43	670 280	0	0	4.5×10^{-6}
Accident testing	1 600 °C iso. FZJ	8	131 200	0		
	1620 °C acc. FZJ	5	82 000	5		
	1 600 °C iso. ITU	6	74 280	0		
	total	19	287 480	5	1.7×10^{-5}	3.7×10^{-5}

iso. = isothermal constant temperature heating test.
acc. = temperature transient heating tests following predicted accident scenario.

The manufacturing data in Table 10 represent two production-scale operation periods where reference 60 mm-diameter spherical elements with LEU UO_2 TRISO fuel were produced by NUKEM in Germany:

- pre-1985: 55 200 elements manufactured with 125 elements destructively examined;
- post-1985: 14 200 elements manufactured with 50 elements destructively examined.

The irradiation tests in Table 10 include:

- HFR-K3, -K5, -K6, FRJ2-K13, -K15, with a total of 19 reference 60 mm-diameter spherical fuel elements with no detectable particle failures at EOL — special tests with other geometries have been used for research studies, but are not included in this statistical evaluation;
- evaluation of the EOL irradiation performance for 24 GLE-3 spheres from the AVR, which has shown zero in-reactor failures (Figure 13 and Figure 14).

The accident simulation heating tests in Table 10 comprise the following:

- eight isothermal 1 600 °C tests with LEU UO_2 TRISO fuel elements conducted at the Forschungszentrum Jülich with the spheres AVR 71/22, 82/9, 82/20, 88/15, 88/33, HFR-K3/1, FRJ2-K13/2 and 4, as reported previously by Schenk (Schenk, et al., 1988) (Nabielek, et al., 2008);

- five accident tests simulating HTR Module core heat-up to 1 620 °C with AVR GLE-3 fuel elements AVR 85/18, 89/13, 90/2 (two failures), 90/5 and 90/20 (three failures) (Schenk, et al., 1991);
- six isothermal 1 600 °C tests with LEU UO_2 TRISO fuel elements conducted at the Institute of Transuranium, Karlsruhe with the spheres AVR 74/18, HFR-K6/2,3 and HFR-EU1bis/1,3,4 (Freis 2010), all without any particle failure.

Collectively, the statistical evaluation for manufacture, irradiation and accident simulation testing is shown in Figure 23. These results, based on the results obtained during manufacture, irradiation in MTRs and in AVR and in accident simulation testing, demonstrate the essential components for a passively safe system insofar as the additional source term due to operation does not exceed the already low level of defects from manufacture. Furthermore, the maximum temperature (1 600 °C) that can be reached in an accident does not lead to a significant additional source term.

4.5. Summary

Inherent safety features of modern small modular HTGRs are, in part, provided by the high level of fuel quality of UO_2 TRISO-coated fuel particles. The work conducted with the German fuel development programme over two decades from 1980 to 1995 constitutes a convincing demonstration of fuel excellence in manufacture, and continuing through irradiation and accident simulation testing. The low levels of particle defects produced during manufacture were significantly altered neither by extensive accelerated and real-time irradiation testing, nor through accident simulation testing in dry and wet environments.

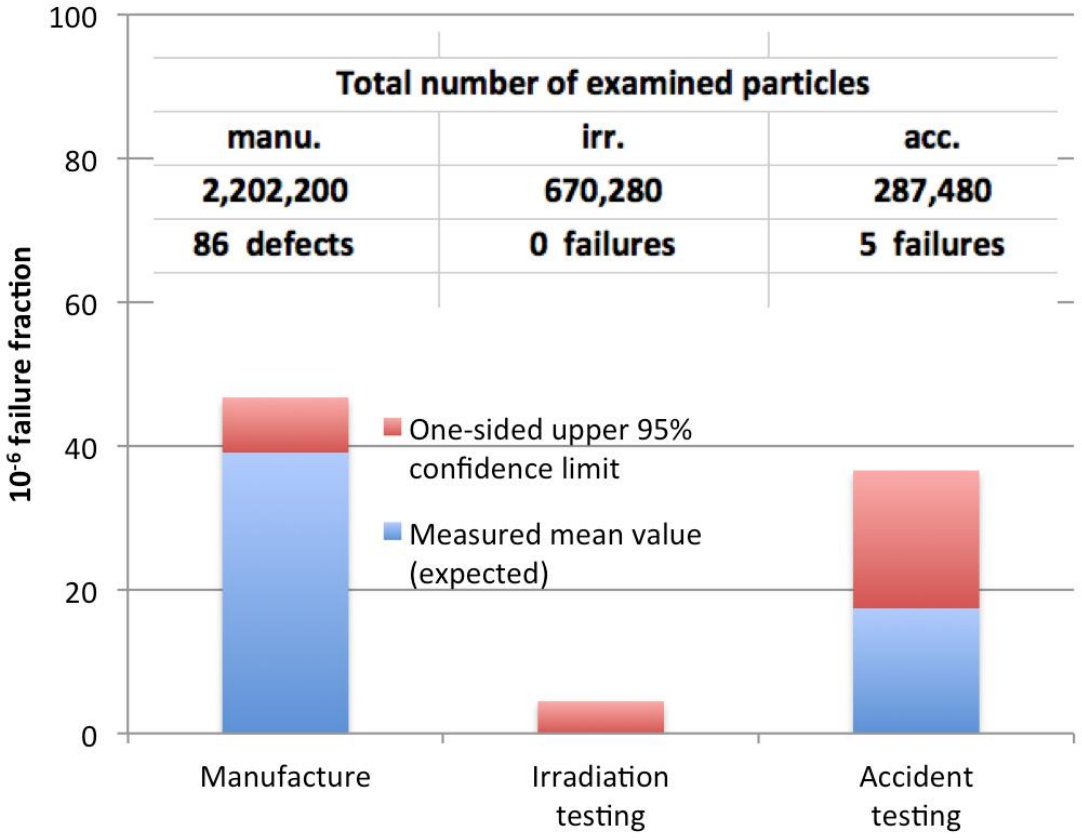

Figure 23: Statistical evaluation of defective and failed LEU UO_2 TRISO particle fractions in reference 60 mm-diameter spherical fuel elements

5. Components

The technology of the HTR Module and its components is based on the experiences of AVR, THTR and the general development of HTR in different countries around the world. The technical details of the concept are explained in the following sections.

5.1. Primary system

The primary system (Figure 24) of each module consists of the following components:

- the reactor pressure vessel together with the inner metallic and graphite structures, the shutdown systems, the fuel-handling system and measurement installations;
- the steam generator vessel, which contains the steam generator bundle and the helium circulator, including the drive;
- the connecting vessel, which contains the hot gas duct;
- the inner concrete cell, which contains the surface cooler.

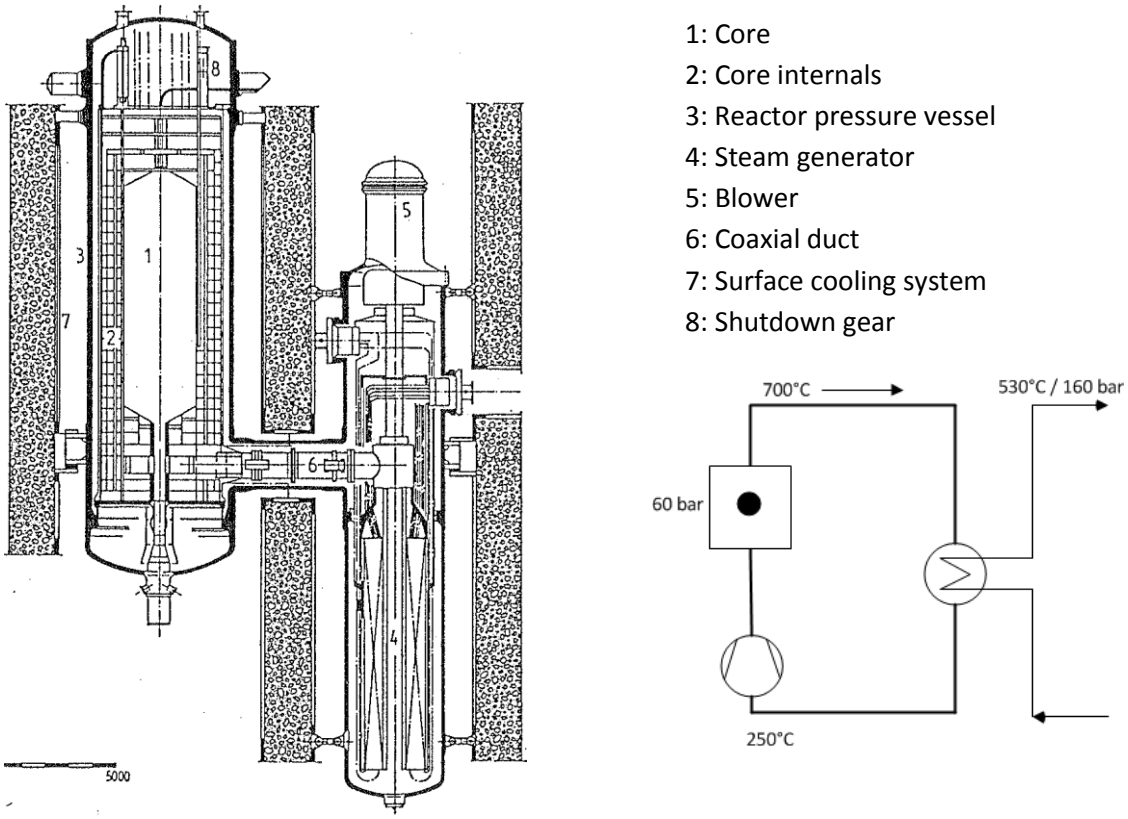

Figure 24: Primary system of an HTR Module (200 MWth)

One very important topic regarding water ingress accidents is the side-by-side arrangement of the reactor and the steam generator, which is positioned geodetically below the core. The two vessels are connected by a third vessel, which contains a hot gas duct.

Furthermore, after total failure of active decay heat removal no natural circulation from the hot core to the steam generator can occur. This component is therefore protected against excessive temperatures. It is practically insulated during this condition of accident. The evaporation in the steam generator is upwards directed and therefore the stability of the process is very good.

Access to the tubes of the steam generator is also possible without opening the primary circuit. Clogging up defect tubes from the outside is possible.

Due to the chosen arrangement of the helium circulator on top of the steam generator vessel, maintenance work on this component is relatively easy and possible without opening of the primary circuit.

The arrangement of the reactor pressure vessel in a concrete cell allows the surface cooler to be put in place surrounding this component. This surface cooler is operated with water and is carried out redundantly.

Decay heat removal via the surface cooler after a ‘total loss of active core cooling’ accident is an effective measure to limit the normal fuel temperature during the accident (1 600 °C in case of the HTR Module). The concrete, furthermore, can store the decay heat if even the surface cooler fails.

The concrete wall between the reactor pressure vessel and the steam generator acts as effective shielding for the steam generator and limits the activation of this component.

The outer reactor building for a plant with two modules, which is designed to withstand the usual loads (earthquake, gas-cloud explosion, aeroplane crash), has a ratio of height to width which is favourable for stability against earthquakes.

After accidents involving small leaks in the primary enclosure the helium is given off via the inner concrete cell and a high-efficiency filter. If larger leaks occur (diameter of 65 mm) the release happens via the containment building, with a relatively lower filter efficiency. If larger leaks will be assumed in the future, improved solutions for the retention of radioactivity can be applied.

Some important data on the primary system are given in Table 11. Data on the main primary components are explained in later specific sections.

Table 11: Some data on the primary system of the HTR Module (1 unit)

Parameter	Dimension	Value	Remark
Thermal power	MW	200	For electricity and process-steam production
Average helium outlet temperature	Celsius	700	Hot streaks
Helium inlet temperature	Celsius	250	
Flow direction in the core		Downwards	
Flow of fuel elements		Downwards	MEDUL
Loading		Continuously	
Number of loops		1	
Steam temperature	Celsius	530	
Steam pressure	bar	180	
Mass flow of steam	kg/s	77	
Arrangement of steam generator		Side by side	
Connection of reactor and steam generator		Coaxial duct	
Concept of primary enclosure		Basic safe	
Earthquake load	G	~ 0.3	
Lifetime of components	Full-power years	40	

5.2. Core structures

The internal core in high-temperature reactors consists of ceramic and metallic components.

The graphite reflector consists of top, side and bottom reflectors. These graphite build-in components serve as containers for fuel elements. The metallic core barrel is installed to support the ceramic structures. This core barrel again consists of a cylindrical part and top and bottom structures. The metallic core barrel is supported in a position above the core connection located in a position at the height of the ceramic core bottom.

Special conditions exist for these graphite components, resulting from the high temperatures of the cooling gas, in case of the THTR of 780 °C, through mechanical forces resulting from the weight and movement of the pebbles and from high radiation doses with fast neutrons. The most important data on the core structures for the THTR are summarised in Table 12. Details are shown in Figure 25 and Figure 26.

Table 12: Data on the ceramic core structures of the THTR

Parameter	Value
Diameter of the core	5.6 m
Height of the core	5.1 m
Filling factor	0.61
Thickness of the radial reflector	1 m
Thickness of the graphite bricks (radial)	0.5 m
Thickness of the top reflector	2 m
Thickness of the bottom reflector	~ 2 m
Weight of the graphite	~ 540 t
Weight of the graphite bricks	~ 35 t

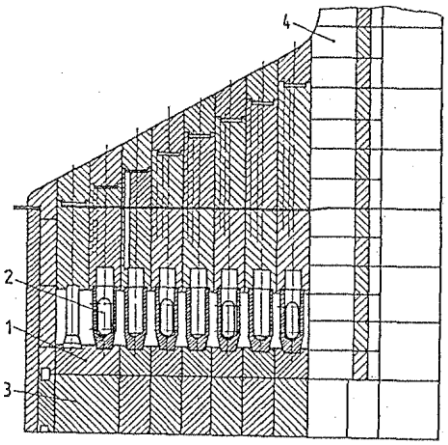

1: Bottom reflector bricks
2: Column of the hot gas chamber
3: Insulation of the bottom
4: Side reflector

Figure 25: Bottom reflector of the THTR

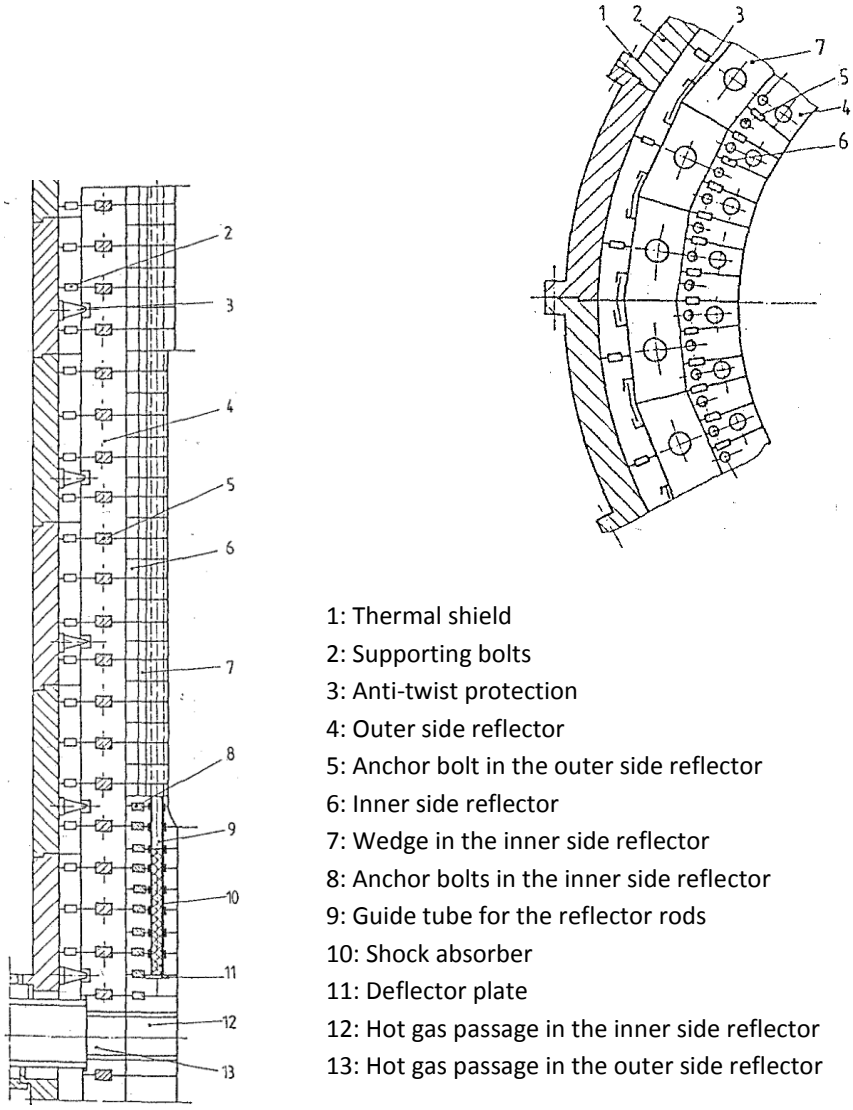

Figure 26: Side reflector of the THTR (left: vertical cross section; right: horizontal cross section)

The top reflector consists of graphite bricks which are connected to the top liner. The cooling gas enters the pebble bed with a temperature of about 250 °C through borings in the top reflector, absorbing the heat in the reflector produced by gamma radiation.

The cylindrical side reflector is also built from graphite bricks, which are connected to each other by anchor bolts and also connected to the surrounding thermal shield. In these bricks there are borings for the absorber rods.

The hot helium gas at approximately 750 °C leaves the core through borings in the bottom reflector. The reflector itself has a conical form with a gradient of 30° to support the draining of the pebbles out of the core. Figure 27 shows the bottom reflector of the HTR-10 pebble-bed reactor.

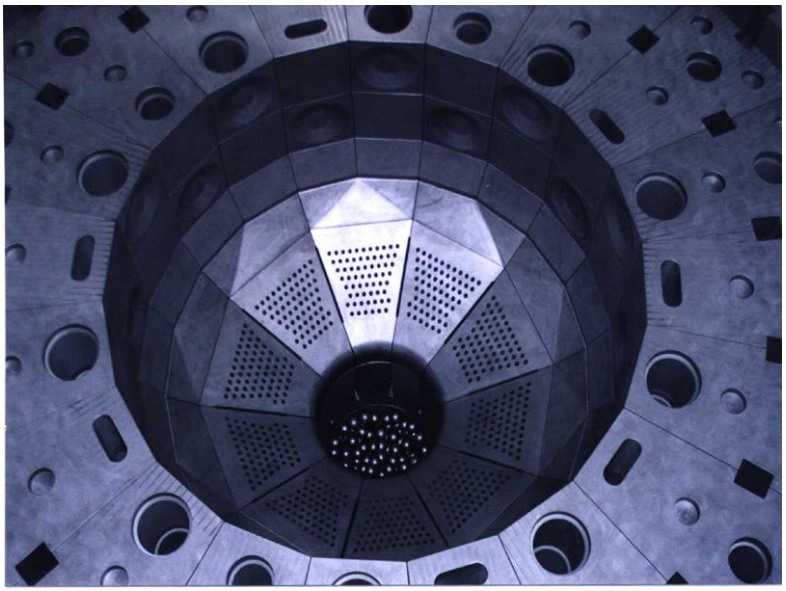

Figure 27: Bottom reflector of the Chinese HTR-10

Concerning the HTR Module, the drives for the control rods and for the second shutdown system (the KLAK system (Kleine Absorber Kugel Systeme)) are mounted at the surface of the thermal top shield. The upper part of the core structure follows the principle, which was realised in the AVR, in which 24 segments are added, consisting of carbon stones because of thermal insulation and shielding.

There are penetrations for seven loading tubes for fuel elements, and for six shutdown rods (first system) and 18 KLAK positions (second system). The side reflector consists of 24 graphite blocks in each layer and carbon stone blocks which are arranged between the graphite and the core barrel.

The connection of the ceramic blocks to the core barrel is based on technologies which are well established in the field of HTR technology (Figure 28).

In the lower part of the reactor there is a new component: the core connection for the hot gas duct (Figure 29). This component is insulated at the position of the penetration through the reactor pressure vessel.

Pipes for fuel loading and further pipes, of the second shutdown system, for the transport of the KLAK elements (B4C balls with a diameter of 1 cm) from the core bottom back to the storage vessels above the top thermal shield are positioned in the space between the ceramic structure and the core barrel.

The bottom of the core is built of ceramic segmented blocks, which contain borings for the hot gas. The bottom has a declination of 30° to allow the safe removal of fuel elements from the core. The fuel elements are removed from the core through the central discharge tube (800 mm in diameter) using a discharge system.

The different layers of the ceramic core structures are designed and optimised to protect the reactor vessel against excessive neutron doses and embrittlement. Therefore, the fast neutron dose over the whole lifetime of the reactor pressure vessel is below 10^{18} n/cm^2.

Table 13 contains some data on the core structures of the HTR Module and, for comparison, the corresponding information for the AVR and THTR. The core structures of both reactors have been licensed, constructed and operated successfully.

The core structure of the AVR has been inspected after more than 15 years of operation in the upper hot part. No changes in graphite structures have been observed. After the unloading of the whole core some damage to the bottom structure has been detected. This indicates that an improved design solution for this part of the graphite should be chosen.

The application of robotic technologies will enable many inspection, maintenance and repair procedures in the future.

Furthermore, a broad experience of graphite structures is available from AGR plants. Design choices for bolting and removal can be taken from this field.

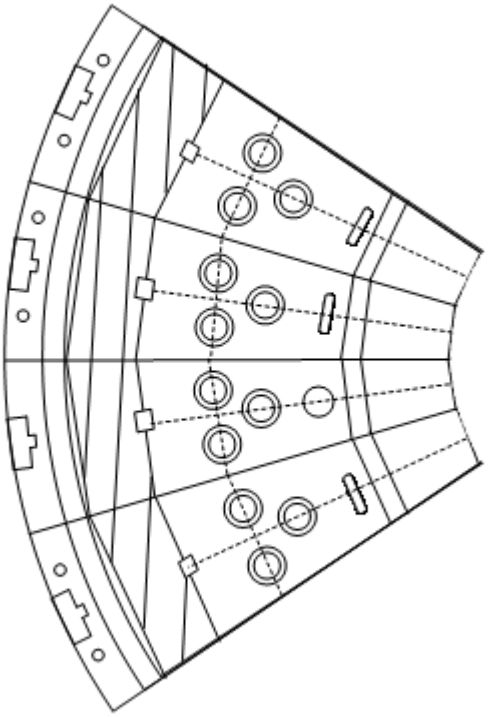

Figure 28: Some details of core structures: connection between ceramic structures and core barrel

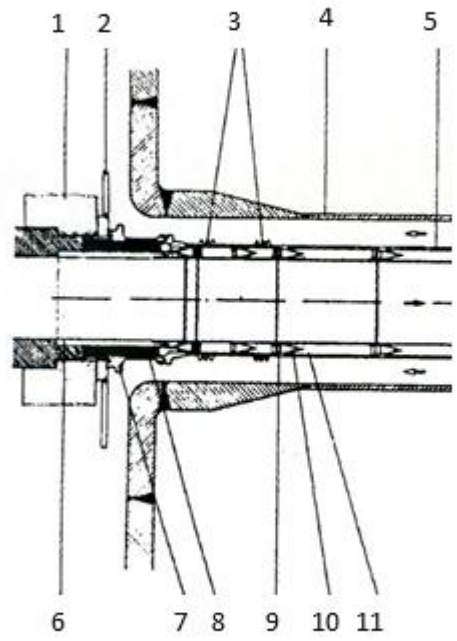

1: Graphite structure
2: Core barrel
3: Compensator
4: Connecting vessel
5: Bearing tube
6: Graphite tube
7: Intermediate flange
8: Fibre insulation
9, 10, 11: Insulation material

Figure 29: Concept of connection of the hot gas duct to the core internals in HTR

Table 13: Data on the core structure of the HTR Module (AVR and THTR data for comparison)

Parameter	Dimension	HTR Module	AVR	THTR
Core diameter	m	3	3	5.2
Core height	m	9.43	3	5.2
Thickness of the side reflector	m	~ 1	~ 1	~ 1
Number of discharge tubes		1	1	1
Fast neutron dose in 20 years	n/cm^2	$< 10^{22}$	$< 10^{22}$	$< 10^{22}$
Max. temperature during operation	Celsius	800	110	850

The ducting of the primary helium in the reactor structures is as follows (Figure 30): the cold gas, leaving the outer annulus of the coaxial duct, enters the reactor pressure vessel, cools the metallic structures at the bottom of the vessel and enters 72 borings in the side reflector.

After arriving at a position above the whole ceramic structure the cold gas is led to an upper cold gas chamber between the top reflector and the top part of the thermal shield. The top reflector contains borings through which the cold gas flows into the upper space above the core. After passing the pebble bed and heating up to the hot gas temperature the gas flows through borings in the bottom

reflector into the hot gas chamber and from there into the hot gas channel. The core bottom structure is designed to mix the gas and to avoid hot streaks.

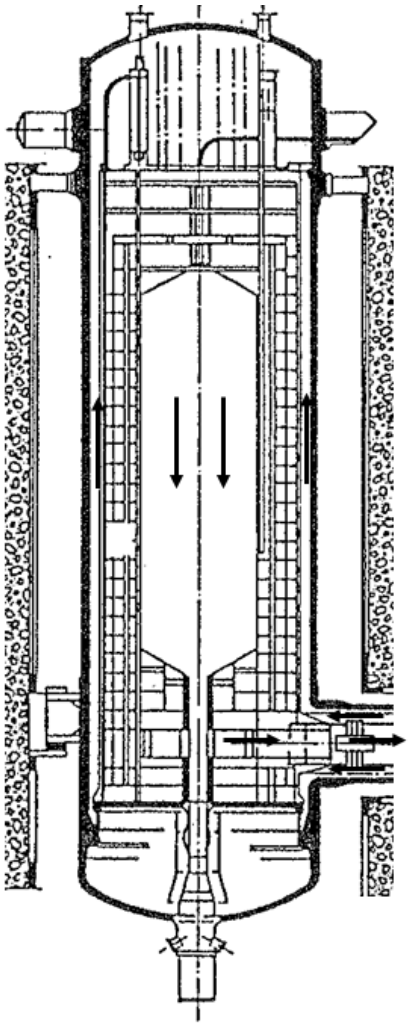

Figure 30: Ducting of the helium in the reactor internals

5.3. Shutdown systems

The shutdown of the HTR Module is carried out by two diverse systems. The first system has to be able to shut down the reactor in the hot stage and in case of accidents, for example due to water ingress. It consists of six rods arranged in the side reflector. The second system must be able to hold the reactor in the cold under-critical state, including the long-term decay of xenon and other relevant isotopes. The system consists of 18 columns of KLAK (small absorber balls) in the side reflector. If the system has to be used the small absorber pebbles (10 mm diameter, graphite with 10 % B_4C) fall under gravity into the borings in the side reflector.

The neutron losses of the core are in the order of 13 %, therefore the arrangement of both systems in the side reflector are possible, with values of around 1.4 % for the first system and of around 10 % for the second system.

Figure 31 shows the arrangement of the borings in the side reflector and summarises the values of demand of reactivity and the worth of the systems.

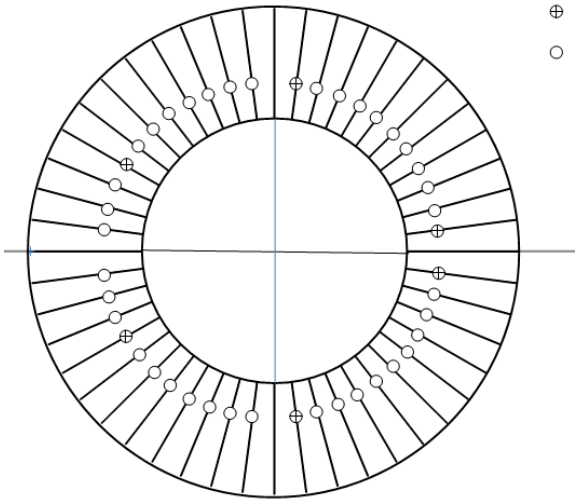

Position of the shutdown elements:

⊕ reflector rod (first system)

○ small absorber (second system).

Demand and worth of the systems:

first system: 1.4 %

second system: 10 %.

Figure 31: Positions of the borings in the side reflector (six reflector rods, 18 KLAK positions)

The first system uses technologies which are well known from THTR and AGR plants. The rods consist of connected single parts which contain Boron carbide as an absorber.

The drives of the reflector rods are mounted above the upper thermal shield plate. Because the room above the plate is separated from the primary helium, this room is accessible for inspection and repair. The rods fall freely into the borings if the electrical energy supply is lost or if they are initiated by the reactor protection system. In this case the electrical supply is also stopped.

The second shutdown system (KLAK) (Figure 32) represents a new concept which still requires qualification. The small balls are contained in storage vessels arranged above the top thermal shield. If necessary they fall into the borings in the side reflector. At the bottom there are closures for each position which can be opened to be able to remove the balls pneumatically back to the storage vessel. The components for transporting the balls are arranged outside the reactor pressure vessel under this component. The transport pipes are inside the reactor pressure vessel between the core barrel and the ceramic structure.

The KLAK system also uses the fail-safe principle: in case of loss of electrical power the storage containers are opened and the balls fall into the borings.

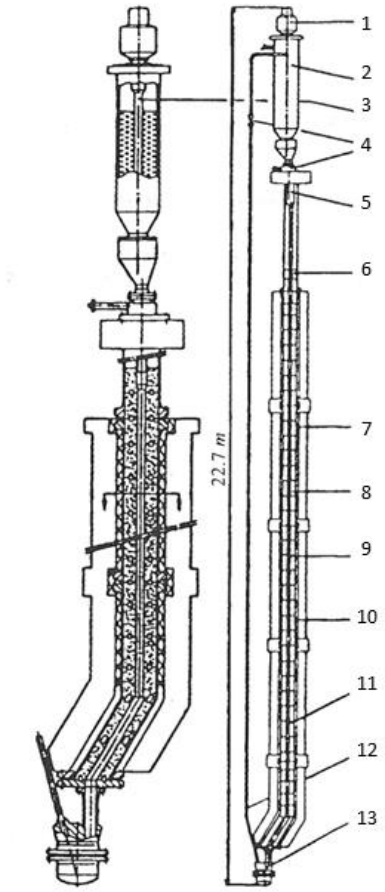

1: Gear
2: Storage tank
3: Detector for filling level
4: Inspection device
5: Shielding
6: Connection brig
7: Side reflector
8: Channel inside the reflector
9: Graphite
10: Guide tube (360 mm in diameter)
11: Connection brig
12: Ball transport pipe
13: Lower collection tank

Figure 32: Principle of the second shutdown system (KLAK) of the HTR Module

5.4. The fuel-handling system

The fuel elements of a pebble-bed reactor are loaded and discharged continuously during normal and full-power operation (Figure 33). They are inserted at the top of the reactor by a special device containing a valve and distribution system. After passing the core the fuel elements are discharged through a sufficiently large discharge tube and a rotating disk with a hole with a diameter of 65 mm. After that they pass a singuliser and a scrap separator, and they are either put into a scrap can or are reused in case of the MEDUL cycle.

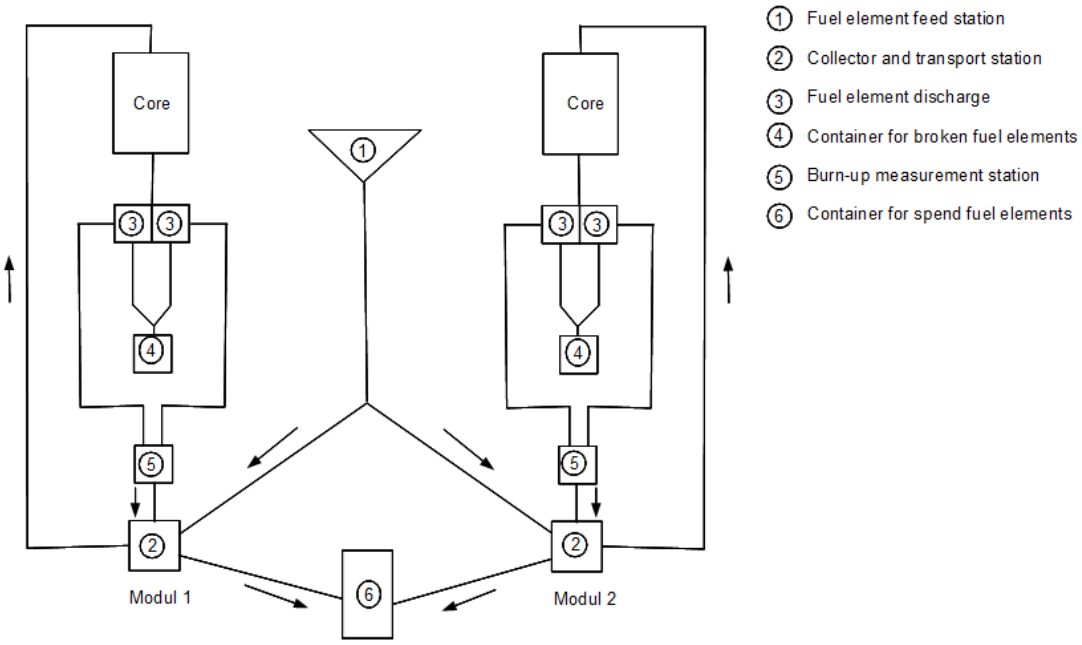

Figure 33: Concept of fuel handling in pebble-bed HTR (MEDUL cycle for a two-module plant)

The intact fuel elements then pass a burnup measurement installation and are either recycled into the core (pneumatically) or they are moved into a vessel for spent fuel elements, from which they are transported into an intermediate storage facility.

All transport processes occur pneumatically and the fuel-handling system allows for very flexible operation of the plant, as demonstrated in the case of the AVR.

Furthermore, there is the possibility, in case of extraordinary repair procedures or other events, to discharge the core totally and to store the fuel elements for a limited time. After that the fuel elements could be transported back to the core again to continue operation. After the water ingress accident in the AVR this possibility has been demonstrated.

In total the core of one module consists of 360 000 fuel elements. If, for example, the MEDUL cycle contains 15 runs through the core, around 120 000 fresh fuel elements have to be added per year and 120 000 spent fuel elements have to be discharged and removed. Around 5.4 million fuel

elements have to be handled per year. Following the experience of the AVR, around 300 damaged fuel elements have to be removed to the scrap canisters.

5.5. Primary enclosure

The primary enclosure of the HTR Module contains three vessels:

- reactor pressure vessel,
- steam generator vessel,
- connecting vessel.

Figure 34 shows the arrangement of the vessels and indicates the special side-by-side positioning of the steam-generator vessel.

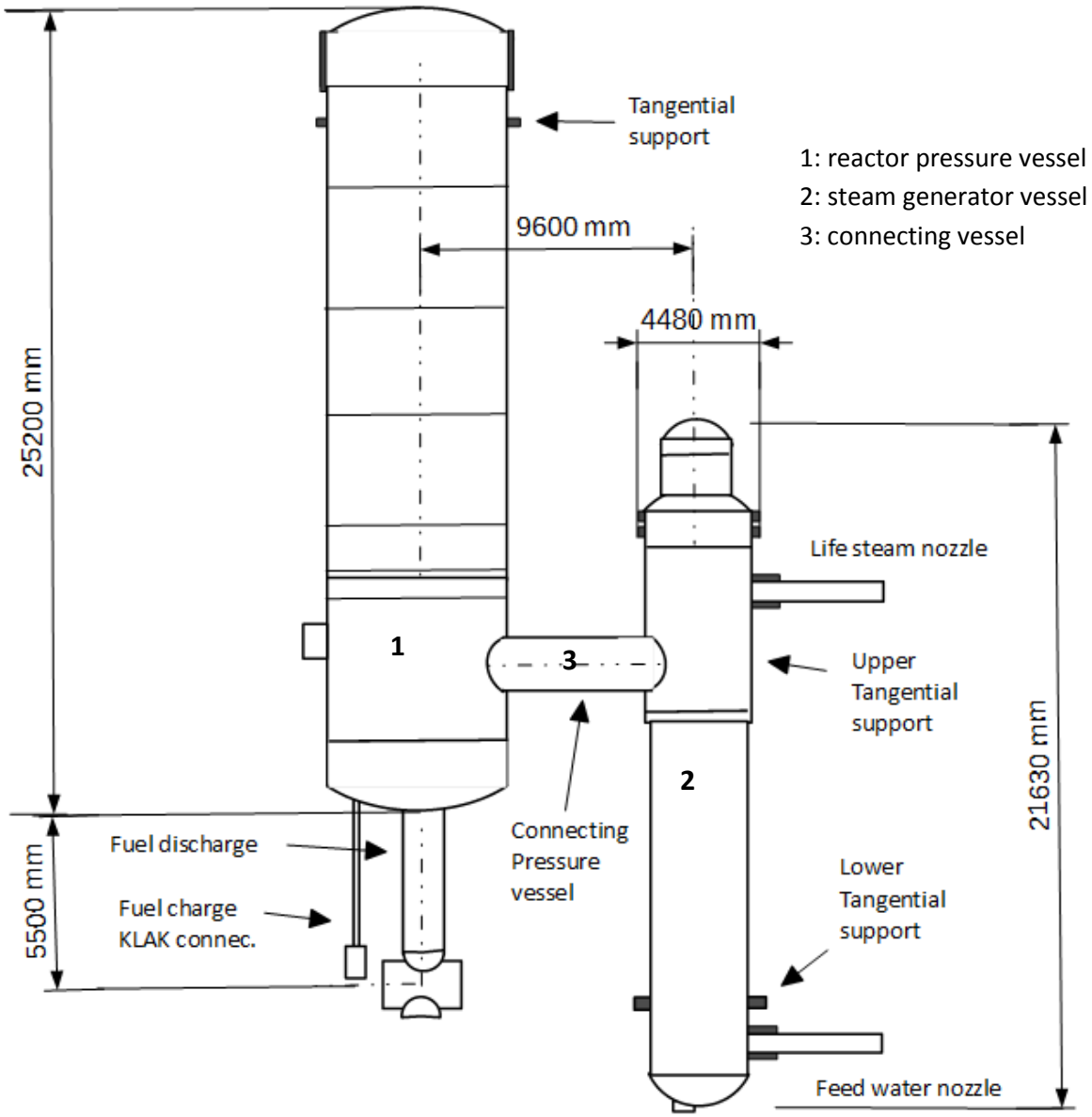

Figure 34: Arrangement of the primary enclosure

Basic data on the three components are contained in Table 14.

Table 14: Data on the vessels of the primary enclosure

Parameter	Dimension	Reactor pressure vessel	Steam generator vessel	Connection vessel
Design pressure	bar	70	70	70
Design temperature	Celsius	350	350	350
Fast neutron dose	n/cm^2	$< 10^{18}$	$< 10^{17}$	$< 10^{17}$

Material		20MnMoNi55	20MnMoNi55	20MnMoNi55
Height	m	25	20	
Inner diameter	m	6	4	1.2
Wall thickness	m	0.1	0.08	0.07
Length	m			6

For all components the material 20MnMoNi55, which is well known from light-water reactor (LWR) technology, was chosen. This material shows good welding properties, high toughness and low embrittlement under irradiation with fast neutrons. The material is applied as forged steel, and mainly rings are welded together. The principle design criterion is that the cold helium temperature is 250 °C and therefore all walls are cooled by the full mass flow of this cold helium.

An extensive programme of quality assurance from the production of the material until the operation of the component, summarised overall as the 'basic safety concept', is applied for the whole primary system. Therefore, it is assumed that the 'leak-before-break criterion' is valid and that the vessel system cannot suffer from bursting.

The reactor pressure vessel has a large nozzle in the centre of the bottom head for the discharge of the fuel elements. The diameter is around 1 m to house the discharge tube.

Another four small nozzles are in the bottom head for the supply of fuel elements (pebbles) and the conveyor gas supply for transportation of the small B4C pellets to the shutdown units.

The thermal cover for the purposes of inspection and maintenance of the reactor pressure vessel is connected to the inner reactor vessel with prestressed bolts, screwed together and sealed with two metallic sealing rings. The removal of the closure of the vessel is not necessary for changing of fuel or for maintenance work.

The reactor pressure vessel has three supports to place it on the structure of the reactor building. The supports are at the elevation of the connecting pressure vessel.

The connecting pressure vessel serves together with the hot (700 °C) helium gas duct as the primary connection between the reactor pressure vessel and the steam generator pressure vessel. The hot gas duct contains insulations and a liner, and is supported by special bearing systems in the connecting vessel.

By counterflow of the cold helium (250 °C) in the outer annulus of the duct, the walls of the connecting vessel are protected in any case against interaction with hot helium. The pressure difference across the inner gas duct wall is in the order of 1 bar.

The penetration through the cylindrical wall of the reactor pressure vessel forms a specific aspect of both components. Designs to reduce stresses have been chosen for this connection.

5.6. Surface cooler

The surface cooler surrounds the reactor pressure vessel at a short distance from the wall (around 1.5 m) and is set tightly against the concrete wall of the inner reactor cell.

The cooling system designed as a plate heat exchanger consists of a lot of tubes which are arranged vertically. The cold water enters at the bottom with a temperature of 35 °C and flows to the top and is sampled there. The system removes around 400 KW during normal operation as heat loss, and in case of a 'total loss of active core cooling' accident removes around 800 KW. In this case the steam generator/helium loop would be out of operation. The cooling system is redundant and normally sends the heat to a cooling tower. In extreme situations the system can be connected to a fire protection installation. Figure 35 shows the arrangement (left) and the flow sheet of the concept (right), while Table 15 contains some data on the cooling system, whereby a value of the mass flow is not specified.

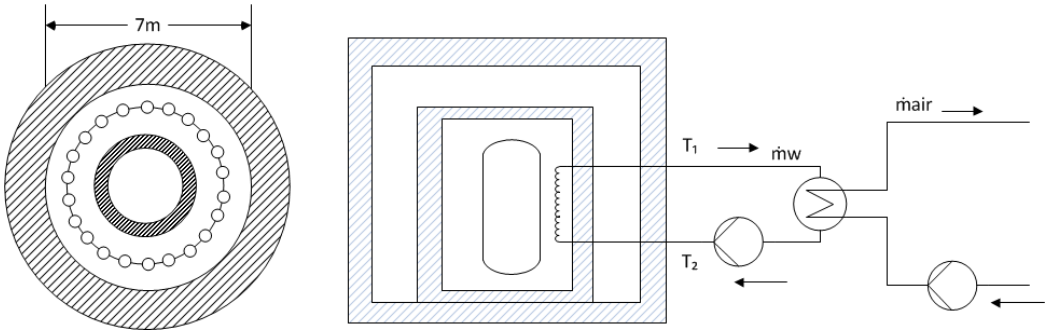

Figure 35: Concept of the surface cooler of the HTR Module

Table 15: Data on the surface cooling system

Parameter	Dimension	Value
Surface	m^2	300
Cooling inlet temperature	Celsius	40
Mass flow	kg/s	
Max. cooling temperature outlet	Celsius	50
Power (normal operation)	KW	400
Power (accident)	KW	800
Grace time	h	20

5.7. Hot gas duct

The hot gas is transported from the hot gas chamber situated in the reactor pressure vessel to the steam generator via a central channel arranged inside the connecting vessel between the two abovementioned components (Figure 34).

The hot gas duct (Figure 36) consists of the bearing tube, insulation and an inner liner, which ducts the hot gas. The duct is supported inside the connecting vessel with the help of special supporting systems.

Changes of length caused by temperature changes are governed by compensators. The hot gas duct is connected to the graphitic core structure by a special core connection, which allows only small leak

rates for the helium. This new component has been tested under extreme conditions of temperature change and for an extreme number of cycles. The connecting vessel has the same quality of material and design as the reactor pressure vessel, including following the concept of 'basic safety' and therefore of the 'leak-before-break' criterion. This includes that bursting of the component is not assumed in the licensing process.

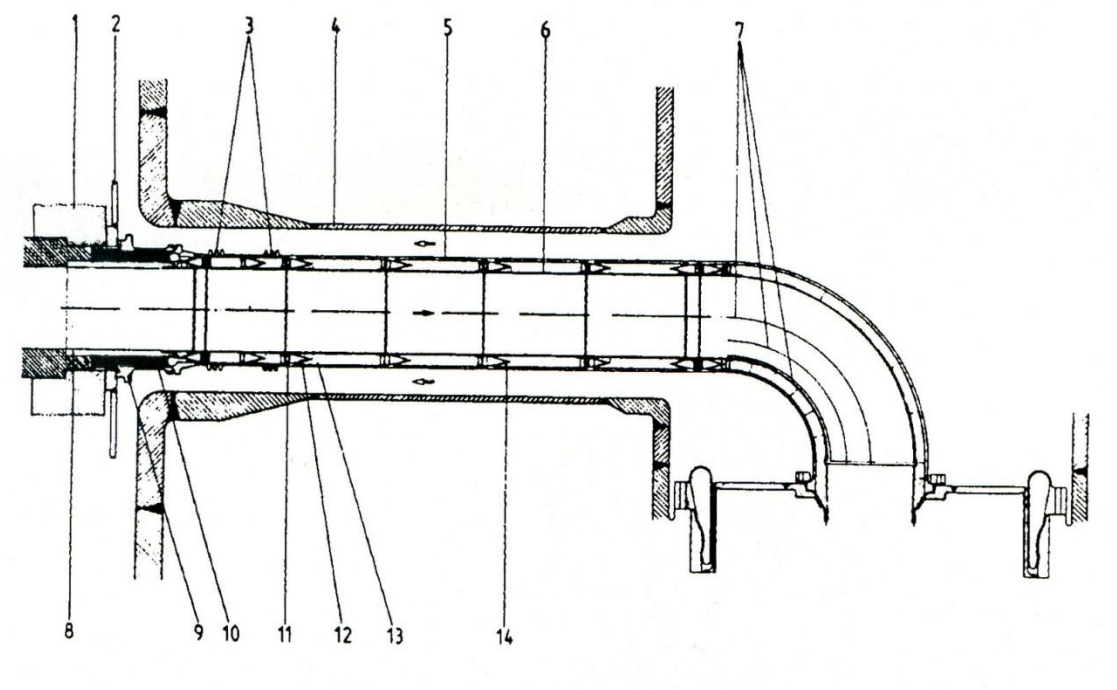

Figure 36: Hot gas duct

Insofar as mechanical loads are concerned the pressure differences between the hot and cold primary helium in the system are small (in the order of 1 bar during normal operation). Only in case of depressurisation accidents could larger pressure differences occur for a very short time.

Vibrations caused by excessive velocities must be prevented by suitable component design. Furthermore, loads from the action of earthquakes must be tolerated by the concept.

Some data on the hot gas duct are contained in Table 16. For comparison, some data are added on the EVO (EnergieVersorgung Oberhausen AG) plant, in which the hot gas ducting system operated very well over many thousands of hours.

Table 16: Data on the hot gas duct of the HTR Module (some data on the EVO plant are added for comparison)

Parameter	Dimension	HTR Module	EVO plant
Power	MW	200	150
Max. helium temperature	Celsius	750	750
Average hot gas temperature	Celsius	700	750
Cold gas temperature	Celsius	250	200
Helium pressure	bar	60	28
Helium mass flow	kg/s	85.5	86
Diameter of the hot gas channel	m	0.75	0.9

Helium velocity (hot gas)	m/s	65	40
Liner		Incoloy 800H	
Insulation		Fibre	Fibre
Length of the duct	m	~ 8	~ 20

Several bendings were included in this design and showed excellent behaviour during operation.

From the experiences of HTR plants and AGR plants which have been in operation until now, and additionally from the results of different large test facilities, it can be stated that the hot gas duct of the HTR Module can be designed for the whole life of the plant.

5.8. Steam generator

The steam generator of the HTR Module is connected to the reactor by a coaxial duct and is arranged geodetically below the core, side by side.

The component uses the principle of Benson-type steam generators and contains a helical-type tube bundle. There are 220 tubes arranged around the central tube (Figure 37). Each tube is coupled to the feed water and the life-steam samplers. Table 17 shows some data.

The hot helium enters the component at the top with an average temperature of 700 °C and is cooled during the flow downwards to 250 °C. The cold helium is deflected at the bottom of the pressure vessel and flows upwards between the wall of the pressure vessel and the casing of the bundle. This choice of gas flow cools the wall of the pressure vessel and limits the temperature to a value of 250 °C. In some positions on the casing insulation is provided to limit the heat exchange. The cold helium arriving at the top of the component is sampled and ducted to the circulator.

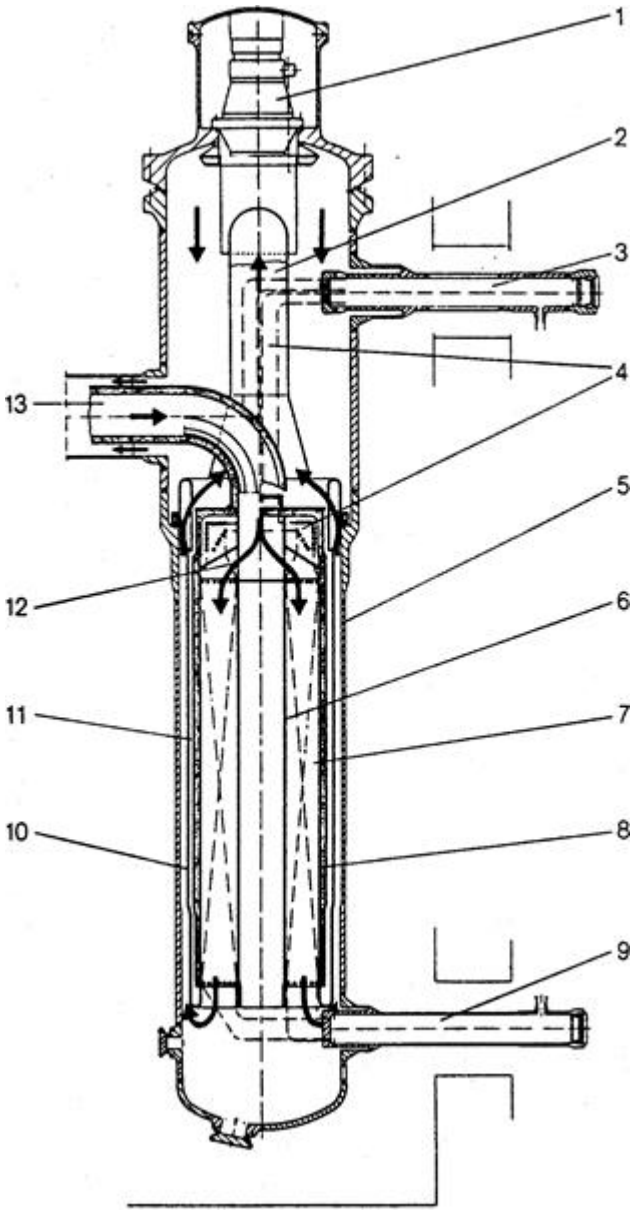

1: Helium circulator
2: Cold gas ducting
3: Sampler for life steam
4: Bundle for compensation
5: Pressure vessel
6: Central tube
7: Helical bundle heat exchanger
8: Gas shroud
9: Pier for feed water
10: Casing for steam generator
11: Gap (pressure)
12: Flow distribution
13: Hot gas duct

Figure 37: Steam generator of the HTR Module — overview of the component

Table 17: Steam generator data

Parameter	Dimension	Value
Power	MW	200
Helium temperature	°C	700 …> 250
Helium pressure	bar	60
Feed-water condition	°C/bar	170/220
Steam conditions	°C/bar	580/180
Helium mass flow	kg/s	85.5
Steam mass flow	kg/s	
Reheat		No
Average heat flux	KW/m^2	80
Heat exchanger surface	m^2	1 200
Number of tubes		200
Length of the tubes	m	~ 100
Dimension of the tubes	mm	22 × 2.5

Material of the tubes		Incoloy 800H
Average power density of the bundle	MW/m^3	5

After compression in the circulator (around 1.3 bar) the helium is pressed into the outer part of the hot gas duct and transported back to the reactor. The cold gas allows the effective cooling of the connecting vessel and of the bearing tube of the hot gas duct.

The heat exchanger bundle is designed with a relatively high heat-transfer number of around 1 200 W/m^{2}k and a high average heat flux of around 80 W/m^{2}k. This results in a total surface for heat exchange of 1 200 m^2 and an average power density of the heat exchanger bundle of around 5 W/m^3.

The feed water enters the component via the sampler with a temperature of 170 °C and a pressure of 220 bar. Inside the component the feed water is preheated, evaporated and superheated to 530 °C/180 bar. The hot life steam leaves the component via a compensation bundle and the sampler for life steam.

The life-steam pipes transport the steam from the reactor through the walls of the inner cell and the containment building to the turbine. The penetrations require special solutions to compensate for the elongation of the hot steam pipes. The concept of helical heat exchangers is fully developed and successful applied in THTR, Fort St. Vrain and in various Magnox and AGR plants.

Additionally, a steam generator depressurisation system is installed. In case of a severe water ingress accident this system allows removal of most of the water from the primary circuit in a short period of time. The steam/water mixture will be condensed in a mixed cooler and will later be released from the plant. Figure 38 shows the flow sheet for this system and indicates that there are two parallel lines provided for.

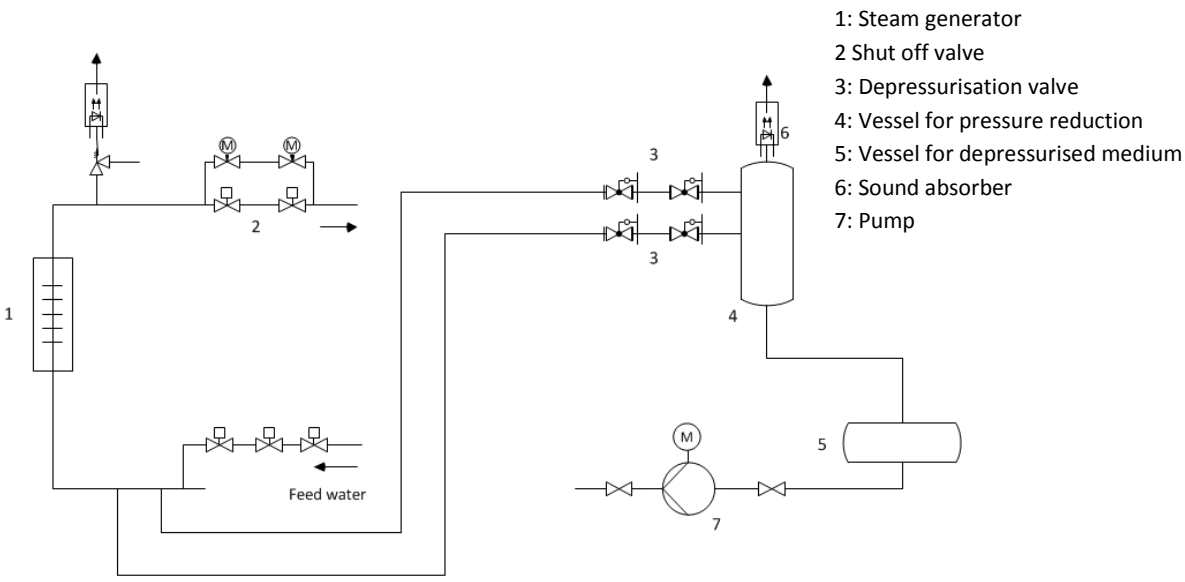

Figure 38: Depressurisation system for the steam generator

5.9. The intermediate heat exchanger

Any combination of a high-temperature gas-cooled reactor with chemical processes will most probably need a decoupling between the primary circuit and the heat utilisation system for the following reasons:

- separation on the nuclear part for safety reasons;
- limitation/exclusion of radioactive contamination of the product (e.g. tritium);
- exclusion of ingress of corrosive process media into the primary circuit;
- near-conventional design of the heat utilisation system;
- ease of maintenance and repair of the heat utilisation system;
- exclusion of contamination of high industrial investment around the nuclear plant.

The intermediate heat exchanger (IHX) is designed as a component to fulfil these requirements and provide a clear separation between the nuclear plant and the heat application. Under normal operating conditions the IHX prevents the primary coolant from accessing the process plant and prevents process gases from being routed through the reactor containment. This physical separation allows the heat application facility to be conventional designed and repair work to be conducted under non-nuclear conditions. The flow diagram of the combination of primary and secondary circuit together with the corresponding T-Q diagram is shown in Figure 39.

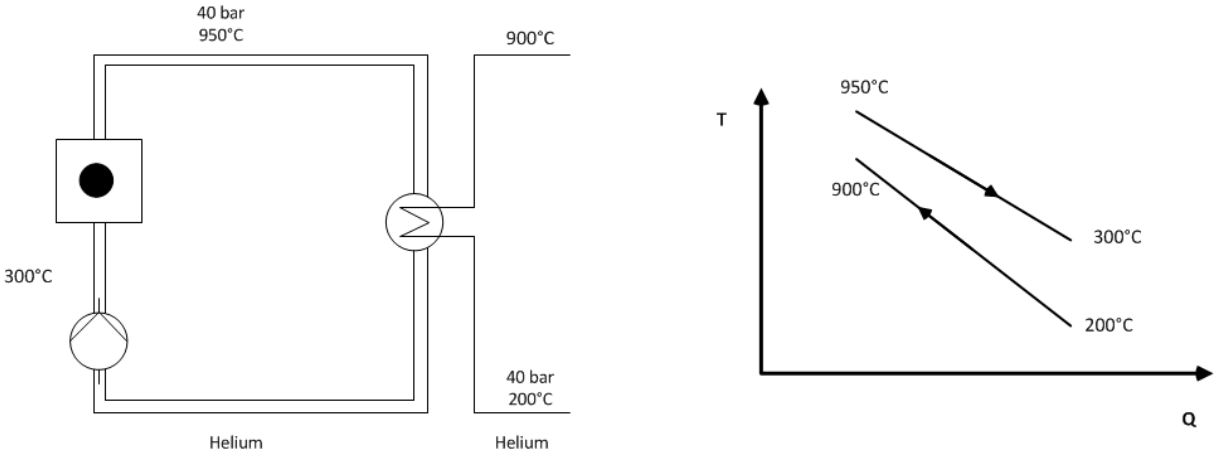

Figure 39: Primary circuit of a modular HTR with IHX (left: principal flow diagram; right: T-Q diagram for use of nuclear heat

The concept of a combination of the HTR Module with an IHX is shown in Figure 40 (Nuclear Energy for Hydrogen Production). The example provided represents the German reference design of a process-heat HTR Module in a side-by-side arrangement of nuclear reactor and IHX vessel for each modular unit. The thermal power of the nuclear reactor and of the IHX is 170 MW; the limitation of power is given by the requirement of self-acting decay heat removal in accidents with a total loss of active cooling. If larger thermal powers were needed an annular core would be required. The limitation in this case is caused by the dimensions and type of reactor pressure vessel. Details of the IHX with a helical tube bundle are shown in Figure 41. Characteristic design data are listed in Table 18.

Table 18: Comparison of IHX data tested in a KVK facility with data on IHX for nuclear application

IHX	KVK		170 MW_{th} HTR Module (IA 1983)		500 MW_{th} PNP (PNP 1981)	
	Helical	U tube	Helical	U tube	Helical	U tube
Material: Tube	Nicrofer 5520	Nicrofer 5520	Inonel 617	Inonel 617		
Size:						
Bundle outer diameter(m)	1.5	2.0	2.78	1.512	2.52	2.098 (hot) 2.815 (cold)
Tube outer diameter (mm)	22	20	22	20	22	20
Tube wall thickness (mm)	2	2	2	2	2.2	2
Tube length (m)			38.2	30.0	40.7	32.7
Number of tubes	117	180	1 612	2 470	1 444	1 900
Primary helium						
Inlet temperature (°C)	950	950	950	950	950	950
Outlet temperature (°C)	293	300	292	292	293	293
Inlet pressure (MPa)	3.99	3.99	3.99	4.05	4.0	3.99
Outlet pressure (MPa)	3.935	3.94	3.97	3.99		
Flow rate (kg/s)	2.95	3.0	50.3	50.3	36.9	36.9
Secondary helium						
Inlet temperature (°C)	220	220	200	200	220	220
Outlet temperature (°C)	900	900	900	900	900	900
Inlet pressure (MPa)	4.19	4.35	4.38	4.35	4.2	4.35
Outlet pressure (MPa)	4.025	4.25	4.19	4.19		
Flow rate (t/h)	2.85	2.9	47.3	47.3	35.6	35.6
Heat-transfer area (m^2)		3 500	4 254	4 700	4 000	3 900
Life time (h)			140 000	140 000	140 000	140 000

The employment of an IHX was also suggested within the PNP project with regard to the steam gasification of hard coal, for which the main characteristic data are also given in the table for comparison.

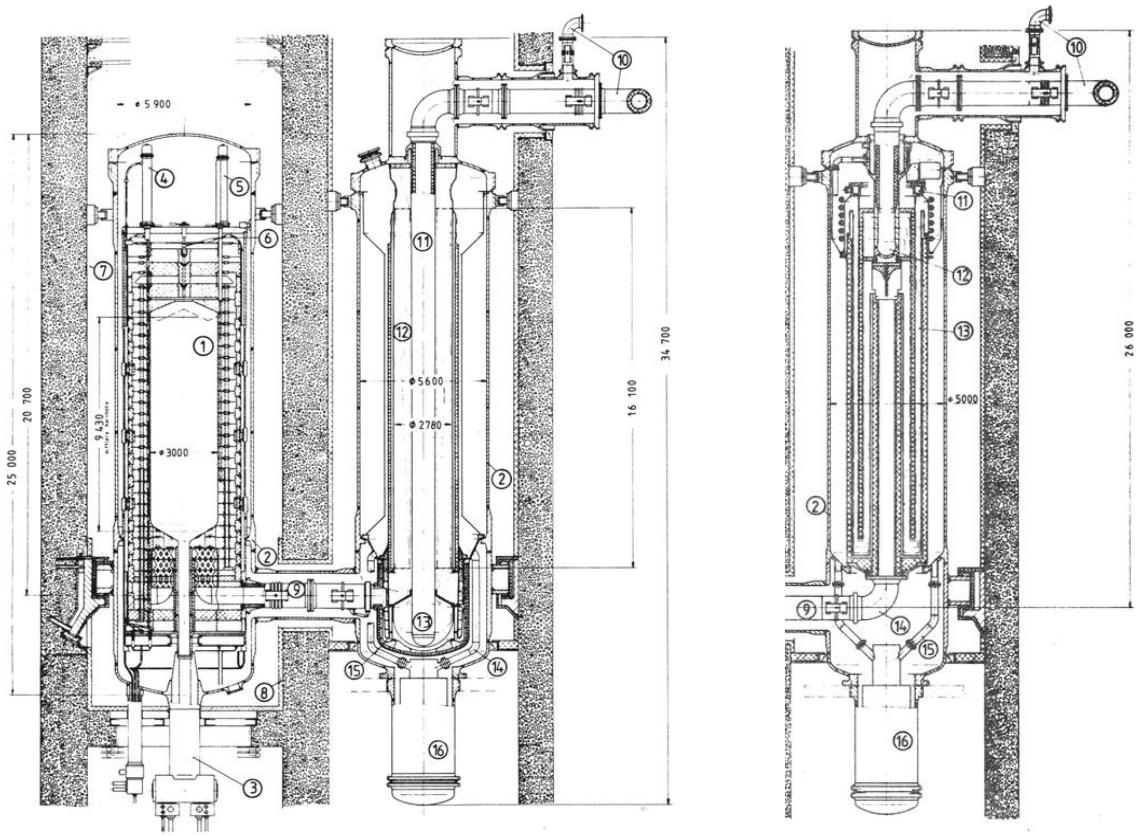

Reactor
1: Pebble bed
2: Reactor pressure vessel
3: Fuel discharge
4: KLAK spheres shutdown system
5: Reflector rods
6: Fuel loading
7: Surface cooler
8: Insulation
9: Hot gas duct

IHX
10: Secondary pipe connections
11: Central secondary hot gas return pipe
12: Tube bundle (helical or U tube)
13: Secondary hot gas header
14: Primary cold gas duct
15: Primary hot gas duct
16: Blower

Figure 40: Arrangement of HTR Module (a) with helix IHX (b) or U tube IHX (c) (Nuclear Energy for Hydrogen Production)

The helical IHX (see Figure 41) consists of a bundle of helical tubes arranged around a central return gas duct for the hot secondary helium. The support system for the tubes consists of support cylinders with star-shaped welded-on support plates serving to take the weight of the bundle. A segmental design of the support structure limits the axial relative expansion caused by the operation temperature. In the upper cold area, the mechanical loads are carried by the vessel cover. This ensures access to the secondary system for in-service inspection and repairs without the necessity to open the primary circuit.

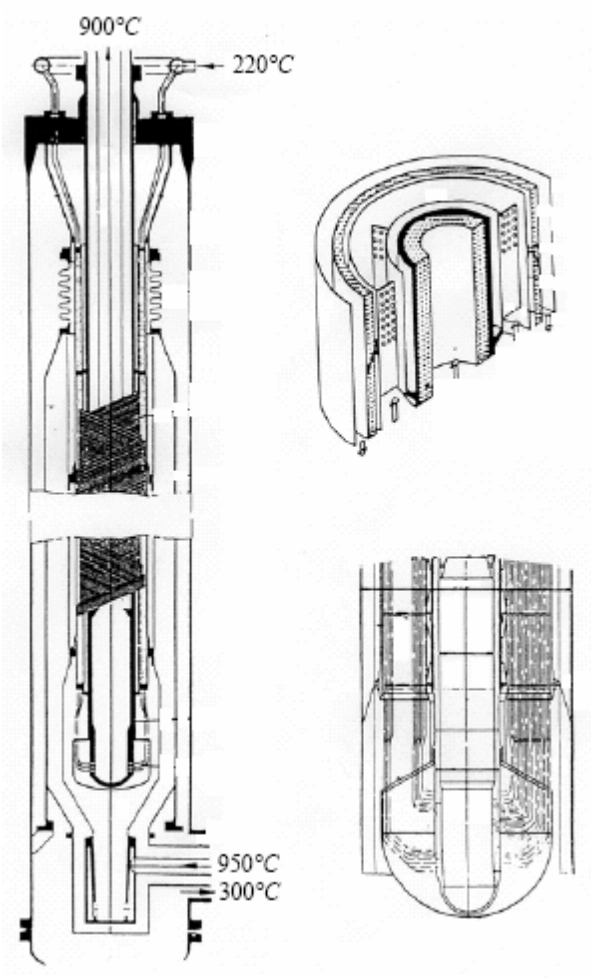

Figure 41: Intermediate heat exchanger for nuclear applications (Technical and Safety Aspects of Processes of Hydrogen Production using Nuclear Energy, 2005) (left: helical tube bundle; right: details of hot gas collector tube and support structures)

A facility for large component testing (Komponenten-Versuchskreislauf — KVK) was constructed and successfully operated by Interatom within the PNP project (Harth, et al., 1990). In a heating system consisting of a heater with steam, a natural gas burner and an electrical heater with a total thermal power of 10 MW, helium was heated up to 950 °C at 4.0 MPa (Figure 42 and Figure 43). This plant also allowed the testing of hot gas ducts with a large diameter, of a steam generator, of valves for hot helium and of other components such as hot headers or auxiliary plants like gas purification.

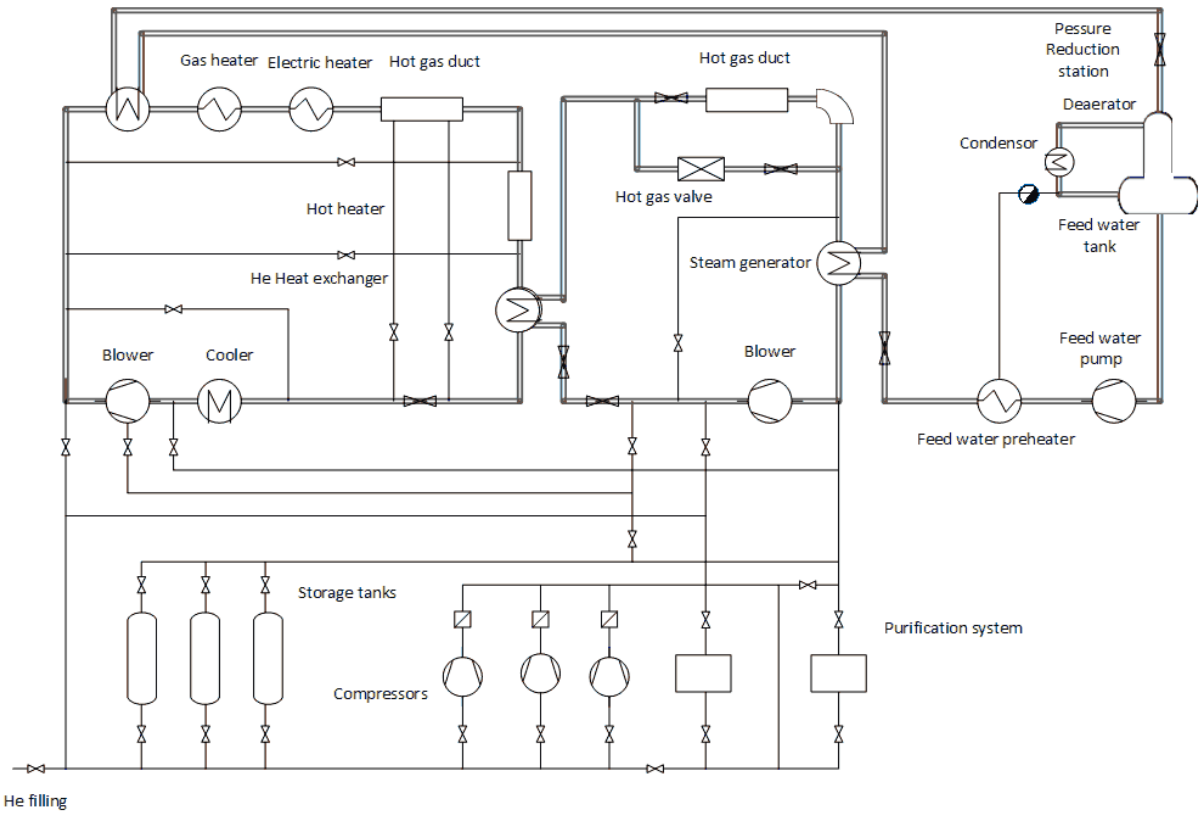

Figure 42: Flow sheet of 10 MW KVK facility for testing nuclear process-heat components

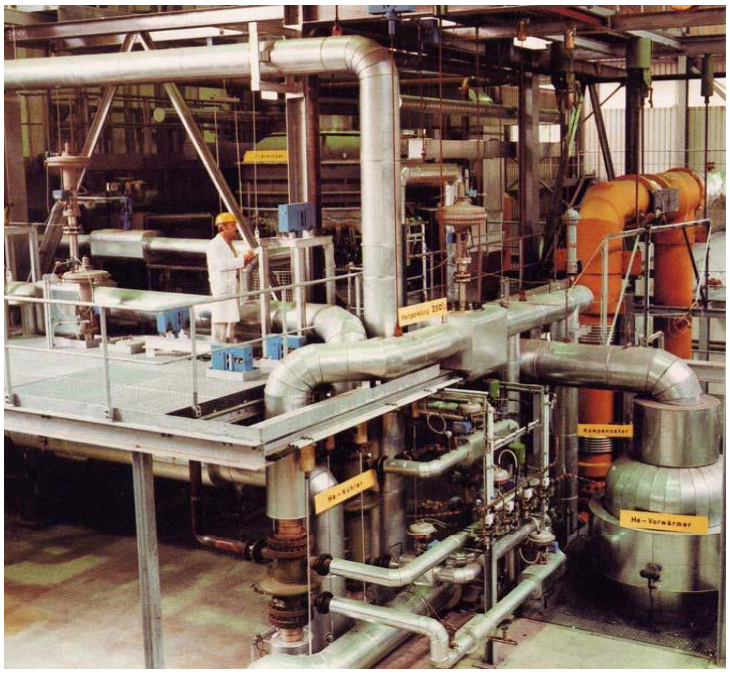

Figure 43: 10MW KVK facility for testing nuclear process-heat components

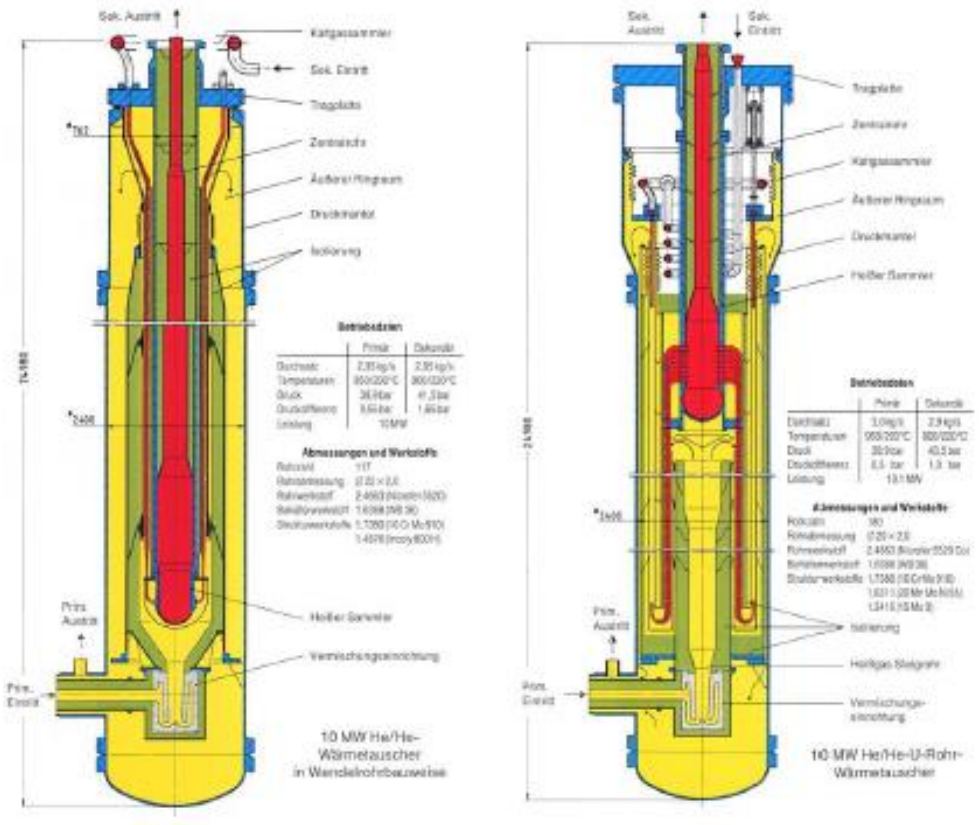

Figure 44: Two IHX components tested in KVK (left: Helical tube bundle by SteinmOller; right: U tube bundle by Balcke-Durr)

Two IHX components were constructed and tested in the KVK loop, one with a helical tube bundle and another one with U tubes. Figure 44 shows schematics of both components.

In the helical IHX, primary hot helium (950 °C) entering the heat exchanger flows via a mixing and deflecting device at the bottom of the component upwards through the bundle and is cooled to 300 °C. The cooled primary helium flows back into the gap between the wall of the reactor pressure vessel and the gas shroud of the heat exchanger to the blower at the bottom of the component.

The secondary helium is entering the component at the top. After entering into a ring conduit, the helium with a temperature of 200 °C is uniformly distributed over the tube bundle and heated up to 900 °C in counterflow. The cycle is closed by the hot header which is insulated on the inside. The hot helium leaves the IHX at the top of the component.

The maximum wall temperature in the tubes under normal operation is 920 °C; the maximum pressure difference between the primary and secondary sides is 0.2 MPa under operational conditions. During depressurisation accidents they have to withstand the full pressure difference in a limited time period.

The relevant data on the IHX test components are contained in Table 18 in comparison to the data on an IHX component to be connected to the two German concepts of a process-heat nuclear reactor. Each component had a thermal power of 10 MW. The most critical part in the design of a helical tube concept, the hot header for the secondary helium, was tested in the 10 MW component at 1:1 scale related to the large component. Both components were operated over several thousands of hours without any difficulty.

The table shows that the specific data on the test components were very similar to those which are planned for the nuclear application. The gas temperatures, pressures and material temperatures in the KVK facility were identical to those of the nuclear design.

In particular, hot gas samplers, as the main sensitive large components of such an heat exchanger, have been tested at 1:1 scale. The tube systems had the same dimensions in test and for nuclear application. The materials for the tubes, the headers, the supporting structures and the gas ducting on the primary side are the same as those planned for the nuclear application.

On the basis of a broad experimental programme in the KVK plant and other related test facilities (HHV plant, EVO plant, insulation test facilities, specific facilities to test, for example, friction, fretting, wear, materials, depressurisation), the following statements can be made with respect to the feasibility of the IHX.

- Two helium-heated IHXs have been successfully tested at the 10 MW power level and at maximum helium heating temperatures of 950 °C (primary) and 900 °C (secondary), respectively. So far, the process parameters have been tested under the real conditions of the nuclear application. The operation time of the helical tube bundle was more than 5000 hours and that of the U tube bundle was more than 4000 hours.
- Parallel to the integral tests of the components, additional testing in KVK was carried out for a hot gas header of the helical tube bundle, for hot gas ducts (including bends and expansion bellows), hot gas valves and a steam generator.

- The thermodynamic data on the heat exchanger designs have been confirmed by the experiments. Average heat fluxes of approximately 40 kW/m^2 can be realised at reasonable pressure drops.
- The components were tested in steady-state operation and under transient conditions. Transients of ± 7 K/min were tolerated by the components without failure.
- Tests have shown leak tightness between the primary and secondary sides of the IHX. The measured vibrations did not result in serious loads on the heat exchanger tubes.
- The bearing forces for the load transfer system of the cold header and the bundle were within the range of calculated values.
- Ultrasonic inspection of IHX tubes after 4700 hours of operation did not reveal any deviations.
- Creep buckling tests on the hot gas header were carried out.
- As many as 656 cycles from 950 °C to 710 °C and the reverse, with a transient of ± 40 K/min, did not cause any damage to the header.
- Tests with a pressure difference of 4.3 MPa between the primary and secondary sides of the hot gas header at 970 °C were carried out over a time period of 455 hours to simulate a depressurisation accident. No damaging influences were identified.
- Insulation and gas-ducting structures inside the tube bundles showed no damage. Overall it was stated that an IHX following one of the two designs investigated (helical tubes and U tubes) can be designed for a power of 170 MW and can be operated for 100 000 hours on the basis of the available experience. In particular, the extensive wall-material testing for high-temperature alloys at a temperature of 950 °C showed that this component can be applied in connection with process-heat HTGRs.

5.10. Helium circulator

The helium circulator has to compensate for total pressure drops in the helium cycle of around 1.5 bar. The helium pressure is 60 bar.

The mechanical power to compensate for the pressure drop in the whole primary circuit can be calculated as follows:

$$N_{mech} = \frac{\dot{m}_{He} * \Delta p}{\rho_1 * \eta_i} \qquad (20)$$

with typical values for THTR:

$\dot{m}_{He} = 298\ KG/s$

$\Delta p = 1.12\ bar$

$\rho_1 = 4.03\ {}^{kg}/_{m^3}$ (at 40 bar and 250 °C)

$\eta_i \approx 0.75$

A total amount of mechanical power in the system of $N_{mech} = 10.8 MW$ is needed. For the THTR with six blowers this results in a single blower power of 1.8 MW.

The total power of the motor is:

$$N_{motor} = \frac{N_{mech}}{\eta_{mech} * \eta_{motor}} \tag{21}$$

with η being the degree of efficiency mechanical and of the motor.

To calculate the specific rotor diameter, the following equations can be used.

For the helium throughput:

$$\dot{V} = {\dot{m}}/{\rho(p,T)} \tag{22}$$

The specific work of the helium flow:

$$y = \frac{\Delta p}{p} = \eta_i * cp * T_1 \left(\left(\frac{p_2}{p_1} \right)^{\frac{R}{\eta_i * cp}} - 1 \right) \tag{23}$$

The specific rotation speed:

$$\sigma_{\gamma M} = 2.108 * n \left({\dot{V}^{0.5}}/{y^{0.75}} \right) \tag{24}$$

The equation for specific rotor diameter is:

$$\delta_{\gamma M} = 1.054 * D * \left({y^{0.25}}/{\dot{V}^{0.5}} \right) \tag{25}$$

The Cordier diagram (Figure 45) shows that the blowers used in the AVR, the THTR and the HTR Module are optimally designed.

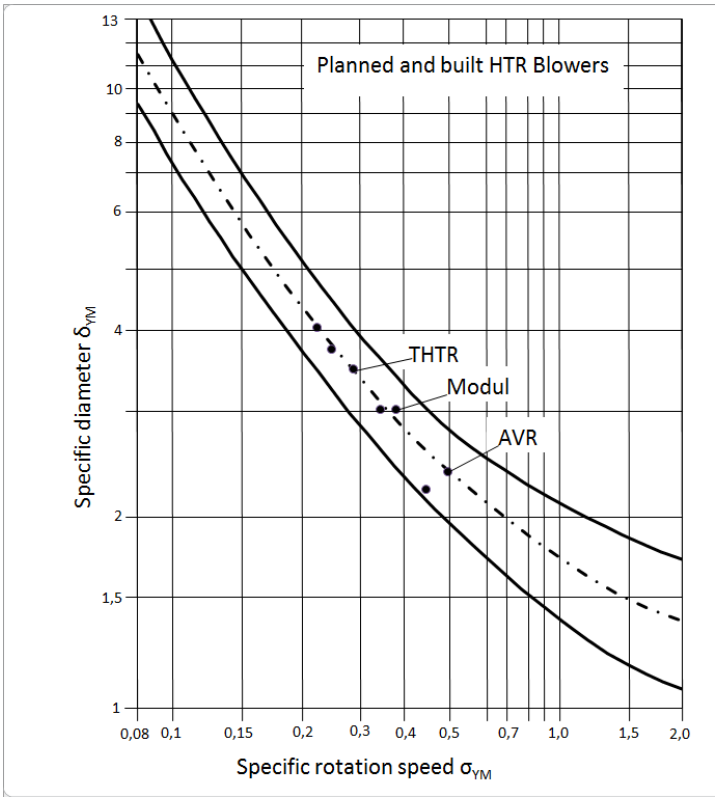

Figure 45: Correlation between specific diameter and specific rotation speed for HTR blower

For the HTR Module a-one stage radial compressor with a vertical shaft (Figure 46) is used. The component is arranged at the top of the steam generator and is fully integrated into the primary circuit. The drive is an asynchronous electrical motor with speed regulation. The bearings of the drive-circulator unit use oil lubrication and helium gas sealing; the cooling is done by water.

The-one stage compressor uses one bearing for the wheel in overhang arrangement. It has a flap on the suction side.

The primary circuit and the housing of the motor are connected via an intermediate flange. The motor can therefore be removed without opening the primary circuit.

The drive for the flap and several pipes for the supply of auxiliary systems are arranged in the housing of the motor . The motor housing has the same helium pressure than the helium cycle.

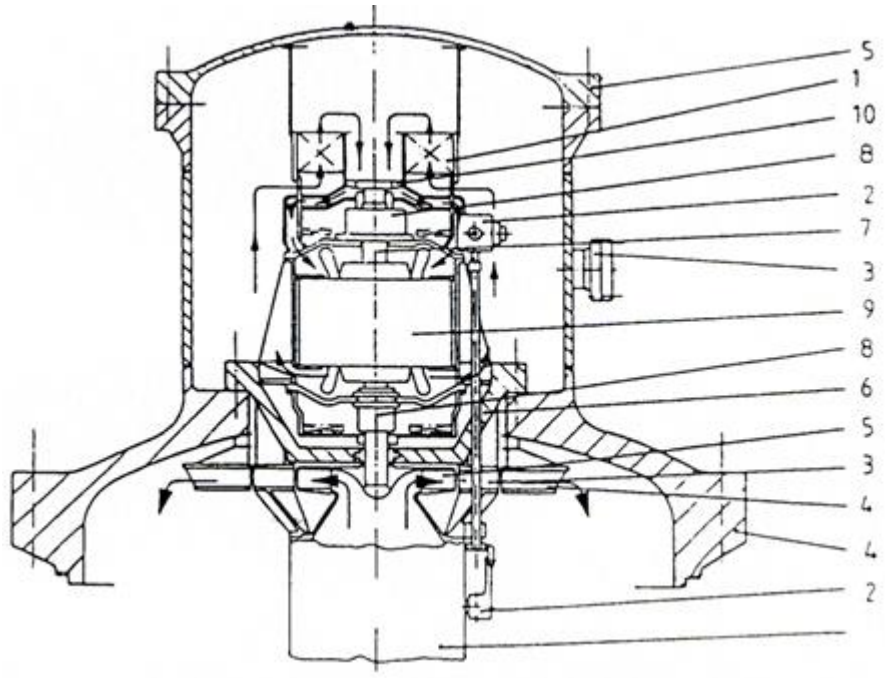

1: Suction
2: Flap
3: Inner diffuser
4: Outer diffuser
5: Wheel
6: Intermediate flange
7: Shaft
8: Oil bearing
9: Motor
10: Auxiliary wheel
11: Gas cooler
12: Drive of flap
13: Gas penetration
14: Flange

Figure 46: Helium circulator of the HTR Module

Some data on the component are contained in Table 19. For comparison, the data on a THTR helium circulator are included in this table.

The development of the HTR technology delivered broad experience on helium circulators and is a good basis for future applications. The many years of successful operation of CO_2-cooled reactors form another large pool of experience for this component.

Table 19: Data on the helium circulator of the HTR Module (THTR circulator data for comparison)

Parameter	Dimension	HTR Module circulator data	THTR circulator data
Number of loops		1	6
Power	MW	2.5	2.3
Mass flow of helium	kg/s	85.5	46.25
Pressure drop	bar	1.5	1.1
Helium pressure	bar	40	60
Helium inlet temperature	°C	250	250
Type of circulator		Radial, 1 stage	Radial, 1 stage
Drive		Electric motor	Electric motor
Bearing		Oil	oil
Speed	Rotations/min	3 000	5 600
Arrangement		Vertical	Horizontal
Support of wheel		Overhang	Overhang

5.11. Helium purification plant

The helium purification plant, together with helium auxiliary systems, has to fulfil different requirements. The helium of the primary circuit must be cleaned to limit the values of H_2, CO, CO_2, N_2, O_2, H_2O and CH_4 to permitted specified values. This is necessary to limit the corrosion of fuel elements and graphite structures to permitted values. Furthermore, tritium has to be removed from the primary circuit. All components and circuits which contain helium have to be supplied with this gas in normal operation, thereby the pressure of the system is controlled too. During extended inspections and repair work the helium has to be removed from the system and storage.

The helium purification of a two-module plant contains three tracks. The third system is mainly used as a reserve unit during inspection and repair and for the purpose of regeneration of one of the other tracks.

Figure 47 shows the concept of the system containing several stages. In the first stage a filter removes dust; in the second stage H_2 and CO are converted to H_2O and CO_2 with help of copper oxide; in the third stage a molecular sieve removes H_2O and CO_2.

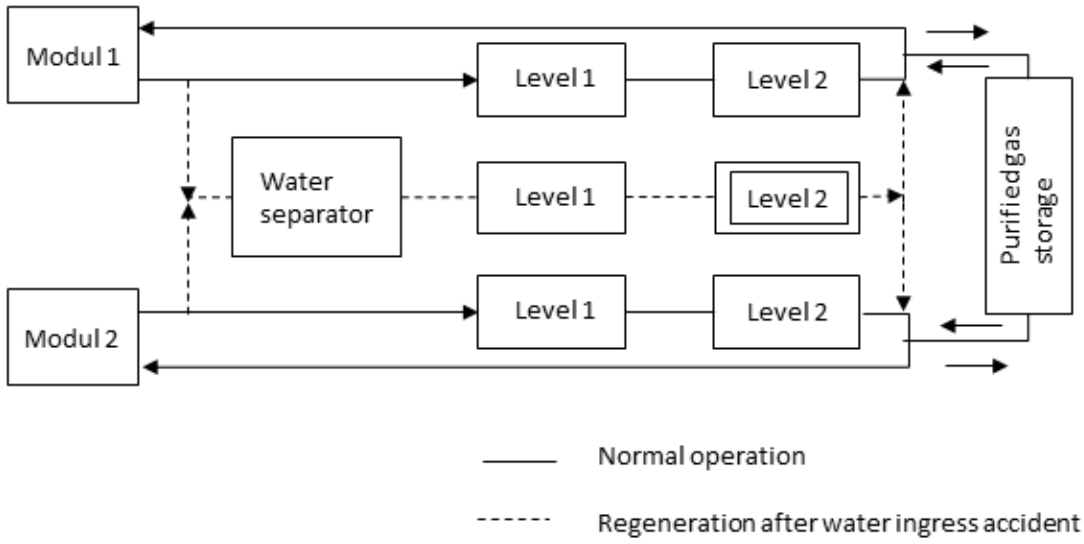

Figure 47: Concept of gas purification of the HTR Module consisting of three tracks

In a further stage the helium is cooled to very low temperatures (~ 180 °C), and this allows CH_4 and N_2 to be removed.

Additionally, fission gases like argon, krypton and xenon are removed. The very small amounts of them in the cooling gas are also reduced.

The purified gas is recycled to the primary system with help of an additional helium circulator. The throughput of the gas purification plant was chosen in the HTR Module to be 5 % per hour related to the primary circuit inventory. This corresponds to a mass flow of helium of nearly 3 kg/s.

The third track in the gas purification of the HTR Module has a special function in case of a 'water ingress into the primary circuit' accident. Water which has entered the primary system can be removed using a water separator especially installed for such an accident. This procedure is helpful in reducing corrosion effects in fuel elements and graphite structures and limiting the formation of water gas.

Furthermore, it allows the rise in pressure of the primary circuit to be limited. The blowing off of helium/steam mixtures into the reactor building is avoided in this case.

The purification plant of the THTR -plant is a good example of the technology explained above (Figure 48)

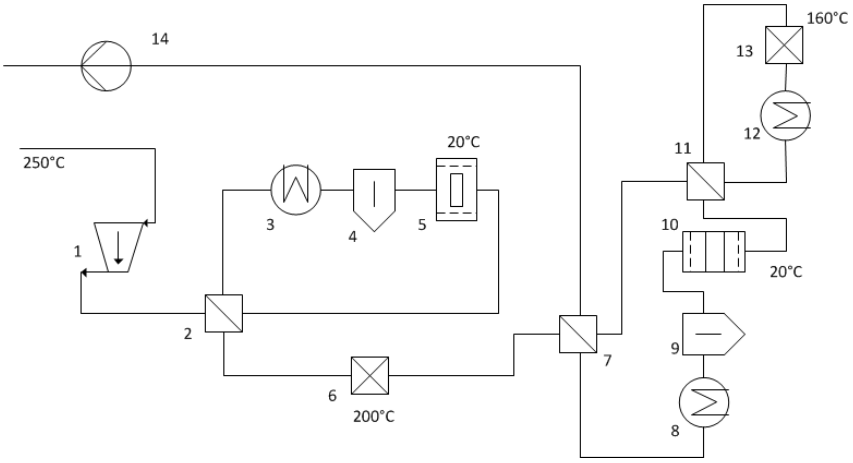

1: Dust filter
2: Recuperator
3: Cooler
4: Separator
5: Active coal filter
6: Copper oxide catalyst
7: Recuperator
8: Cooler
9: Separator
10: Molecular sieve
11: Recuperator
12: Cooler
13: Active coal filter
14: Helium compressor

Figure 48: Flow sheets of THTR gas purification plant

5.12. Depressurisation systems

The primary system has a depressurisation system. It protects the primary enclosure in case of excessive pressure (around 69 bar). A higher pressure could be caused, for example, by the loss of the main heat sink and the pressure regulation at the same time or in case of severe water ingress accidents.

The system consists of two parallel tracks which contain valves, safety valves, pressure holding valves and burst discs.

One track is designed for a flow section of 1 cm^2 for small leaks and one of 30 cm^2 corresponding to a break with diameter of 65 mm. In the first case very effective filtering of the effluent gas takes place; in the second case the gas is ducted directly into the channel for depressurisation and released via the stack. Corresponding to the permitted release of radioactivity at the time of planning, the radiological consequences were assumed to be tolerable. For future concepts in this case, filtering could even be envisaged, and could be required in the licensing process. Figure 49 shows the arrangement of the components of the depressurisation system.

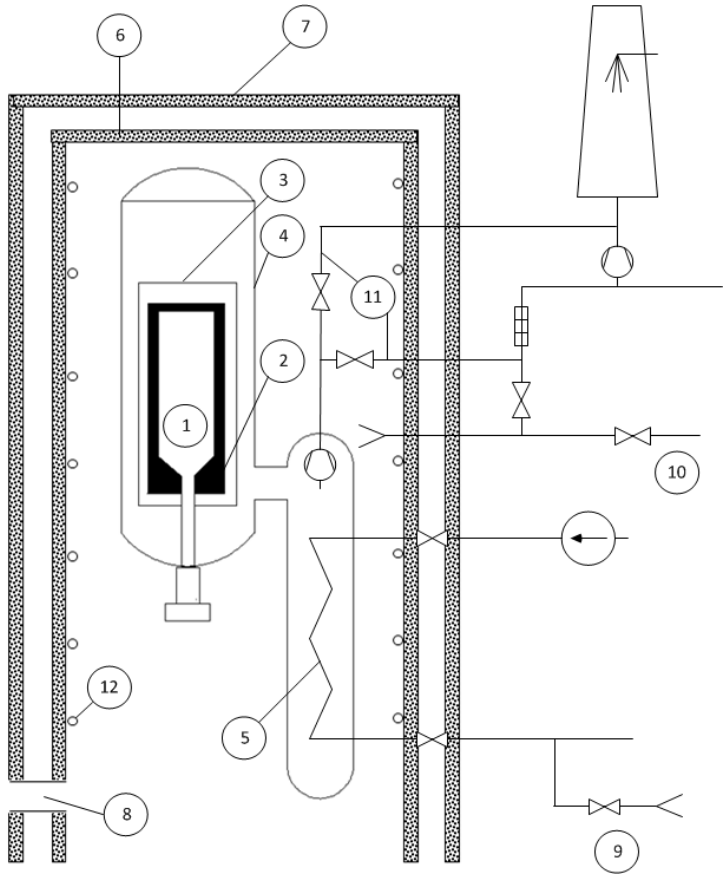

1: Pebble bed core
2: Graphite reflector
3: Core container
4: Pressure vessel
5: Steam generator
6: Reactor cell
7: Reactor building
8: Pressure-relief system of reactor cell
9: Steam generator dump line
10: Exhaust air system
11: Pressure-relief system
12: Surface cooler

Figure 49: System for the depressurisation of the primary system

Furthermore, a system is available to depressurise the steam generator if large amounts of water have penetrated into the primary circuit. The system will limit the amount of water which will stay in the steam generator pressure vessel, and it is designed in such a way that the pressure becomes smaller than the primary pressure, thereby a release via a leak in the steam generator is avoided. Gas purification allows the total removal of the water after the accident has happened. Steam will be condensed and the helium will be pumped into the gas storage.

Two tracks allow a redundant design of the systems consisting of valves and vessels which are provided for steam condensation.

Finally the concrete cell inside the reactor building is equipped with a depressurisation system to protect this room against excessive pressure in case of 'loss of coolant' accidents.

All rooms with pressurised pipes are connected via a central pressure exoneration channel to the stack and the environment, and during accidents this measure avoids excessive pressures in these rooms. All rooms have openings into this channel. These openings are normally closed by flaps which allow the rooms to operate in under-pressure conditions

5.13. Decay heat removal installations

The normal situation of decay heat removal from the reactor is the operation of the production loop, consisting of the gas duct, the steam generator and the helium circulator. This system has several possibilities of feed-water supply and steam condensation or blow-off. Figure 50 shows this concept.

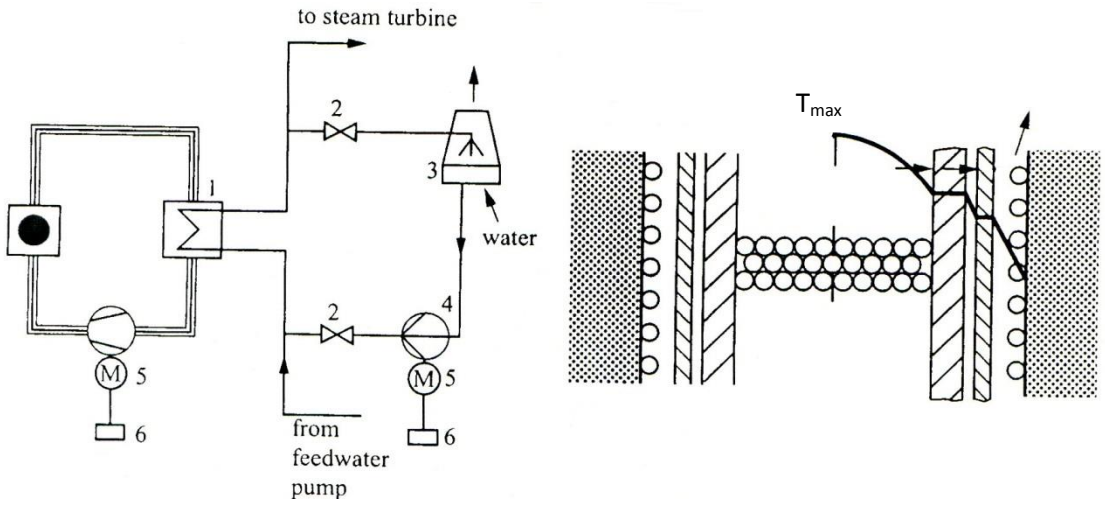

Figure 50: Decay heat removal in a modular HTR

There are several possibilities feeding in water into the steam generator. Furthermore there are several diverse possibilities to condensate the steam or release it to the environment.

Despite of all these efforts the non-availability of this chain of decay heat removal is relatively large, and is estimated at around 10^{-1} per year. Therefore, in some concepts of modular HTRs separate additional decay heat removal systems are provided for. As an example, in the GAC-600 design a small auxiliary loop (layout for full pressure of the primary system) is planned to be situated at the bottom of the reactor pressure vessel. Naturally, a similar solution of a small loop located side-by-side with the reactor could also be used in the case of the HTR Module. The electricity supply of this loop should have high availability. If the active decay heat removal has failed, the surface cooler, situated around the reactor pressure vessel, acts as heat sink. This cooler is built from three tracks and has simple supply systems for water and cooling towers outside the reactor building. Figure 51 shows a principal flow sheet for this installation.

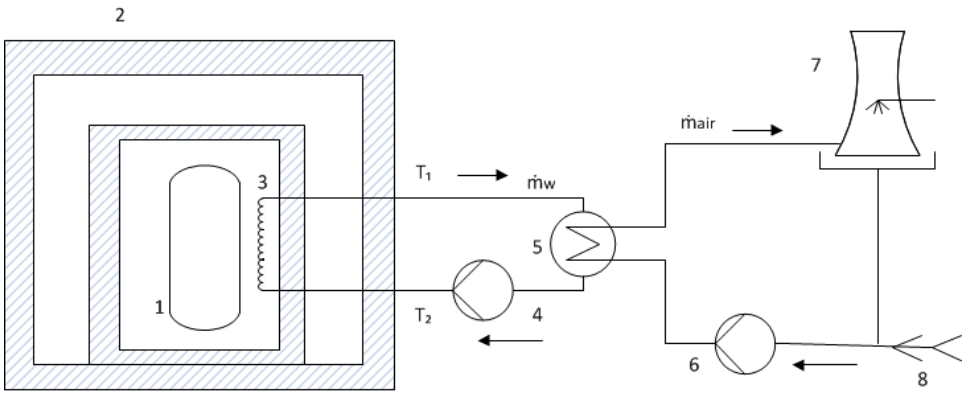

1: Reactor pressure vessel
2: Wall of reactor building
3: Surface cooler
4: Pump
5: Intermediate heat exchanger
6: Pump
7: Cooling tower
8: Auxiliary water supply

Figure 51: Concept of surface cooler

If the surface cooling system were also to fail the decay heat would penetrate into the concrete of

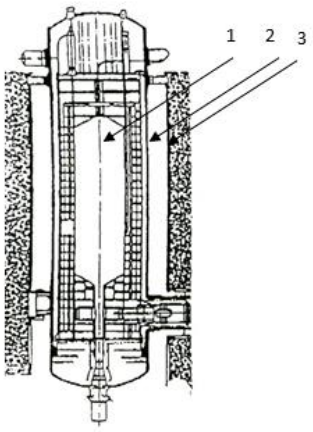

the inner cell (

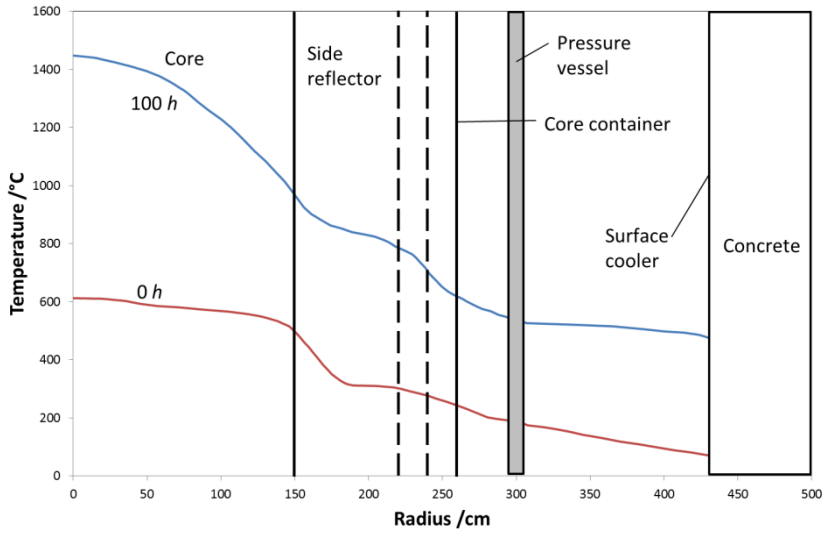

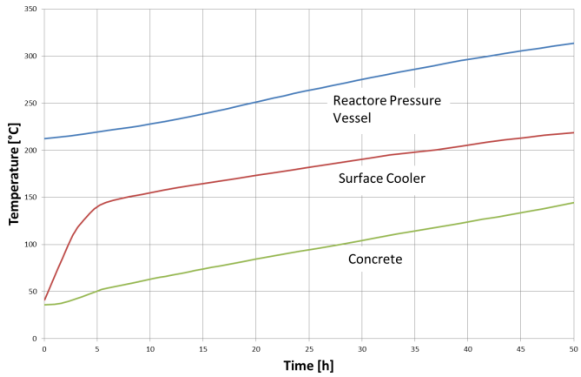

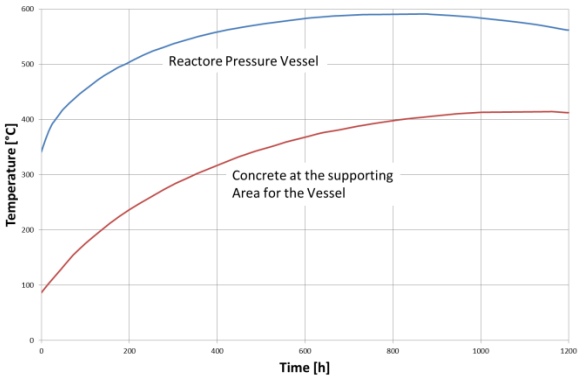

Figure 52). It would be stored there and finally released into the environment. In all cases the maximum temperature of 1 600 °C during these accidents would not be reached.

Further intervention methods to cool the reactor are possible, for example feeding water into the surface cooler after long grace time, cooling the concrete cell or cooling the reactor pressure vessel using nitrogen.

Without any measure of active cooling, however, the principle of self-acting decay heat (see chapter 7.2) would be suited to limit the maximum fuel temperature to values of 1 600 °C.

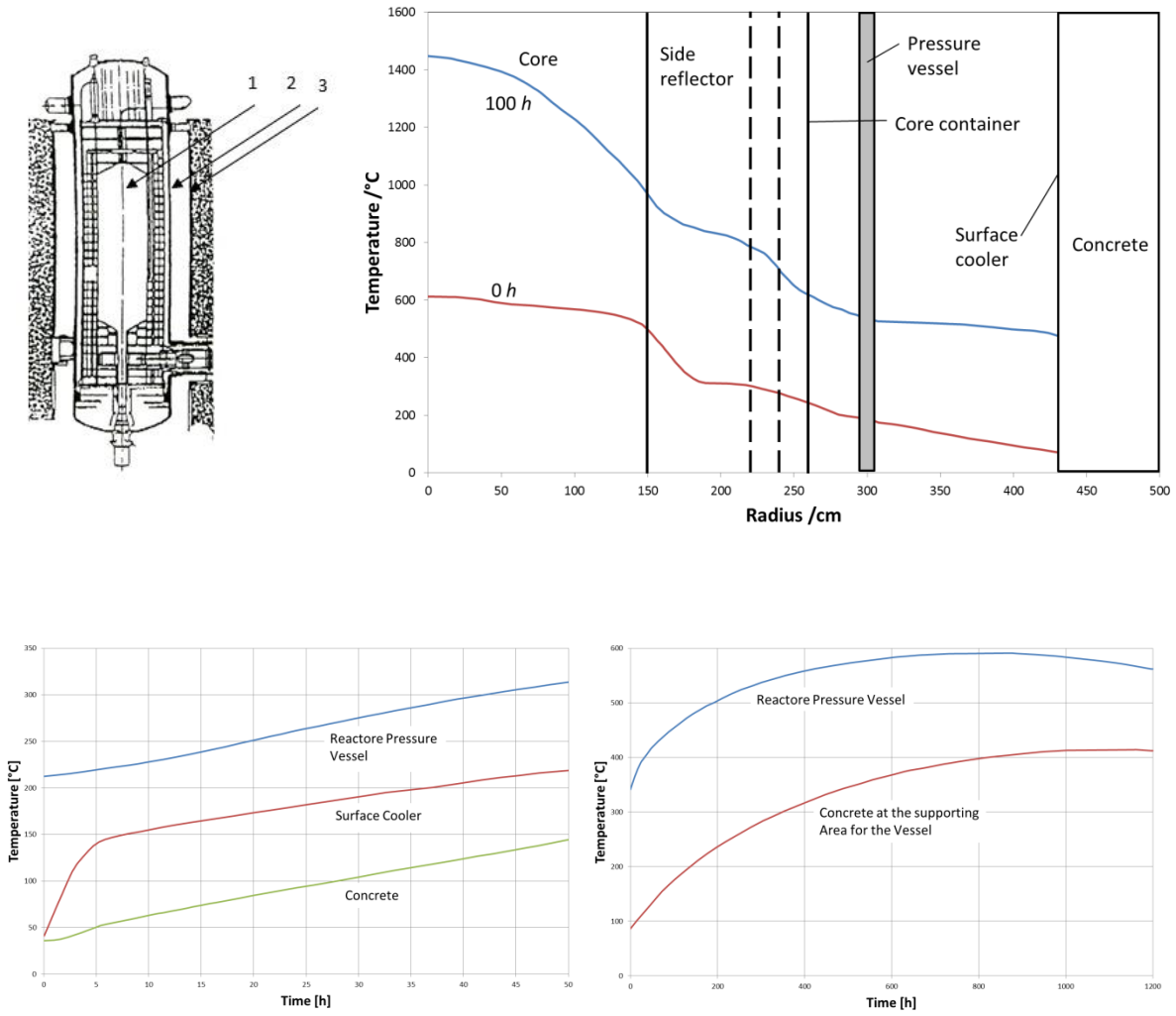

Figure 52: Results for a 'total loss of active cooling' accident; failure of the surface cooler; storage and transport of heat in the concrete cell (HTR Module, 200 MWth)

5.14. Reactor protection system

As usual in nuclear technology each modular unit possesses a reactor protection system. The systems for single modules are not coupled and work without interactions.

In case of accident the afflicted unit will be shut down and protection system actions will be initiated in this reactor.

Figure 53: Connections in the reactor protection system of the HTR Module

Figure 53 shows an overview of the connections between measured data, assumed accidents and actions initiated by the reactor protection system.

The measurement of the following process parameters allows the detection of accidents due to both internal reasons and outer impacts:

- neutron flux (reactor power),
- helium inlet temperature to core,
- helium outlet temperature from core,
- humidity in primary helium,
- pressure in primary helium circuit,
- pressure in secondary circuit,
- mass flow of primary helium,
- mass flow of feed water.

The concept of measurement of data and the logical connection of these data will be taken over from the established technologies for light-water reactors.

The actions of safety systems, which are initiated by the reactor protection system, are (see Figure 53):

- insertion (free fall) of the six reflector rods of the first shutdown system;
- shutdown of the primary helium circulator;
- closure of the secondary circuit (feed-water valves, life-steam valves);
- depressurisation of the steam generator until it reaches the same pressure as the primary system;
- locking of primary circuit closures.

The following accidents are governed by this concept of the reactor protection system in the case of the HTR Module:

- uncontrolled removal of reflector rods during the start-up procedure;
- uncontrolled insertion of reflector rods during normal power operation;
- loss of pressure in the primary system;
- break in steam generator tubes;
- failure of the helium circulator;
- malfunction of the helium circulator flap;
- break in the feed-water line;
- break in the life-steam line;
- loss of electrical power.

Normally, several process variables are used to detect the accident and they initiate different actions. For example, in case of a break in a steam generator tube the humidity in the primary system and the primary pressure initiate actions (1), (2), (3) and (4) via the reactor protection system.

Accidents	Logical matches	Threshold value	Process variables	Safety actions		
Uncontrolled move out of control rods during start-up				①	②	③
Uncontrolled move in of control rods during normal operation				①	②	③
Uncontrolled move out of control rods during normal operation				①	②	③
Pressure loss in the primary circuit				①	②	③
Break in tubes in the steam generator				①	②	③ ④
Blower failure/erratic behaviour of blower flaps				①	② ③	④ ⑤
Break in feed-water line				①	②	③
Break in life-steam line				①	②	③
Emergency power				①	②	③
	1 of 2	Period to low	Neutron flux in the middle area			
	1 of 2	$\Phi to\ high$	Neutron flux in the middle area			
	2 of 3	$\Phi/\Phi_0 > 1.1$	Thermal corrected neutron flux			
	2 of 3		Thermal corrected neutron flux			
	2 of 3	$T_H \geq T_{Hmax}$	Hot gas temperature			
	2 of 3		Hot gas temperature			
	2 of 3	$T_K \geq T_{Kmax}$	Cold gas temperature			
	2 of 3	$F \geq F_{max}$	Humidity in the primary system			
	2 of 3	$P \geq P_{max}$	Pressure in the primary system			
	2 of 3		Pressure in the primary system			
	2 of 3		Primary gas/feed-water throughput			
	2 of 3	$\Delta P \leq \Delta P_{max}$	Pressure diff. primary system/steam generator			

Figure 53: Connections in the reactor protection system of the HTR Module

The number of the safety actions in Figure 53 can be described as follows:

① levelling of the six control rods through gravity (scram);

② switch off the blower in the primary circuit;

③ blocking of the secondary circuit (feed-water and life-steam instruments);

④ unloading the steam generator until pressure equilibrium with the primary system is reached;

⑤ blocking of the primary system closure.

5.15. Steam turbine plant

For a power plant for cogeneration consisting of two modular reactors two turbines were envisaged (Figure 54). Alternatively, the application of one turbine is possible. This is a question of optimisation between investment costs and plant availability.

The process steam will be produced using steam leaving the high-pressure part of the steam turbine system. The water consumed is substituted with deionised water from storage. Steam which is not required for the production of process steam is used in the medium- and low-pressure turbines for electricity production. The condensate leaving the low-pressure turbines is condensed and pumped back into both feed-water storage vessels.

From these vessels the feed-water pumps carry the water back to the steam generators. Some important data on the steam cycle are included in Table 20. This process corresponds to well-known technologies, often applied in conventional energy technology.

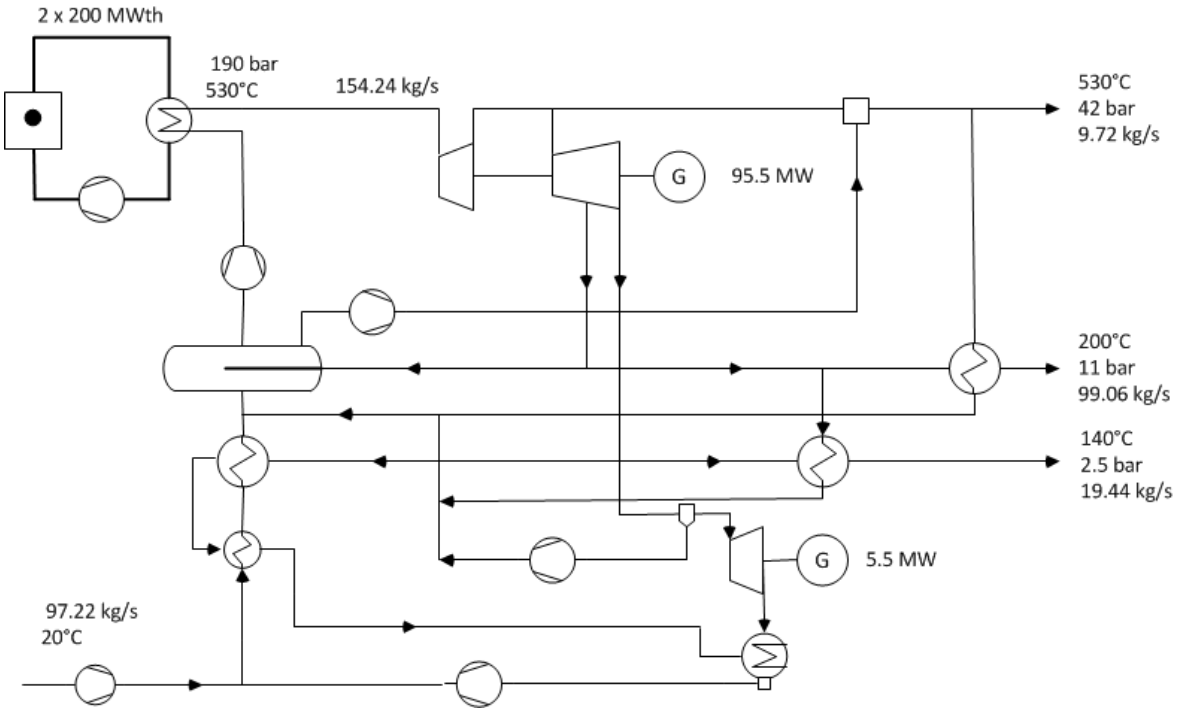

Figure 54: Steam turbine system for process-steam delivery from a power plant with two modular HTRs and two turbines

The detailed layout of the turbine process is possible on the basis of the operation of prototype plants, for example THTR and Fort St. Vrain. Table 21 shows pre-calculated and measured values for the THTR and demonstrates the excellent agreement of the data.

A special question for this process of steam production by cogeneration is the tritium content of the product. Based on the experience of HTR plants which were in operation and on many measurements in special test facilities for tritium permeation, it can be stated that the tritium content of the products is very low, and is smaller than licensed levels. The introduction of a steam transformer is a major precondition for the limitation of tritium.

Table 20: Some data on the steam turbine plant for the production of process heat by cogeneration

Parameter	Dimension	Value	Remark
Thermal power	MW	2 × 200	
Electric power	MW	95	Flexible
Power of process-steam delivery	MW	130	Flexible
Life-steam conditions	°C/bar	530/190	
Process steam-conditions	°C/bar	240/42, 200/11	
Mass flow of process steam	t/h		
Concept of the turbine		Extraction	
Separation of process heat		Steam transformer	

Cooling method		Wet cooling tower	

Table 21: Pre-calculated and measured values of THTR

Parameter	Dimension	Measured value	Calculated value
Thermal power of the core and internals	MW	756	755
Circulator speed	min^{-1}	5 407	5 380
Helium flow rate	kg/s	48.26	49.12
Feed-water flow rate	t/h	151.6	151.7
Mass flow through the reheater	t/h	144.7	144.1
Hot gas temperature at the SG inlet	°C	750.3	750
Hot gas temperature at the SG outlet		246.8	246.3
Main steam temperature	°C	534.2	535
Main steam pressure	MPa(abs)	18.69	18.67
Reheat steam temperature	°C	530.6	527
Reheat steam pressure	MPa(abs)	4.85	4.84
Generator active power	MW	303.3	301.3
Cooling water temperature	°C	27.6	26.5

5.16. Cooling system

The cooling system of the plant contains the following parts.

- A main cooling system for the steam turbine plant. A condenser and a wet cooling tower release the waste heat into the environment. Some additional water is necessary to operate this cooling system.
- Start-up and shutdown systems for each module are necessary for the operation; each system has its own cooling system.
- Separate intermediate cooling systems; all heat losses occurring in different components of the plant are released via this system containing separate cooling towers.
- A separate cooling system for the surface cooler, which is built in three tracks. Some effort is required to make this system as reliable as possible. Also, after a long grace time water can be injected into this system from different sources (e.g. by the fire brigade).

Some more details on these cooling systems can be seen in Figure 55.

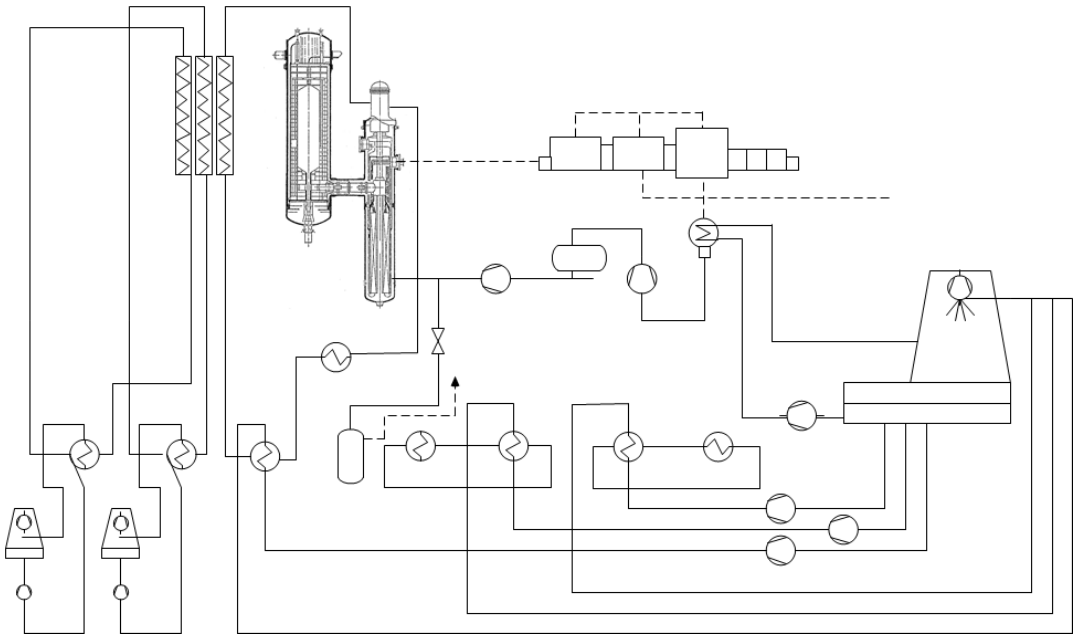

Figure 55: Overview of cooling systems of the HTR Module

5.17. Handling of radioactivity

There are several streams of material containing radioactive substances during operation of the HTR Module.

- Spent fuel elements are highly radioactive waste — around 300 spherical fuel elements have to be brought into the intermediate storage per day during full-power operation of one modular HTR.
- Air containing radioactive, polluted helium is released from the plant via filtering and the stack.
- Releases of waste water occur and the water has to be cleaned up. Finally the cleaned water has to be released into the environment.
- There are various paths to treat solid-waste mainly containing low radioactive substances. They have to be conditioned and stored in special intermediate storage containers.

An overview of the different paths to handle waste and the conditioning of these materials is given in Figure 56.

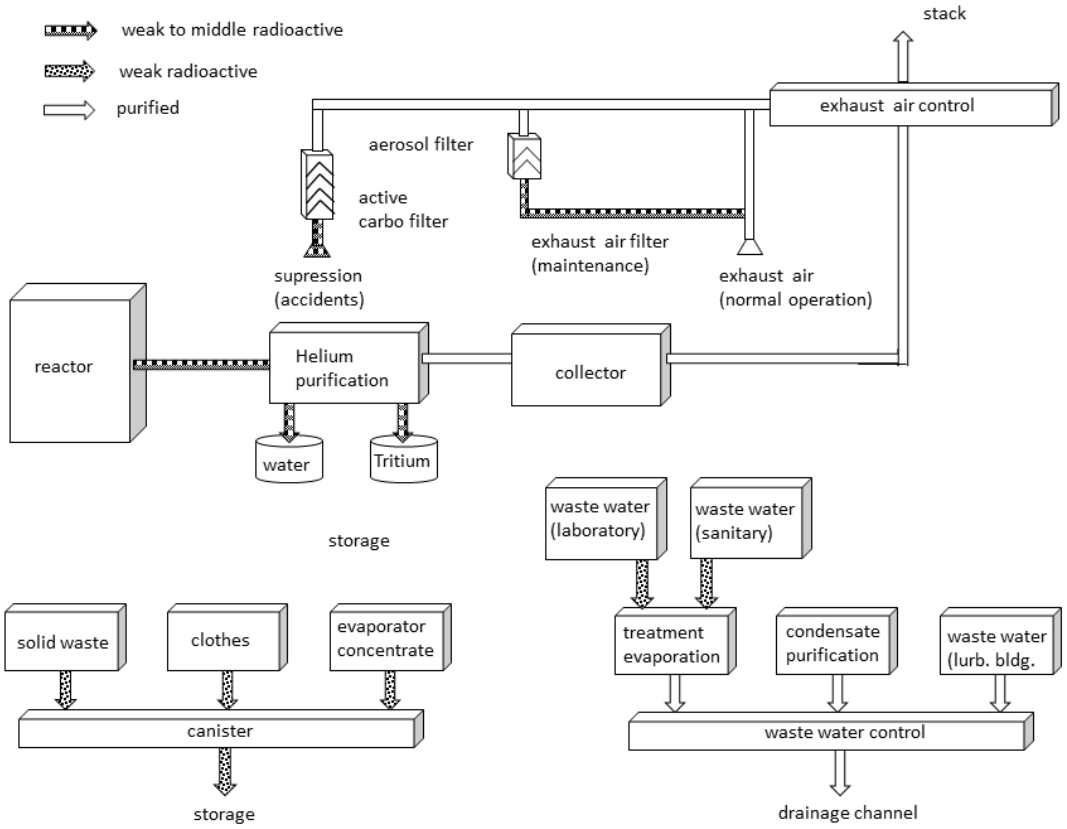

Figure 56: Flow of activity which is envisaged for the HTR Module

The concept of storing spent fuel is a very well-established concept in AVR and THTR, and rules for future licensing processes can be adopted from LWR technology too. The intermediate storage technology is extremely safe, even for cases of very strong impacts from the outside.

Gaseous waste is produced in the gas purification plant. The gases removed in this plant are pumped into special storage vessels, and later they are released in a controlled manner via the stack. The regeneration of the stages of the gas purification causes the release of very small amounts of noble gases (^{85}Kr, ^{133}Xe), tritium and carbon (^{14}C).

A very small contribution to the radioactivity formed during operation comes from neutron-activated isotopes like argon (^{41}Ar), mainly inside the reactor building. These impurities are released via the air ventilation system.

Leakages of helium from the primary system can contain very small amounts of gaseous activity too. Following the experience of HTR plants and large facilities in which helium was handled, around 50 % to 100 % of the helium inventory leaks per year. Again this release of radioactivity is very low. Releases during inspection, maintenance and repair require special attention.

Overall the expectations for the HTR Module are as given in Table 22.

Table 22: Estimate of yearly releases of radioactive isotopes from an HTR Module plant

Released activity	Bq/yr	Ci/ye
Noble gases	7.4×10^{13}	2 000
- Main gas argon (^{41}Ar)	1.2×10^{13}	320
Iodine (^{131}I)	2.2×10^{7}	0.0006
Aerosol (long half-life)	3.7×10^{7}	0.001
Tritium (^{3}H)	3.7×10^{12}	100
- Main release in turbine building	8.9×10^{11}	24
Carbon (^{14}C)	8.9×10^{11}	24

Contaminated water is collected and treated. Treatment processes mainly consist of evaporation. Water can originate from washing processes, laboratories or decontamination processes.

The processed waste water is routed to three waste-water vessels, each having a storage capacity of 20 m^3.The water content of a waste-water vessel is only allowed to be released into the environment according to applicable guidelines. The limit for this is 1.85×10^{7} Bq/m^3 (5×10^{-4} Ci/m^3). If the radioactivity is higher than the limit the water must undergo an additional water-treatment cycle. The average concentration in the sewage will, in general, be substantially below the permitted release limits.

In general, the following annual values should be applied in a future plant specific location for an HTR Module power station:

- radioactivity in treated water 9.2×10^{9} Bq/yr (0.25 Ci/yr)
- Tritium H_3, 3.7×10^{12} Bq/yr (100 Ci/yr)

Condensate that contains tritium which is separated in the helium cleaning system, and in case of accidents when it is stored in separate storage vessels, is accumulated in the reactor building or in the reactor auxiliary systems building and is not released to the surroundings.

Solid waste, beside spent fuel elements, which is produced during operation is treated and stored in the power plant or in special intermediate storage buildings before later being taken for final storage.

The values estimated above correspond to experiences from the operation of AVRs and THTRs. Table 23 for example contains some values gained over 20 years of AVR operation.

Table 23: Values of release of radioactivity during AVR operation: (a) release of radioactive substances into the atmosphere; (b) transfer of radioactive water from the AVR In the KFA

Year	From the secondary circuit to the storage basin				From waste-water storage							
					to the vaporiser unit				to storage basin			
	Amount m^3	Alpha emitter Bq	Beta emitter without Tritium Bq	Tritium Bq	Amount m^3	Alpha emitter Bq	Beta emitter without Tritium Bq	Tritium BQ	Amount m^3	Alpha emitter Bq	Beta emitter without Tritium Bq	Tritium Bq
1968	13 282		1.19E09	2.223e11					296.3		3.80E07	1.90E10
1975	18 022		1.03E10	3.40e12	5.6		2.68EE09	2.6E08	568.9		2.38E08	4.13E10
1986	9 426		4.50E08	1.35E11	244.2	1.44E08	9.73E10	4.26E10	268.2	1.57E04	3.73E06	3.07E08
1987	8 624		2.15E08	2.04E11	363.5	3.12E07	4.88E10	4.30E11	363.6	1.28E05	1.04E07	1.62E09
1988	10 030		7.58E07	1.23E11	261.6	1.34E06	1.34E10	1.61E10	284.6	7.93E03	3.5E06	8.65E08

Year	Noble gas Bq	Aerosol Bq	^{90}Sr Bq	^{89}Sr Bq	^{3}H Bq	^{14}C Bq	^{131}I Bq	^{82}Br Bq	Outlet air m^3
1968	5.81E11	< DT	NM	NM	NM	NM	NM	NM	1.75E08
1986	4.77E11	1.61E04	1.6E05	3.09E05	1.71E12	3.38E10	1.62e04	4.65E05	3.22E08
1987	2.20E11	8.33E03	4.75E04	8.55E03	1.66E12	3.83E10	2.03E03	7.60E05	2.97E08
1988	2.78E11	< DT	1.17E05	1.05E04	1.70E12	4.42E10	DT	8.79E05	2.89E08

5.18. Status of development of components and the concept of the HTR Module for cogeneration

In practice, the components and concepts described in the previous chapters have already been used in LWR or HTR plants. As Table 25 indicates, broad experience is available for all components.

The most important component, the spherical fuel element, has been tested extensively in the AVR, the THTR and many irradiation and heating experiments. The operational temperature, fast neutron dose and burnup values required in the HTR Module concept are significantly lower than those which have been used in development up to now.

The core design of the reactor uses the experience of all HTR plants, especially that of the AVR, which has the same core diameter. The long-term experience from the graphitic core structures of AGR plants furthermore supports the use of the core structures of the HTR Module.

The first shutdown system is well known from the THTR. For the second shutdown system (KLAK), experiences from Fort St. Vrain can be adopted, however this system still requires additional qualification work.

The loading and unloading system is fully developed and can be derived from the AVR and the THTR. Some further improvements are possible.

The reactor pressure vessel and the steam generator vessel can be adopted from LWR technology. Because of the use of helium as coolant, no inner protection layers against corrosion, as in the PWR,

are necessary. The steam generator vessel follows similar principles of design to the reactor pressure vessel. The concept of designing and evaluating the connecting system with the hot gas duct and the cold annulus as a connecting vessel is new in nuclear technology.

For the whole primary enclosure the principle of 'basic safe design' and following the requirement to use the 'leak-before-break' concept must be fulfilled. This is well-established technology for LWRs today. The arrangement of the components of the primary system chosen for the HTR Module has a good example in the development of the AGR. The Windscale AGR (WAGR), as the prototype of AGR development, used the same concept of arrangement of the primary circuit and has worked for more than 10 years with good success. However, the arrangement is turned by 180° compared to the HTR Module.

The steam generator bundle, compensation and support systems inside this component can be derived from technologies applied in the THTR, Fort St. Vrain, Dragon and several CO_2-cooled reactors. Furthermore, heat exchangers with helical farmed surfaces are well known from fast breeders and from many fields of conventional technology too.

The helium circulator corresponds to technical solutions used in all HTR plants and in CO_2-cooled reactors. The component applied in the HTR Module can be directly derived from that of the THTR.

The hot gas duct has been tested at 1:1-scale (with a displacement body) in the Interatom component test facility KVK (*KomponentenVersuchsKreislauf*) and in the large ADI facility with good success. Elements of these components (insulation, liner, support) can be taken from other HTR projects. An important component joined to the hot gas duct is the core connection. This component has also been tested extensively at 1:1-scale in the KVK facility, and it was shown that a connection with very small leak rate can be used.

Auxiliary systems such as gas purification, helium circuits, helium technology in general and helium measurement methods can be carried over fully developed from HTR plants and many test facilities.

The control systems, the reactor protection system and electrical systems are fully developed and can be transferred from nuclear technologies developed up to now.

The concept of the inner concrete cell, which houses the primary system, is also well established in nuclear technology. For example, the WAGR uses a similar arrangement of an inner cell and an outer reactor building. In the case of the HTR Module the inner concrete cell is dense and connected to a filter system. The outer reactor building is not dense but protects against impacts from outside. The filter systems are well known and introduced in nuclear technology.

Containment structures, especially those designed against strong impacts from the outside, are now a well-established technology. Conventional systems for the plant, such as cooling systems, steam/water circuits, turbine generator units, secondary electrical systems and further concepts, are well known worldwide and can be carried over to the HTR Module.

The intermediate storage of spent fuel elements will be the waste management solution for several decades in many countries (e.g. Germany). The technologies developed for the AVR, the THTR and in the field of LWR can be carried over to the HTR Module. Dry storage vessels with self-acting decay heat removal offer an extremely high standard of safety.

A very important topic for the components operating at high temperature, such as the hot gas duct, the core connection and the steam generator, is the materials used. The alloy relevant for this application up to an average helium temperature of 700 °C is Incoloy 800H. For this material a broad qualification programme has been carried out and showed that these components can be designed for the whole lifetime with high safety factors.

Table 24 contains some comparisons and valuations of safety aspects and safety relevant features of AVR and HTR Module. Further improvements in case of modular HTR are possible, especially regarding air ingress accidents and very strong impacts from the outside.

Table 24: Safety concept of HTR Module compared to that of AVR

Main design data		
	HTR Module	**AVR**
Power, power density	200 MWth, 3 MWth/m^3	46 MWth/m^3
Pressure, temperature	60 bar, 250/700 °C	10.8 bar, 275/950 °C
Core radius/height	1.5/9.4 m	1.5/2.4m
Heavy metal	7 g/fuel element	6 g/fuel element
Safety concept		
Reactivity control	inherent	inherent
Temperature coefficient	-5×10^{-5}/°C	-9×10^{-5}/°C
Excess activity	1.0 nile	1.2 nile
Shutdown systems	6 reflector rods (hot) 18 reflector KLAK systems (cold)	4 reflector rods (hot, cold)
Decay heat removal	passive, operating system only (cavity cooler for component protection)	passive, operating system only (seal gap cooler for component protection)
Safety enclosure	fuel elements (T_{max} < 1 600 °C) pressure vessel unit vented confinement	fuel elements inner and outer pressure vessel gastight containment
Water ingress control	volume limitation (leak insulation) vessel configuration: slight under-moderation	volume limitation (leak insulation)
Air ingress control	volume limitation (vessel excluding failure, small reactor building)	volume limitation (multiple vessel excluding failure)
Reactor protection system		
Criteria	Pressure, temperature, flow rate, flux (moisture)	Pressure, flow rate, flux, moisture
Actions	Plant shutdown — hot standby (steam generator relief)	reactor shutdown — cold run (steam generator insulation, relief)

The questions of licensing, application of existing rules of nuclear technology, development of new rules and design prescriptions always require new considerations corresponding to the development of the state of science and technology. Furthermore, changing conditions regarding politics and acceptance have brought large amounts of uncertainty and delays in many nuclear projects,

especially in Germany. The licensing process of the AVR and the THTR was carried out completely and successfully; the licensing process of the HTR Module was nearly finished, but was stopped for political reasons. There was no doubt, however, that on the basis of the work of the companies, the advisers, the TÜV and the German Reactor Safety Commission (RSK) this reactor concept was licensable.

Table 25 contains some important components of modular HTRs. It is clear that there is a broad basis available to use these components and systems.

Table 25: Evaluation of components of the HTR Module

Fuel element	HTR reactor and test facilities
Fuel-handling system	AVR,THTR
Ceramic core internals	AVR,THTR, other HTR plants, AGR
Metallic core internals	AVR,THTR, other HTR plants, AGR
First shutdown system	THTR, AGR
Second shutdown system	Fort St. Vrain
Concept of primary enclosure	LWR (PWR, BWR), AVR, Dragon, Peach Bottom
Arrangement of the primary system	WAGR
Support of the vessels of the primary system	LWR (PWR, BWR)
Core connection	KVK tests
Hot gas duct	KVK tests, EVO,HHV,ADI, several plants
Steam generator bundle	THTR, Fort St. Vrain, several AGRs
Helium circulator	THTR, all other HTR plants, AGRs
Helium purification	AVR, THTR, all other HTR plants, large test facilities
Helium circuits, Helium technology	AVR, THTR, all other HTR plants, large test facilities
Inner concrete cell	WAGR, LWR (PWR, BWR)
Filter systems	LWR (PWR, BWR)
Surface cooler in inner concrete cell	Conventional technology (boilers)
Outer reactor containment building	All reactors
Instrumentation of the primary circuit	AVR, THTR, KVK,PWR
Reactor protection system	LWR (PWR, BWR), THTR
Secondary cycle (stem/water cycle, turbine)	THTR, Fort St. Vrain, AGR, all conventional plants
Intermediate storage for spent fuel elements	AVR, THTR, LWR (PWR, BWR)

6. Materials

The need for reliable material property data is an important requirement for the HTR and (V)HTR. The development of advanced HTR concepts requires an understanding of material behaviour plus data information under representative reactor operating conditions for the main HTR components important to safety and feasibility. The following sections provide the position on materials development issues for the HTR, making use of information from previous projects (such as those in Germany, the United Kingdom and the United States) and more recently developed information from R & D projects managed within the European Commission's fifth (Martin-Bermejo, et al., 2001), sixth (Raphael) and seventh (Archer) framework programmes. For consistency the materials issues and available information are discussed under similar headings to those listed in the previous section on components.

6.1. Primary system and primary enclosure

The primary system components are largely metallic (e.g. reactor pressure vessel — RPV), except for those of the reactor core, which are constructed using graphite and composite materials (used for straps etc.). The components covered here are as follows:

- the reactor pressure vessel together with the inner metallic and graphite structures, the shutdown systems, the fuel-handling system and measurement installations;
- the steam generator vessel, which contains the steam generator bundle and the helium circulator, including the drive;
- the connecting vessel, which contains the hot gas duct;
- the inner concrete cell, which contains the surface cooler.

The non-metallic materials for the core are discussed in the next section.

Materials issues for the reactor pressure vessel, the steam generator vessel and the connecting vessel which use a similar material for the pressure boundary (depending on the temperature) are discussed here. For the HTR the LWR materials technology provides a firm basis. For the VHTR a stronger material capable of operating at higher temperatures is needed. Such a material (Mod 9Cr 1Mo steel) has been investigated in the HTR-M & M1 (Buckthorpe, 2004) and Raphael projects (Buckthorpe, et al., 2008).

For the HTR RPV the design pressures and internal diameters fall within a relatively narrow range. This is because of the constraints imposed by requirements for passive heat removal under 'loss of circulation' or 'loss of coolant' scenarios and the requirement to meet the allowable stress levels in various design codes. As a result two types of material are used, depending on whether the temperature of the pressure boundary under normal operation or design conditions exceeds the limit for LWR/PWR pressure vessel operation. Different ferritic materials have been used for the RPV in both current and past test reactor systems. Comparisons between material types and between grades of the same material suggest the following materials are possible:

- various grades of 2-1/4 Cr-1Mo steel (ASME Grade 22 Class 1, the normalised or quenched and tempered grades of RCC-MR);
- Mn-Ni-Mo steel (PWR grades);
- ASME Grade 91 and RCC-MR mod 9Cr-1MoVNb.

Comparisons of tensile and creep data for matching grades indicate that there are differences in the minimum stress to rupture (Sr) and the primary stress intensity (St) design values for these materials, particularly for modified 9Cr1Mo steel, which exhibits great strength at elevated temperatures (see Figure 57). There is also a need for long-term creep data at moderate creep temperatures (425-500 °C) to confirm long-term values of Sr and St for both the 2-1/4 Cr-1Mo and modified 9Cr-1Mo types of steel, particularly if these are to be used for the pressure boundary.

In China, silicon killed C-Mn steel to ASME SA 516-70 has been specified for both the HTR-10 test reactor and future power reactors. This material is similar to the C-Mn steels used in the United Kingdom for the construction of both steel and concrete pressure vessels in CO_2-cooled reactors of the Magnox and AGR types. Long-term operating and/or design temperatures are limited to 370 °C. Similar limits apply to the SA 508 forgings used widely in LWR pressure vessels and proposed for the pebble-bed modular reactor (PBMR) in South Africa. It should be noted that the SA 508 specification covers a number of grades, some of which are not suitable for pressure vessels. In terms of the current designations in ASME specifications, 'SA 508 type' material is taken to mean SA 508 Grade 3 Class 1 or the equivalent material in plate form, SA 533 Type B Class 1. Equivalent European designations are 20MnMoNi 5 5 (Germany) and 15MND 5 or 18MND 5 (France). Except for HTR-10 the above systems have core inlet gas temperatures close to 550 °C, so the integrity of the RPV also depends on the performance of the insulation, which might be in the form of fibre blanket and/or stagnant/flowing layers of helium.

For the HTTR test reactor and larger power reactors of 450-600 MWth the RPV temperature is close to the core inlet temperature due to the passage of inlet (or intermediate) temperature helium to cool the inside surface of the vessel. Vessel temperatures are in the range 395-460 °C under normal operating conditions. The HTTR inlet temperature of 400 °C allows the use of 2-1/4 Cr-1Mo steel with a margin of about 25 % on allowable stress and about 40 °C on temperature. Modified 9Cr1Mo steel has also been specified for both large and small reactors with the beltline region of the vessel running at the core inlet temperature. This material has not yet been qualified for pressure vessel use according to most design codes. Work has however been carried out within the European framework programme Raphael (Buckthorpe, et al., 2008) to investigate the issues connected with material qualification for RPV application, including the effects of irradiation and environment with a specific thick section (150 mm) welded plate manufactured for testing.

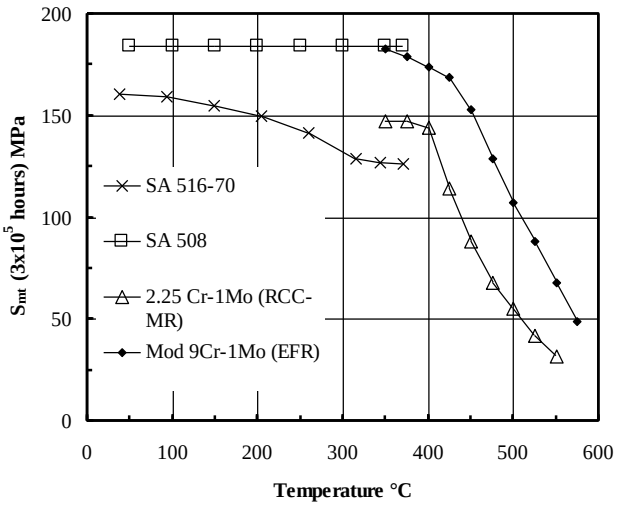

Figure 57: Vessel steels — comparison of allowable strengths

For an RPV application the fabrication and qualification of the vessel steel material has to be extremely thorough. Investigations have to be carried out in a very measured way. Issues that should be addressed include areas such as weld strength, manufacturing and adherence to design codes and procedures. These three areas are addressed briefly below.

Weld strength

The main concerns for the VHTR RPV are in the vicinity of the welds. The welds carry an additional requirement to satisfy the safety analysis methodology and safety studies (defect location and defect size), and have to be assessed from the point of view of non-destructive examination and potential for failure or leakage.

The main damage mechanisms to be addressed are fracture, fatigue and creep-fatigue. These have to be evaluated from an initiation aspect and for crack growth of defects under fluctuating thermal and mechanical loads. The potential effects of the environment (temperature, irradiation, ageing) all have to be taken into account. The important issues to address are toughness and creep behaviour under as-fabricated and simulated end-of-life conditions. This is to provide an understanding of the welding processes, weld metals and post-weld heat treatment required for thick welds and weld factors to be applied on the base material properties. The strength issues for HTR and VHTR vessels are summarised in Table 26 below:

Table 26: Qualification issues for HTR/VHTR reactor pressure vessel

LWR vessel steel (HTR temperatures)	Mod 9Cr 1Mo steel (VHTR temperatures)
LWR experience provides filler materials. Toughness properties well matched. Irradiation embrittlement less than 1dpa as for LWR- low P and Cu. Thermal ageing embrittlement — most	No previous experience on thick section RPV welds. Short term strength — HAZ; long term strength by Type IV cracking. Irradiation embrittlement — increases with

likely in the HAZ — only for transients at higher temperatures (10s to 100s of hours). Carburisation/corrosion — HTR gas chemistry.	lower temperature — no data on welds. Thermal aging embrittlement — operation above 450 °C — no data on welds. Carburisation/corrosion — HTR gas chemistry.

Other sensitive zones that are important are areas that feature thicker sections (potential for reduced properties and strength), hotspots and regions important from a functionality point of view. This includes the flange area and belt line, which have to satisfy primary and secondary stress-limit requirements and progressive deformation mechanisms.

The HTR and VHTR helium gas chemistry is dominated by the impurities H_2, H_2O, CO, CO_2 and CH_4 that exist within the gas. Low concentrations of H_2O and H_2 are produced by leakage and/or desorption from both metal surfaces and graphite. CO, CO_2 and CH_4 may be produced by coolant/graphite reactions at high temperatures.

Design codes usually instruct the designer to take into consideration the effects of corrosion without specifying in detail how this should be done. In practice two measures are usually adopted.

- An allowance for metal losses over its lifetime is added to the minimum design thickness of a pressure vessel.
- Fatigue and creep-fatigue damage calculations made with design data include allowances for data scatter, ‘mild’ (oxidising) environments and the characteristics of typical pressure vessel surfaces. Additional margins are necessary only where the environment has different and/or more severe effects on fatigue and creep by carburising the exposed surfaces or by producing intergranular oxidation to a significant depth.

The chemical attack from the impurities within the helium is temperature dependent, and its effects have to be checked at all operating temperatures where the material is expected to experience a significant period of operating time. Depending on the partial pressure of the impurities the resulting atmosphere can either be oxidising, carburising or decarburising, with damage either at the surface or diffusing to significant depths in the metallic matrices (internal oxidation or carburisation or decarburisation) which may result in a loss of mechanical properties. Phase diagrams (Figure 58) can be used to determine the neutrality of the chemical activity and to determine whether compatibility issues are likely to have a strong impact on material behaviour and performance.

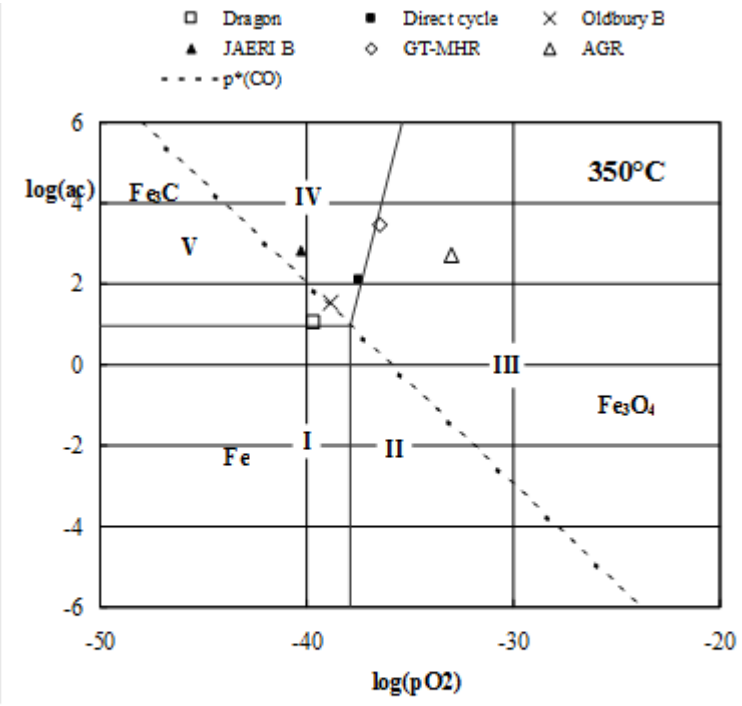

Regions I and II: Severe decarburisation

Region III: Protective oxidation plus slight carburisation

Region IV: Carburisation; Region V: De-carburisation

Figure 58: Phase diagram for Fe at 350 °C

The RPV in the HTR will be irradiated with neutrons, which cause damage within the material and will result in a change in mechanical behaviour of the material and in the welds. Depending on the operating conditions of the HTR and (V)HTR, this irradiation can take place at temperatures between 120 °C and 450 °C, where 120 °C is considered representative of the lower temperature of the LWR material option and 375 °C the lower temperature of the Mod 9Cr 1Mo steel material option, with 450 °C the upper end of the Mod 9Cr 1Mo steel material temperature operating window.

The effects of irradiation on the toughness of LWR steels have been studied extensively and reviews have been undertaken as part of the work programme of the CEC-supported AMES network (Ageing, Materials Evaluation and Studies), where CEC is the abbreviation of “Commission for Environmental Cooperation”. Reports from this group, along with publications in the open literature, are highly relevant to the materials and operating conditions of LWR steel HTR vessels given that LWR vessels operate at 250-300 °C with similar end-of-life fluences to HTR vessels.

The major effect in these materials is an increase in the ductile brittle transition temperature (DBTT) and ΔDBTT due to the combined effects of matrix hardening and grain-boundary weakening associated mainly with the residual elements P and Cu. Various empirical relationships between composition, fluence and ΔDBTT have been proposed on the basis of results from test reactors and LWR surveillance programmes (Western PWRs and Russian LWRs). Common features of the formulae are the importance of the Cu and P contents as well as synergistic effects of the Ni content. The range of behaviour predicted for Mn-Ni-Mo, 2-3/4 Cr-Mo-V and 2-1/4 Cr-Ni-Mo-V pressure vessel steels is shown in Figure 59. The upper bounds correspond to steels used in the 1960s and 1970s which had relatively high levels of either Cu (PWR steels) or P (WWER steels). Specifications for

modern pressure vessel steels and weld metal contain special limits on Cu and P for material to be used in the most highly irradiated (beltline) region of LWRs:

- 0.008 %P and 0.08 % Cu in RCC-M;
- 0.012 %P and 0.12 % Cu in the ASME Code;
- 0.010 % P and 0.08 % Cu in WWER rules.

The above limits can be met comfortably using modern steelmaking techniques. They ensure that the predicted end of life ΔDBTT for a LWR vessel operating at 250-300 °C is small in relation to the data scatter.

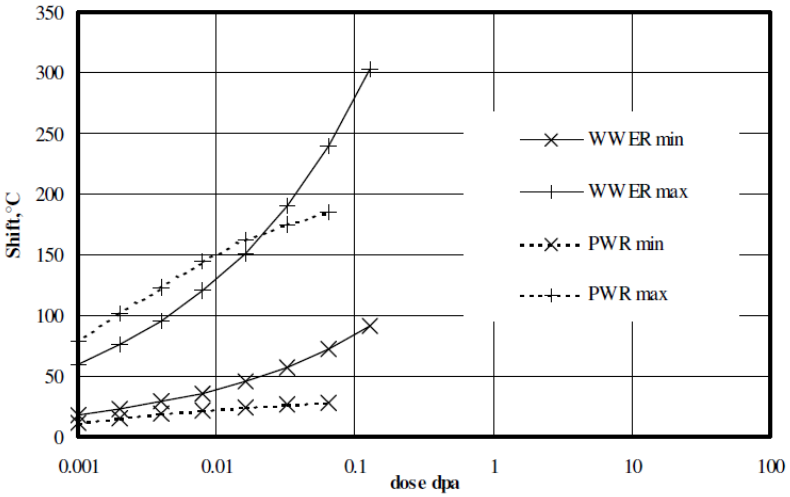

Figure 59: PWR and WWER regulatory guides — shift in DBTT with dpa dose

Material ageing describes a continuous time or operational degradation of the material due to operating condition, (excluding 'design' and 'beyond design basis' accidents). As a result of ageing degradation the plant or component state could vary through the operating life.

Material ageing or thermal ageing embrittlement (TAE), sometimes called temper embrittlement (TE), may involve hardening due to precipitation of carbides and intermetallic compounds, along with grain-boundary segregation of trace elements (P, Sn, As, Sb). The term 'temper embrittlement' came into use because slow cooling after tempering was sufficient to embrittle steels with relatively high levels of the trace elements. More severe effects could be induced by step cooling from the tempering temperature followed by holding at approximately 450 °C and/or slow (furnace) cooling to room temperature. TE is not usually a problem in modern steels with very low levels of P and the other trace elements. TAE can however occur after long-term service at temperatures in the 350-550 °C range. The severity of the effect depends on a number of factors including:

- the prior austenite grain size of the material;
- the concentration and distribution of the trace elements (P, Sn, As, Sb);
- the cooling cycle after tempering;
- time at temperature(s) within the critical range;
- the property considered.

The base materials and weld metals for both the LWR steel and Mod 9Cr 1Mo steel vessel options normally have very fine grain sizes. The most likely embrittlement location is therefore the coarse-grained heat-affected zone. Because the LWR-cooled vessels operate at temperatures below the embrittlement range of the material, it usually can only occur for this material during transients

involving exposure to higher temperatures for tens or hundreds of hours. Warm (non-cooled) vessels (Mod 9Cr 1Mo steel) can operate at higher temperature and in the ageing temperature range throughout their lifetime, and so for the Mod. 9Cr 1Mo steel vessel ageing can be more important to integrity. The approximate duration after which ageing effects can be significant can be in the order of 20-30 years, and its predictability depends upon technical understanding of the conditions and the quality of the operational experience data. It predictability is also dependent on the ability to monitor the condition of the component and to model it. For Mod 9 Cr 1 Mo steel investigations have been carried out in the HTR-M & M1 projects (Buckthorpe, 2006) and Raphael (Buckthorpe, et al., 2010) on both irradiation and ageing effects with specific experiments performed.

Manufacturing

The technology developed for building LWR vessels from heavy section ring forgings provides a sound basis for manufacture covering:

- procurement specifications for forgings;
- welding procedures and filler metal selection;
- manufacturing sequences including weld examinations and post-weld heat treatment.

HTR vessel wall thicknesses are within the PWR range but the diameters of HTR vessels (6-8.5 m) are much greater than for PWR (up to 4.5 m). There is therefore a need to establish a capability to produce forged parts of the required dimensions with the required mechanical properties. If this cannot be done it will be necessary to manufacture the vessel from formed plates. In this case there are implications for both design and manufacturing. The most important design consideration is the introduction of axial welds with higher cross-weld stresses. Manufacturing requirements include provision of procurement specifications, forming facilities and forming procedures for heavy plates. On-site welding and post-weld heat treatment (PWHT) of the reactor vessel–cross vessel–PCS vessel assembly can introduce a requirement that does not arise in LWR manufacture:

- a validated local heat treatment procedures for Mn-Ni-Mo steel;
- a site heat treatment facility that can accommodate the whole reactor vessel–cross vessel–PCS vessel assembly.

The above considerations also apply to vessels using 2-1/4 Cr-1Mo steel. There is manufacturing experience in France for one grade and it can be extended to other grades of 2-1/4 Cr-1Mo steel. Appropriate filler metals exist but the properties of welded joints require evaluation. Russian experience of WWER-1000 vessel manufacture in 2-1/4 Cr-Ni-Mo-V steel is also relevant. The PWHT temperature for 2-1/4 Cr-1Mo steel is 630-660 °C compared with 620 °C for Mn-Ni-Mo steel. This difference may have a significant effect on cost, particularly in the case of a site PWHT facility.

In the case of modified 9Cr-1Mo steel the above-noted manufacturing problems introduce greater difficulties, as detailed below.

- A lower limit on the mass of single cast or ingot for high-Cr steel compared with 2¼Cr-1Mo steel.
- Difficulties in selecting filler metals to achieve the required levels of resistance to hot cracking, high toughness at 0 °C and creep strength.

- A much higher PWHT temperature (> 750 °C) compared with 2¼Cr-1Mo steel (630-660 °C). Local heat treatment at > 750 °C of welds in the RPV/cross vessel assembly would be particularly difficult to validate.
- The design temperature of the PCS vessel for GT-MHR is 150 °C compared with 440 °C for the RPV and cross vessel. It is possible therefore to specify C-Mn, Mn-Ni-Mo or 2¼Cr-1Mo steel for the PCS vessel. A transition joint between modified 9Cr-1Mo steel and any one of the other candidate material types would involve a mismatch of 100-150 °C in their PWHT temperatures. It might be necessary in this case to validate the use of a filler metal such as Alloy 82 and a 'buttering' technique to permit separate PWHT at temperatures appropriate to each base material prior to completion of the closure weld.

Manufacturing issues for HTR and VHTR vessels are summarised below in Table 27:

Table 27: Qualification issues for HTR/VHTR reactor pressure vessel

LWR vessel steel (HTR temperatures)	Mod 9Cr 1Mo steel (VHTR temperatures)
Technology for LWR provides a sound basis: • procurement specifications, • welding procedures, • manufacturing sequences and examinations. Larger-diameter forgings than LWR. On-site welding produces additional requirements — on-site heat treatments.	No previous similar experience in manufacture with this material. Selection of filler material. Higher PWHT temperatures (> 750 °C). Possibility of needing transition welds if cross vessel is of a different material. Potential for PWHT mismatch of 100-150 °C.

Codes and standards

Pressure vessel design and construction codes provide mandatory rules for calculation of material thickness, allowable materials for construction, welding, NDE, testing and regulatory documentation. The pressure vessel code(s) applicable to the location of installation must be followed for mechanical design and construction. There are several commonly accepted design codes that can and have been used for the metallic materials of the primary circuit:

- ASME BPVC — American Society of Mechanical Engineers, Boiler and Pressure Vessel Code;
- (KTA3221, 2015) 'Metallische HTR Komponenten' Parts 1 to 3 (Draft);
- (KTA3201, 2015) Light-Water Reactors;
- (EN13445, 2012) EN 13445 — the European standard, harmonised with the pressure equipment directive (PED);
- (AFCEN, 2012) RCC-MRx — design and construction rules for mechanical components of nuclear installations.

Within such codes key damage mechanisms are addressed:

- DM 1. Instantaneous excessive deformation;
- DM 2. Delayed excessive deformation;

- DM 3. Ratcheting;
- DM 4. Fatigue;
- DM 5. Creep-fatigue.

DMs 1 and 2 are of major significance to the design of pressure vessels because they lead directly to the primary stress limits Sm (instantaneous limit based on tensile properties) and St (delayed limit based on creep properties). The crossover temperature θ_{co} above which St applies is an important parameter for RPV materials selection since it is necessary to show that time-dependent effects are negligible. For the pressure vessel structures this means that normal operating temperatures must be below the negligible creep limit of the material. The areas relevant to DMs 3-5 are identified below.

- Parts of the vessel where wall temperatures are highest may be subject to creep damage.
- Nozzles and openings including the cross-vessel connection and penetrations in the hemispherical bottom and lid may be subject to fatigue.
- The internal support attachments may be subject to fatigue and ratcheting.
- The RPV and PCU support to foundation may be subject to fatigue with mean stress effects. The designs of the two supports need to be compatible.
- Welds. Results from thick section welds at such temperatures are very scarce and such data are very important not only for understanding weld behaviour but also for confirming a maximum normal operating temperature (and hence, for non-cooled designs, the gas inlet temperature) for vessel operation.

Section III, Division 1, Subsection NB of the ASME Code is fully applicable to the design of LWR-type HTR pressure vessels operating at up to 371 °C and the RCC-M Code provides a European set of rules for these vessels. Both ASME III NB and RCC-M incorporate extensive LWR experience and are easily available. They can be regarded as having equivalent status from the standpoint of an HTR vessel design and validation approach. The ASME III Division 1, Subsection NH and the RCC-MR rules provide limited coverage for HTR vessels made from 2 ¼ Cr-1Mo steel and Mod 9Cr 1Mo steel.

Codes and standards issues for HTR and VHTR vessels are summarised below in Table 28.

Table 28: Codes and standards issues for HTR/VHTR reactor pressure vessel

LWR vessel steel (HTR temperatures)	Mod 9Cr 1Mo steel (VHTR temperatures)
Data and experience of LWR provides sound basis. Property data plus fracture and fatigue crack growth information. ASME/RCC-M Code — exclude effect of environment — but procedures substantiated by years of successful operation in service.	No previous service experience. Property data available — RCC-MR design rules — some gaps Long term data required at 425-500 °C. Experimental programmes required for irradiation and thermal ageing. P91 approved code material for ASME subsection NH.

6.2. Reactor core

The graphite core is a key component that affects the safety and operability of the reactor. It provides structural support, coolant channels, moderation and shielding while operating in a high-temperature helium environment. Its performance is critically dependent on the graphite properties, which are irradiation dependent. The final choice of graphite for the core should be based on a number of factors, although the most important will be the effects of fast neutron irradiation on its properties up to the peak doses envisaged. Given the best graphite available, it is the task of the core designer to produce a design that will operate safely over the design life of the reactor. The most important considerations are component integrity and changes in core geometry, both of which are affected by the dimensional change (see Figure 60).

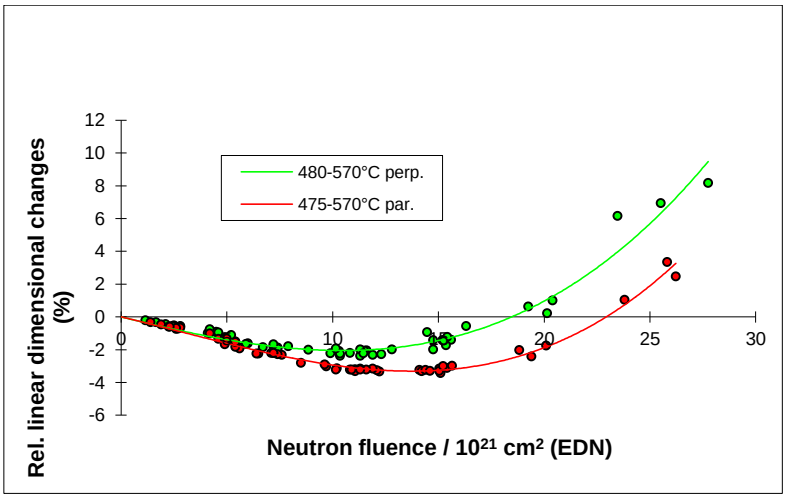

Figure 60: Effect of irradiation on dimensional change

Many of the graphites used in previous core designs are no longer available and there has been a serious decline in the ability to manufacture nuclear-grade graphite in large quantities since the 1980s. The main questions concern the long-term availability of the coke and manufacturing procedure. Current HTGR projects — HTTR (Japan) and HTR-10 (China) — use a Japanese graphite called IG110, which, with its high strength, is suitable for exchangeable core components where low fast neutron fluences are applicable.

Much of the available irradiated materials data are obtained from various materials test reactors, and often it is not possible to complete an irradiated materials property database for a particular graphite in advance of a reactor's design and construction phases. In such cases design databases can be used to arrive at the required information, developed from previously irradiated graphites of similar microstructure and an understanding of irradiation damage in the polycrystalline graphites. R & D activities have been undertaken in a number of countries to investigate graphite properties.

Two of the most significant experimental programmes in the past were for the European Dragon HTR programme and the German HTR programme. Unfortunately most of the data obtained by other countries are confidential and so far have not been published in open literature. Work performed on the review and collection of graphite properties considers the accessible information on the IAEA database, internal information and published information at seminars and conferences. The IAEA database was established to help the development of International programmes on graphite-

moderated reactors, assist safety authorities in assessment of safety aspects and serve as a source of scientific information for nuclear and non-nuclear technology.

The data relevant to the irradiation temperature and neutron fluence domains for new HTRs will largely come from the new tests and be built up for each graphite grade and sample orientation, and contain the appropriate details of the graphite, i.e. grade, manufacturer, coke source, grain size and manufacturing method. These data are being collated into a set format for use and development representing the experimental data on the new graphites in the form of recommended 'design curves' for each required material property.

For nuclear applications, the graphite has to be as free as possible from impurities. Most of the impurities present will become activated during the operating life of the reactor, which will give rise to operational problems, as well as decommissioning and final disposal problems. Most impurities, however, are volatile and so disappear during graphitisation. To remove as much of the remainder as possible, halogens are added generally during graphitisation to aid the conversion of metal impurities, and boron particularly, to their more volatile halides. (Extremely low boron levels are important from a reactor physics point of view, as it is a very strong neutron absorber.)

Table 29: Typical range of graphite grades in an irradiation experiment

Manufacturer	Grade	Coke	Grain size	Process	Classification
GrafTech	PCEA	Petroleum	Medium	Extrusion	Major
	PPEA	Pitch	Medium	Extrusion	Major
	PCIB-SFG	Petroleum	Super-fine	Iso-moulding	Minor
	LPEB/BAN	Petroleum	Medium	Extrusion	Minor
SGL	NBG-10	Pitch	Medium	Extrusion	Major
	NBG-25	Petroleum	Fine	Iso-moulding	Minor
	NBG-18	Pitch	Medium	Vibro-moulding	Major
	NBG-17	Pitch	Medium	Vibro-moulding	Minor
Toyo Tanso	IG-110	Petroleum	Fine	Iso-moulding	Minor
	IG-430	Pitch	Fine	Iso-moulding	Minor

The choice of graphite for the reactor core is limited to those that are currently recommended and available from manufacturers (see Table 29). Discussions with graphite manufactures will establish suitable graphites produced using a range of methods (extruded, iso-moulded and viro-moulded graphites), which can be investigated using a graphite irradiation programme. Such a programme has been carried out in Europe (over the 2000-2015 period) within EU framework programmes **(Martin-Bermejo, et al., 2001) (Raphael) (Archer)** to provide results over a low, medium and high dose levels suitable for both the prismatic and pebble-bed HTR designs. The experiments examine material behaviour at two nominal temperatures (750 °C and 950 °C) relevant to the HTR and VHTR cores (see

Figure 61). A further irradiation programme can be performed (under load) including the effects of creep **(Ratton, 2005)**, but these types of experiment are significantly more expensive and should be considered to be a second step after general selection. Such irradiation programmes performed on selected graphites can be used to determine the variations in their physical and mechanical properties over low/medium/high irradiation doses and used for design.

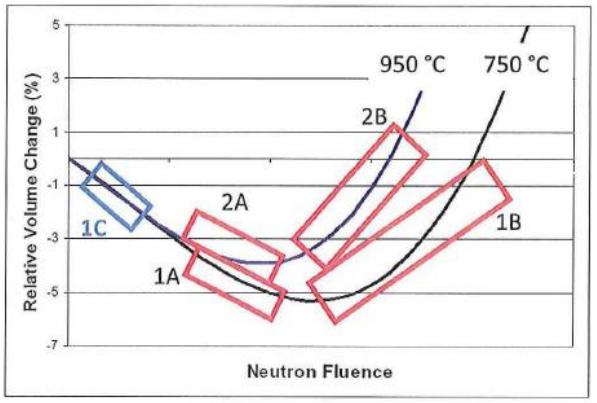

Innograph-1A 750 °C, low/medium dose (FP5)
Innograph-1B 750 °C, high dose (Raphael)
Innograph-2A 950 °C, low/medium dose (Raphael)
Innograph-2B 950 °C, high dose (Raphael)
Innograph-1C 750 °C, low dose (Archer)

Figure 61: Schematic overview of the graphite irradiation experiments

For the experiments above the focus has been on the determination of engineering design curves which can be used for the core design process:

- dimensional change (DC)
- dynamic Young's modulus (DYM)
- coefficient of thermal expansion (CTE)
- thermal conductivity/diffusivity (TC/TD)

The effects of irradiation can change all these properties and it is important to have representative curves for design. There can also be significant differences in the with-grain (WG) and against-grain (AG) directions, because of the non-isotropic nature of the graphite material. A typical curve for dynamic modulus variation with irradiation dose is shown in Figure 62 below. The DYM data show the expected increase at lower dose to a plateau, followed by a further increase at medium dose and finally a decrease at high dose. The CTE decreases with irradiation dose to a stable plateau at medium dose and a slight increase at high dose. The TD and TC values typically fall rapidly at low dose and reach a plateau at medium dose.

Since investigations into the effects of neutron irradiation rely heavily on testing (such as that described above), and given that suitable facilities for such testing are both scarce and expensive to use and that manufacturers are continually developing and offering new graphites for such applications, in the longer term it is also important to develop an alternative modelling approach (in parallel with the tests) that will both facilitate the longer-term development of graphites and minimise and reduce the extent and requirement for future irradiation testing. One such technique uses X-ray tomography in conjunction with model simulations to predict behaviour which can be applied to both non-irradiated and irradiated samples from experiments (Halli, 2004). Such investigations can indicate that irradiation-induced microstructural (pore) changes can be detected and can give confidence that they can be used to gain further insight into the microstructural changes within the graphite and their predictive models.

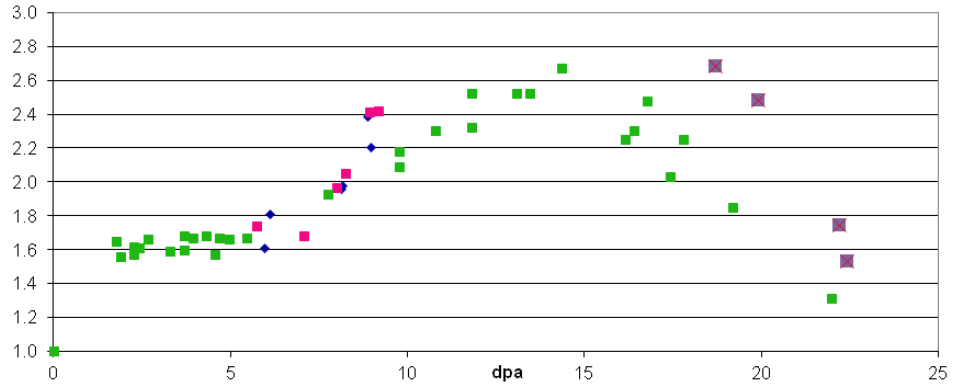

Figure 62: Change in E/Eo with irradiation dose for graphite

Oxidation of the graphite also takes place during normal operation of the HTR core due to impurities in the cooling gases. In such cases however the oxidation rate of the graphite is extremely low. Tests in oxygen and air at temperatures up to 1 500 °C (accident and normal operation) to establish graphite property requirements and specifications can provide useful information on graphite behaviour, with the rapid oxidation data derived (Kuhn, et al., 2003) providing information on reactivity for the graphites investigated. Such tests can identify differences between grades and between the inner and outer parts of a block which can be explained by density and impurity differences between centre and edge specimens in the block.

Work has been carried out in Germany to develop SiC coatings for graphite materials to protect the graphite against oxidation from air or steam ingress under severe accidents. Investigations were done using the matrix German graphite A3-3 to measure the corrosion rate for temperatures up to 1 200 °C, and on coated pebbles using different graphites. Such tests involve corrosion tests, irradiation tests and PIE tests to assess coating integrity and different coating methods (chemical vapour deposition (CVD), paste siliconisation (PS)). Although the original objective, to develop a coating for A3-3 graphite, was not achieved, these results gave a very positive indicator and provide a useful basis for further investigation.

Other issues that need to be addressed are the tribological performance, like on like for the core; graphite on metal like on like (Core/Core); and graphite on metal for the core against internals. Such investigations need to be carried out at pressure and under load for accident and normal operating conditions. Results from these investigations are summarised in Buckthorpe (Buckthorpe, et al., 2008).

In summary, graphite material issues and requirements for the HTR and VHTR core can be summarised as follows.

Table 30: Graphite core material issues and requirements

Graphite core (HTR and VHTR temperatures)
Graphite impurity levels and disposal. Changes in physical and mechanical properties with

irradiation dose.
Investigations under load to determine properties with irradiation creep.
Increase and saturate the data range required for design.
Oxidation under normal operation and accident conditions to establish corrosion resistance and protection.
Tribology tests and simulations.
Link between testing behaviour and design, establishing design curves representative of the physical property variation with irradiation dose and temperature.
Graphite microstructural modelling and simulation.

6.3. Shutdown system

For the control rod, which compensates for fuel burnup and power variation reactivity effects, used to control the reactor operation under fast normal operating modes and to shut down the reactor system, available metallic materials (such as Alloy 800H) are prime candidates. Material property data at elevated temperature are available in codes such as ASME to enable a metallic arrangement to be designed and operated. Such a material can be employed in the HTR but is considered to be at its operational limit for the VHTR. For the VHTR, new carbon fibre reinforced materials can be considered as alternatives. Such materials are expected to give potential for improved reactivity control during shutdown and to allow the normal operating temperatures of future reactors to be increased.

The characteristics of composites are usually governed by their individual base constituents. This is the main advantage of employing composites over conventional materials, having that 'unique' mix of different properties delivered by its fibres and matrix components. This provides the potential for composites to deal with severe nuclear environments. Most composites for industrial use are based on polymeric matrices, i.e. thermosets and thermoplastics. These are usually reinforced with aligned ceramic fibres, such as carbon. Aligned reinforced composites or 1D reinforced composites have two distinct orientations: parallel to the fibre reinforcements (z-axis) and transverse to the fibre reinforcements (x- and y-axes). The orientations parallel to the fibres possess superior properties.

The use of carbon-carbon composite and carbon fibre material composites for control rods (Figure 63) is not, however, a proven technology. Consultation with manufacturers on possible candidate materials is important and necessary. The material sits permanently in a neutron field accumulating fast fluences that change its structure and properties. The selection of the material is very important. Manufacture involves specialised (and expensive) processing. Certain fabrication parameters (e.g. fibre and yarn properties, matrix bonding of fibres, porosity, architecture, graphitisation) have a strong influence on mechanical properties. The mechanical properties of the composites are however remarkably stable up to temperatures of 2 000 °C. As with other carbon-based materials (and graphite), significant changes in the physical and mechanical properties occur due to the effect of irradiation and temperature, and material investigations as discussed for the graphite core are considered important for the validation of such materials for this application.

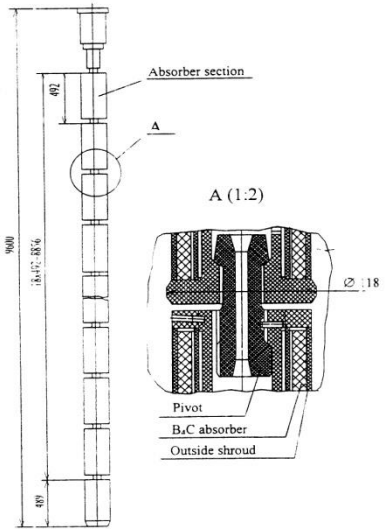

Figure 63: An arrangement for a carbon-fibre composite control rod

In summary, control rod material issues and requirements for the HTR and VHTR can be summarised as follows.

Table 31: Control rod material issues and requirements for the HTR and VHTR

Control rod (HTR and VHTR temperatures)
Alloy 800H a candidate metallic material for HTR application. Material property data at elevated temperature are available in codes such as ASME. The use of carbon-carbon (C/C) composite and carbon fibre material composites is possible for VHTR conditions, but this is not a proven technology. Consultation with manufacturers on possible candidate C/C materials is needed. Fast fluences change its structure and properties as with graphite. Issues associated with graphite core will need to be investigated if a C/C or fibre-reinforced composite is to be used (e.g. impurity levels, oxidation and corrosion, property changes with irradiation, modelling).

6.4. Hot gas duct

The hot gas duct is used to transfer the hot helium from the reactor core to the power conversion circuit components such as heat exchangers and turbines (in the case of the direct cycle). The duct is usually insulated to increase efficiency and limit thermal loads.

The lifetime of the hot gas ducts is the same as that of the reactor with no repairs or maintenance required with the option to repair or replace the component reserved for unforeseen circumstances. Materials that could be considered include high-strength alloys such as Alloy 800H, ODS materials and composites. Some investigations have been carried out in the past using such materials and these need to be extended, taking full advantage of new and potential material developments.

The hot gas duct can be of horizontal or vertical design, usually of coaxial flow (hot on inside, cold on the outside). Temperatures are in the 465-480 °C range on the outside and the 680-850 °C range on the inside. A design was recommended for the hot gas duct and the thermal insulation which could be used at the turbine inlet (straight duct configuration). Thermomechanical analysis of such a concept has been performed as part of the past German experience and within the fifth framework programme project HTR-E (Buckthorpe, et al., 2008). For the design, fibre packed insulation is used between the inner liner and the outer support pipe in the region of the thermo-sleeves. Wrapped fibre insulation is used between the outer liner and the depressurisation gap liner.

The metallic materials used are classed as materials for elevated temperatures with sufficient tensile strength and creep resistance in the < 550 °C temperature range. For the insulation, fibrous materials consisting of at least Al2O3 can be used at temperatures above 600 °C, with mixed-oxide fibres at lower temperatures and mineral insulation below 400 °C.

The design rules used are those important to safety, with initial sizing based on international rules and regulations (e.g. in Germany AD specifications, technical rules for steam boilers). Stress, deformation and fatigue analyses can be performed in accordance with the ASME Code and KTA Safety Standards using approaches consistent with the ASME Code.

In summary, hot gas duct material issues and requirements for the HTR and VHTR can be summarised as follows.

Table 32: Hot gas duct material issues and requirements for the HTR and VHTR

Hot gas duct (HTR and VHTR temperatures)
Alloy 800H a candidate metallic material for HTR application. Material property data at elevated temperature are available in codes such as ASME. Helium: impurities, potential for carburisation/decarburisation possible above 700 °C. Radiation issues (negligible); ageing issues (possible). The use of carbon-carbon (C/C) composite and carbon fibre material composites and ceramics is possible for VHTR conditions, but this is not a proven technology. Consultation with manufacturers on possible candidate C/C and insulation materials is needed.

6.5. Circulator

Gas circulation in HTR and VHTR is required for a number of different purposes (e.g. turbo-compressors/turbo-generators for direct cycle helium gas turbine plants, start-up blower system for the turbo compressor, operational coolant gas circulation for heat transfer to the heat exchangers, coolant gas blowers in intermediate helium circuits, etc.). Turbo compressors and turbo generators generally attract most attention within R & D programmes, however other applications for blowers and compressors are equally important for the functionality and availability of the complete reactor system.

For the HTR with indirect cycles, the design of the gas circulator, the impeller, the electric motor and the bearings (e.g. electromagnetic bearings + catcher bearings and/or permanent magnetic bearings) is important under normal operation and also under external loads from the process transients. For

the power rotor, benefit can be taken from the materials investigations on the turbine (see below). For the 600 MWth VHTR a blower power of 10 to 15 MW is required, which is much higher than in former HTRs (maximum 4 MW).

A study of former designs (Buckthorpe, et al., 2008), including bearings, lubrication, control and drive, showed in many cases that the technology is based on the broad experience with CO_2 circulators from the Magnox and AGR plants in the United Kingdom and in France. In most cases, one-stage radial circulators with an overhung wheel have been applied, and the overall experience is very good with high availability.

With regard to the selection of materials, those used for the IHX (such as Alloy 800H for HTR) should provide necessary creep strength for the casing. The material IN 607 has been established for steam turbine rotors, and this should represent a suitable impeller material. Other possible materials are Hastalloy, IN 6I7, IN 625 or Haynes 230 for the casing and IN 638 or IN 608 for the centrifugal impeller. There are more materials options for smaller discs. Temperatures in the vicinity of the circulator are expected to be < 700 °C, hence corrosion may not be a problem. The final materials are most likely to be influenced by the manufacturer's choice.

The design approach and information on materials behaviour is likely to be commercial and held by the gas turbine manufacturers. The ASME Code case for Ni-based alloys is in progress and should provide an elevated temperature procedure for relevant materials. For a gas temperature of 465 °C, non-cooled options should be acceptable. Coatings are also possible for protection against activation (cobalt). For the disc, there may be a limit on the diameter because of forging capacity. For the large centrifugal impeller there may be a need to use casting or a more advanced sintering/hipping process. The use of casting/hipping processes for the impeller as an alternative to casting may require the development of specific standards.

In summary, circulator material issues and requirements for the HTR and VHTR can be summarised as follows in Table 33.

Table 33: Circulator material issues and requirements for the HTR and VHTR

Circulator (HTR and VHTR temperatures)
Materials used for IHX should provide necessary creep strength for the casing. Alloy 800H a candidate metallic material for HTR application. Also Hastalloy, IN 6I7, IN 625 or Haynes 230. Materials property data at elevated temperature for Alloy 800H are available in codes such as ASME. KTA has extensive property data for Alloy 617. IN 607 established for steam turbine rotors and impellers. Greater number of materials options for smaller discs. Temperatures < 700 °C hence corrosion may not be problem. High-velocity impingement of dust and particles (possible). Radiation issues (negligible). Ageing issues (possible). For the disc there may be limit on the diameter because of forging capacity. For large the centrifugal impeller there may be a need to use casting. The alternative is more advanced sintering/hipping processes. Materials most likely influenced by manufacturer's choice.

6.6. Steam generator

Steam generator concepts are currently in use in several HTR demonstrators overseas. All seven constructed HTRs, including prototypes and the grid-connected THTR-300, deliver their heat to steam generators operating at temperatures significantly lower than the reactor's capabilities. Steam generators are also in use in the UK AGRs, which operate with gas outlet temperatures ~ 640°C.

Possible options for the SGU include the straight-tube and helical-tube designs. The helical-coil-tube-type steam generator was used in the THTR-300 (see Figure 64), which consisted of a shell and three tube bundles. The small bundle on the bottom of the steam generator (SG) provides the reheat section and, for manufacturing reasons, there are two high-pressure bundles above it that contain the superheater, evaporator and economiser. The thermal-expansion helical tubes are located on top of the steam generator. On the secondary side, water enters the helical tubes on top of the HP bundle. The water flow is downwards. First the water is preheated in the economiser, then evaporated and at last superheated before leaving the steam generator.

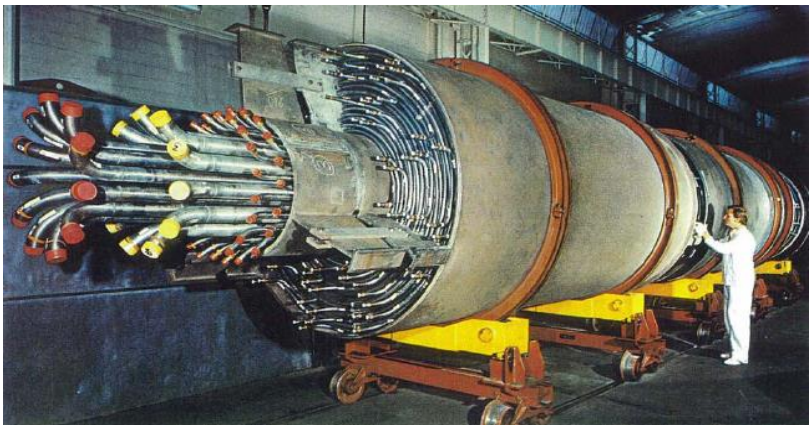

Figure 64: HTR cooler THTR 300

The use of appropriate materials and their data is an important issue, and the materials used in the superheater sections, which must withstand the highest temperatures and the target lifetimes of 500 000 hours, are of primary importance. The need to avoid stress-corrosion cracking has influenced material selection at lower temperatures, and the shell material is similarly required to withstand prolonged durations, while maintaining the pressure boundary due to its connection to the reactor vessel. For the THTR, Alloy 800H was selected for the helical coil material.

Within the Archer project (Archer) the helical design was selected for the HTR since this can accommodate thermal expansion more readily, and Alloy 800H was chosen as the tubing material. At VHTR temperatures an improved high-temperature-strength material would be needed, and Alloy 617 and Haynes 230 are considered good candidates for long operating periods (< 850 °C) and potential transients. Alloy 617 already has a very large database with numerous mechanical properties, and creep data measured in air and a helium atmosphere.

For the design the ASME Code is applicable and contains many of the material design information needs. The section ASME III-NH provides the material specification together with all requirements necessary for the material to be properly specified. This includes both ferrous (common steels) and non-ferrous materials, for example Alloy 800H tubes. Most of the temperature-dependent material properties (allowable stress, yield strength, modulus of elasticity, etc.) are listed. Of primary interest too are the location and stressing of any dissimilar metal welds (DWMs) which may arise when connecting the higher-strength Alloy 800H with a lower-cost carbon material such as SA-335 Grade P11 used at lower temperatures.

Over the past 40 years or so there has been much research on DMWs, examining such effects as

- carbon migration across the weld interface;
- diffusion of other metallic alloying elements;
- effect of post-weld heat treatments;
- effect of exposure at temperature;
- effect of oxidation/corrosion;
- consequent changes in mechanical properties at the microscopic scale and how this effects large-scale properties;
- selection of filler metals with a view to reducing thermal expansion mismatch.

Many problems have been overcome, but as temperatures have increased the associated mismatch in expansion possess an increased risk. In addition the manufacture will require many thousands of tube-to-tube welds and necessitate high-quality advanced manufacturing methods to produce and inspect welds on a routine basis by non-destructive testing.

At present the materials data requirements for the steam generator seem no more complex than for other HTR components. Since there is current experience in using similar technology elsewhere there seem to be no fundamental barriers with respect to materials for the successful development of steam generators for HTR applications

In summary, steam generator materials issues and requirements for the HTR and VHTR can be summarised as follows in Table 34.

Table 34: Steam Generator material issues and requirements for the HTR and VHTR

SGU (HTR and VHTR temperatures)
For the tube and plate designs the thick section requires development. Consistency of properties (midsection) is important. Issues of tribology in an inert helium environment. Requirement for coatings for resistance to fretting, etc. (vibration). Materials candidates: Alloy 800H and Alloy 617 identified by vendors as primary candidates for HTR application. Materials selection: creep rupture — use of tertiary creep for development of allowable; creep-fatigue could be more developed. Weldability: Alloy 800H has good capabilities, as does Alloy 617. Automated processes are available for manufacture. Alloy 230 welding possible but difficult, especially in thicker section. All candidates need precautions to avoid hot cracking. Corrosion depends on exact He coolant composition and temperature: possible degradation due to carburisation, decarburisation and oxidation.

Cold work can affect the creep properties of materials such as Alloy 617 and Haynes 230 leading to a reduction in strength. A suitable limit for manufacture should be defined.

6.7. Intermediate heat exchanger

The heat exchanger component is vital in any nuclear power plant, and particularly in process-heat or cogeneration applications (Groot, et al., 2013). Its compactness and efficiency has been highlighted to be of particular importance in the VHTR.

The intermediate heat exchanger (IHX) is perhaps the most critical part of the VHTR and HTR. Its development relies on selecting specific materials that can deal with high operating temperatures and pressure drops. The thermal, environmental and service life of the reactor makes selecting high-temperature materials a significant challenge, especially for the VHTR conditions (> 950 °C). Alloy 800H and Alloy 617 already have a very large database with numerous mechanical properties and creep data measured in air and a helium atmosphere and are regarded as a possible material for HTR conditions. For VHTR conditions established industrial materials (such as Alloy 617, Haynes 230, Hastalloy X, Hastalloy XR and Alloy 800H) are at or near their limit and new range of materials (oxide dispersion strength (ODS) alloys, ceramics) may have to be considered for development, however these require significant manufacturing advances before they are suitable for this application. The need for materials capable of tolerating very high temperatures is especially true when used with the iodine-sulphur hydrogen generation process.

The thermomechanical conditions of the IHX that affect material selection are as follows

- the normal operating temperatures range from 350 °C to 1 000 °C (maximum);
- the expected mechanical load is from the pressure, i.e. 1 to 10 MPa;
- impurities in the helium are a major concern for metals, since they can lead to environmentally induced degradation;
- ageing effects and embrittlement are important since they can affect performance, especially during thermal transients;
- welding and fabrication issues in relation to design.

Materials selection and optimisation for the once-through AGR boilers, for example, were uniquely influenced by corrosion considerations from both the primary and secondary water/steam environments, where a 250 000-hour design lifetime was required. There are four boilers in each reactor and each boiler comprises three once-through HP units and three reheater units, and in normal operation generates steam to drive the main turbine. These units have demonstrated proven control and reliability in service.

Tube-and-shell arrangement

The conventional form of IHX component is the tube-and-shell design, which is housed within a pressure vessel connected to the reactor vessel by a coaxial cross-duct. Its components are: the tube bundle; secondary-side headers; the primary gas circulator with its electric motor and cooler; and the primary-side gas baffles. The concept of a heat exchanger with an integrated circulator offers the

greatest protection to the primary circuit components and provides for the whole pressure boundary to be cooled by the primary coolant.

An important design principle of the IHX is that the tube bundle had to be free to expand within the shell to minimise stresses within the tubes and the tube plates. A further design principle is that neither hot primary nor hot secondary gas should come into contact with the primary pressure boundary. To comply with the first principle, the tube bundle and its headers can be designed to be fully floating with respect to the IHX shell. The second principle can be fulfilled by using a system of internal baffles and engineered leak paths to ensure that the entire internal surface of the shell is cooled by primary coolant at the reactor inlet temperature.

Compact arrangement

The effective transfer of heat is an important requirement for the HTR. For higher temperature exchanges, the gas-to-gas IHX is likely to offer a cheaper, more robust and compact solution. Temperatures are close to the core outlet temperature for most of its lifetime, which requires considerable design development to achieve a solution capable of resisting to such temperatures for long periods of time.

The plate stamped heat exchanger (PSHE) design offers the most promising solution. This design of a compact IHX is being investigated in the EU projects Raphael and Archer. Such a design uses a series of flat, thin plates assembled together in such a way that a counterflow of hot and cool gas can be achieved to transfer heat. Plate-type heat exchangers (PHEs) were formerly used for milk pasteurisation and gradually became the standard choice for heat treatment in the liquid food industry. The facility to dismantle plate heat exchangers is one the main reasons for their wide use in the food industry. Furthermore, as the heat-transfer coefficients are high, the fluid path length is shorter and relatively well defined. With the developments of larger plates, their use began to grow quickly in the chemical, petrochemical, district heating and power industries, but essentially for single-phase duties.

Adaption of this type of technology for the IHX was first applied to the recuperator and was investigated in Raphael (Buckthorpe, et al., 2008). Table 35 below provides some characteristics in terms of hydraulic and thermal considerations for the direct and indirect cycle HTR options.

Table 35: Main characteristics for direct and indirect from hydraulic and thermal consideration

	Direct cycles	Indirect cycles
Fluid	He/He	He/mixture: combined cycles He/He: Heat production
Nominal working P (bar)	P HP ~ 72 P BP ~ 26	P primary side ~ 55 P secondary side ~ 50
Differential of pressure between circuits (bar)	~ 50	~ 5
Maximum nominal temperature (°C)	510	850 or 750
Thermal duty (MW)	635	600
Thermal efficiency (%)	95	90

The PSHE comprises a stack of corrugated plates generating mechanical contact points between the plates (see Figure 65). However, it is necessary to apply external pressure to ensure the rigidity of the system. Depending on the application, the plates are mechanically maintained by tied bars or by an external pressure higher than that of the fluids.

Figure 65: Plate heat exchanger (flow direction and mock-up)

Iterative sizing and CFD/FEM calculation were performed to minimise the thermomechanical stresses under steady and transient conditions so that the length and the height were chosen to give smooth thermal gradients. The technology task also involved exploring different types of welding processes (laser, plasma, diffusion bonding, etc. — see Figure 66) and an important challenge was to set the welding parameters and complete welding tests on single and stacked plates to validate their application.

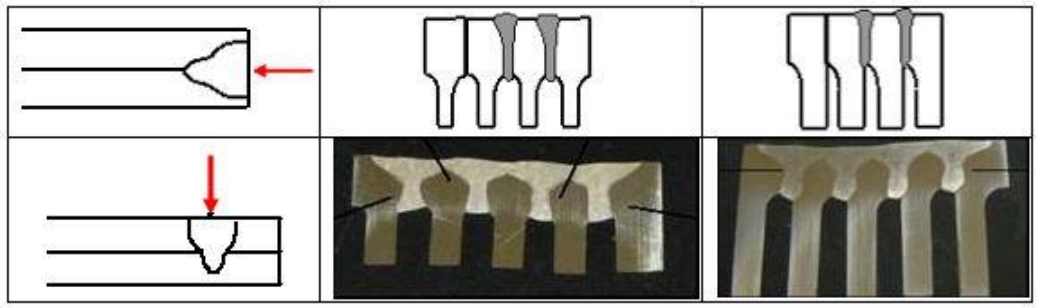

Figure 66: Examples of welding involved in joining the plates

Within Archer (Buckthorpe, 2014) a mock-up was made with Alloy 800H material of the same size as a real IHX module with fewer plates — 20 instead of 300. Welding and machining processes were optimised to ensure the quality of the component. The compact heat exchanger was tested under transient high-temperature conditions to evaluate its integrity and potential.

With regard to materials, Alloy 800H was chosen as this has a strong background in heat exchanger development at temperatures up to 750 °C and has an extensive range of design material properties available for the development of such a technology. The ASME Code recently produced design property data that extends to temperatures above this and includes information on higher-temperature alternatives such as Alloy 617.

In summary, IHX material issues and requirements for the HTR and VHTR can be summarised as shown in Table 36 below.

Table 36: IHX material issues and requirements for the HTR and VHTR

IHX (HTR and VHTR temperatures)
For the tube and plate designs the thick section requires development. Consistency of properties (midsection) is important. Issues of tribology in an inert helium environment. Requirement for coatings for resistance to fretting etc. (vibration). Materials candidates: Alloy 800H and Alloy 617 identified by vendors as the primary candidate, with Alloy 230 or Alloy X, XR as alternatives. Materials selection: creep rupture — use of tertiary creep for development of allowable; creep-fatigue could be more developed. Weldability: Alloy 230 possible but difficult, especially in thicker section — other candidates are easier to weld but need precautions to avoid hot cracking. Corrosion depends on exact He coolant composition and temperature: possible degradation due to carburisation, decarburisation and oxidation. Cold work can affect the creep properties of materials such as Alloy 617 and Haynes 230 leading to a reduction in strength. A suitable limit for manufacture should be defined.

6.8. Turbine for direct cycle and turbine plant

The HTR or VHTR can be developed as a direct-cycle or an indirect-cycle system. The direct-cycle system based on the Brayton cycle utilises a gas turbine placed directly into the hot gas leaving the reactor and converts it into rotational energy and electricity via a generator. The indirect-cycle system uses a steam generator or intermediate heat exchanger introduced into the heat transport circuit to transfer the heat energy into steam or hot gas for electricity via a process-heat application. The following sections consider the materials issues for the turbine for these two types of system.

Turbine plant

Turbine components are subjected to:

- rotation velocities of ~ 3 000 rpm (50 Hz), which lead to centrifugal forces in disks and blades;
- aerodynamic forces;
- thermal gradients;
- contact forces between blades and their corresponding disk;
- axial retention of blades in their disk socket.

Materials issues concern the selection of materials for the turbine blades and lead turbine disc.

For the turbine blades failure modes such as creep, high cycle fatigue and low cycle fatigue have to be taken into account. The gas radial temperature variation often peaks typically in the middle third of the blade, with steep temperature gradients across the blade section that vary according to the transient and steady-state conditions. All regions of the blade profile therefore undergo complex stress-strain cycling with reversed plasticity in some areas.

For turbine discs there is a requirement to limit the permanent growth and distortion to within typical design life targets. Critical regions for the disc are the hottest and highly stressed parts (high stress and moderate temperature at the hub, low stress and high temperature at the rim). For large

diameter disks, IN706 can operate successfully at temperatures of 550-600 °C (steam turbines) and IN718 is a further possible material for higher temperature.

Turbine for direct cycle

High temperatures and environmental degradation are again main concerns for the direct-cycle system utilising a turbine in the hot outlet gas leaving the reactor.

For the turbine materials, resistance to high temperatures (above 750 °C) and long-term endurance (60 000 hours) are key issues. The main concerns in areas such as the turbine blades and discs are creep plus the influence of the environment.

Manufacturing considerations are also especially important for the rotor and blades. Candidate alloys for the disc must have good forging properties and proven thermal stability. For the blades cast material is not sufficient, and so directionally solidified or single crystal alloys have to be considered. The need for cooling is also an important issue for both disc and blades. For current disc materials the temperature limits are in the region of 750 °C, suggesting that a cooled disc could be required for the VHTR design.

The environment in an HTR is composed of helium with impurities as CH_4, CO, H_2O and H_2 at μbar levels. The impurities can interact with the core graphite and metallic components and cause some degradation of their properties. Low concentrations of H_2O and H_2 are produced by leakage and/or desorption from both metal surfaces and graphite. CO, CO_2 and CH_4 may be produced by coolant/graphite reactions at high temperatures. Depending on the partial pressure of the impurities, the atmosphere can be either oxidising (high P_{O2}, low a_c) or carburising (low P_{O2}, high a_c) for the alloys selected.

The carburisation can be limited by a protective Cr oxide layer, provided that the oxygen partial pressure is sufficiently high for a stable Cr oxide scale to be formed (see Ellingham diagram). The experience gained in the past German projects has shown that the oxygen partial pressure may not in all cases be high enough for the formation of a stable Cr oxide scale. For this case, Al oxide formers should be considered in the selection of blade alloys because Al oxide forms even at extremely low oxygen partial pressures.

Damage can either be at the surface or can diffuse to significant depths in the metallic matrices (internal oxidation or carburisation or decarburisation), resulting in a loss of mechanical properties over a significant thickness of the material. As with the RPV, phase diagrams are used to determine the neutrality of the chemical activity and to determine whether compatibility issues are likely to have a strong impact on materials selection. For Ni-based alloys phase diagrams were constructed based on Cr levels. Typical zones for carburisation and decarburisation and the formation of protective oxidation were identified at different temperatures and used to aid materials selection.

Impurities in helium atmospheres, arising from decomposition of methane under extremely low oxygen partial pressures, are heavily carburising and can cause a significant shortening of the material creep life and accelerated creep crack growth rates. The presence of alloying elements such as cobalt (which is in most of the currently available turbine disc and blade materials) is also difficult to avoid. The main issues are the potential for plate-out and lift-off of particles and their activation and prevention of transport through the core.

Table 37: Chemical composition of IN 792 DS and CM 247 LC DS blade materials (weight %)

	C	Si	Mn	Cr	Mo	Ni	Ta	Ti	W	Co	Fe	Al	Hf	V	Zr
CM 247	0.074	< 0.03	< 0.03	8.16	0.43	Bal.	3.21	0.68	9.55	9.364	0.03	5.63	1.42	< 0.03	0.015
	Cu	**B**	**P**	**S**	**Pb**	**Ag**	**Bi**	**Te**	**Tl**	**Sb**	**Sn**	**Zn**	**Cd**		
	< 0.03	0.0155	< 0.005	6 ppm	< 2 ppm	< 2 ppm	< 0.3 ppm	< 1 ppm	< 1 ppm	< 3 ppm	< 3 ppm	< 2 ppm	< 0.5 ppm		

	C	Si	Mn	Cr	Mo	Ni	Nb	Ti	Ta	Al	Fe	Co	Cu	Hf	W
IN 792	0.079	< 0.05	< 0.05	12.63	1.82	Bal.	< 0.1	3.91	4.18	3.52	0.02	9.08	0.03	1.34	4.25
	B	**Zr**	**P**	**S**	**Ag**	**As**	**Bi**	**Mg**	**N**	**O**	**Pb**	**Se**	**Te**	**Tl**	
	0.017	0.02	< 0.002	< 20 ppm	< 0.1 ppm	< 5 ppm	< 0.1 ppm	< 6 ppm	< 11 ppm	< 12 ppm	< 0.3 ppm	< 2 ppm	< 1 ppm	< 0.2 ppm	

Suitable materials investigated in the EU HTR-M-M1 projects (Martin-Bermejo, et al., 2001) include Udimet 720 for the disc material and CM 247 LC DS and IN 792 DS blade materials (see Table 37). Investigations have been carried out to verify their strength properties (tensile, impact, fatigue and creep) to evaluate their performance under carburising and decarburising atmospheres. Such investigations are required to confirm the effects of the corrosion on material properties. Alternative approaches include the use of large test loops which can investigate material degradation under representative reactor environments.

With regard to codes and standards most information is commercial (gas turbine manufacturers). No nuclear coded design data are available for these materials. An ASME Code case for Ni-based alloys is being developed. Cooled discs could be used for a gas temperature of 850 °C, and non-cooled blades and coatings are possible for protection against corrosion/activation (cobalt).

For the fabrication of the disc there is a limit on diameter with materials such as IN 706 because of their forging capacity. For the blades cast versions are considered insufficient for HTR — direction-solidified and single-crystal versions are possible.

In summary, turbine material issues and requirements for the HTR and VHTR can be summarised as follows in Table 38.

Table 38: Turbine material issues and requirements for the HTR and VHTR

Turbine disc (HTR and VHTR)	Turbine blades (HTR and VHTR)
Life assessment methodology (standards, design rules, 1D, 2D or 3D simulations?). List of possible critical defects (bore, hole, metallurgical defect). Critical mechanical criteria for design (creep or fatigue); cumulative damage laws. Minimum required ductility of alloys (non-aged	Life assessment methodology (standards, design rules). Identification of critical defects (metallurgical defect, machining). Creep design rules and damage assessment. Minimum required ductility of alloys (non-

and aged conditions). Vibration analysis (critical speeds, possible failure location due to vibration). Stress relaxation properties/Fatigue and creep design rules (1 % plastic deformation in creep?). High-velocity impingement of dust and particles (possible). Radiation issues (negligible). Thermal ageing (impurity level (for carburising or oxidising environment). Possible plate-out by fission products. Specific design criteria related to environment. Recommendations on alloy composition (Co) due to plate-out.	aged and aged conditions). Vibration analysis. Impurity level (for carburising or oxidising environment). Possible plate-out by fission products (Cs, Ag, Te). Specific design criteria related to environment. Recommendations on alloy composition (Co) due to plate-out. High velocity impingement of dust and particles (possible). Radiation issues (negligible). Ageing issues (possible).

7. Safety

7.1. Relevant accident scenarios

In case of an accident, the behaviour of the reactor during severe accidents that are beyond an emergency shutdown is of considerable interest. Many possibilities of disturbance of the heat balance of the reactor have to be considered, especially during the licensing process and beyond, in discussions about the acceptance of nuclear technology.

Concerning possible accident scenarios, accidents due to inner or outer reasons must be distinguished. Furthermore, many events are foreseeable, while others are beyond expectations, for example terrorist attacks (Figure 67).

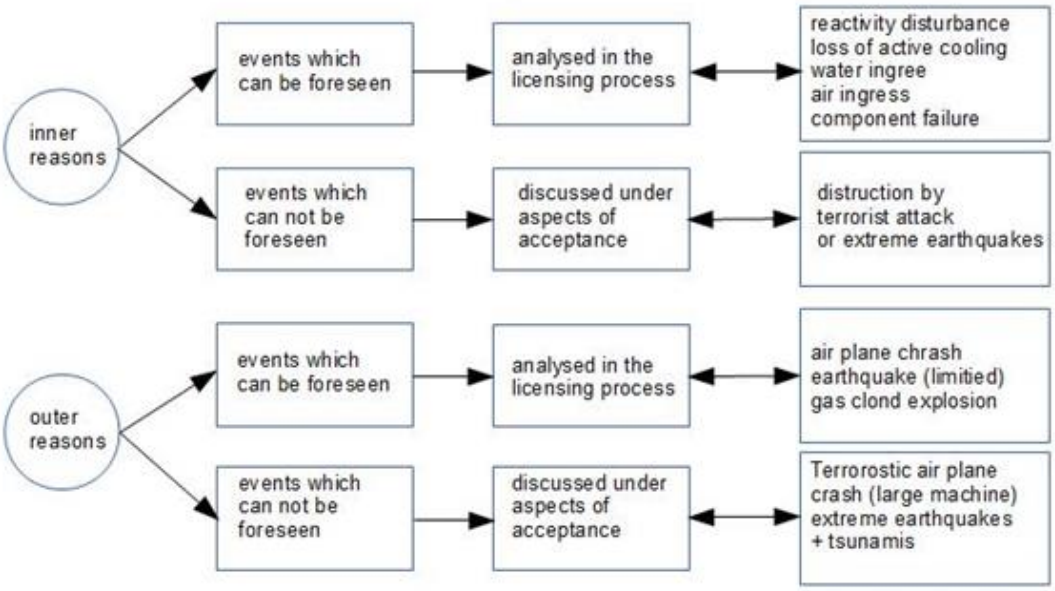

Figure 67: Overview of possible impacts and events in nuclear power plants: proposal for classification

From this list the accidents can be grouped as shown in Table 39.

Table 39: Regarded severe accidents and their probability (P)

Design-basis accident	DBA	$P \approx 10^{-2} \ldots 10^{-3}$/1 year
Beyond design-basis accident	BDBA	$P \approx 10^{-3} \ldots 10^{-6}$/1 year
Extreme assumed accident	EAA	$P << 10^{-6}$/ year

For the future it would be helpful to have a classification of accidents with regard to their severity.

- DBA events (design-basis accidents). These are analysed in the licensing process und the plants have to withstand these loads. In particular, the decay heat removal, the shutdown and the barriers to retain the radioactive substances must stay intact.
- BDBA events (beyond design-basis accidents). Assuming these loads it should be possible to show that no catastrophic release of radioactivity from the plant can occur.
- EAA events (extreme assumed accidents). There are very extreme assumptions behind this type of accident. They should be discussed to analyse the robustness of a nuclear system against extreme impacts from outside. There can be special solutions to ensure safety even against these very extreme accidents, for example underground siting and cores that can never melt, and EAA events are explained in Figure 68 and Figure 69. They are related to the severity of earthquakes. For many years the layout against a horizontal acceleration of approximately 0.2-0.3 g seemed to be sufficient for most sites. This would correspond to a magnitude of 7 to 8 (the Richter scale). The probability for this event was estimated as 10^{-6} per year. One could interpret this scenario as a DBA accident. Earthquakes with an acceleration of 0.3-0.4 g can be classified as a BDBA event with a smaller probability of 10^{-7} to 10^{-8} per year (German conditions). Stronger earthquakes cannot be excluded. However, their occurrence is very unlikely so that they can be regarded as EAA events.

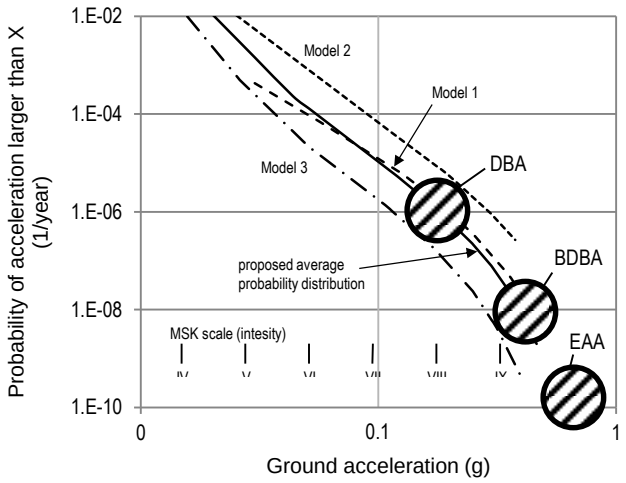

Figure 68: Aspects of earthquakes: (a) estimated annular probability that an earthquakes (as large as the value on the X-axis) could occur (e.g. THTR 300, Germany (20)); (b) probability of damaging components depending on the acceleration

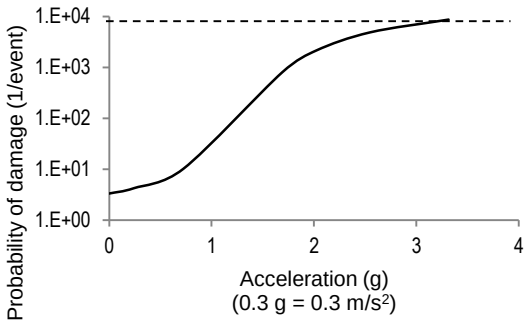

Figure 69: Probability of damaging components depending on the acceleration

The question of an aeroplane crash has totally changed. At the beginning of the development of nuclear technology (~ 1960) this topic was not important and was not considered. During the following decades the requirement rose to the assumption that a military aeroplane (e.g. McDonnel Douglas F-4 Phantom) could damage the containment. The last three German convoy plants (1 300 MWel, PWR) were built fulfilling this requirement. The crash of a Phantom could correspond to a DBA event, but today very few nuclear installations have similar protection (2 m-thick wall of concrete for the containment) (Dräger, 2001) (VDI, 2001).

Since the terroristic attacks on buildings in the United States in 2001 (World Trade Center, Pentagon) the crash of large commercial aeroplanes into nuclear power plants has been discussed. This event could be classified as a BDBA event. The very new situation is, additionally, that no probabilistic numbers can be identified for these events. Sometimes even stronger impacts on nuclear plants are discussed, for example very large aeroplanes, which can carry a large load, flying into the nuclear power plant. A characteristic example could be a turbine shaft with a weight of many tons. Such events have to be classified as EAA events. Figure 70 shows the forces depending on time (DBA event

for a Phantom aeroplane crashing into the containment) and Table 40 the aeroplane characterisation for DBA, BDBA and EAA events.

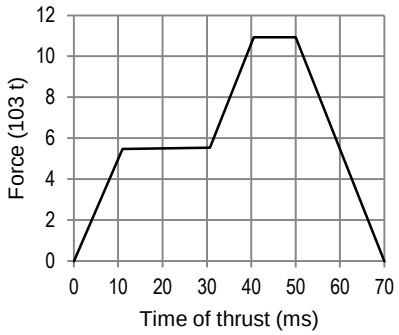

Figure 70: Forces of an aeroplane crashing into the containment (different DBA, BDBA and EAA events)

Table 40: Comparison of some data on aeroplanes for DBA, BDBA and EAA events

Parameter	DBA	BDBA	EAA
Aeroplane	Phantom	B 747	Antonov
Total mass (t)	20	400	500
Mass of turbine (t)	1	1	> 10*
Mass of kerosene (t)	5	200	50
Necessary wall thickness (m)	1.5-2	> 2	> 3

The limits of possible considerations on accidents at nuclear installation become clear looking at two examples: special weapons (including atomic bombs) or meteorites (of sufficient large size) could possibly damage plants.

Accidents relevant for self-acting decay heat removal in HTRs are summarised in Table 41 and are discussed briefly below using the HTR Module as a representative modular HTGR design.

Table 41: Accidents relevant for self-acting decay heat removal

Event	Conditions of primary system	Assumption	Accident case	Characterisation
Failure of the active decay heat removal	Normal helium of primary system available	Helium circulation fails	A	DBA
		Steam generator fails		
		Outer surface cooler works		
	Depressurisation of the primary system	Helium cycle fails	B	DBA
		Outer surface cooler works		
		Helium cycle fails, outer surface cooler does not work; heat is stored in concrete inner cell	C	BDBA

		Inner concrete cell is destroyed by extreme event; heat transport through rubble	D	EAA

7.1.1. Accident case A: reactor under full pressure, loss of forced cooling

If the reactor is under full pressure, but the helium circulator fails, the forced helium flow through the core stops and the helium flow is driven by natural convection. By this mechanism the heat is distributed inside the reactor system. Part of the heat is already removed via the surface of the reactor pressure vessel (approximately 1 M W for the HTR Module — Figure 71).

The maximum fuel temperatures will stay below 1 250 °C in this accident. A value of 1 250 °C corresponds to the specification of the coated particles under normal operation (TRISO particles with LEU fuel). Therefore, the fission-product release from the fuel elements will stay well below the desirable limits. The amount of heat removed is nearly the same as that during normal operation (Melese, et al., 1984).

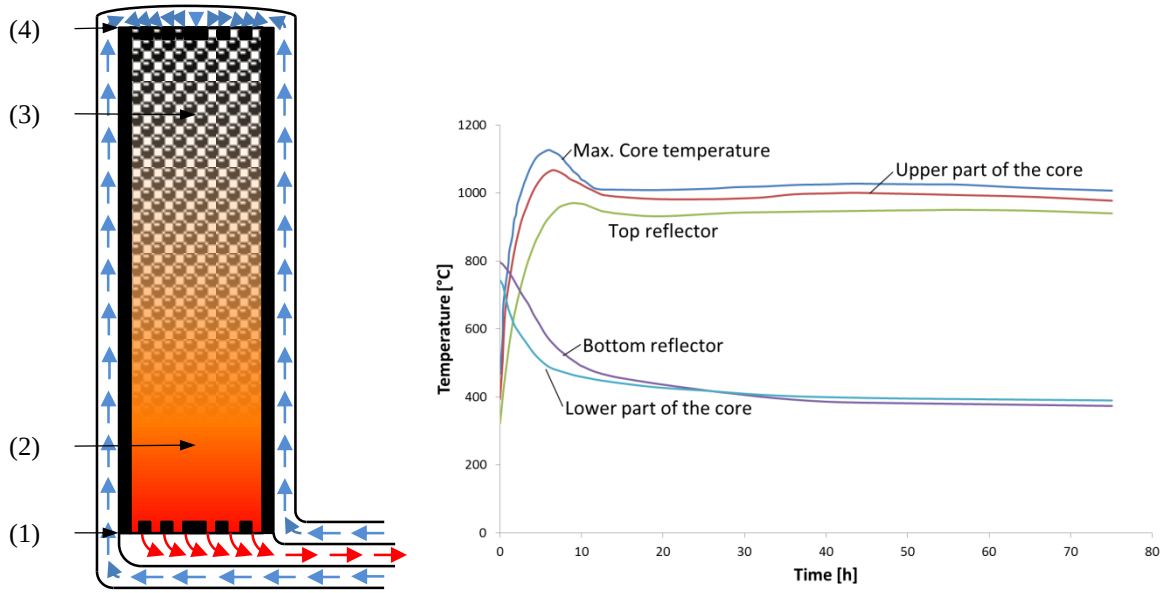

Figure 71: Temperatures (right) in the core in case of loss of forced convection in a modular HTR core, here HTR Module, 200 MWth (illustrated at left), at full helium pressure

The natural convection of the helium leads to heat distribution within the reactor structures. The temperatures of the upper part of the reactor internals will be higher than they are during normal operation. Figure 71 shows the temperatures at the top reflector and at the control rod drives as they would rise from approximately 250 °C to approximately 400 °C. Due to the rising temperatures it must be ensured that, after a 'loss of coolant flow' accident, the pressure of the system does not stay too high over a long period of time.

In this accident case the supplying of electric energy is totally unnecessary. The operation of the surface cooling system can be interrupted for a long period of time. Even after a very long 'grace period' (several hundred hours), it would be possible to feed the surface cooling system with water.

The special behaviour of HTR — this long 'grace period' before feeding the surface cooling system — has already been accepted in the licensing process in Germany. In the THTR 300, for example, it was

acknowledged by the regulator that the reactor will be able to remain without active cooling for 5 hours (Figure 72) (Verfondern, et al., 1979) (Verfondern, 1983).

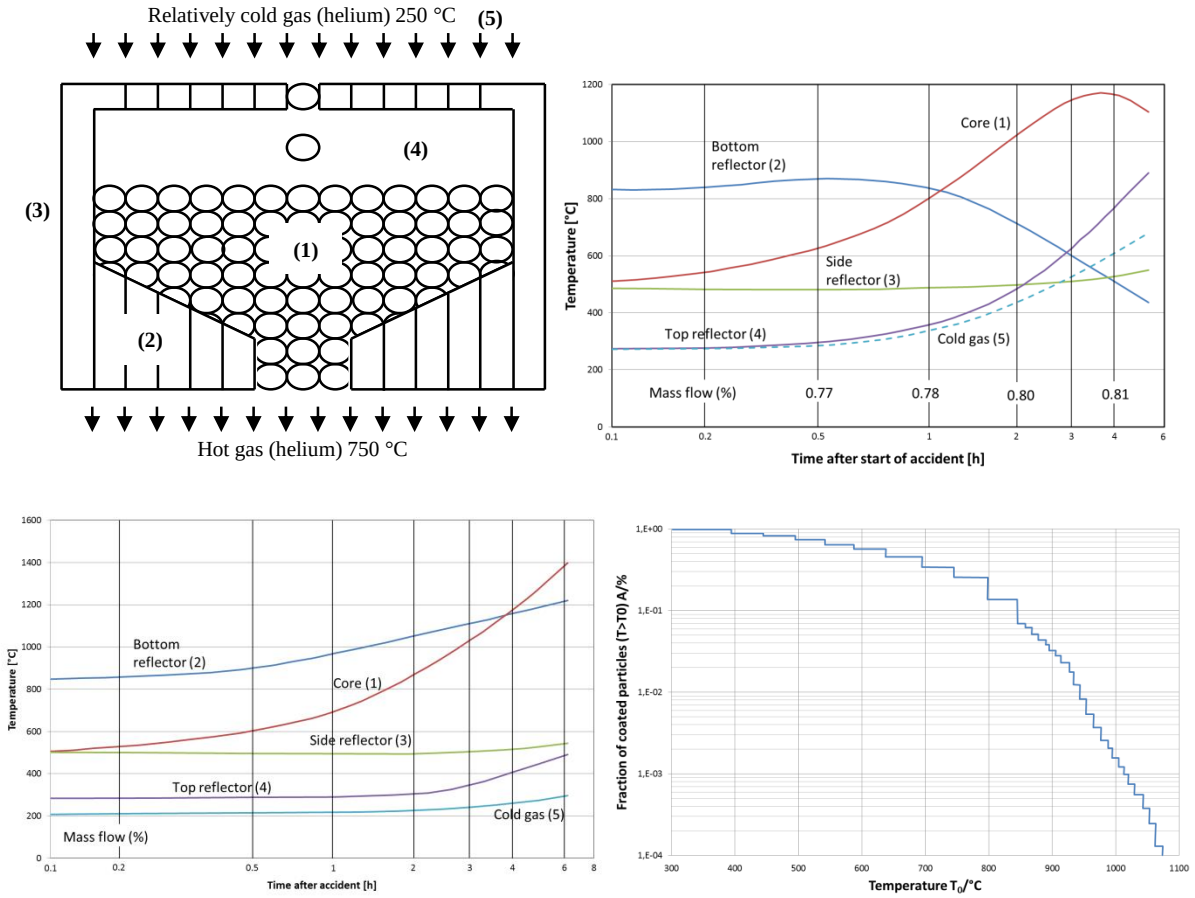

Figure 72: Results of calculations for the THTR 300 (750 MWth) in case of 'loss of active cooling' accident

The top left figure shows the positions (1 to 5) of important temperatures; top right the time dependence of some characteristic temperatures in the THTR core (assumption: failure of circulators, reactor at pressure of 40 bar, hot water operation of steam generators); bottom left the time dependence of some characteristic temperatures in the THTR core (assumption: failure of helium circulators and of steam generators, reactor at 40 bar pressure); and bottom right the histogram of fuel temperatures in normal operation.

Even in this reactor, with a much larger power density than the HTR Module, the fuel temperatures would have stayed below 1 250 °C and the temperatures of the top reflector structures would have stayed below 500 °C within the first 5 hours.

This was the first time that the principle of self-acting decay heat removal played an important role in a licensing process and was accepted by the official licensing body. It would have permitted repair works to be carried out to re-establish cooling systems after failures. Furthermore, it offered time spans for carrying out efficient interventions for specific cooling measures.

7.1.2. Accident case B: reactor at normal pressure, surface cooler working

In this case the heat is transported from the core through the internal structures of the reactor to the surface of the reactor pressure vessel. From the surface the heat is conducted to the surface cooler, which surrounds the reactor pressure vessel. This transport uses only heat conduction, heat radiation and free convection of air. The surface cooling system can either work with small pumps that are applied to circulate the water or by natural convection.

The temperature distribution within in the core of the modular HTR can be calculated using 3D program systems (Rehm, et al., 1985) (Holzkamp, 1987).

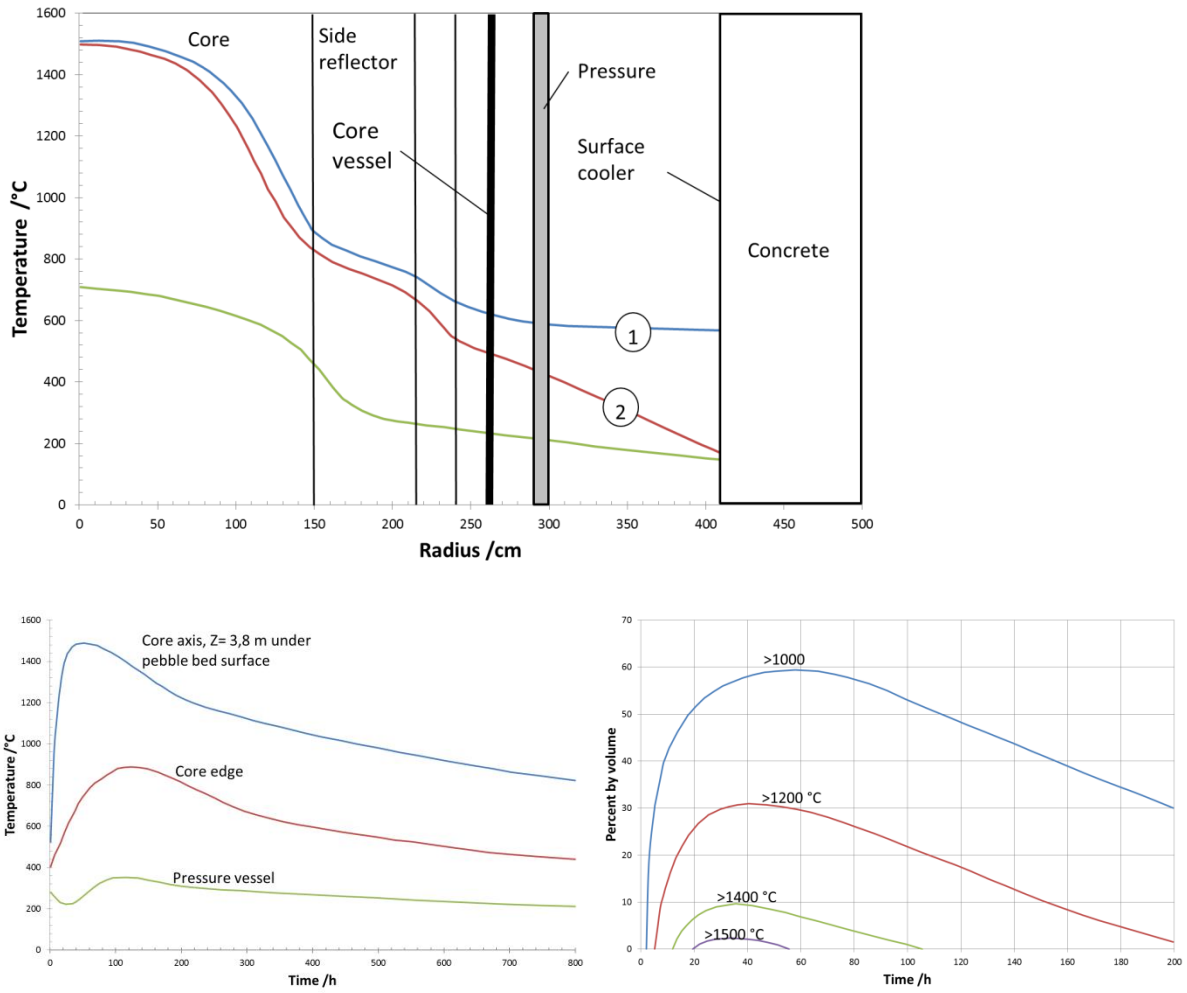

Figure 73: Results for the total loss of coolant and active cooling; failure of the surface cooler; storage and transport of heat in the concrete cell accident (HTR Module 200 Mth)

The top figure shows the radial dependence of temperatures at different times (t = 0, t = 100 hours) and the bottom figures the time dependency of the temperatures, the maximum fuel temperature (left) and the temperature of the reactor pressure vessel (right).

After 30 hours the maximum fuel temperature reaches 1 500 °C. After reaching the maximum the temperature decreases. During the accident case the temperature of the reactor pressure vessel stays below 400 °C. Therefore, this component stays intact.

The time schedules for these heating and cooling processes are very long (approximately 800 hours as shown in Figure 73). Therefore, it is very likely that there would be enough time to cool the system using simple or tentative methods to cool the core (e.g. nitrogen injection). If cooling the reactor the possibility of subcriticality occurring has to be considered (see Figure 74).

Due to xenon decay and a strong negative temperature coefficient in the core, neutron-absorbing material has to be added to the core, otherwise a small amount of additional heat production due to fission will occur.

The analysis showed that only a few per cent of the fuel elements — less than 5 % — stay at temperatures between 1 500 °C and an upper limit of ~ 1550 °C. The time span for which these fuel elements stay under these conditions is relatively short — approximately 30 hours. The other fuel elements reach lower, partly much lower, temperatures during this accident case.

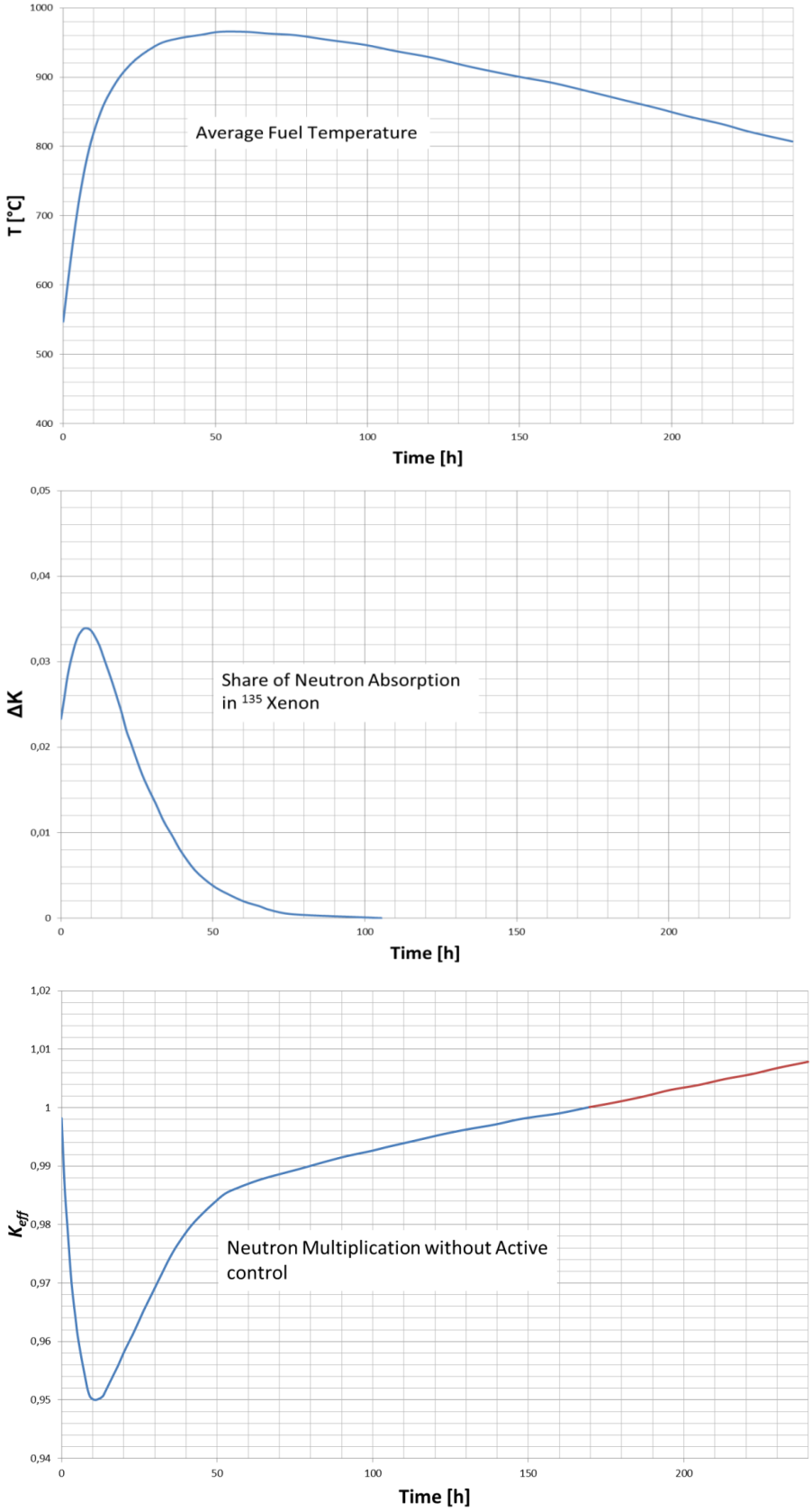

Figure 74: Neutron multiplication in the core of a modular HTR without active shutdown (examples: HTR Module, 200 MWth)

The top figure shows the average fuel temperature, the figure in the middle neutron absorption in xenon I35 and the lower figure the time dependence of criticality without active shutdown.

7.1.3. Accident case C: reactor under normal pressure, surface cooler fails

The probability of this accident case is very low as a failure of the surface cooler can nearly be avoided using a redundant design of the surface cooling system. Moreover, the possibility of effective countermeasures is provided due to the long 'grace period' of the reactor. However, as detailed calculations show, even under these assumptions the maximum fuel temperature is quite similar to an accident case with a working surface cooler as the heat is given to the concrete structure of the inner concrete cell. Figure 75 shows that the maximum temperature of the reactor pressure vessel would rise to approximately 600 °C and the concrete temperature would reach nearly 500 °C (Siemens/Interatom, 1988). The histogram of the fuel temperatures changes insofar as the percentage of fuel elements with temperatures higher than 1 250 °C will be larger and the time these fuel elements have to withstand the heat will be longer. The important property of the fuel elements — to nearly retain all fission products — will not be changed drastically.

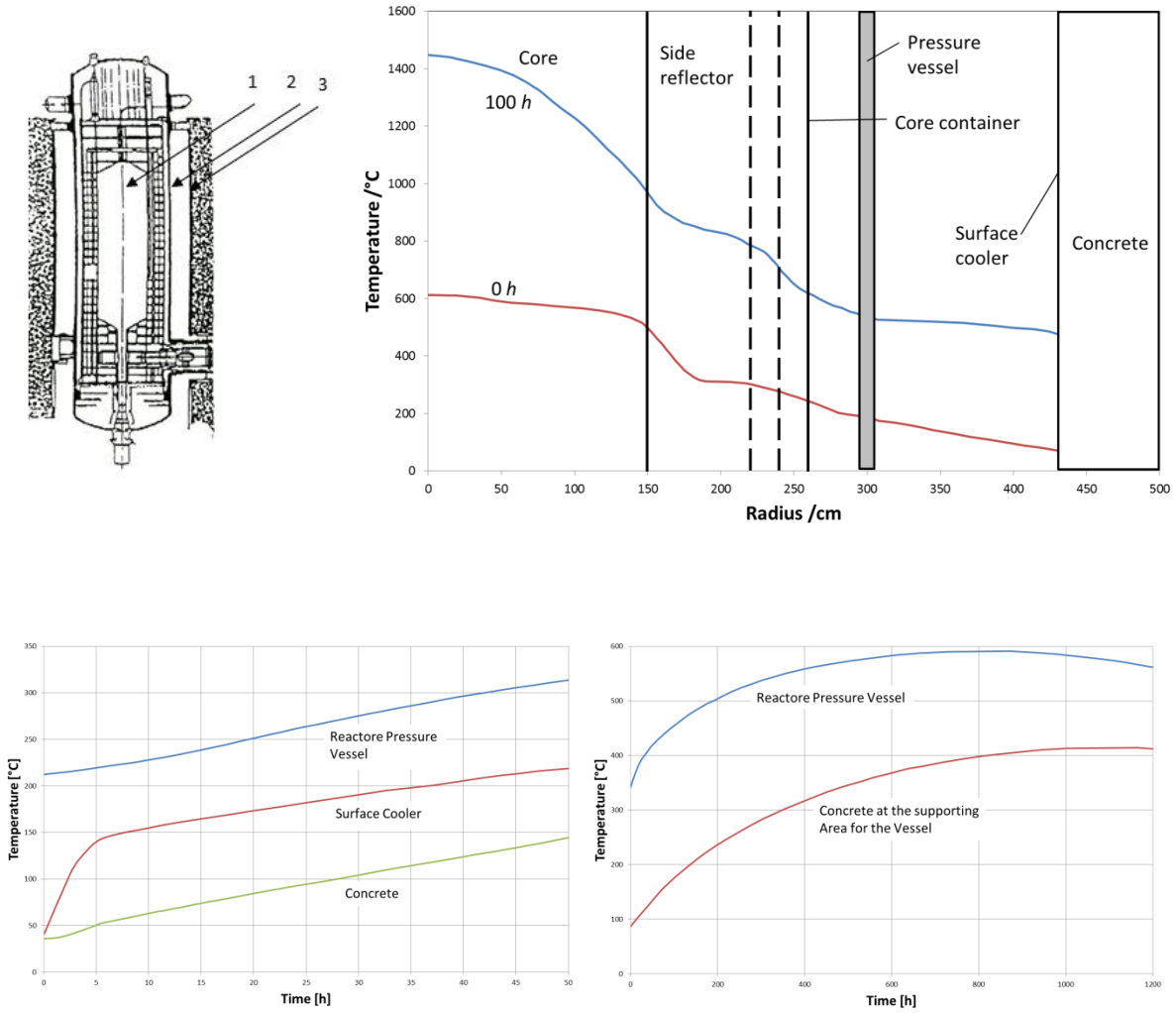

Figure 75: Results for the accident: total loss of active cooling; failure of the surface cooler; storage and transport of heat in the concrete cell (HTR Module, 200 MWth)

In the scheme of the reactor (top left) the characteristic points (1, 2, 3) are denoted where temperature distributions are shown. The top right figure shows the radial dependence of

temperatures after 0 h and after 100 h. The figures below show the time dependence of the reactor pressure vessel and surface cooler after a short time (left) and after a long time (right).

7.1.4. Water ingress into the primary circuit

Even though the steam generator or possible separate water-powered decay heat removal systems of an HTR system are manufactured, monitored and operated with great care, it is still possible that leaks may occur or pipes may burst during operation. As a result of such incidents quantities of water may enter the primary circuit. The amount of water entering depends on the design of the heat exchanger as well as the size and location of the leak. The ingress of water into the helium circuit of an HTR basically has the following consequences. The penetrated water evaporates or enters in the form of vapour, which consequently leads to a pressure increase in the primary helium circuit. Either the existing reactor volume has to be sufficiently large so that the penetrated water can be saved as a vapour within acceptable pressure limits in the primary circuit, or after exceeding an allowable overpressure redundant existing safety valves or rupture discs need to open so that the primary circuit can be depressurised. The steam is then collected in a 'mixed condenser', which effects condensation of the vapour in a water trap or a suitably dimensioned heat store so that the vapour can be transferred into a liquid phase again. Steam in the primary system may lead to corrosion of the hot graphite structures of the fuel or the core structures. As a result of this structural weaknesses may occur. The products of this water-gas reaction are hydrogen and carbon monoxide. These gases can mix with the helium in the primary circuit and the unreacted steam in the reactor building. The gas mixture may furthermore mix with the air present in the reactor building. This multicomponent system (air/helium/hydrogen/carbon monoxide) can be explosive in certain mixtures.

In addition, water entering the primary circuit can result in increased reactivity of the core since the water acts as a moderator.

Subsequent damage to components that are not directly related to reactor safety but may impact the availability of the overall system will be mentioned only briefly here. Considerable damage may be caused to the insulation, the blower and components of the shutdown and charging system.

The pressure increase in the primary circuit due to water ingress may be estimated according to equation 1.

$$\frac{dm}{dt} \sim f\sqrt{2\partial\Delta p} \tag{26}$$

f describes the area of the leak in a steam generator and ∂ is the density of the water in the steam generator close to the leak. Δp may be the pressure difference between the primary and secondary circuits. The pressure differences changes over time (equation 2).

$$\Delta p \sim \Delta p_0(1 - \alpha t) \tag{27}$$

Using changing pressure differences may lead to equation 3.

$$\frac{dm}{dt} \sim f\sqrt{2\partial\Delta p} \cdot \left(1 - \frac{a}{2}t\right) = \dot{m}_0(1 - \frac{a}{2}t) \tag{28}$$

Equation 4 may be used to estimate the mass leaving the secondary circuit over time t.

$$M(t) = \int_0^t \frac{dm}{dt'} dt' = \dot{m}_0(t - \frac{a}{2}t^2) \tag{29}$$

The volume of the water entering the primary circuit can then be estimated as follows.

$$V_D(t) = \frac{M(t)}{\partial D} \tag{30}$$

with ∂D accounting for the steam density.

Assuming that safety valves or other measures used to decrease the pressure in the primary circuit do not react instantly the steam concentration in the primary circuit may be determined using equation 6.

$$k_d(t) = \frac{V_D(t)}{V_C(t) + V_{He}} \approx \frac{V_D}{V_{He}} \tag{31}$$

At the beginning $V_D << V_{He}$ is assumed. Hence the pressure increase in the primary circuit can be expressed as follows.

$$p(t) = p_0 \frac{1}{1 - k_d(t)} \approx p_0\big(1 + k_d(t)\big) \tag{32}$$

$$p(t) \sim p_0 \left(1 + \frac{V_D(t)}{V_{He}}\right) = p_0(1 + \frac{M(t)}{\partial(t) \cdot V_{He}}) \tag{33}$$

Time dependent:

$$p(t) \approx p_0 \left(1 + \frac{\dot{m}_0}{\partial(t) \cdot V_{He}} \cdot \left(t - \frac{a}{4} t^2\right)\right) \quad (34)$$

A leak with f = 1 mm^2, an initial pressure difference of 150 bar and a rupture resulting in $\partial = \partial_W$ = 1 000 kg/m^3 water loss may be used as an example here. The amount of water at the beginning of the incident flowing into the primary circuit is given as $\dot{m}_0 \approx 0.2\ kg/s$. In this example it is assumed that moisture detectors in the primary system notice the water ingress after 10 seconds, resulting in activation of the shutdown valves after 30 seconds. The amount of water that may penetrate the primary circuit this way can be estimated taking the capacity of the damaged steam generator sections into account. Ideally, the steam generator allows locking of different sections so that the amount of water entering the primary circuit can be reduced. For instance, 10 steam generator tubes result in a tube length of around 100 m with a total capacity of about 200 kg of water. Assuming a completely ruptured heat exchanger tube from the super heater, the amount of water entering the primary circuit may be as follows:

f = 4 cm^2, $\partial_D = 60\ kg$/m^3, $\Delta p \approx$ 150 bar resulting in $\dot{m}_0$ zu ≈ 17 kg/s. It is evident that in addition to the content of the tube a significant contribution of water occurs, as the valves are not closed immediately but after 30 seconds. This process can be estimated using the following equation.

$$t \sim \left(\frac{p}{p_0} - 1\right) \frac{\partial(t) \cdot V_{He}}{\dot{m}_0} \quad (35)$$

In reality condensation processes may occur prior to reaching the final pressure, therefore the total pressure may not be reached. Figure 76 displays the result of a more accurate quantitative analysis of the time-dependent pressure increase in the THTR primary circuit system in case of demolition of a steam generator tube.

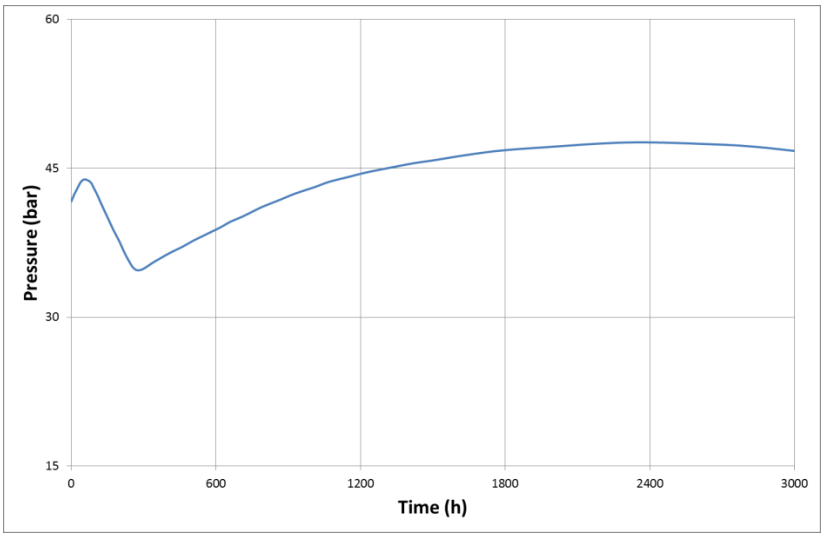

Figure 76: Pressure as function of time in the THTR primary circuit due to water penetration from a defective steam generator tube (operating pressure 40 bar)

For new HTR concepts this accident scenario may occur as follows. After detecting a tube rupture using moisture detectors, pressure increase, neutron flux changes or blower power changes the reactor is shut down. The water supply is stopped and the leak will be detected using moisture-measurement techniques. In such an incident the pressure is usually around 20 % above the design pressure, therefore the abovementioned pressure-relief devices of the primary circuit may be opened. The steam/helium mixture is thereby injected into condensers. The steam condenses and the helium flows into the reactor protection building. Depending on the design of the overpressure protection system of the primary circuit this event may result in 1 bar operating pressure or normal operating pressure. The decay heat removal system is put into operation and cools the reactor to such an extent that corrosion processes occur only very slowly. This means that the surface temperature of the graphite in the core region is lowered to below 700 °C. In addition to the pressure increase, corrosion effects need to be investigated further. Based on the determined heterogeneous water-gas reaction:

$$C + H_2O \rightarrow CO + H_2, \Delta H\text{=119 kJ/mol (endotherm)} \quad (36)$$

the following amount of material may react:

$$1kg\ C + 1.5\ kg\ H_2O \rightarrow 1.87m^3CO + 1.87m^3H_2 \quad (37)$$

The reaction speed is dependent on the pressures and the temperature of the components involved.

$$r' = \frac{k_1 \cdot p_{H_2O}}{1 + k_2 \cdot p_{H_2O} + k_3 \cdot p_{CO}} \quad (38)$$

With:

$$k_i = C_i \cdot e^{-\frac{E_i}{kT}} \quad (39)$$

Experiments with graphite suitable for reactor application determined the following relationship:

$$r = r_0 \sqrt{\frac{p_{H_2O}}{p}} \cdot e^{\frac{E}{R}\left(\frac{1}{T_0} - \frac{1}{T}\right)} \quad (40)$$

in which:

r = reaction rate (mg/cm^{2}h),

p_{H_2O} = water pressure (bar),

p = overall pressure (bar),

E = activation energy (kJ/mol),

R = gas constant (kJ/mol K),

T_0 = nominal temperature (K),

T = material temperature (K),

r_0 = nominal reaction rate (mg/cm^{2}h).

The nominal reaction rate r_0 is usually for T_0 = 950 °C, p = 1 bar and a specified volume fraction of 3 % steam in helium. The value of r_0 is for A3 graphite at 1.3 mg/cm^{2}h. The dependence of the reaction rate r (mg/cm^{2}h) to temperature, total pressure and water vapour partial pressure is shown in Figure 77 and Figure 78. Here a burnup of 2 % was used. The dependence of the reaction rate of the burnup has also being taken into account in accurate analyses. It is shown in Figure 79. The curves indicate that data higher than 1 000 °C was extrapolated. This high graphite temperature occurs only in extreme incidents. In all design-basis accidents the core is rapidly cooled below 1 000 °C. Moreover, corrosion rates of over 2 % go beyond the scope of design-basis accidents. A modification of the corrosion rates by catalytic effects of alkali metals is known, but the magnitude of this effect is below these values.

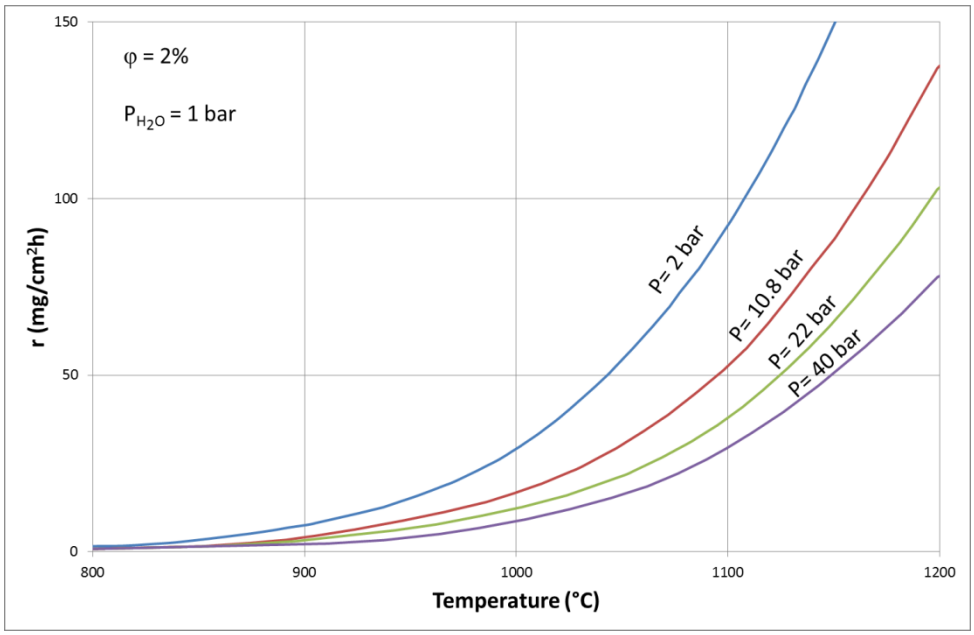

Figure 77: Corrosion rate of A3 graphite in water vapour as a function of temperature

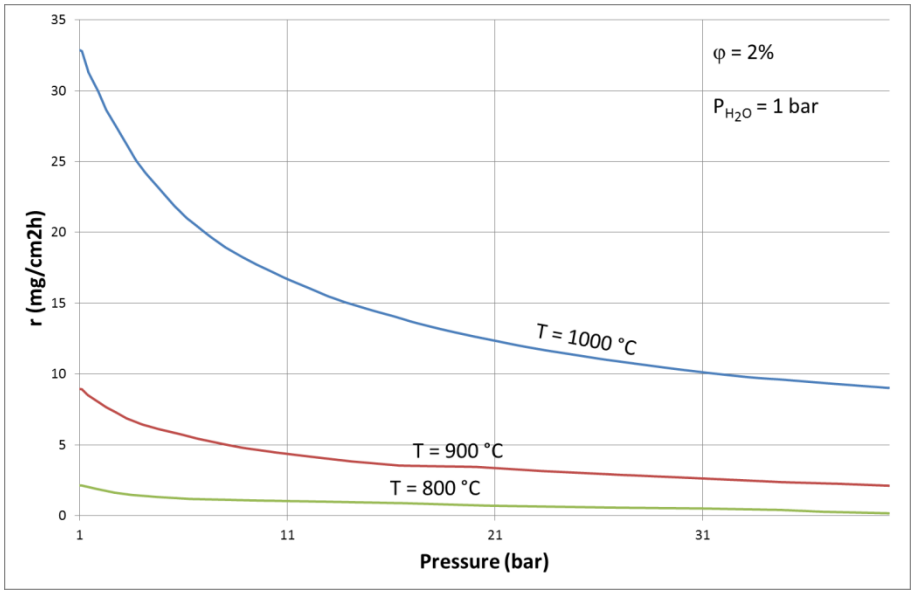

Figure 78: Corrosion rate of A3 graphite in water vapour as a function of total pressure p

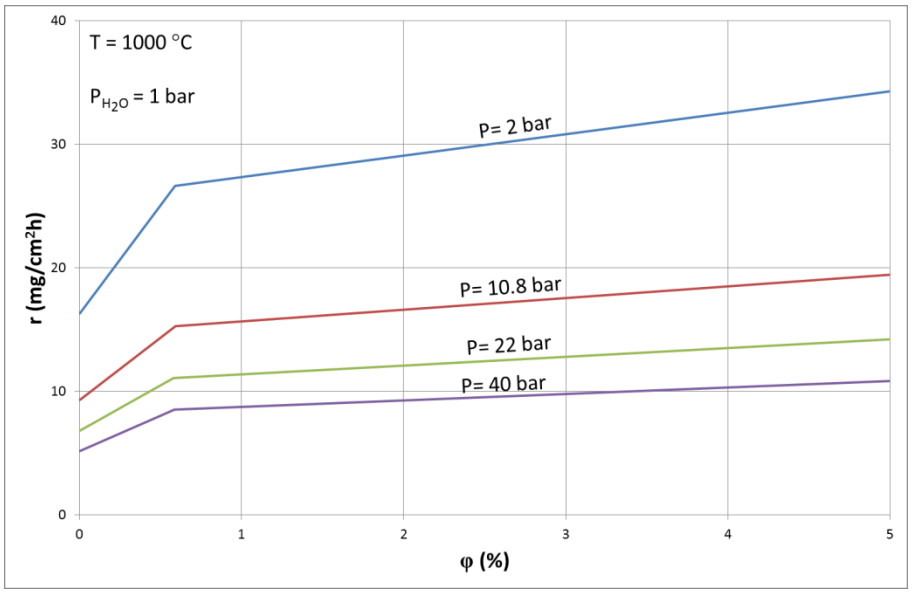

Figure 79: Corrosion rate of A3 graphite in water vapour as a function of burnup

To illustrate the effect of water vapour corrosion of fuel, the following example is considered. A fuel assembly with surface $A = 4\pi R^2 = 113\ cm^2$ will be exposed for 1 hour to water vapour attack (1 bar partial pressure in helium) at 1 000 C and 40 bar total pressure. The reaction rate under these conditions is about 10 mg/cm^2h. Consequently, in this period, a graphite amount of about 1.1 g, corresponding to 0.6 wt % relative mass loss is plotted on the entire fuel assembly due to corrosion. The corresponding layer is 6×10^{-2} mm, therefore it is essentially not significant. Also, a substantial adverse effect on the stability of the fuel is not yet connected to such a low burnup, as shown in Figure 80. Only if a longer-lasting corrosion attack is relevant does this become important.

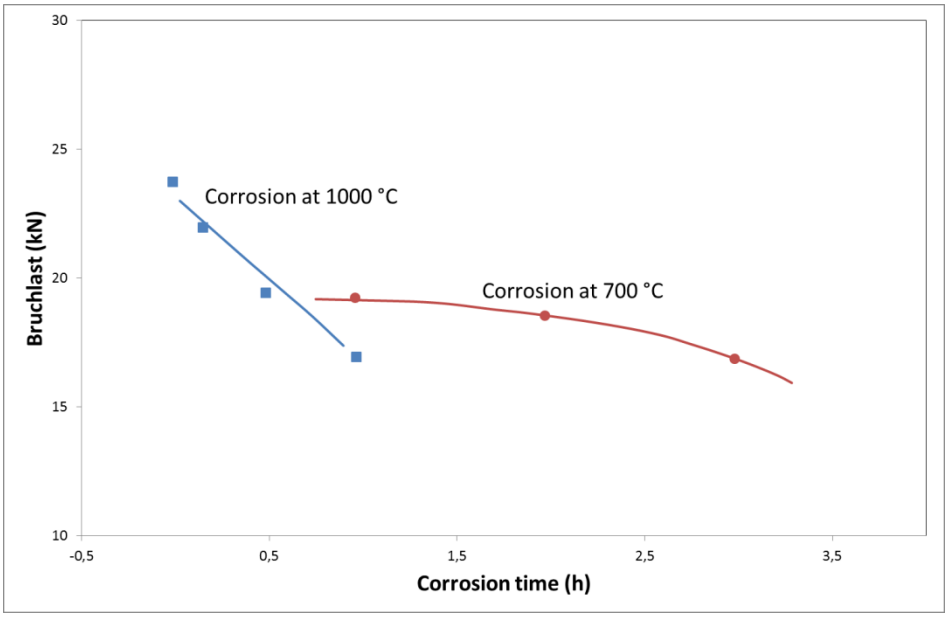

Figure 80: Decrease in the strength of the fuel due to corrosion in steam (6:42)

The total area of the reflector hot graphite structures shall be subject to the flooding event. In steam-generating systems the core area or the hot gas chamber is located in a temperature range from 700 to 750 °C. These temperatures are similar to fuel element graphite at 950 °C. During process-heat applications, reflector graphite structures are affected by water vapour corrosion. Figure 81 shows measured corrosion rates for various reactor graphite materials with A3 graphite inclusions for fuel elements. In this case a reaction rate r (in %/h) related to the entire surface plotted against the increasing burnup is assumed. The rate is to be regarded as an integral rate.

It can be noticed that in standard conditions, depending on the grade of graphite, around 0.1 % to 0.4 % of the amount of graphite would be transferred by water vapour corrosion if no cooling of the graphite structures were carried out before. Reflector structures which are operated normally during operation below temperatures of 800 °C are therefore not endangered by multiple flooding incidents during the system life cycle, as relatively small reaction rates are to be set for such events.

A method for dealing with the effects of a flooding incident on the integral corrosion behaviour of an HTR core's space- and time-dependent temperature fields must be determined for all graphite surfaces, overlaid with the temperature, burnup, and partial pressure dependent corrosion rates.

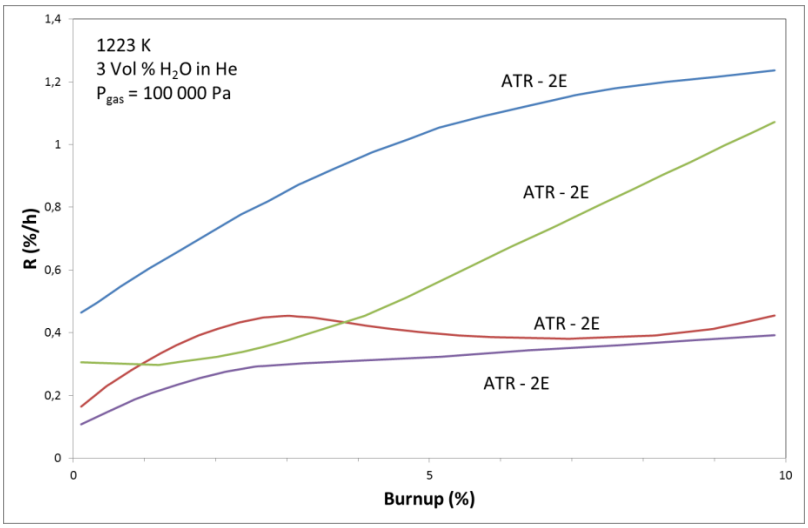

Figure 81: Integral corrosion rate in water vapour as a function of burnup for standard conditions. Reflector graphite ATR-2E and ASR 1RS and fuel element graphite A3-3 and A3-27 (6:37)

In general, it can be assumed that the corrosion of the reactor internals of the core due to water vapour can be limited by timely cooling of the core by the decay heat removal system within tolerable limits. In addition, only a few fuel elements in the HTR core see temperatures that are relevant to water vapour corrosion (the surface temperature of the fuel element is about 700 C). As mentioned above, reactions with 1.5 kg of water vapour on 1 kg of graphite by the heterogeneous water-gas reaction results in a total of 3.74 m^3 of hydrogen and carbon monoxide. Thus if, as mentioned above, for example in a tube damage accident, around 400 kg of water enters the primary circuit of an HTR, then about 1 500 m^3 of water gas is formed when complete conversion of the water is assumed. These gases do not come there to relieve the pressure of the primary circuit, therefore they must be removed after shutting down the reactor through the gas cleaning system (see 'Components' section). If, additionally, the relieving of the pressure of the primary circuit is assumed, a gas mixture consisting of helium/air/water gas forms in the reactor protection building. A portion of the incoming air from the containment is displaced by the incoming helium-water mixture.

Under certain conditions the composition of such a mixture is explosive. The diagrams below show potential explosion areas, to assess the usefulness of the relationships (Figure 82). Thus, the area of ignitable mixtures with increasing temperature shifts. As a security boundary, values for the fuel gas contents of an inert gas fuel gas-air mixture can be defined where for any dilution with air no ignitable mixtures will emerge. For ambient temperatures, therefore, this stands at 17.85 %. With precise analysis the effect of pressure and water vapour is taken into account. A further limitation of the quantities of water during flooding can be achieved through changes to the steam generator concept. When using gas turbine systems the question becomes less relevant.

In general it can be said that the formation of gas would extend after flooding over a period of several hours and that cooling of the graphite usually already occurs during this period, therefore the amount of water gas remains very limited regarding reactivity changes which are to be expected in connection with water ingress in an HTR core.

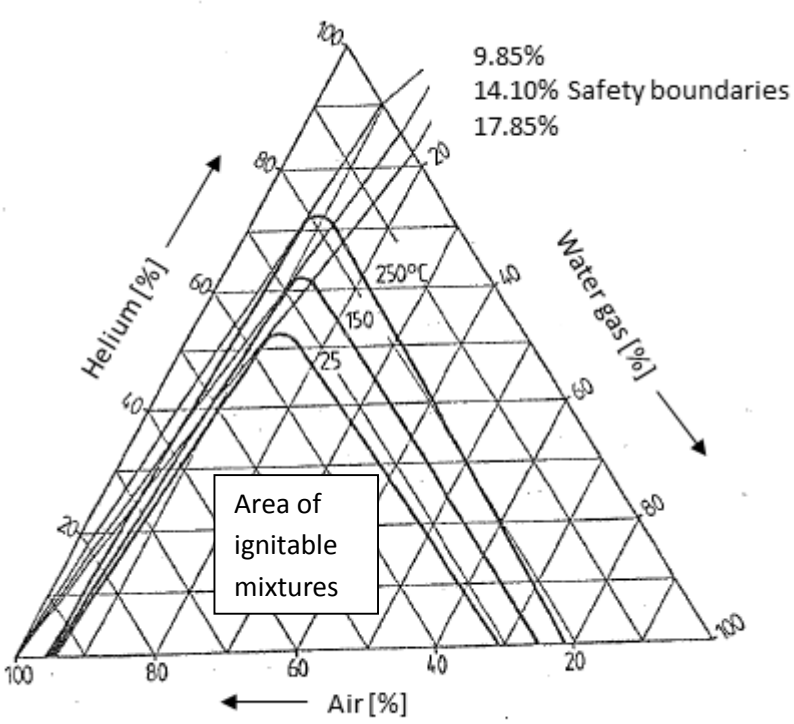

Figure 82: Flammability of water-gas helium-air mixtures at different temperatures

7.1.5. Air ingress into the primary circuit

Quantities of air that enter into the helium circuit of an HTR can trigger reactions depending on the size and location of one or more leaks and can possibly lead to safety-related incidents in the hot core. Specifically, fuel and graphite internals may be damaged and their structural behaviour adversely affected by combustion of graphite. If too much erosion occurs fission products may be released from the graphite matrix or from defective particles, in addition to incomplete oxidation of the graphite carbon dioxide and carbon monoxide, which has to be considered in connection with

the formation of explosive gas mixtures in the reactor building protection. Exothermic reactions that may lead to fires may cause further heating of the internal structures. The amount of air that can penetrate into the core is determined by the expiration of convection processes, by the contraction or compression of the primary cycle gas content, by cooling and fluctuations in air pressure and by diffusion processes. Whilst for the THTR chosen design principle of the inclusion of the entire primary circuit system in a prestressed and mon bursting concrete container leaking cross sections of 65 mm in diameter can be assumed, other leaking cross sections and incident possibilities for different HTR concepts are conceivable. As part of these considerations, other fragment sizes incidents possibilities are conceivable. As part of these considerations chimney effects may also be assumed considering two leaks. These incidents are classified in the range of hypothetical accidents.

First the reactions may be explained using simple stoichiometric considerations. The basic reactions are as follows.

$$C + O_2 \rightarrow CO_2, \Delta H = -393.9 \frac{kJ}{mol} (exotherm) \quad (41)$$

$$C + \frac{1}{2} O_2 \rightarrow CO, \Delta H = -111.2 \frac{kJ}{mol} (exotherm) \quad (42)$$

$$C + O_2 \rightarrow 2CO, \Delta H = +170.5 \frac{kJ}{mol} (endoherm) \quad (43)$$

$$CO + \frac{1}{2} O_2 \rightarrow CO_2, \Delta H = -281.7 \frac{kJ}{mol} (exotherm) \quad (44)$$

The first two reactions mentioned lead to the following quantities of air reaction.

$$1\ kg\ C + 2.667\ kg\ O_2 \rightarrow 3.667\ CO_2 \quad (45)$$

$$1\ kg\ C + 8.92 m^3\ air\ \rightarrow 1.87 m^3\ CO_2 + 6.87 m^3 N_2 \quad (46)$$

or

$$1\ kg\ C + 1.33\ kg\ O_2 \rightarrow 2.33\ kg\ CO_2 \quad (47)$$

$$1\ kg\ C + 4.96\ air\ \rightarrow 1.86 m^3\ CO + 3.48 m^3 N_2 \quad (48)$$

The distribution of the reaction processes to the responses of CO_2 or CO formation is based on present experience such that below a reaction temperature of about 1 000 °C significant amounts of CO_2 and increasing amounts of CO are formed. The equilibrium and the CO–CO_2 ratio are shown as a function of temperature in Figure 83.

The reaction rate of graphite with oxygen or air is known from a variety of measurements. Essential parameters for the conversion rate are: the temperature T, the oxygen partial pressure ψO_2, the flow rate of air v_L and the pre-burnup of the graphite Δm. In the range below a temperature of about 700 °C in the graphite, called the pore diffusion region, the corrosion rate increases exponentially with temperature, and the dependence on the oxygen partial pressure is linear. In this area the chemical reaction is dominant for the reaction rate and the flow rate of air has virtually no effect on the reaction rate R (mg/cm2h).

$$R \sim \exp(-\frac{A}{T}) \cdot T^{-0.125} \cdot \psi O_2 \cdot \frac{P}{P_0} (1 - \frac{\Delta m}{m})^{0.66} \quad (49)$$

The relationship above is in close agreement with past measurements. At reaction temperatures above 900 °C in the boundary layer region the flow speed determines all of the oxygen which is introduced to the graphite surface because of the high temperature. In this area, the reaction rate can be expressed by:

$$R \sim T^{0.53} \cdot v_L^{0.437} \cdot \psi O_2 \cdot \frac{P}{P_0} (1 - \frac{\Delta m}{m})^{0.66} \quad (50)$$

In the transition region of 700 °C < 900 °C the following equation can be used:

$$R \sim \varphi(T, v_L) \cdot \psi O_2 \cdot \frac{P}{P_0} (1 - \frac{\Delta m}{m})^{0.66} \quad (51)$$

Function φ takes both effects, diffusion and reaction, into account. Experimental results for the reaction rates of graphite pebble beds are shown together with the aforementioned theoretical relationships in Figure 84, and show close agreement between theory and experiment.

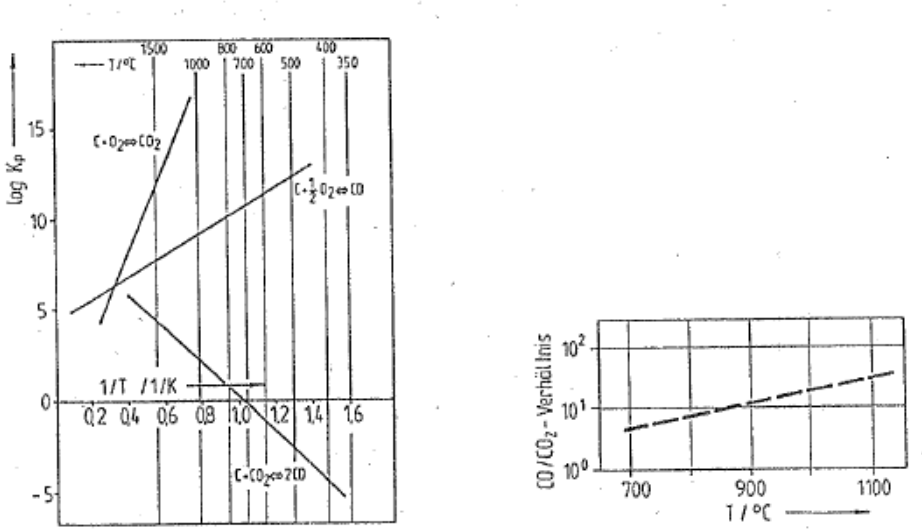

Figure 83: equilibrium and ration of CO/CO_2

The effect of air entering the primary circuit of an HTR to the fuel is here illustrated by the following simple estimation: at a temperature of 1 000 °C and a flow rate of 2.35 cm/s, a reaction rate of about 200 mg/cm^{2}h in the corrosion of A3 graphite can be expected in air. When a fuel assembly remains for 1 hour in air it loses about 23 g of its graphite matrix by burning. The corrosion would occur evenly distributed over the surface, so a graphite shell would be ablated with a thickness of about 13 mm. Consequently the fuel matrix is not affected.

However, in case of direct exposure of the fuel elements to air the graphite is not attacked uniformly but a certain 'shaping' of the fuel elements is observed. The material removal is not evenly distributed over the spherical surface. This phenomenon leads to more detailed considerations beyond the scope of the assumptions employed here. In case of material removal the properties of the fuel or the graphitic core structures are unfavourably altered. For example, the strength of the fuel is decreased by graphite corrosion (Figure 85) over time.

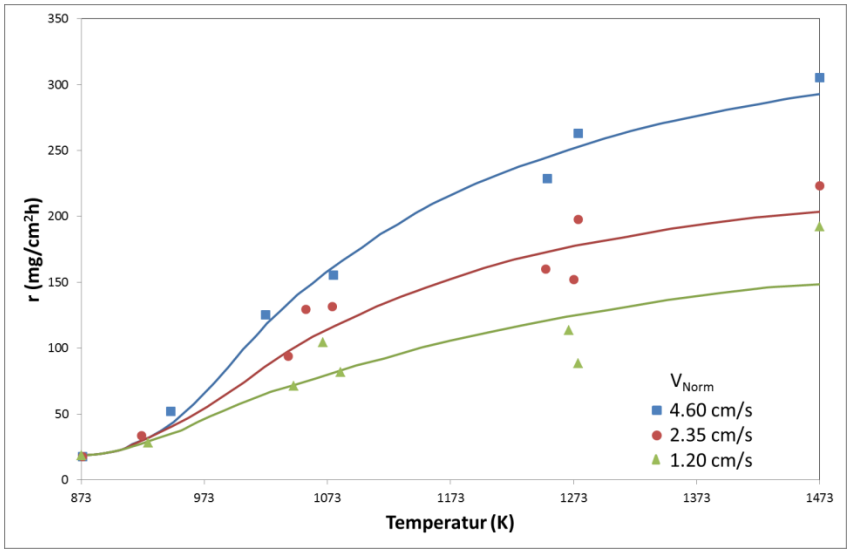

Figure 84: Measured reaction rates of corrosion of graphite pebble beds by air

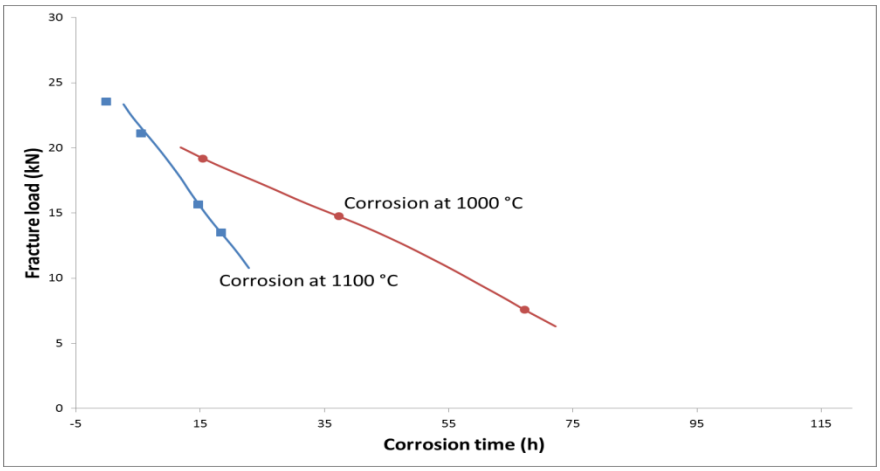

Figure 85: Decrease of the maximum load before rupture of the fuel elements depending on the corrosion time at variable temperatures (corrosion in air)

According to the stoichiometric considerations initially employed about 0.4 m^3 of CO is produced per 1 m^3 of air. In air, carbon monoxide is formed in a volume range of 14 % to 73 % ignitable mixtures. By including helium, which would be available in certain quantities during air ingress accidents in the reactor protection building, the flammability limits are moved (Figure 86). If the total helium share is above 40 % ignitable mixtures are not possible. For more accurate analyses local gas compositions and the influence of water vapour and may be dust have to be taken into account.

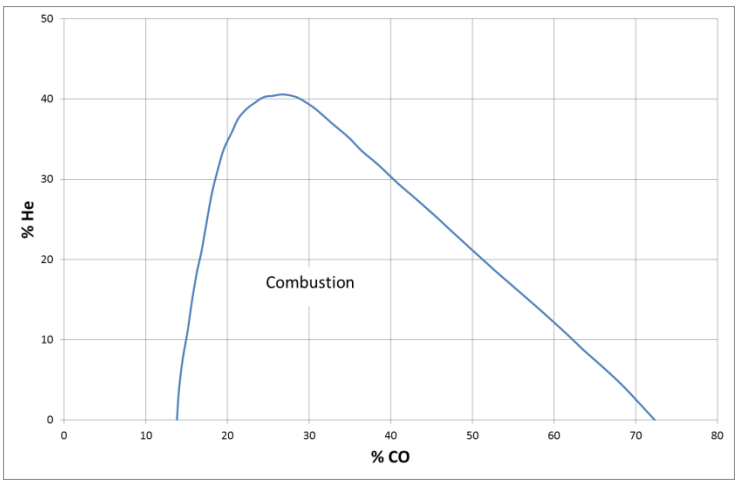

Figure 86: Flammability limits for the air/carbon monoxide/helium system

A prerequisite for the occurrence of significant graphite burning in both fuel elements and graphite structures is that sufficient quantities of air can penetrate into the reactor core. In particular, the chimney effect through the reactor is worth mentioning in this context. A hypothetical accident situation is considered here (Figure 87).

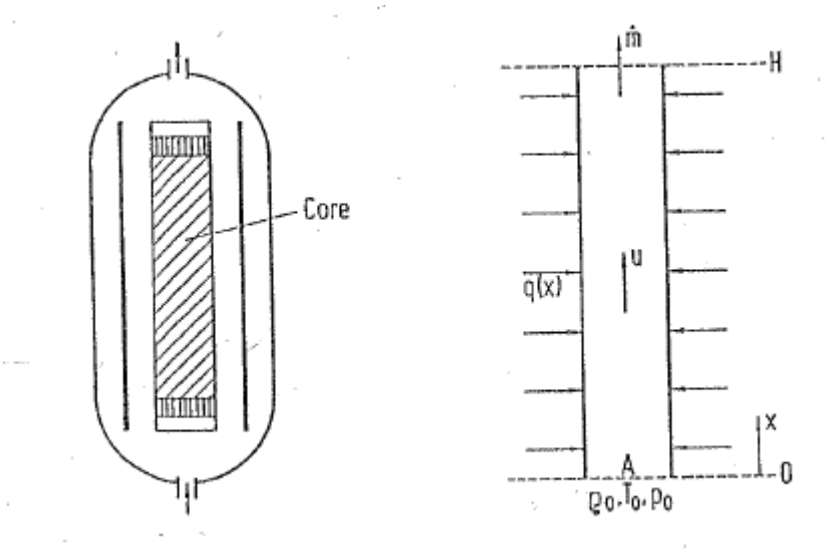

Figure 87: Schematic diagram of the chimney effect during air ingress into the HTR core

An opening is available at both the upper and lower ends of the reactor pressure vessel, therefore a chimney can form through the reactor. The air mass flow, which is established in the primary circuit, can then be determined from the conservation equations. The conservation of mass, which was first seen in the chimney approximated without chemical reaction, yields the stationary case:

$$\frac{d}{dx}(\partial \cdot u \cdot A) = 0, \dot{m} = \partial \cdot u \cdot A = const \quad (52)$$

Application of the pulse conservation law leads to:

$$\partial \cdot u \cdot \frac{du}{dx} = -\frac{dp}{dx} - g \cdot \partial - K_\alpha(T) \cdot \dot{m}^\alpha \quad (53)$$

The energy law finally gives:

$$\partial \cdot c_p \cdot u \cdot \frac{dT}{dx} = \frac{q(x)}{A} \quad (54)$$

q(x) may represent the heat in the core of the air stream here, and the size A is the free cross section. The part $K_\alpha \cdot \dot{m}_\alpha$ accounts for the frictional pressure loss. Taking into account the temperature dependence of density and toughness this leads to:

$$\partial = \partial_0 \cdot \frac{T_0}{T}, \eta \sim C \cdot T^{1/2}, v = \frac{\eta}{\partial} \sim C^* \cdot T^{3/2} \quad (55)$$

After appropriate transformation of the equations the correlation between mass air flow, the height of the system H, the heat input q(x) into the system and the free cross section A is given as:

$$\varphi(x) = \frac{1}{m \cdot c_P \cdot T_0} \cdot \int_0^x q(x')dx' \quad (56)$$

where:

$$\frac{\dot{m}^2}{\partial_0 \cdot A^2}\left(\frac{1}{2} + \varphi(H)\right) = \partial_0 \cdot g \cdot \int_0^H \left(1 - \frac{1}{\varphi(x)}\right) dx - K_\alpha \cdot \dot{m}^\alpha \cdot \int_0^H (1 + \varphi(x))^{(2-\alpha/2)} dx \quad (57)$$

In the case of laminar flow (α = 1) is given as K_α where:

$$K_\alpha \sim C_1 \cdot T^{3/2} \quad (58)$$

while for turbulent flow (α = 2):

$$K_\alpha \sim C_2 \cdot T \quad (59)$$

is given. In Figure 88 the results of calculations that include the dependence of the invading air mass flow rates of the most important parameters are listed for a module reactor. With one ingress and the passage of 10 m^3/h of air through a chimney HTR basis (this is shown in Figure 88) for two openings (nominal diameter 60 mm) this leads to a burn rate of about 1.1 kg C/h. This could mean the destruction of up to 10 fuel assemblies per hour. However, this effect would occur only after the various layers of the bottom reflector are burned through (these are about 2 m thick). This leads to a period of at least 10 hours before fuel is affected. This delay allows the implementation of simple and effective countermeasures to prevent air intrusion.

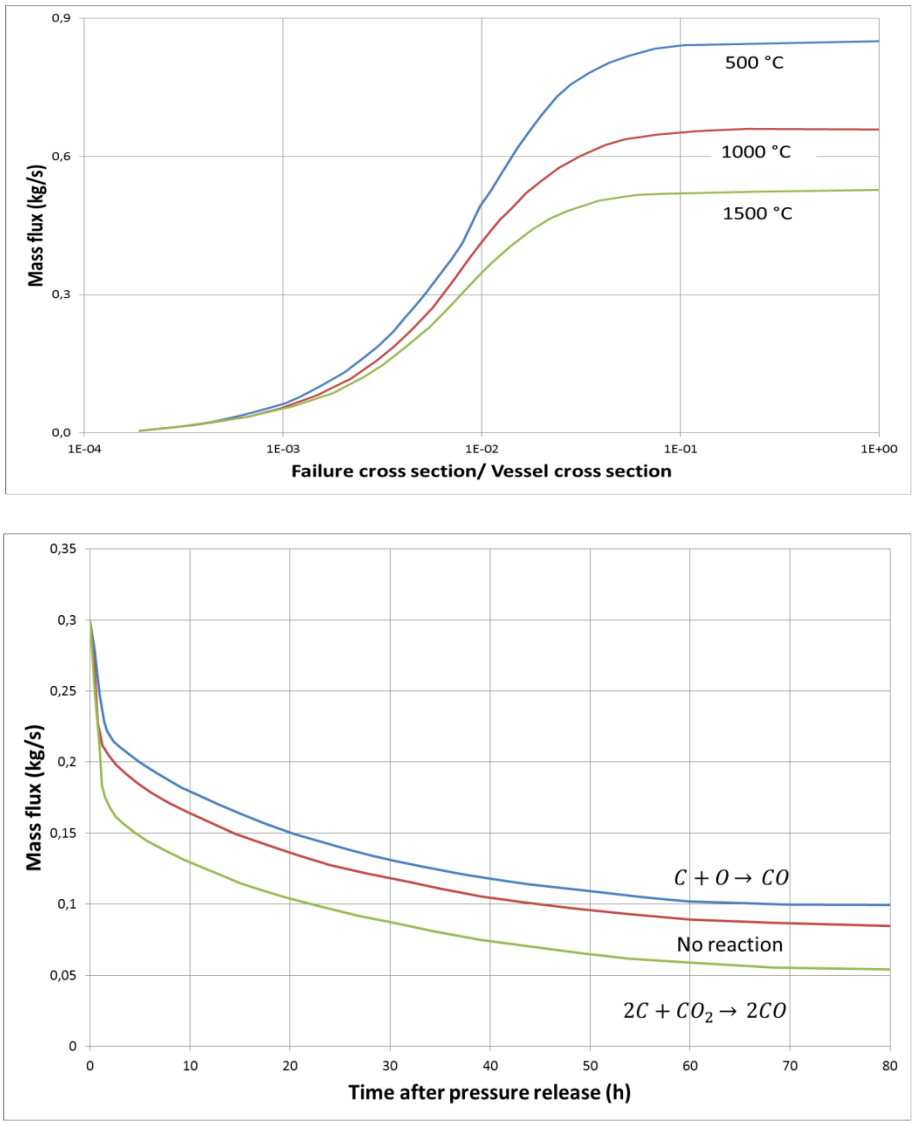

Figure 88: Mass flow depending on the leakage cross section and on the temperature in the core (measured from the reactor module)

For larger leak cross sections, which are discussed for hypothetical accidents here, the abovementioned shall apply. For larger leak cross sections, which are discussed for hypothetical accidents here, the abovementioned shall apply. From such considerations it can be concluded that for an HTR system it must be ensured by design and construction of the primary circuit enclosure, that air infiltration is very unlikely and if the amount remains very limited. In particular, prestressed reactor vessels meet these requirements in a particular way. For interventions, that is, interventions where air leak can be stopped, very long periods of time at all HTR concepts remain. In particular, such interventions are feasible because the facilities remain under all possible incidents virtually contamination free and accessible for long periods of time.

7.1.6. Accident case D: concrete structures of the reactor system are destroyed; the reactor is covered with rubble

Due to a terrorist attack or the crashing of a large aeroplane, or as a consequence of a very strong earthquake with a strength much larger than the design value, the concrete structure of a modular

HTR could be totally destroyed. It must be assumed that the reactor pressure vessel is covered with rubble and that therefore the conditions for the self-acting removal of decay heat are changed. Figure 89 briefly illustrates this situation.

Although the conditions and integrity of the reactor pressure vessel and the core structures are totally unknown, under the assumption that the reactor pressure is intact calculations of temperature fields deliver the dependencies shown in Figure 89. Even in this extreme case the maximum fuel temperature stays below 1 600 °C. The temperature of the reactor pressure vessel would (depending on the heat transport capabilities of the rubble structure) reach 600 °C to 1 000 °C (Rütten, 2007) (Hauck, 2003).

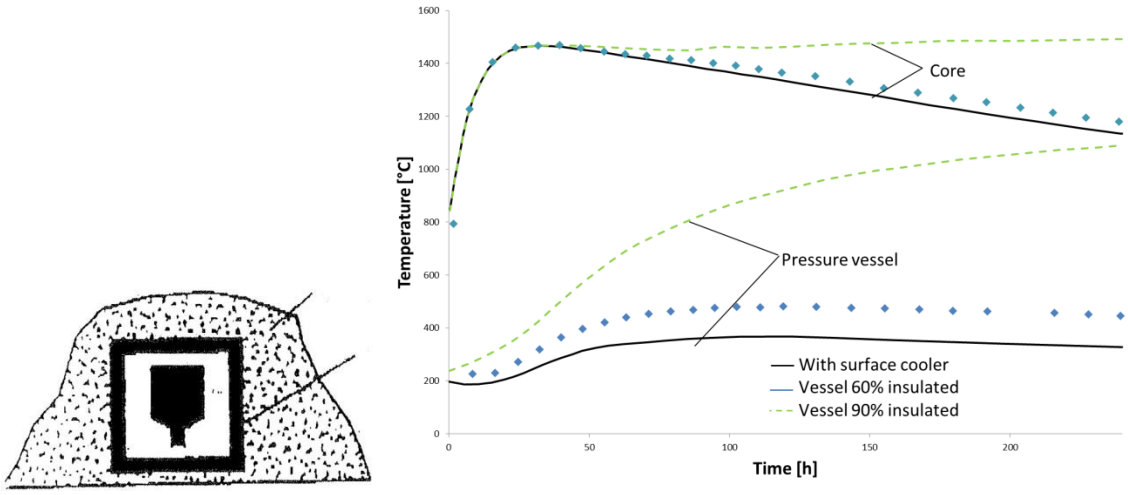

Figure 89: Accident case D — concrete structures are destroyed, reactor is covered with rubble: (a) model for calculations; (b) results of calculations for the time dependence of relevant temperatures

Generally the outer parts of the core become hotter than in the accident cases discussed before. However, under the assumption of an intact reactor pressure vessel it can be stated that even this extreme disturbance of the decay heat removal system does not cause the reactor to heat up towards temperatures that would destroy the fuel elements. Even in this case the fission-product release would be limited.

Another interesting point is linked to very strong seismic events is that a change in the density of the pebble bed core could happen. In the normal non-compacted state the packing fraction of the pebble bed is assumed to have an average value of 0.61. The results of seismic event simulations in a large test facility showed that, depending on the magnitude of horizontal acceleration and the acceleration period, very small changes in the packing factor occur. For an acceleration of 0.3 g, for example, characteristic values of a maximum 2 % change of density are reasonable. Hence, this is of no relevance for the reactivity balance and for the cooling conditions of a modular HTR.

7.2. Self-acting decay heat removal

7.2.1. Overview of the concept

Self-acting decay heat removal uses physical means, namely conduction, convection and radiation, to remove decay heat without using active or passive machinery. Figure 90 explains the principle of heat transport from the core to the environment. In case of severe accidents in the modular HTGR a total loss of coolant and a total loss of active decay heat removal is assumed. In this case the self-acting removal of decay heat takes place and a possible meltdown of the reactor core is avoided as the fuel temperatures do not reach concerning temperatures. In fact, theoretically no fission-product release from the fuel elements occurs (Mertens, et al., 1985) (Schenk, et al., 1986) (Schenk, et al., 1989). This inherent feature cannot fail because of accidents due to internal and external reasons.

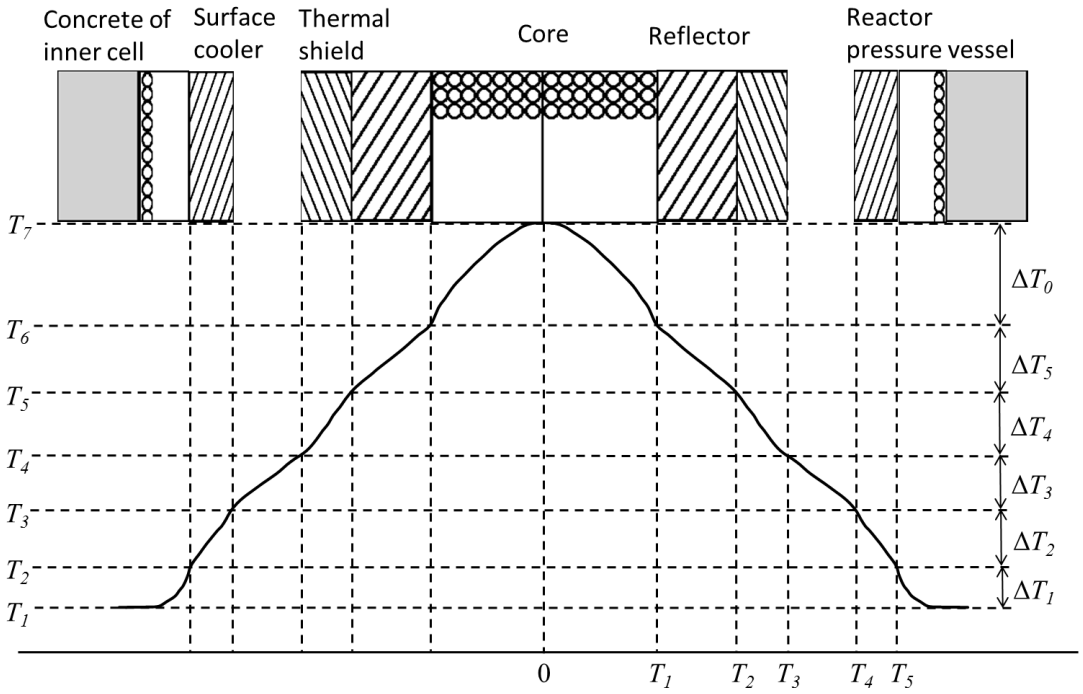

Figure 90: Stationary radial temperature profile in case of self-acting decay heat removal in a modular HTR (Tmax in the hottest part of the core)

Some further explanations on the concept, as far as heat transport mechanism and limitations of temperatures in the components are considered, are contained in Table 42.

Table 42: Heat transport mechanism and temperature limits: (a) heat transport mechanism in different structures; (b) limiting parameters for the concept (e.g. HTR Module, 200 MWth)

Position	Conduction	Radiation	Free convection
Core	●	●	●
Reflector	●		
Reflector -> thermal shield		●	●
Thermal shield	●	●	
Thermal shield -> reactor vessel		●	●
Reactor vessel	●		
Reactor vessel -> cooling system			
Reactor vessel -> concrete	●	●	●

Parameter	Condition	Characteristic value
Fuel temperature	$T_{fuel} < T_{fuel}(\max.)$	$T_{fuel}(\max.) < 1\,600℃$
Temperature of the reactor pressure vessel	$T_{rpv} < T_{rpv}(\max.)$	$T_{rpv}(\max.) < 600℃$
Temperature of the concrete	$T_{conc} < T_{conc}(\max.)$	$T_{conc}(\max.) < 400℃$
Heat removal	$\dot{Q} > \dot{Q}(min.)$	$\dot{Q}(min.) \approx 800K$

The main requirement is that the heat is released from the core by these self-acting mechanisms in such conditions that the maximum fuel temperature stays below a value of T_{max}. Currently T_{max} has the value of 1 600 °C for coated particle fuel (TRISO particles). In these conditions the fission products stay almost completely inside the coated particle. If a reactor releases the decay heat by self-acting processes and the maximum fuel temperature stays below this permitted level (< 1 600 °C) the reactor system is called thermally stable. Some results from annealing experiments using irradiated pebble bed fuel elements with TRISO particles are explained in Figure 91.

The top figure shows the release of ^{85}Kr as a function of the temperature, the lower figure the release of ^{90}Sr, ^{137}Cs and ^{85}Kr depending on the heating time at a temperature of 1 600 °C.

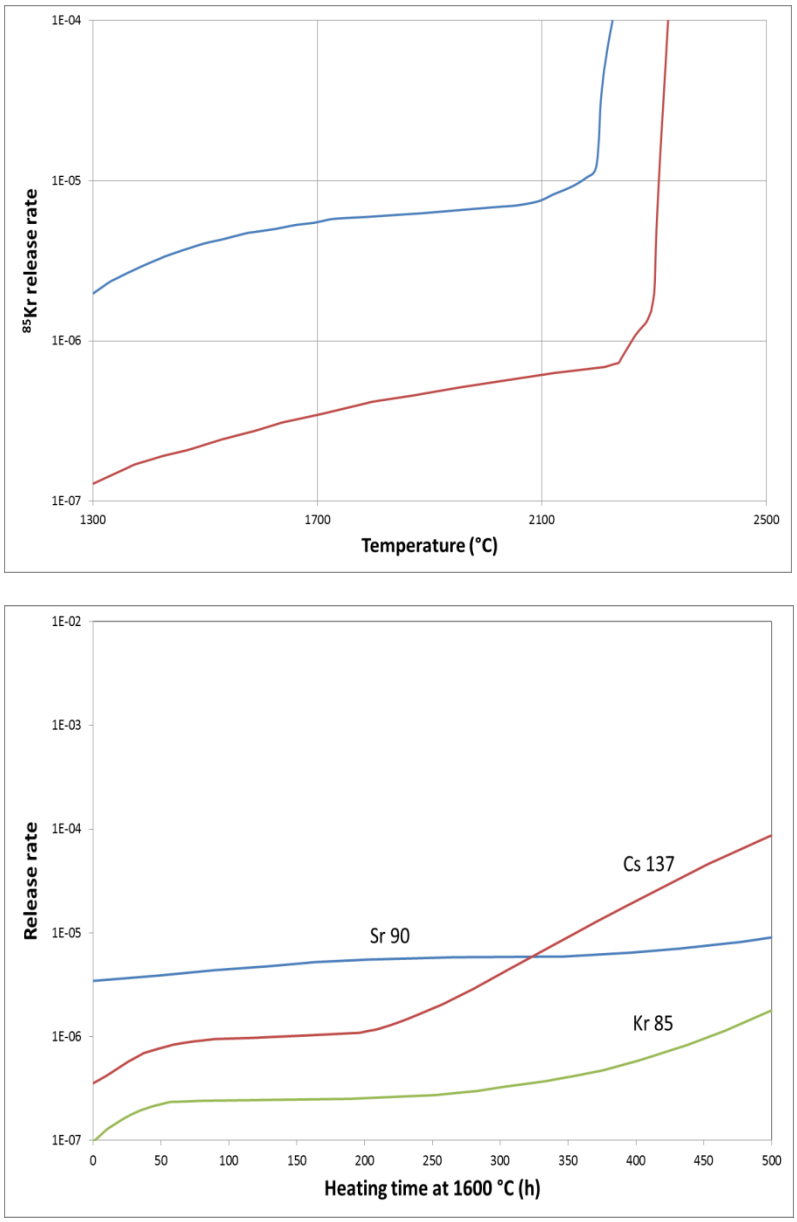

Figure 91: Release fraction of fission products from pebble bed fuel elements containing TRISO-coated particles

The release fractions of noble gases or of iodine dependent on temperature and time are indeed very low even after a long period of annelation of the solid fission products, such as for ^{137}Cs and ^{90}Sr.

The principles of heat transport, characterised here, can never fail if the system is designed in the right way and if the parameters of the core and the core internals are chosen corresponding to the requirement of temperature limitation.

7.2.2. Valuation of parameters influencing the decay heat removal concept

As already indicated in Figure 92, the heat removal depends on several parameters that are connected to the core design and the layout of the internal structures that influence the fuel temperatures in normal operation, shutdown or emergency cases.

Also as already indicated, heat removal depends on several parameters that are connected to the core design and the layout of the internal structures that influence the fuel temperatures in normal operation, shutdown or emergency cases.

The influence of the main parameters characterising the working of this principle can be discussed on behalf of the qualitative estimations of self-acting decay heat removal shown in Figure 92.

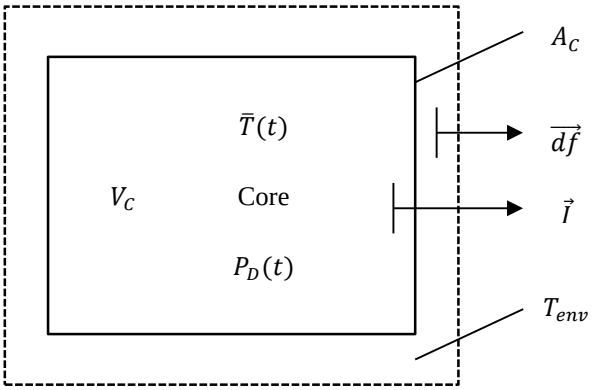

Figure 92: Schematic system for balancing decay heat production and dissipation from the core

Energy balance of the core:

$$\frac{dE}{dt} = P_D(t) - \int_{(a_c)} \bar{J} d\bar{f} \tag{60}$$

Energy in the core:

$$E(t) = \int_{(V_B)} p \cdot c \cdot T(\bar{r}, t) \cdot dV \tag{61}$$

Decay heat production:

$$P_D(t) = \int_{(V_C)} \dot{q}_D^{'''}(\bar{r}, t) \cdot dV \tag{62}$$

Energy balance of the core:

$$\frac{d}{dt} \int_{(V_C)} \rho \cdot c_p \cdot T(\bar{r}, t) \cdot dV = \int_{(V_C)} \dot{q}_D^{'''}(\bar{r}, t) \cdot dV - \int_{(A_C)} \bar{J} \, d\bar{f} \tag{63}$$

Average value of the core temperature:

$$\bar{T}(t) = \int_{(V_c)} \frac{T(\bar{r}, t) \cdot dV}{V_C} \tag{64}$$

Decay heat production:

$$\int_{(V_C)} q_D^{'''}(\bar{r}, t) \cdot dV = \overline{\dot{q}_D^{0'''}} \cdot f_{D(t)} \cdot V_c = \overline{\dot{q}_D^{0'''}} \cdot V_c \cdot 0.062 \cdot t^{-0.2} \tag{65}$$

Equation of the time dependence of temperature:

$$\bar{\rho} \cdot \bar{c_p} \cdot V_C \frac{d\bar{T}}{dt} = \dot{q}_D^{0'''} \cdot V_C \cdot 0.062 \cdot t^{-0.2} - k \cdot A_C \cdot (\bar{T} - T_{env}) \tag{66}$$

This differential equation provides a rough estimate of the time dependence of the average temperature in the core and shows the influence of the main parameters: $\bar{\rho} \cdot \bar{c_p}$. k, A_C, V_C. The solution of the dependence of the average temperature in the core can be derived using the following equations.

From the approximation of the decay heat function by an exponential function:

$$t^{-0.2} \approx A \cdot \exp(-a \cdot t) \tag{67}$$

the constants c_1 and c_2:

$$c_1 = \overline{\dot{q}_0'''} \cdot A/\overline{\rho \cdot c_p} \tag{68}$$

$$c_2 = K \cdot A_C/V_C \cdot \frac{1}{\overline{\rho \cdot c_p}} \tag{69}$$

and the starting condition:

$$t = 0: \bar{T}(t = 0) = \bar{T} \tag{70}$$

one gets the solution:

$$T(t) = T_u\,(1 - e^{-c_2 \cdot t}) + \left(\overline{T_0} - \frac{c_1}{c_2 - \alpha}\right) \cdot e^{-c_2 \cdot t} + \frac{c_1}{c_2 - \alpha} \cdot e^{-\alpha \cdot t} \tag{71}$$

The qualitative solution of this is illustrated in Figure 93.

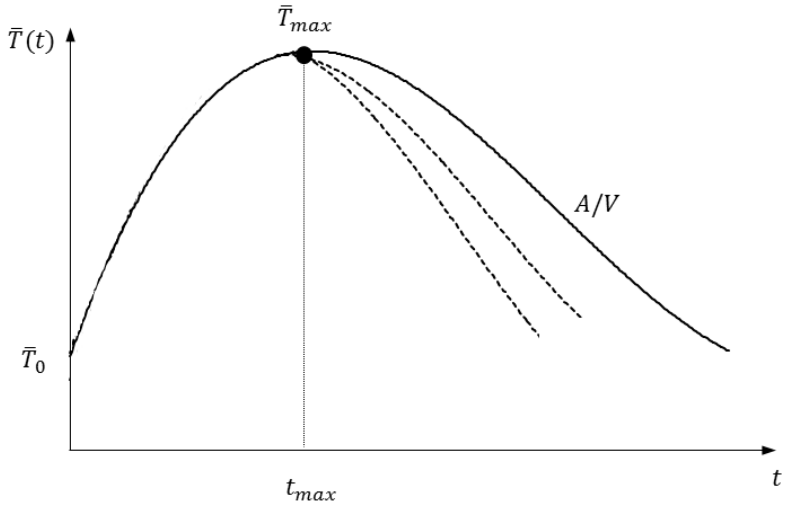

Figure 93: Qualitative picture of the above-derived solution

It can be assumed that during the first phase of the accident most of the decay heat is stored in the core and the surrounding graphite structures. The transient of an average temperature, adiabatic condition, can be expressed as follows:

$$\frac{d\bar{T}}{dt} = \overline{\dot{q}_c'''} \cdot \frac{V_C}{V_t} \cdot \frac{1}{\rho \cdot c_p} \cdot 0.062 \cdot t^{-0.2} \quad (72)$$

$$\bar{T}\ (t) = \overline{T_0}(t) \cdot \frac{V_C}{V_t} \cdot \frac{1}{\rho c_p} \cdot \frac{0.062}{0.8} t^{0.8} \quad (73)$$

With values of:

$$\overline{\dot{q}_c'''} = 3\ MW/m^3,\ V_C/V_t \approx 0.7, p \cdot c_p \approx 2\ J/K \quad (74)$$

the maximum temperature transient at the beginning of the accident is calculated to be in the order of:

$$d\bar{T}/dt \approx 100\,°C/h \quad (75)$$

After $t = 10$ hours an average value of $\bar{T} \approx 1\,000$ °C is reached if the initial temperature of the system was 500 °C. Hence, the core of an HTGR is very robust against 'loss of cooling' accidents.

A more detailed evaluation of the solution derived above delivers for the time t_{max} a value for $\bar{T}_{max.}$, where:

$P_D/P_{th} \approx 0.4$ % (after around 30 hours for t_{max}),

$$\overline{\dot{q}_c'''} = 3\ MW/m^3, k = 10\ W/m^2K, A_C/V_c = 150\,m^2/66\,m^2 = 2.3\,m^{-1}$$

a value of:

$$\bar{T}_{max} - T_{env} \approx 1\,000\,°C$$

Further important results of this simple estimate are:

$$\overline{\dot{q}_c'''} = \frac{P_D}{P_{th}} \approx 1.2 \cdot 10^{-2}\ \mathrm{MW/m^3} \quad (76)$$

$$\bar{k} \cdot \frac{A_c}{V_c} (\bar{T}_{max} - T_{u)} \approx 2 \cdot 10^{-2}\ \mathrm{MW/m^3} \quad (77)$$

Thus, after some time (t*), the heat losses from the surface are larger than the decay heat production. In the time span before, the decay heat is mainly stored in the ceramic fuel elements without any danger of them being destroyed. Additionally, there is a radial temperature profile inside the core and the structures of the reactor.

To get an impression of what parameters influence this radial heat transfer the following estimate may help considering the stationary heat transport inside the core. One can assume a specific point in time, for example the time at which the maximum fuel temperature occurs, and apply the stationary heat transport equation:

$$0 = \int_{(V_C)} \dot{q}_D'''(\bar{r}, t) \cdot dV - \int_{(A_c)} \bar{j} \cdot \bar{df} \quad (78)$$

The application of Gauss's law delivers:

$$\int_{(A_B)} \bar{J} \cdot \mathrm{df} = \int_{(V_B)} div\, \bar{J} \cdot dV \tag{79}$$

The radial dependence of temperature is a result of the differential equation:

$$\dot{q}_C^{0'''} = 0.062 \cdot t^{*-0.2} + \lambda_{eff} \cdot \Delta\tilde{T} = 0 \tag{80}$$

where Δ is the Laplace operator and λ_{eff} an effective heat conductivity in the core, in which all processes of conduction, radiation and free convection are included.

The ordinary differential equation:

$$\frac{d^2\tilde{T}}{dr^2} + \frac{1}{r} * \frac{d\tilde{T}}{dr} + \bar{\dot{q}}_D{}''' * \frac{0.062 * t^{*-0.2}}{\lambda_{eff}} = 0 \tag{81}$$

has to be solved with the boundary conditions:

$$\bar{T}(r = R) = \bar{T}_r, \bar{T}(r = 0) = \bar{T}_0 \tag{82}$$

As a result the radial temperature profile in the core can be determined as:

$$\bar{T}_0 - \bar{T}_r \approx \bar{\dot{q}}_c{}''' * f_D(t^*) * \beta * \frac{R^2}{4\bar{\lambda}_{eff}} \tag{83}$$

where β is the peak factor:

$f_D(t^*) \approx 0.4\,\%$ for $t^* = 30h$

$\bar{\lambda}_{eff}$ is suitable effective heat conductivity inside the pebble bed. Here an average value for $\bar{\lambda}_{eff}$ is assumed.

Figure 94 contains a qualitative figure of the radial temperature profile in the reactor at a specific time, for instanced at $t = t^*$.

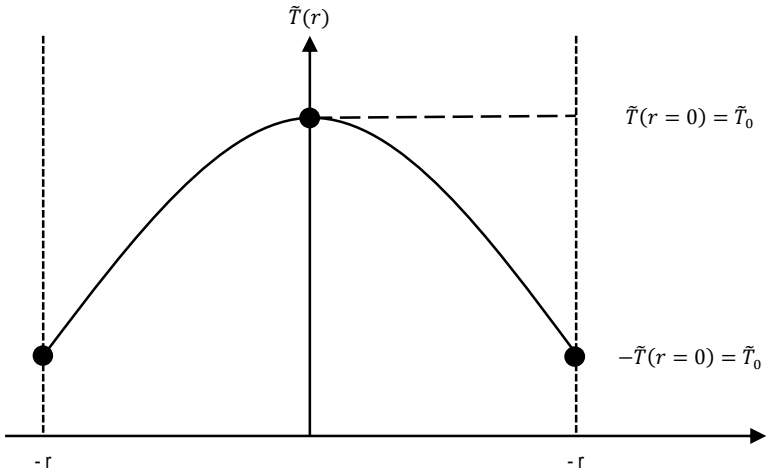

Figure 94: Qualitative dependence of a radial temperature profile in the core (at $t = t^*$ with $f_D(t^*)$)

As a result the differential equation to estimate the radial dependence of the temperature at a special time t^* can be calculated. This can be done applying some typical values of the HTR Module (Lohnert, 1990) such as:

$$\beta = 1.6, \bar{\dot{q}}''' = 3\frac{MW}{m^3}, f_D(t^*) = 4 * 10^{-3}, R = 1.5\ m\ and\ \bar{\lambda}_{eff} = 15W/mK$$

The computation of this formula results in a temperature difference across the core of approximately:
$\Delta T_{max} = 720^\circ\ C$

This value has to be taken into consideration to get an impression of the peak temperature inside the reactor. Taking into account a temperature of 800 °C on the reflector boundary, the maximum temperature is around 1 500 °C in the hotspot region of the HTR Module after 30 hours. This temperature is well below the maximum temperature limit of the fuel elements of 1 600 °C. Detailed three-dimensional computer calculations deliver results similar to those explained before. The heat transport between the gaps inside the reactor structures can also be estimated with simple models. Figure 95 illustrates the heat removal in small gaps in the reactor structures.

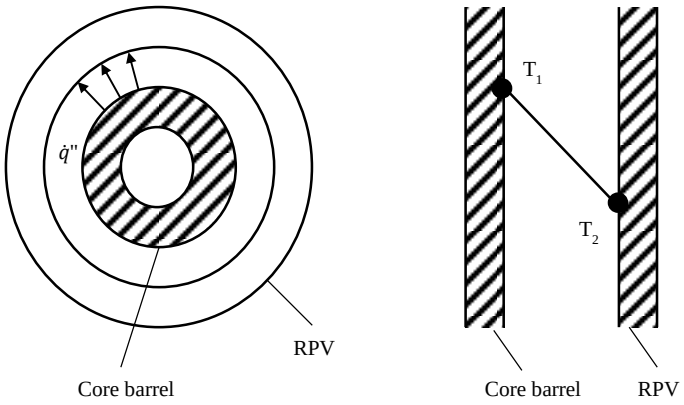

Figure 95: Heat transport across gaps in the core

Here the heat removal is mainly driven by conduction through gas and heat radiation. In case of depressurisation the conduction through the primary coolant in the gaps is negligible, therefore, for example, only radiation and free convection have to be taken into account.

The transport by radiation is described by the following equation:

$$\dot{Q}/_A = \dot{q}'' = \varepsilon * C_s * \left(\left(\frac{T_1}{100}\right)^4 - \left(\frac{T_2}{100}\right)^4\right)$$

with the values in the core structures of modular HTR (200 MWth) being:

$$\varepsilon = 0.6, C_s = 5.6\frac{W}{m^2K4}, \dot{q}^* \approx \frac{600KW}{150m^2} = \frac{4KW}{m^2}$$

This brief calculation leads to a temperature T_1 of approximately 433 °C for the pressure vessel if the outside of the core barrel is T_2 = 600 K.

A gap in the core structures between relevant structural zones (graphite reflector/thermal shield; thermal shield/reactor pressure vessel) delivers a temperature difference in the order of 100 °C each.

Finally, the decay heat must leave the surface of the RPV without overheating this component. A rough estimation of the heat balance for the time t^* delivers:

$$P_{th} * f_D(t^*) = 2\pi * R_2 * H_c * \bar{\alpha} * (T_{RPV} - T_{env}) \quad (84)$$

in which $\bar{\alpha}$ is the heat-transfer number at the outer surface of the reactor pressure vessel.

Applying characteristic values of an HTR Module (200 MWth):

$$R_2 = 3m, \bar{\alpha} = 10\,{}^{W}/_{m^2K}, T_{RPV} - T_{env} \approx 300K, f_D(t^*) \approx 0.4\,\% \quad (85)$$

the following limiting value is derived:

$${}^{P_{th}}/_{H_c} \approx 22\,{}^{MW}/_{m} \quad (86)$$

as a permitted linear power rating for self-acting heat transfer from the surface of the RPV. If the limiting maximum fuel temperature of $T_{max} < 1\,600^{\circ}\mathrm{C}$ is applied the core height of the HTR Module reactor is limited to 9.4 m. A thermal power of 200 MW fulfils this boundary condition. The temperature difference in the RPV wall itself is relatively small:

$$\Delta T_{RPV} = \dot{q}'' * \frac{s}{\lambda} \quad (87)$$

in which:

$\dot{q}''$= the heat flux through the wall;
s = the wall thickness; and
λ = the heat conductivity of steel.

With a heat flux of 4.0 kW/m^2 at time t^* $s = 0.1m, \lambda = 30\,W/mk$, ΔT_{RPV} results in a value of 13 °C, which causes no intolerable additional stresses as secondary loads.

From the considerations given above it can be stated that the following features of the reactor core are essential for the self-acting decay heat removal so as to prevent core melting and the superheating of fuel elements above tolerable temperature limits:

- low power density ($\bar{\dot{q}}'''$) in the core;
- high effective heat conductivity (λ_{eff}) in the core;
- short distance (R) for the transport of heat inside the core;
- high heat-storage ($\overline{\rho c_p}$) capability of the core;
- high temperature stability of the core materials;
- high heat-transfer numbers ($\bar{\alpha}$) through the core structures;

- high ratio of surface to volume (A_R/V_R) for the core;
- permanent outer heat sink outside the RPV.

Additionally, there are some further requirements for the integrity of the fuel elements in case of extreme accidents:

- avoid large amounts of air ingress into the primary system or use corrosion protected fuel elements — this first requirement can be fulfilled by a suitable design of the inner concrete cell together will a self-acting closure of the cell after depressurisation;
- use of a core in which unwanted rises of fuel temperatures because of strong nuclear reactivity transients are impossible;
- avoid the ingress of large amounts of water or steam into the core after accidents in the steam generator — this can be ensured by a suitable design of the steam generator system, for instance in such a way that the steam generator is placed below the core.

If the very extreme accident case is considered in which the total outer surface of the reactor pressure vessel is insulated or covered by rubble, which could be the case after an extremely strong earthquake, the following simplified estimate helps to identify the important parameters for the transient behaviour of the system (Figure 96).

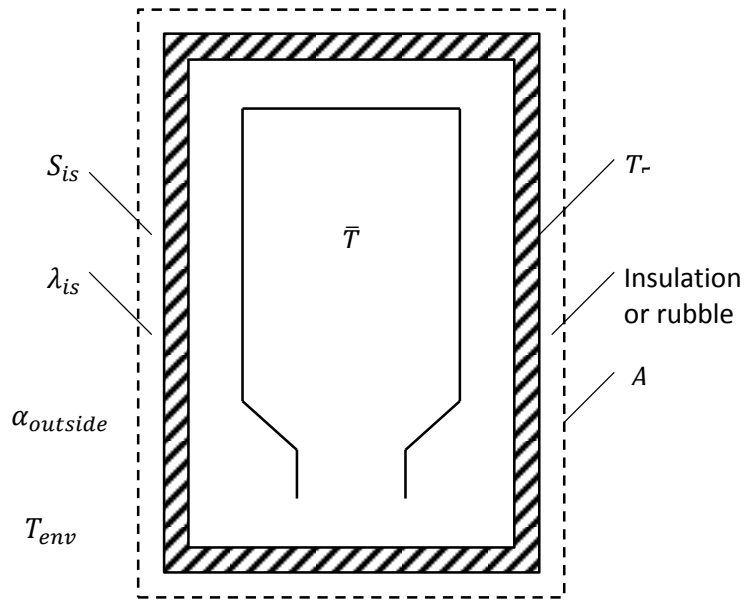

Figure 96: Simplified model to evaluate the system in a very extreme accident

The energy balance delivers the relation for this case in the following form:

$$\frac{dE}{dt} = \frac{d}{dt}\int_{V_v} \rho * c_p * T * dV = P_D(t) - \dot{Q}_L(t) \tag{88}$$

An average temperature $\bar{T}$ of the system with a volume V_R of the reactor is defined by:

$$\frac{d}{dt}\int_{V_R} \rho * c_p * T * dV \approx \sum_i \rho_i * c_{p_i} * V_i * \frac{d\bar{T}}{dt} \tag{89}$$

i indicates the different parts of the reactor (core, internal structures, RPV), which may store heat. The decay heat is approximated in the form:

$$P_D(t) = P_0 * 0.0622 * (t^{-0.2} - (t_0 + t)^{-0.2}) \quad (90)$$

The heat losses can be described by the simplified expression:

$$\dot{Q}_L = A * (\bar{T}_s - T_{env}) * \bar{\alpha} \quad (91)$$

in which $\bar{T}_s$ is the surface temperature of the vessel and T_{env} is the temperature outside the total configuration. The heat-transfer number α mainly contains the heat conductivity λ_{is} and the mean thickness δ_{is} of the insulating material, as well as the heat-transfer coefficient or the outside of the total arrangement:

$$\frac{1}{\bar{\alpha}} + \frac{1}{\lambda_{is}/\delta_{is}} + \frac{1}{\alpha_{outs}} \quad (92)$$

A is the surface of the total configuration of the rubble, α_{outs} characterises the heat-transfer coefficient on the outside of this material zone, caused by radiation and free convection of air. In a first approximation T_s might have the same value as $\bar{T}$.

Thus, the final differential equation results in the form:

$$\frac{d\bar{T}}{dt} = \frac{P_{th}}{\sum_i \rho_i * c_{p_i} * V_i} * 0.062 * t^{-0.2} - \frac{\bar{k} * A}{\sum_i \rho_i * c_{p_i} * V_i} * (\bar{T} - T_u) \quad (93)$$

A solution to this differential equation delivers functions is shown in Figure 97.

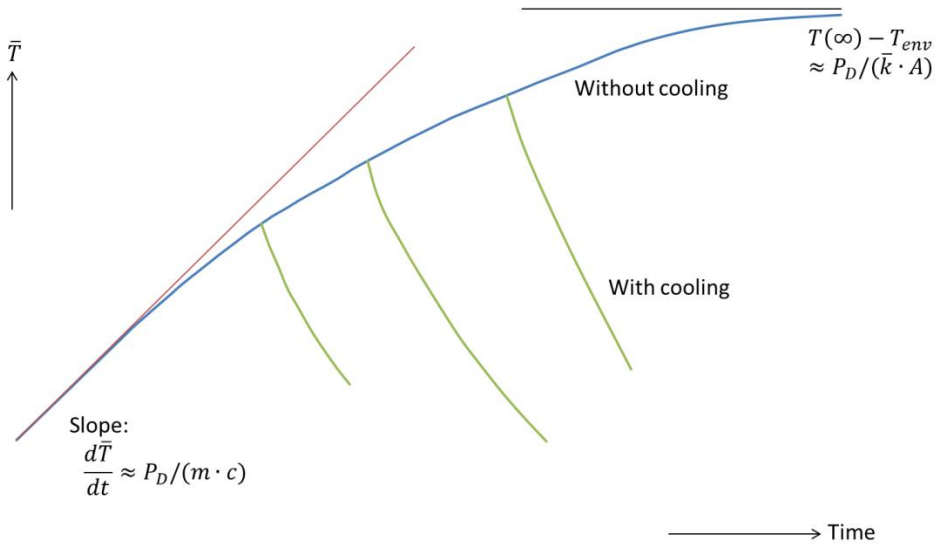

Figure 97: Qualitative values of temperature of reactor pressure vessel and fuel dependent on time

The maximum increase in temperature in a first phase can be estimated by the following equation:

$$\frac{d\bar{T}}{dt} = \frac{P_{th}}{\sum_i \rho_i * c_{p_i} * V_i} * 0.062 * t^{-0.2} \quad (94)$$

Again some values for the structures of the HTR Module may be used for better illustration:

$$P_{th} = 200MW, \sum_i \rho_i * c_{p_i} * V_i = 4 * 10^8 \, {}^{Ws}/_{K} \quad (95)$$

This results in a transient of approximately 5 K/h after 30 hours. After that time, a major part of decay heat enters the wall of the reactor pressure vessel, which acts as a main heat sink. Assuming a decay heat fraction of 0.3 % of the thermal power and a storage capacity of 50 MJ/K, a temperature transient of approximately 4.5 K/h results. Assuming an adiabatic system, the vessel would fail after 500 hours due to melting of the steel.

From the beginning of the accident a part of the heat is passed to the rubble and released into the environment. Non-adiabatic limiting temperatures of the system can be derived from the following equation:

$$P_D \approx \dot{Q}_{losses} \approx \bar{k} * A(T(\infty) - T_{env}) \quad (96)$$

If the decay heat is assumed to be 400 KW for a longer time (corresponding to 2 ‰ in case of an HTR Module, 200 MWth) the outer surface A to be approximately 1 000 m^2 and the heat-transfer coefficient $\bar{k}$ to be 0.5 W/m^{2}K the adiabatic temperature $T(\infty) \approx 800K$ is obtained.

Calculations using more dimensional computer codes have already shown this. One of the important results is the fact that even in these extreme accident cases the maximum fuel temperature is very similar to the accident cases discussed before. However, the outer structures and their heat conductivities are very important for the transient. If the surrounding infrastructure is not completely destroyed, man-made interventions in time (e.g. additional cooling using nitrogen) could cool the system earlier.

These results show in a very convincing manner that the concept of self-acting decay heat removal works even in case of extreme accidents. In all accident scenarios the maximum fuel temperature stays below the tolerable 1 600 °C. Furthermore, there should be enough time to apply very simple emergency cooling procedures. Some examples for these measures are:

- injection of nitrogen into the reactor pressure vessel, if this is possible, by direct access of machines;
- injection of nitrogen into the rubble;
- spraying with water.

The ‘grace period’ would be in the order of some days, before damage (e.g. from air ingress) would have to be considered.

7.2.3. Influence of uncertainties relating to the different steps of the transport chain for decay heat removal on the maximum fuel temperature

If a maximum fuel temperature of 1 600 °C is assumed as the tolerable temperature limit in a ‘total loss of active cooling’ accident a safety margin between this value and the calculated value needs to be assumed. Therefore, uncertainties of calculation for the maximum temperature have to be analysed and considered. By applying a simple approximation:

$$T_{fuel}(max) = T_{fuel}(nominal) + \Delta T_{fuel} \quad (97)$$

a value of $+\Delta T_{fuel} \approx 100\ ^{\circ}$ C is considered to be a suitable additional safety margin. For the nominal value the temperature of the hottest fuel element can be derived as follows:

$$T_{fuel}(nominal) = \overline{\dot{q}^*} * \beta * f_D(t^*) * \Phi(r_i, \lambda_i, \alpha_i,) \quad (98)$$

in which:

$\overline{\dot{q}^*}$ = average power density in the core

β = peak factor of power density

$f_D(t^*)$ = factor of the decay function, of approximately. 3×10^{-3} after time $t^* \approx 30h$ for the HTR Module of around 200 MWth

$\Phi(r_i, \lambda_i, \alpha_i,)$ function describing all steps of heat transfer in the core and internals

$$\Phi = \frac{{r_1}^2}{4\lambda_{eff}} + \frac{r_1}{2} * \frac{(r_2 - r_1)}{\lambda_G} + \frac{r_1}{2} * \frac{r_1}{r_3} * \frac{(r_2 - r_1)}{\lambda_S} + \frac{r_1}{2} * \frac{r_1}{r_4} * \frac{1}{\bar{\alpha}_s} + \frac{r_1}{2} * \frac{r_1}{r_5} * \frac{(r_5 - r_4)}{\lambda_S} + \frac{r_1}{2} * \frac{r_1}{r_5} * \frac{1}{\bar{\alpha}_a} \quad (99)$$

Uncertainties can be correlated to this function by expressions such as the one given below:

$$\Delta T_{fuel} = \sum_i \frac{\partial T_{fuel(nominal)}}{\partial \xi_i} * \Delta \xi_i \quad (100)$$

Regarding the uncertainty of the fuel temperature in relation to the nominal value this would result in the following equations:

$$\frac{\Delta T_{fuel}}{T_{fuel}} \approx \frac{\Delta \overline{\dot{q}'''}}{\overline{\dot{q}'''}} + \frac{\Delta \beta}{\beta} + \frac{\Delta f_D(t^*)}{f_D(t^*)} + \frac{\Delta \Phi}{\Phi} \quad (101)$$

$$\frac{\Delta \Phi}{\Phi} \approx \frac{\Delta \lambda_{eff}}{\lambda_{eff}} \quad (102)$$

$\Delta\Phi/\Phi$ is approximated in simplified form if the uncertainties of the heat conductivity in the pebble bed are considered to be the main uncertainties for the function Φ.

The uncertainties relating to the various other factors can be derived in detail from the measured curves for the relevant parameters. These are mainly $\lambda_{eff}(T)$ in the core, $\alpha_{eff}(T)$ in gaps, $\overline{\propto}_a\ (T)$ or the heat release from the reactor pressure vessel and naturally the uncertainties connected with the decay heat production. In particular, the factor β requires attention as it depends very much on the furnace cycle.

Figure 98 shows exemplary measurements of the effective heat conductivity in the core. Furthermore, the heat conductivity of graphite and values of the emissivity are given. The differences between the 'nominal' values in the curve of $\lambda_{eff}(T)$ and the 'lower' values are in the order of 10 %. The uncertainty of the emissivity plays an important role for the heat transfer on the outer surface and in the gaps. Certain values measured are given in Figure 98.

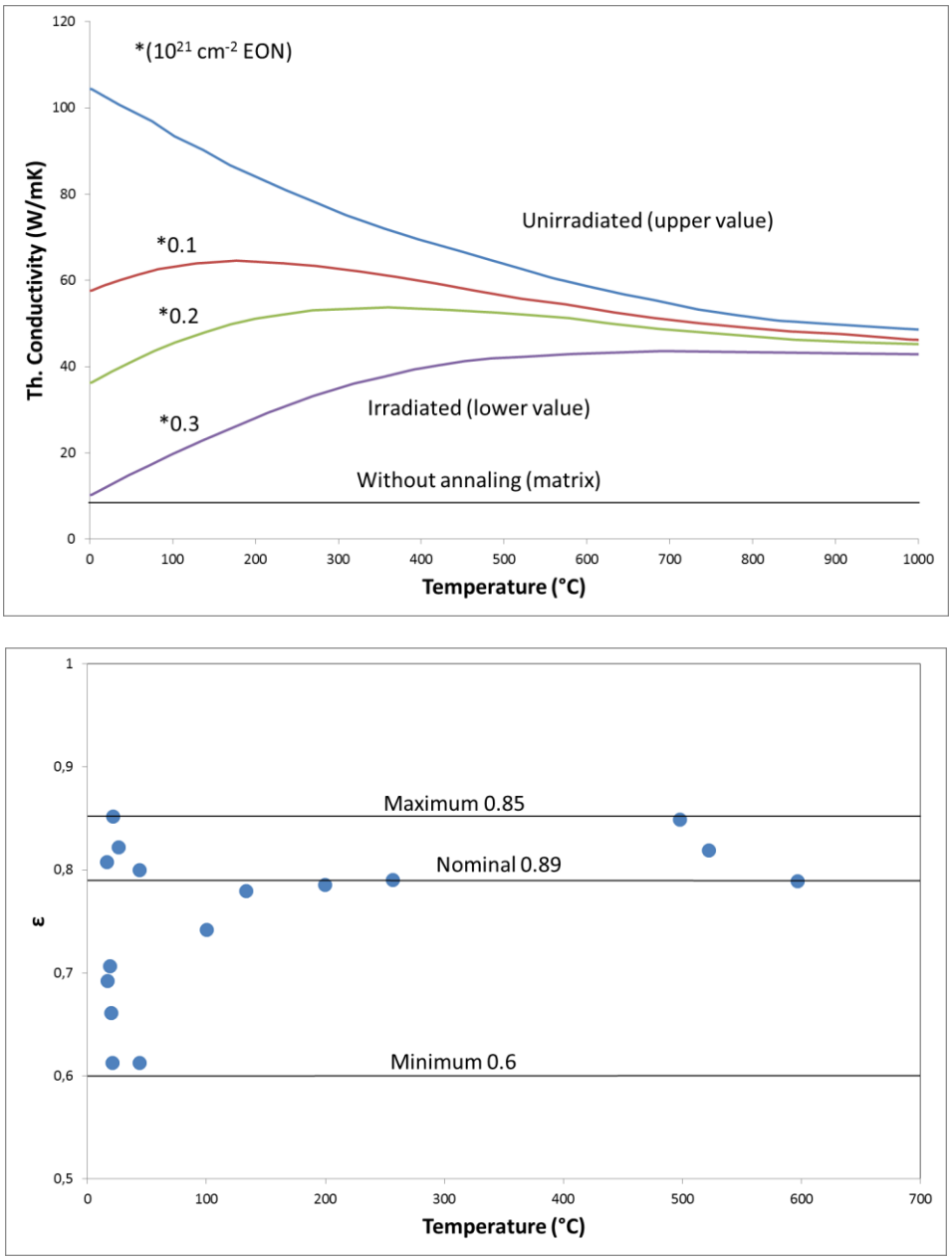

Figure 98: Uncertainties relating to measured parameters for the heat transport in the reactor system in case of a 'total loss of active cooling' accident:

Figure 98 shows the heat conductivity in the pebble bed (top), and for the reflector graphite (example AVR) the measured values of the ε.

There are some uncertainties in the definition of the status of the core at the start of the accident, which have to be analysed in detail. In particular, the height of the peak factor β depends on the type of the fuel cycle (e.g. the number of passes through the core clearly influences this parameter).

Due to the described uncertainties in calculations temperature measurements in the reactor core are desirable. In light-water reactors the temperature in the core is approximated using time-dependent hot channel factors. The pebble-bed reactor uses online refuelling so that, in contrast to an LWR, blind elements can be used to measure the temperature in the core.

In the AVR, for instance, blind elements have been fed to the reactor in order to determine the temperature in the core. These pebbles were equipped with melting wires. Figure 99 shows one of these elements.

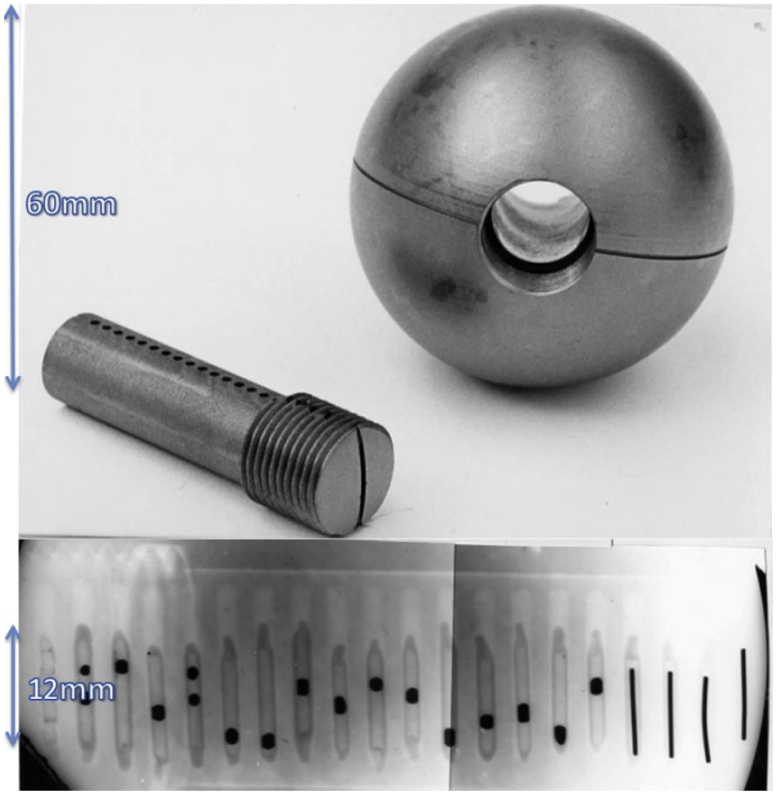

Figure 99: Spheres for temperature measurements in the core of the AVR (with melt-wires — the X-ray below shows the molten wires)

Table 43 provides specific information on the melting temperatures of the specific wires shown in Figure 99. Each element contained 20 wires. After they had passed the reactor and were removed from the fuel-handling cycle, they were post examined and the molten wires allowed the maximum temperature that the element examined experienced while passing the reactor core to be estimated.

Table 43: Characteristics of the wires shown in Figure 99

Sample number	Metal alloy components	Composition	Melting temperature (°C)
1	Al/Fe	99.2/0.8	655
2	Ag/Cu/In	60/27/13	700
3	Ag/Cu	72/28	780
4	Ag/Cu/Pd	68.4/26.6/5	810
5	Ag/Au/Cu	20/60/20	840
6	Ag/Cu	47/53	878
7	Ag/Cu/Pd	52/28/20	900
8	Ag/Cu	35/65	920
9	Ag/Cu/Pd	54/21/25	940
10	Ag	100	960
11	Au/Cu	46/54	982
12	Ag/Pd	95/5	1 000

13	Au/Cu	33.5/66.5	1 020
14	Au/Cu	25/75	1 050
15	Au/Cu	10.5/89.5	1 072
16	Cu/Pd	82/18	1 088
17	Cu/Ni	90/10	1 120
18	Cu/Ni	84/16	1 150
19	Ag/Pd/Mn	64/33/3	1 200
20	Pd/Cu	70/30	1 280

In some regions of the reactor (especially in the outer core) higher temperatures than previously calculated have been obtained (Figure 100). The difference between measurements and calculations were partly in the order of 150 °C. Explanations were given by considering, first, the influence of the graphite noses, second, of bypasses in the core structures or, third, by a large bypass on the cold side of the total gas flow.

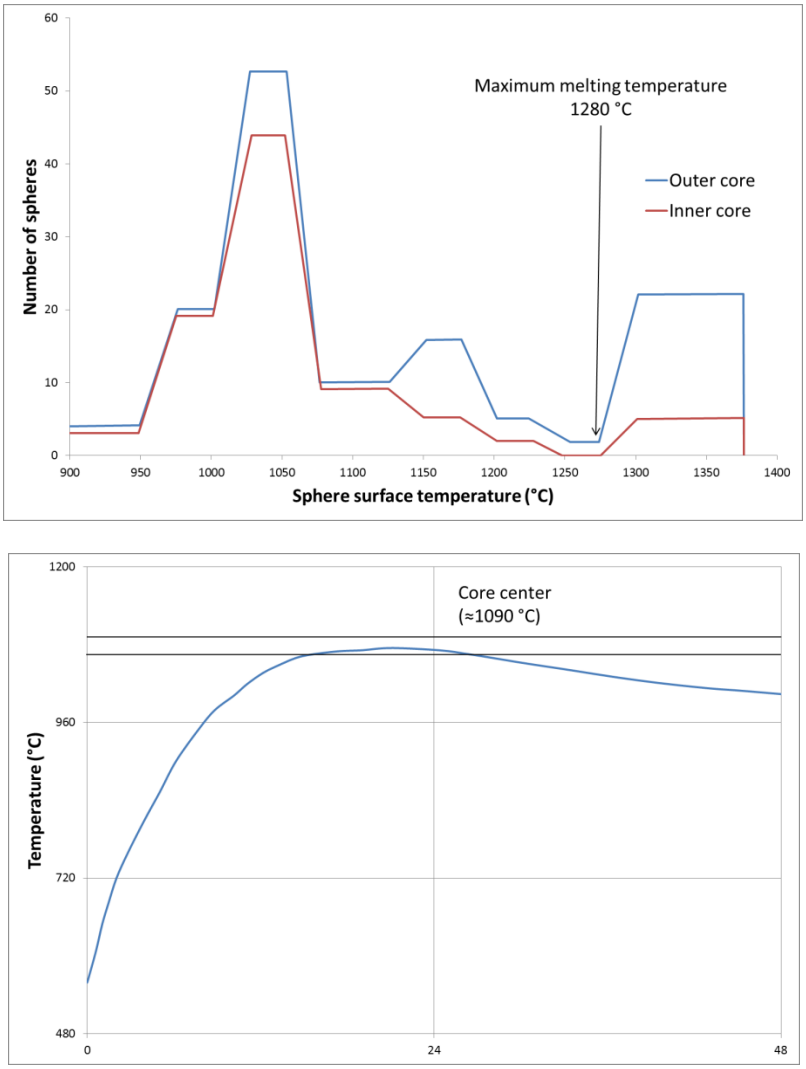

Figure 100: Aspects of temperature measurements in the AVR: (a) temperatures obtained from melt-wire experiments; (b) calculated maximum temperature in core

These elevated temperature values during normal operation were characteristic for the AVR, where fresh fuel elements were put into core regions with the highest gas temperatures (counterflow of

fuel elements and cooling gas). For future pebble-bed HTR concepts the method tested here is an excellent concept to measure in core temperatures during operation.

Table 44 gives a rough overview of the uncertainties in case of a 'total loss of active cooling' accident (e.g. HTR Module, 200 MWth). The nominal value of the maximum fuel temperature is calculated to be as high as 1 450 °C. The maximum value is determined to be as high as 1 615 °C. In practice a value of around 100 °C to 150 °C as an additional safety margin seems to be adequate for the design and the licensing process.

Table 44: Estimates of the influence of uncertainties on the fuel temperature in case of a 'total loss of cooling' accident

Parameter	Dimension	Characteristic value of design	Uncertainties	Possible upper value	Remark
Power density by decay heat production	MW/m^3	0.01	+ 10 %	0.011	After around 30 hours
Temperature difference in the core (λ_{eff})	°C	700	+ 10 %	770	Including surface effects
Temperature difference in the reflector	°C	100	+ 20 %	120	Irradiation in 40 years
Temperature difference gap 1 (α_a)	°C	120	+ 20 %	144	Reflector/ thermal shield
Temperature difference gap 2	°C	120	+ 20 %	144	Thermal shield reactor vessel
Temperature difference on outside RPV	°C	350	+ 10 %	385	Surface cooler works
Total	°C	1 450	165	1 650	Including $T_{cooling} = 50^0$C

8. Appendix A

8.1. Irradiation tests in MTRs and in AVR

The irradiation testing of German HTGR fuels began in 1972 and has lasted for four decades. Table 45 provides a historical overview of the significant irradiation tests, categorised by the primary objectives of the individual tests.

Two features present in each of the major R & D programmes are that irradiation testing occurred in both accelerated neutron environments and real-time HTGR environments. All the important particle variants have been evaluated in this manner since the beginning of the fuel development effort. Accelerated neutron environments were made available in European MTRs:

- Dragon Reactor (DR) — England;
- FRJ2 Reactor — Germany;
- BR2 Reactor — Belgium;
- R2 Reactor — Sweden;
- High Flux Reactor (HFR) — Netherlands;
- Siloë Reactor (SL) — France.

The real-time environment is represented by the AVR in Jülich, Germany.

Fuel spheres intended for AVR irradiation testing were manufactured in large numbers with the purpose of bulk testing in a real-time HTGR environment. Small fuel-sphere lots were specially manufactured for the German LEU Phase 1 irradiation test programme and for the proof test fuel for the HTR Module. Irradiation testing of Phase 1 fuel elements began in European MTRs in May 1982 and continued until November 1990 (Mehner, et al., 1990).

Real-time testing in the AVR began with AVR 19 in July 1982, followed by AVR 21 in February 1984 and AVR 21-2 in October 1987. Irradiation testing of the HTR Module proof test fuel in HFR Petten began with HFR-K5 and K6 in June 1990 and continued until May 1994 (Nickel, et al., 2002).

Table 45: Historical overview of German irradiation tests in the development of coated particles from 1972 to 2010 (IAEA 2012)

R & D programme	Old LEUs	HEU programme for process-heat and gas turbine applications			LEU programme
	1972-76	1977-1981			1982-2010
		Variant 1	Variant 2	Variant 3	
Coated particle	UO_2 TRISO UO_2 BISO	(Th, U) O_2 BISO	(Th, U) O_2 TRISO	UC_2/UCO TRISO + ThO_2 TRISO	UO_2 TRISO
Test goal					
Coated particle tests					
Particle performance	HFR-M5 DR-S6	BR2-P24	BR2-P25	BR2-P23	HFR-P4 SL-P1
Fission product transport in intact particles	DR-S4	FRJ2-P22	FRJ2-P23	-	FRJ2-P27
Release from kernel	-	FRJ2-P25	FRJ2-P25	FRJ2-P25	FRJ2-P28
Chemical effects	FRJ2-P16	-	-	HFR-P3	HFR-P5

Fuel element tests					
Fuel element performance	DR-K5	HFR-K1	R2-K12 R2-K13	R2-K12	HFR-K3
FE fission product transport	-	-	FRJ2-K11	FRJ2-K10	FRJ2-K13 FRJ2-K15
Large-scale demonstration	AVR 6	AVR 14 AVR 18	AVR 15 AVR 20	AVR 13	AVR 19 AVR 21
Proof tests					HFR-K5 HFR-K6
High burnup tests					FRJ2-K15 HFR-EU1
High temperature test					HFR-EU1bis

After a 10-year pause, irradiation testing resumed in 2004 with the European Union-sponsored test HFR-EU1bis (Fütterer, et al., 2008) (Fütterer 2008) (September 2004 to October 2005) and in 2006 with HFR-EU1 (Laurie, et al., 2010) (September 2006 to February 2010). In both of these tests, fuel elements from the AVR 21-2 production (GLE-4/2 elements) were subjected to accelerated irradiation conditions in the HFR. Test HFR-EU1 also contained two Chinese spherical fuel elements from the HTR-10 production (Tang, et al., 2010).

8.2. Irradiation envelope

All of the irradiation tests listed in Table 45 (with the exception of large-scale demonstration tests) were conducted in the accelerated neutron environments of MTRs as opposed to a real-time HTGR neutron environment like the AVR. The European MTRs utilised for the accelerated testing of the modern LEU UO_2 TRISO fuel typically have higher thermal, epithermal and fast neutron fluxes than an actual HTGR. In such an environment, fissile fuel burnups and accumulated neutron fluences can be achieved in 1-2 years, as opposed to 4 years in an HTGR. Thus, 'accelerated' refers to an irradiation under higher thermal and/or fast neutron flux environments for the purpose of speeding up the normal rate of fuel burnup and fast fluence accumulation.

Table 46 lists the nominal maximum operating conditions for the primary parameters — operating temperature, fuel burnup and fast neutron fluence. These parameters are listed in the order of their importance in defining the irradiation environment a fuel specimen is subjected to in an irradiation test. Table 47 lists these irradiation test operating parameters for all the MTR accelerated irradiation tests conducted on modern LEU UO_2 TRISO-coated particles. Table 47 also contains the BOL and EOL 85mKr release rates that are indicative of in-reactor fuel performance.

Table 46: The nominal maximum HTGR design operating conditions, for which the MTR irradiation tests were patterned

Operating parameter	General HTGR design (Phase 1)	HTR Module
Spherical element central temperature (°C)	1 068	870 (cycled)
Burnup (% FIMA)	10.1	8.9
Fast neutron fluence (10^{25} n/m^2, E > 16 fJ)	2.7	2.1

The presence of active temperature-monitoring systems in all of the MTR accelerated irradiation tests made it possible to record temperatures and to measure the release rates of gaseous fission products from the fuel under irradiation. Sampling the helium and neon purge gas on the outlet side of the test capsules, followed by quantitative gamma-spectrometry of the gas sample, makes it possible to identify and quantify the fission gas isotopes of Kr and Xe present as a function of irradiation time.

Using this technique, and knowing the sample volume and purge gas flow rate at the time of sampling, a measure of the release rate (Ri) for a specific gas isotope from the irradiated fuel can be determined. Comparing the measured release rate to the computed birth rate (Bi) for specific fission gas isotopes provides a measure of the steady-state release behaviour of fuel under irradiation. Monitoring the fission gas R/Bs is the standard methodology of assessing in-reactor fuel performance.

A comparison of the nominal range of fuel burnup versus operating temperature limits for various HTGR designs with those achieved in MTR and AVR tests is shown in Figure 101, and these data are also presented in Table 47. The later HFR-EU1 and HFR-EU1bis tests are not shown here because data are still under review (Fütterer, et al., 2008) (Laurie, et al., 2010) (Tang, et al., 2010).

Test specimens irradiated in HFR-K3/3, middle positions of HFR-P4/legs 1, 2 and 3 and FRJ2-K13/2 achieved burnups above the nominal maximum burnup limit at operating temperatures well above the maximum limit. For those specimens irradiated in SL-P1, HFR-K3/2 and FRJ2-K15/1 and 3, the maximum burnup limits were exceeded in nearly all cases. However, the operating temperatures were not above the maximum limit in most instances. For the specimens irradiated in FRJ2-P27/1, 2 and 3, FRJ2-K13/1 and 2 and HFR-K3/1, the nominal burnup maximum was above 7 % FIMA, but did not exceed the nominal HTR Module maximum limit; however, they were accumulated at operating temperatures that exceeded the nominal maximum limit.

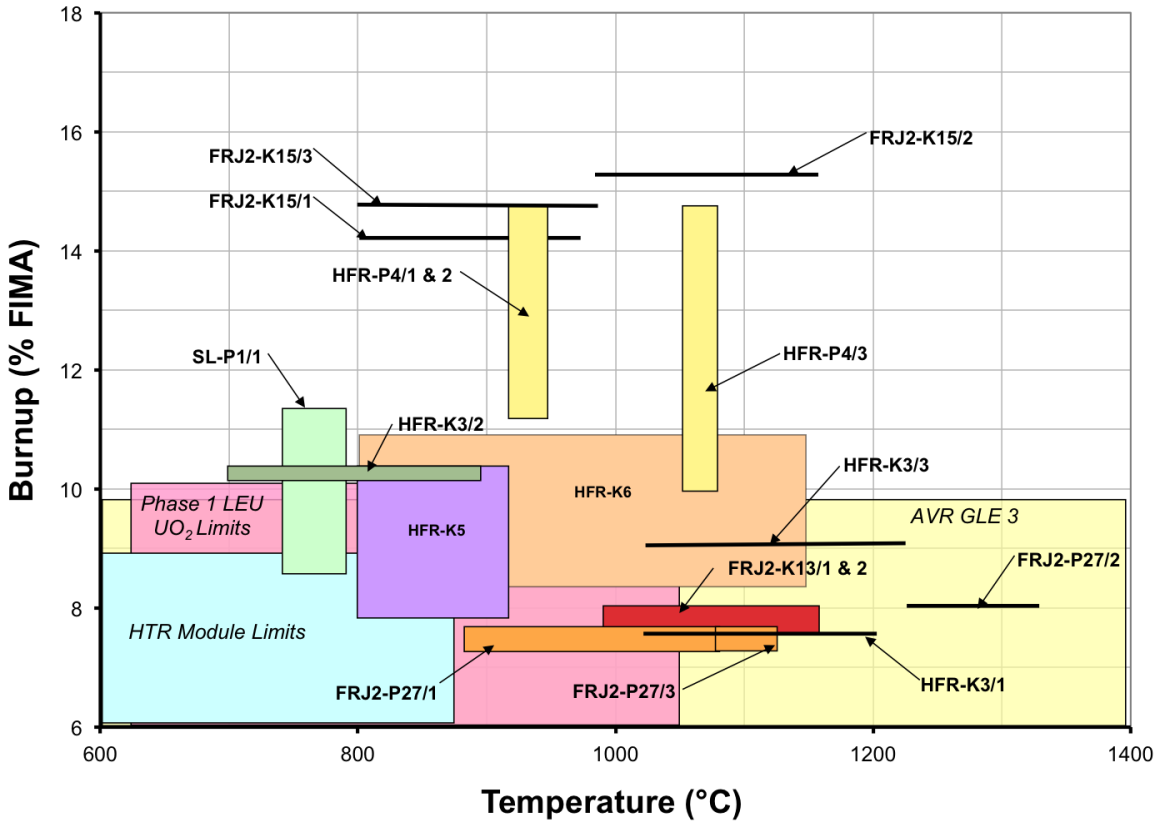

Figure 101: Irradiation envelope of fuel burnup versus mean operating temperature for LEU UO_2 TRISO particles in accelerated irradiation tests in European MTRs and in AVR prior to 2000

The in-reactor operational test data are presented in Table 47. Test specimens irradiated in HFR-K3/1 and 4 and HFR-P4/legs 1 and 3 well exceeded the nominal maximum fluence and temperature limits. For those specimens in HFR-K3/2 and SL-P1/1, the nominal fast neutron fluence limit was exceeded, but the operating temperatures did not exceed limits. For specimens irradiated in FRJ2-K13/1 and 2, FRJ2-P27/1, 2 and 3 and FRJ2- K15/2, the fluence limits were not exceeded: the fluences were all accumulated at temperatures higher than the nominal maximum operating temperature limit. It was only for FRJ2-K15/1 and 3, where the nominal maximum limits for fast neutron fluence and operating temperature, although above 800 °C, were not exceeded.

Figure 101 shows that HTGR irradiation requirements are fully enveloped by experimental results from the German fuel development programme database. However, the actual performance limits of the LEU UO_2 TRISO-coated particle had not been established in the 1980s. The recent HFR-EU1bis and HFR-EU1 irradiation tests were designed to explore irradiation loads that might reach these limits, but these tests are still under evaluation.

In 2004, irradiation testing of modern German HTGR fuel resumed with experiment HFR EU1bis (Fütterer 2008) in the HFR at Petten. Sponsored by the European Commission, the primary objective of HFR-EU1bis was to demonstrate the feasibility of LEU UO_2 fuel particle failure under normal operating conditions with extended operating temperatures up to and beyond 1 250 °C and peak fuel burnup to 16 % FIMA. The HFR-EU1bis experimental test rig contains five GLE-4/2 spherical elements in a single capsule.

Table 47: In-reactor operating parameters for the MTR irradiation tests conducted on modern high-quality LEU UO_2 TRISO fuel particles irradiated in the German fuel development programme

Irradiation test element	Operating temperature range (°C) subscr. transient	Burnup range (% FIMA)	Fluence (10^{25} n/m^2, E > 16 fJ)	^{85m}Kr R/B	
				BOL	EOL
MTR irradiation tests, Phase 1, LEU UO_2 TRISO fuels					
SL-P1***	740-790	8.6-11.3	5-6.8	5.8×10^{-7}	1.2×10^{-6}
HFR-P4/					
leg 1	915-940	11.1-14.7	5.5-8	3.5×10^{-9}	8×10^{-8}
leg 3	1 050-1 075	9.9-14.7	5.5-8	3.6×10^{-9}	8×10^{-9}
HFR-K3/					
1	1 020-1 200	7.5	4.0	1×10^{-9}	2×10^{-7}
2-3	700-900	10.1-10.2	5.9	9×10^{-10}	1×10^{-7}
4	1 020-1 220	9	4.9	2×10^{-9}	3×10^{-7}
FRJ2-K13/					
1-2	985-1 150	7.5-8	< 0.2	2×10^{-9}	1.6×10^{-8}
3-4	980-1 150	7.6-7.9	< 0.2	8×10^{-10}	7×10^{-9}
FRJ2-K15/					
1	800-970	14.1	< 0.2	2.0×10^{-10}	1.2×10^{-8}
2	980-1 $150_{1\ 280}$	15.3	< 0.2	2.5×10^{-10}	5×10^{-9}
3	800-$990_{1\ 280}$	14.8	< 0.2	2.0×10^{-10}	3×10^{-9}
FRJ2-P27/					
1*	880-1 080	7.2-7.6	1.4	1.0×10^{-6}	1.6×10^{-6}
2	1 220-1 320	8.0	1.7	8.6×10^{-7}	1.0×10^{-5}
3	1 080-1 130	7.2-7.6	1.3	2.0×10^{-8}	1.2×10^{-7}
HTR Module proof tests					
HFR-K5/					
1	800-$923_{1\ 200}$	7.8	4.0	4.8×10^{-10}	1.7×10^{-7}
2	800-$909_{1\ 250}$	10.1	5.8	2.7×10^{-10}	3.0×10^{-7}
3	800-$903_{1\ 260}$	10.3	5.9	2.5×10^{-7}	3.6×10^{-7}
4*	800-$921_{1\ 200}$	9.3	4.9		
HFR-K6/					
1	800-1 $090_{1\ 200}$	8.3	3.2	5.0×10^{-10}	2.0×10^{-7}
2	800-1 $130_{1\ 250}$	10.6	4.6	3.0×10^{-10}	3.0×10^{-7}
3	800-1 $140_{1\ 260}$	10.9	4.8	4.5×10^{-7}	9.0×10^{-7}
4**	800-1 $130_{1\ 240}$	9.9	4.5		

* One manufacturing defect, no additional failures during irradiation.
** Two manufacturing defects, no additional failures during irradiation.
*** Five manufacturing defects, no additional failures during irradiation.

The irradiation began in September 2004 and was terminated in October 2005 after 250 full-power days. Average operating temperatures were in the range of 900 °C to 1200 °C, and peak values well beyond 1 250 °C were achieved. The EOL noble fission gas R/B data were much higher than expected, ranging from 3×10^{-6} to 8×10^{-6} for the short-lived Kr and Xe isotopes. Post-irradiation examination testing began in 2006 followed by accident simulation testing in the years 2008 to 2012.

In 2006 the irradiation experiment HFR-EU1 began irradiation in Petten. This experiment consists of two independent irradiation test capsules. The upper capsule contains two Chinese spherical

elements from recent HTR-10 production. The lower irradiation capsule contains three German GLE 4/2 spherical elements, the same as HFR-EU1bis. The irradiation of HFR-EU1 began in September 2006 and continued into February 2010. The results were reported recently (Laurie, et al., 2010) (Tang, et al., 2010).

8.3. MTR irradiation analysis

The beginning-of-life 85mKr R/B values for the MTR irradiation tests that contained reference 60 mm-diameter spherical elements (HFR-K3, K5, K6, FRJ2-K13 and FRJ2 K15) ranged from 2×10^{-10} to 4×10^{-9} (Table 47). These R/B values are extremely low and characteristic of as-manufactured fuel specimens with no defective fuel particles and very low levels of uranium contamination in the fuel element matrix. The end-of-life 85mKr R/B values for these same irradiation test capsules were also very low, ranging from 3×10^{-9} to 3×10^{-7} (Table 47). These three MTR irradiation tests with reference spherical fuel elements contained an inventory of 159 880 LEU UO_2 TRISO-coated particles. For all of the MTR tests on Phase 1 LEU UO_2, including those tests with non-reference-sized fuel elements (SL-P1, HFR-P4, and FRJ2-P27), a total of 240 452 TRISO-coated particles were irradiated.

By comparing the measured end-of-life 85mKr R/B values with the prediction of a failed TRISO-coated fuel particle, the fraction of failed particles responsible for the release can be determined by:

$$\eta = \frac{\left(R_i / B_i\right)_{EOL}}{\left(R_i / B_i\right)_f} \tag{103}$$

where:

η = fraction of failed particles;

$\left(R_i / B_i\right)_{EOL}$ = measured EOL R/B ratio for isotope i;

$\left(R_i / B_i\right)_f$ = predicted R/B ratio for isotope i in exposed fuel.

The fractional release from a failed LEU UO_2 TRISO particle can be predicted from the equivalent sphere model (Boothe, 1957) (Nabielek, et al., 1974) (Krohn, 1982). Thus, the number of failed particles present is just the product of the failure fraction and the particle population that the release measurement represents.

The 85mKr was determined at EOL fuel-kernel temperatures obtained from thermocouple measurements and thermodynamic calculations at the respective burnup and fluence levels. Knowledge of the initial thorium and uranium contamination values and the number of initially defective particles was considered in the evaluation of the derived failure fraction.

Table 48: LEU UO_2 TRISO-coated particle fuel performance in accelerated MTR irradiation tests based on EOL Kr R/B values and the temperature-dependent fractional release values for an exposed oxide fuel kernel

Irradiation test element	BOL		EOL			
	^{85m}Kr $\left(R/B\right)_{BOL}$	Equivalent failed particles	^{85m}Kr $\left(R/B\right)_{EOL}$	Contribution due to contamination	Equivalent in-reactor failed particles	One-sided upper 95 % confidence limit of irradiation induced failure fraction
SL-P1 with 19 572 particles in 12 mini spheres						
1	5.8×10^{-7}	~ 5	1.2×10^{-6}	~ 60 %*	~ 4	$\leq 4.7 \times 10^{-4}$
HFR-P4 with 39 144 particles in 24 mini spheres						
1	3.5×10^{-9}	~ 0	8×10^{-8}	~ 100 %	~ 0	
3	3.6×10^{-9}		8×10^{-9}	~ 100 %	~ 0	$\leq 7.7 \times 10^{-5}$
HFR-K3 with 65 600 particles in 4 spherical fuel elements						
1	1×10^{-9}	~ 0	2×10^{-7}	~ 100 %	~ 0	
2,3	9×10^{-10}	~ 0	1×10^{-7}	~ 100 %	~ 0	
4	2×10^{-9}	~ 0	3×10^{-7}	~ 100 %	~ 0	$\leq 4.6 \times 10^{-5}$
FRJ2-K13 with 65 600 particles in 4 spherical fuel elements						
1,2	2×10^{-9}	~ 0	1.6×10^{-8}	~ 100 %	~ 0	
3,4	8×10^{-10}	~ 0	7×10^{-9}	~ 100 %	~ 0	$\leq 4.6 \times 10^{-5}$
FRJ2-K15 with 28 680 particles in 3 spherical fuel elements						
1	2.0×10^{-10}	~ 0	1.2×10^{-8}	~ 100 %	~ 0	
2	2.5×10^{-10}	~ 0	5×10^{-9}	~ 100 %	~ 0	
3	2.0×10^{-10}	~ 0	3×10^{-9}	~ 100 %	~ 0	$\leq 1.0 \times 10^{-4}$
FRJ2-P27 with 21 856 in 9 annular compacts and 6 coupons						
1	1.0×10^{-6}	~ 1	1.6×10^{-6}	~ 65 %*	~ 1	
2	8.6×10^{-7}	~ 0	1.0×10^{-5}	~ 10 %*	~ 4	
3	$2. \times 10^{-8}$	~ 0	1.2×10^{-7}	~ 100 %	~ 0	$\leq 4.8 \times 10^{-4}$
Total for entire Phase 1 with LEU UO_2 population (240 452)					~ 9	$\leq 6.5 \times 10^{-5}$
Total for LEU UO_2 population in 60 mm-diameter fuel spheres (159 880)					~ 0	$\leq 1.9 \times 10^{-5}$
HFR-K5 with 58 400 particles in 4 spherical fuel elements						
1	4.8×10^{-10}	~ 0	1.7×10^{-7}	~ 100 %	~ 0	
2	2.7×10^{-10}	~ 0	3.0×10^{-7}	~ 100 %	~ 0	
3	‘	~ 0	‘	~ 100 %	~ 0	
4	2.5×10^{-7}	~ 1	3.6×10^{-7}	~ 100 %	~ 0**	$\leq 5.1 \times 10^{-5}$
HFR-K6 with 58 400 particles in 4 spherical fuel elements						
1	5×10^{-10}	~ 0	2.0×10^{-7}	~ 100 %	~ 0	$\leq 5.1 \times 10^{-5}$
2	3×10^{-10}	~ 0	3.0×10^{-7}	~ 100 %	~ 0	
3	‘	~ 0	‘	~ 100 %	~ 0	
4	4.5×10^{-7}	~ 2	9.0×10^{-7}	~ 100 %	~ 0**	
Total for proof test LEU UO_2 population (116 800)					~ 0	$\leq 2.6 \times 10^{-5}$

* A portion of EOL noble gas release is due to the breeding of fissile material into the initial uranium and thorium contamination in fuel matrix and capsule graphite materials.

** The initial evaluation predicted ~ 1 equivalent particle failure. However, the fission gas release analysis conducted on HFR-K5/K6 strongly suggests that the increase in noble gas release at EOL is likely due to the breeding of fissile materials into the initial uranium and thorium contamination in fuel element matrix and irradiation capsule graphite materials.

Employing this methodology, a total of nine in-reactor LEU UO_2 TRISO particles were determined to have failed out of all the LEU UO_2 TRISO particles irradiated (240 452) in the accelerated MTR tests of Phase 1 production material. All nine of these failed particles were from MTR irradiation tests SL-P1 and FRJ2-P27 and contained in special, non-reference fuel elements (20 mm-diameter spheres, cylindrical compacts or coupons). No in-reactor failed particles were detected in the non-reference elements in HFR-P4.

Based on the R/B data at EOL for the three MTR tests (HFR-K3, FRJ2-K13 and -K15) that contained only reference 60 mm-diameter fuel elements, no in-reactor particle failures were observed. These 11 reference fuel elements contained a total of 159 880 LEU UO_2 TRISO particles and, with zero failures, this represents a failure fraction of $\leq 1.9 \times 10^{-5}$ at the upper 95 % confidence limit according to Equation 2.

8.4. HTR Module proof test analysis

A comparison of initial R/B values monitored in HFR-K5 and HFR-K6 shows a significant difference for fuel elements 1, 2 and 3 compared to element 4 in both tests (Table 48 and Figure 102). The BOL 85mKr R/B values in the top capsules are $< 5 \times 10^{-10}$ for both tests, compared to 2.5×10^{-7} and 4×10^{-7} in HFR-K5/4 and K6/4, respectively. These differences of four orders of magnitude in R/B values are a result of as-fabricated defective fuel particles present in element 4 for each irradiation capsule. Other releases of fission gases are from contamination in the A3 sphere matrix and in the graphite cups that surround the spheres.

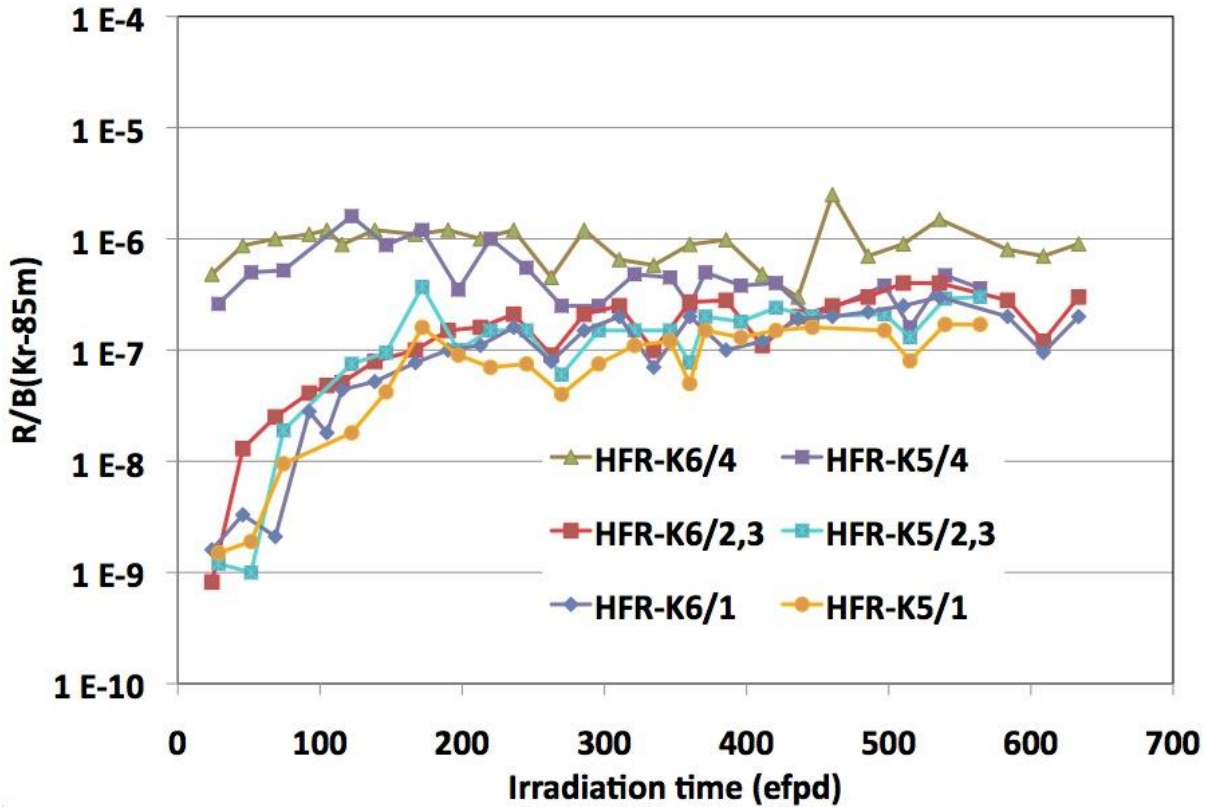

Figure 102: Measured 85mKr release rates during the irradiation of tests HFR-K5 and HFR-K6

In both HFR-K5 and K6 the upper capsules 1, 2 and 3 with very low BOL R/B values are representative of elements with no defective fuel particles and very low levels of uranium and thorium contamination in the fuel matrix. The fuel element HFR-K5/4 with a 85mKr R/B value of 2.5×10^{-7} at the start is representative of one equivalent defective fuel particle from manufacture. In HFR-K6/4 with a BOL 85mKr R/B value of 4.5×10^{-7} there are approximately two equivalent defective particles. This is within the limits of defective particles from manufacture (six elements with zero defects plus one element with one defect plus one element with two defects, i.e. three defects in 116 800 particles represent a 2.6×10^{-5} defect fraction and this is within acceptable limits).

The effect heavy-metal contamination in fuel-sphere matrix material has on fission gas release rates was also investigated (Röllig, 1977) (Röllig, 1993) (Merwe, 2004) (Merwe, 2004b) (Merwe, et al., 2007) to explain the higher-than-expected EOL R/B data observed in the proof tests. Natural uranium (~ 99.28 wt % ^{238}U + 0.72 wt % ^{235}U) and thorium (^{232}Th) are present as natural contamination. The fertile isotopes (^{232}Th and ^{238}U) capture neutrons and breed fissile materials such as ^{233}U, ^{239}Pu and ^{241}Pu. This phenomenon is of importance in the accelerated irradiation environments of an MTR where flux levels in the epithermal region are greatly accelerated compared to real-time HTGR environments (~ 2 to 5 times higher).

The analysis demonstrated that, for the HFR-K6 experiment, fuel elements increased their equivalent initial fissile contamination fraction of 7.2×10^{-8} by factors of 15 to 20 by the end of the 634 effective full-power days of irradiation. This increase is attributed to the production of ^{233}U, ^{239}Pu and ^{241}Pu fissile materials in the fuel matrix and in the graphite crucibles that surround each fuel element and hold them in place during irradiation. Similar results were obtained for the elements in HFR-K5. The ^{88}Kr release predicted for fuel elements 2 and 3 in HFR-K6 is compared to the online ^{88}Kr R/B measurements in Figure 9 with close agreement. Similar results were also established for the short-lived xenon gas isotopes (Merwe, 2004) (Merwe, 2004b) (Merwe, et al., 2007).

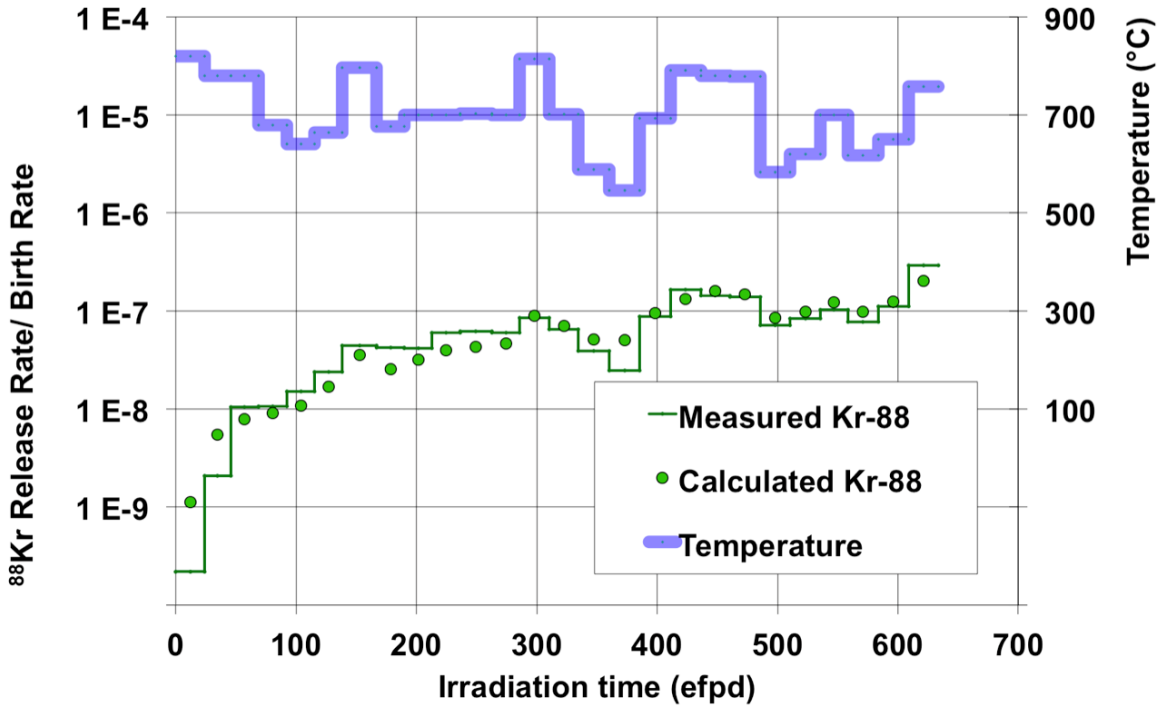

Figure 103: Detailed comparison of measured and calculated ^{88}Kr release rates for fuel elements HFR-K6/2 and 3 throughout the 634 full-power days of irradiation. Also shown are the measured temperatures at the spheres' surface. Release source terms are from contamination

For the fuel elements HFR-K5/4 and HFR-K6/4, which contained as-manufactured defective fuel particles, the amount of free uranium not contained within a SiC barrier is much larger at the start of irradiation. The free ^{235}U due to one defective fuel particle at BOL is ~ 1 000 times that due to matrix contamination.

Zero in-reactor particle failures were observed in HTR Module proof tests HFR-K6 and HFR-K6 out of a total irradiation population of 116 800 LEU UO_2 TRISO-coated particles. This represents a failure fraction of $\leq 2.6 \times 10^{-5}$ at the upper 95 % confidence limit as shown in Table 48.

8.5. AVR real-time irradiation testing

The 46 MW(th) AVR in Jülich, Germany operated from 1967 through 1988 and generated 1.7×10^9 kWh of electric power. During its operation the AVR provided invaluable information on spherical fuel element development, fuel particle development with many particle variants (kernel material, enrichments, coating designs) and HTGR fuel cycles (Sauer, 1990). Nearly 290 000 spherical fuel elements of five different types, containing more than 6×10^9 coated fuel particles, were inserted into its core over its operating lifetime from 1967 to 1988, Figure 104. Spheres with high-quality TRISO particles of type GO-2, GLE-3 and GLE-4 came late to the AVR with around 50 % at the end.

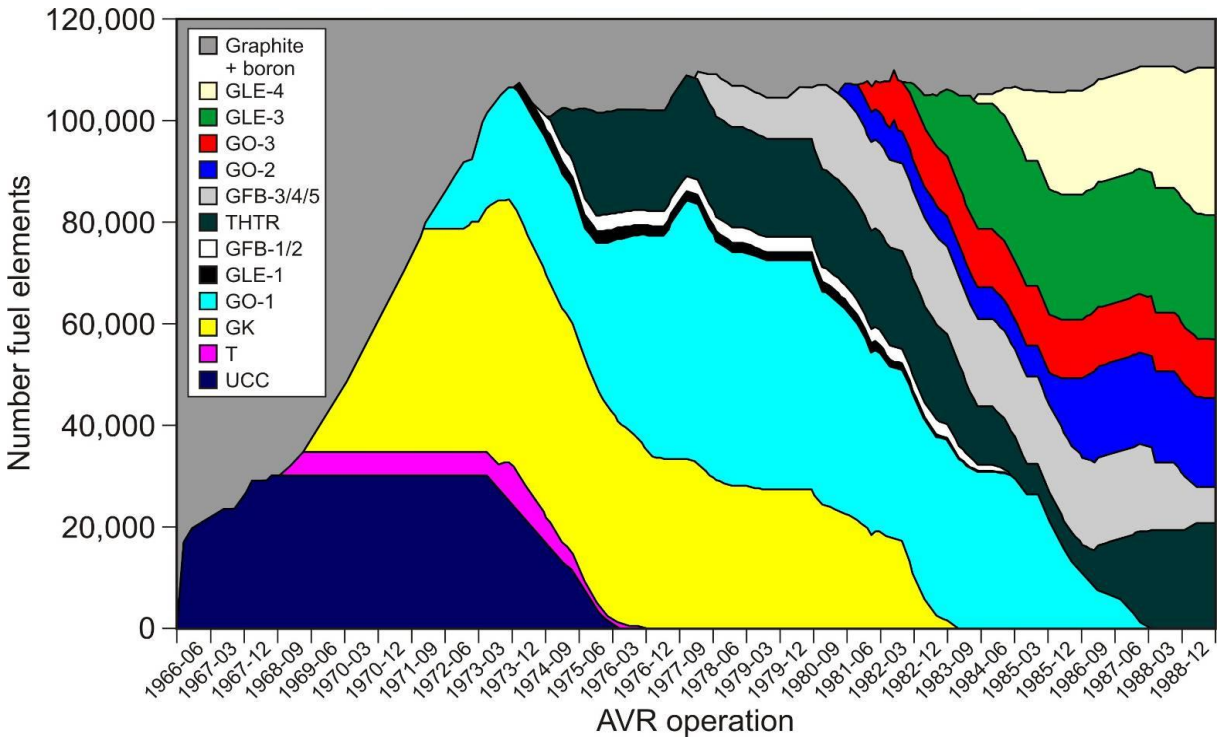

Figure 104: Distribution of spherical fuel element types in the AVR core as a function of operating history (Verfondern, 2007)

For a 7-year period from 1982 to 1988, these fuel element types were inserted into the AVR and experienced real-time HTGR operating conditions. At periodic intervals over this period, a number of irradiated elements would be randomly drawn from the core for post-irradiation evaluation and accident condition testing. In 7 years of irradiation, a total of 240 GLE-3 and GLE-4 elements were withdrawn and evaluated at the Jülich Research Centre. Peak burnups of the withdrawn elements were 9.8 % FIMA for the GLE-3 elements and 13 % FIMA for the GLE-4 elements. Peak accumulated fast fluences were ~ 2.9×10^{25} m^{-2}, E > 16 fJ for the GLE-3 elements and ~ 2.3×10^{25} m^{-2}, E > 16 fJ, for the GLE-4 elements. Post-irradiation evaluations include fission product inventory measurements (burnup), out-of-reactor gas release measurements and accident simulation testing.

Assessing the operating temperatures experienced by the fuel elements as they traverse, on multiple passes, through the AVR pebble-bed core during their irradiation lifetime has been a difficult situation. Predictions based on model calculations were always available, but no experimental measurements were made until the mid 1980s. In 1986 a 'melt-wire experiment' was conducted during the period relevant to when the GLE-3 and GLE-4 fuel elements were present in the AVR. This experiment inserted into the AVR specially designed graphite matrix spheres which incorporated a set of 20 quartz capsules, each containing a single melt-wire (Figure 99). The melt-wires were fabricated from specific alloy compositions that would melt if specific temperatures were exceeded. A total of 190 of these monitoring spheres were added into the AVR core through standard fuel loading procedures: 102 to the centre and 22 to each of the four outer feed lines.

Upon discharge, 140 of the monitoring spheres were X-rayed to assess the momentary maximum peak temperatures experienced during their passage through the AVR: 15 % of the monitoring

spheres experienced operating temperatures ≥ 1 244 °C, at which all the melt-wires in the quartz capsules had melted (Derz, et al., 1990) (Gottaut H., 1990) (Stoker, et al., 2010).

Based on the melt-wire measurement results, the underlying temperature distribution was extracted by constructing a quantile–quantile (Devore 2004) plot based upon the probability properties of the histogram distribution. Two Gaussian distributions with peak temperatures of 1 100 ± 66 °C and 1 220 ± 100 °C were found that define the variation of momentary maximum fuel element surface temperatures in the AVR between the inner core and outer core locations. Peak central temperatures were calculated to be 37.3 °C and 75.6 °C higher for the inner and outer locations, respectively. Both are significantly higher than the coolant gas exit temperature because of substantial core bypass flows. The resulting temperature distributions are shown in Figure 105.

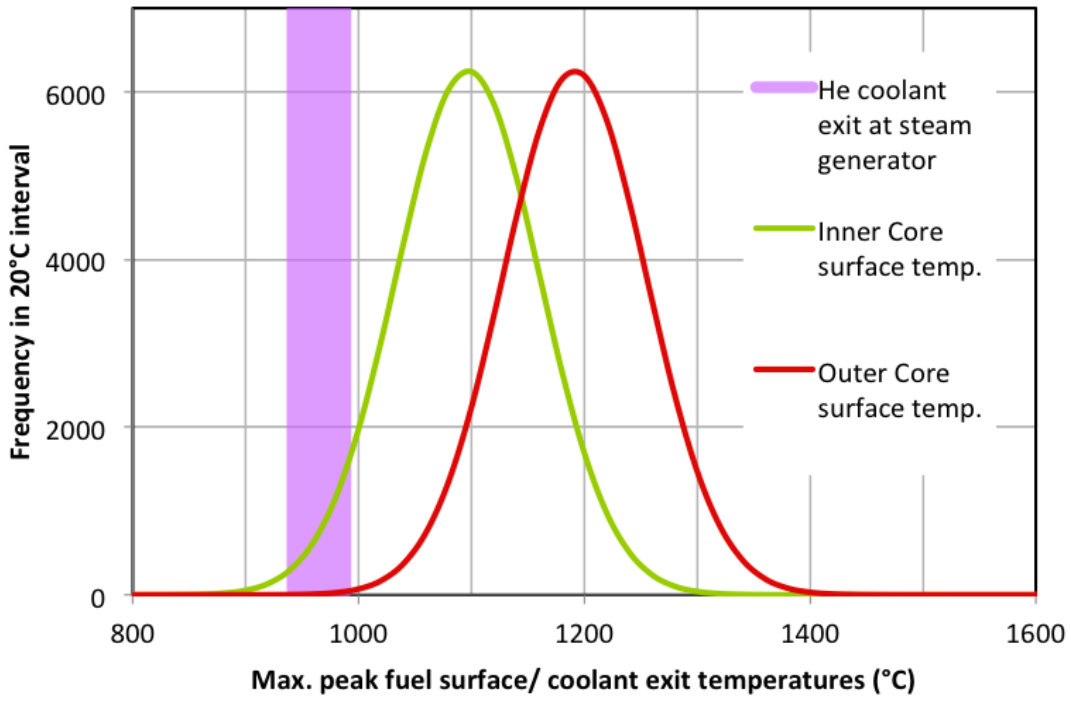

Figure 105: Distribution of AVR inner core maximum fuel element surface temperatures and outer core maximum fuel element surface temperatures as obtained from the 1986 melt-wire tests

To assess the EOL performance of GLE-3 and GLE-4 AVR fuel elements, a methodology was developed based upon fission gas release measurement during the temperature increase in the early phase of accident condition testing (Schenk, 1977) (Schenk, 1978) (Schenk, 1983) (Schenk, et al., 1988) (Schenk, et al., 1990) (Schenk, et al., 1993). The heat-up process begins at room temperature, progresses over a series of heating ramps to specific temperatures (300 °C, 1 050 °C and 1 250 °C) and hold periods until the desired accident simulation temperature is reached. Two of these hold points, 1 050 °C and 1 250 °C, are designed to equilibrate the irradiated fuel particles in the fuel element at or near their prior irradiation temperature. This allows the fuel to develop a stable

internal environment before being heating to an elevated temperature not previously experienced by the fuel particles. The 1 050 °C hold point was considered the mean working temperature for fuel specimens from accelerated MTR irradiation tests, and the 1 250 °C hold point was considered the typical working temperature for AVR fuel elements.

During heating, the test facility is purged with a sweep gas and continuously monitored for release of the long-lived ^{85}Kr noble fission gas, half-life 10.76 years. Detection of any significant activity in the sweep gas is an indicator of failed or defective fuel particles present in the irradiated fuel element (Figure 106).

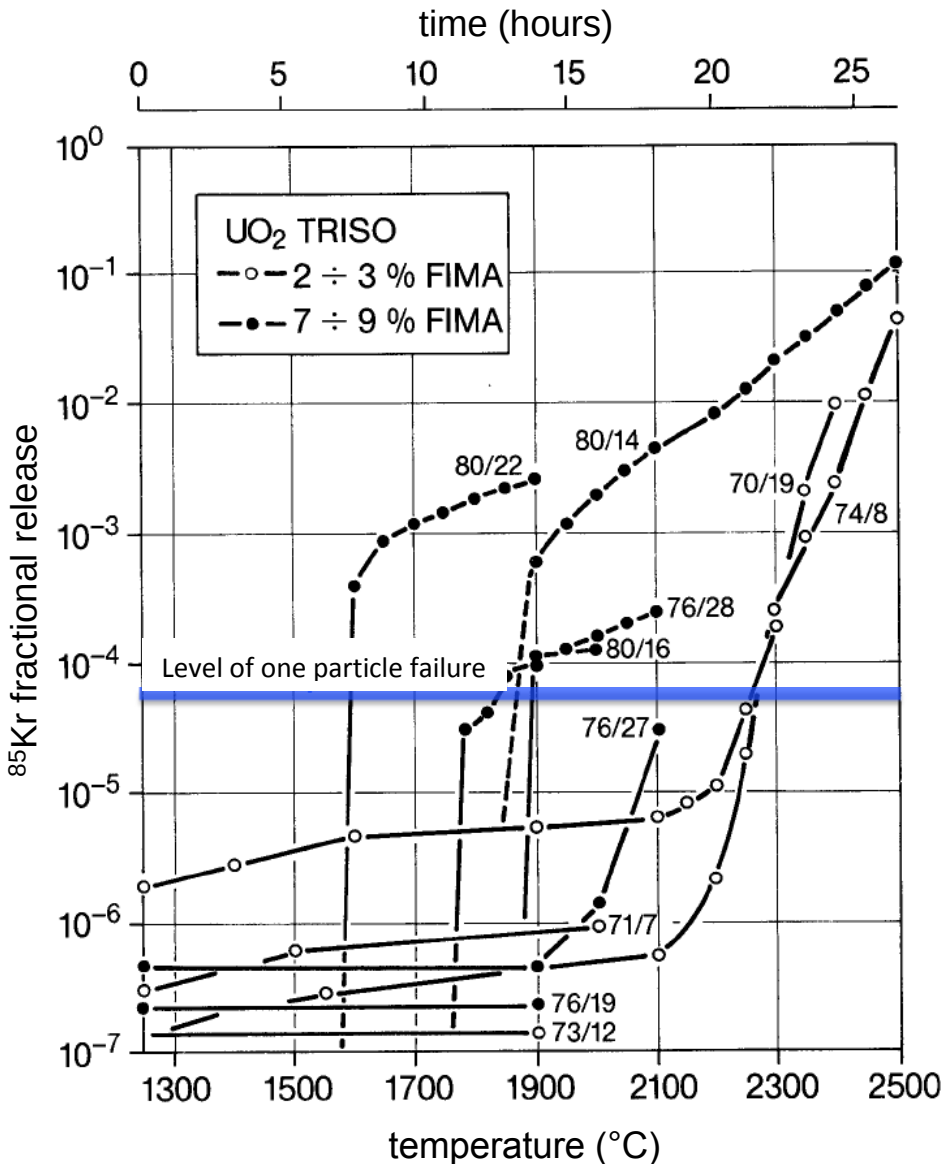

Figure 106: Release of ^{85}Kr measured during accident simulation testing of GLE-3 spherical fuel elements irradiated to various burnups in the AVR. The first part of the two-digit number refers to the consecutive AVR sampling event, and the second is a sequential s

Table 49 is a detailed list of 29 GLE-3 fuel elements that have been subjected to accident simulation testing. Of these, 24 were used to analyse AVR EOL irradiation performance. Five were excluded

because of the lack of detailed ^{85}Kr release data at testing temperatures near those expected in the AVR.

Table 49: ^{85}Kr fractional release measurements made during the 1 250 °C+ hold temperature on AVR type GLE-3 fuel elements prior to accident simulation tests at higher temperatures

Fuel element (AVR sample No/specimen No)	Burnup (% FIMA)	Measurement temperature (°C) of ^{85}Kr release	^{85}Kr release fraction	Peak temperature (°C) of accident simulation test
Isothermal accident simulation tests				
AVR 70/33	1.6	1 250	3.8×10^{-6}	1 800
AVR 73/21 (ITU)	2.5	NI	NDR < 1 600 °C	1 800
AVR 71/22	3.5	1 250	4.5×10^{-8}	1 600
AVR 74/18 (ITU)	4.8	1 600	5.9×10^{-6}	1 600
AVR 74/10	5.5	1 250	$< 8.0 \times 10^{-7}$	1 800
AVR 74/11	6.2	1 250	1.3×10^{-7}	1 700
AVR 76/18	7.1	1 250	1.6×10^{-8}	1 800
AVR 88/41	7.6	1 250	1.3×10^{-8}	1 800
AVR 88/33	8.5	1 250	$< 4.2 \times 10^{-8}$	1 600/1 800
AVR 82/20	8.6	1 250	5.5×10^{-8}	1 600
AVR 88/15	8.7	1 250	6.3×10^{-8}	1 600/1 800
AVR 82/9	8.9	1 250	1.3×10^{-8}	1 600
HTR Module 'depressurised loss of forced cooling' (DLOFC) event profile				
AVR 91/31	9.0	1 500	1.0×10^{-8}	1 700
AVR 89/13	9.1	1 490	6.7×10^{-8}	1 620
AVR 85/18	9.2	1 495	2.6×10^{-8}	1 620
AVR 90/5	9.2	1 495	5.3×10^{-8}	1 620
AVR 90/2	9.3	1 495	9.2×10^{-8}	1 620
AVR 90/20	9.8	1 500	5.7×10^{-8}	1 620
Ramp accident simulation tests				
AVR 71/7	1.8	1 250	3.1×10^{-7}	2 000
AVR 70/19	2.2	1 200	1.9×10^{-6}	2 400
AVR 74/8	2.9	1 250	1.4×10^{-7}	2 500
AVR 73/12	3.1	1 250	$< 1.4 \times 10^{-7}$	1 900
AVR 74/6	5.6	1 250	1.3×10^{-7}	2 100
AVR 76/28	6.9	1 250/NI	NDR < 1 750 °C	2 100
AVR 76/19	7.3	1 250	2.3×10^{-7}	1 900
AVR 76/27	7.4	1 250	4.6×10^{-7}	2 100
AVR 80/16	7.8	1 250/NI	NDR < 1 900 °C	2 000
AVR 80/14	8.4	1 250/NI	NDR < 1 900 °C	2 500
AVR 80/22	9.1	1 250/NI	NDR < 1 600 °C	1 900
Accident simulation tests on MTR and HTR Module proof test elements				
HFR-K3/1	7.7	1 250	$< 5.6 \times 10^{-8}$	1 600
HFR-K3/3	10.2	1 250	1.5×10^{-7}	1 800
FRJ2-K13/2	8.1	1 250	5.3×10^{-7}	1 600
FRJ2-K13/4	7.8	1 250	4.5×10^{-8}	1 600/1 800
HFR-K6/2 (ITU)	9.7	1 050	1.0×10^{-8}	1 600
HFR-K6/3 (ITU)	9.8	1 050	3.2×10^{-6}	1 600

Figure 107 presents the fractional release data for these elements whereby the heat-up 1 250 °C hold temperature reproduces EOL conditions. The release data represent AVR EOL irradiation conditions and are characteristic of fuel element performance. Eleven of the GLE-3 elements were ultimately subjected to isothermal tests from 1 600 °C or 1 800 °C, six elements were subjected to a simulated HTR Module design basis depressurised event temperature profile up to 1 620 °C or 1 700 °C and seven elements were subjected to ramp tests ranging from 1900 °C to 2 500 °C.

Included in the figure, for comparison purposes, are the ^{85}Kr fractional release measurements made on six MTR and HTR Module proof test elements, also subjected to design basis accident simulation testing. The fractional release data were similarly obtained during the 1 250 °C hold temperature during the heat-up phase of test simulation.

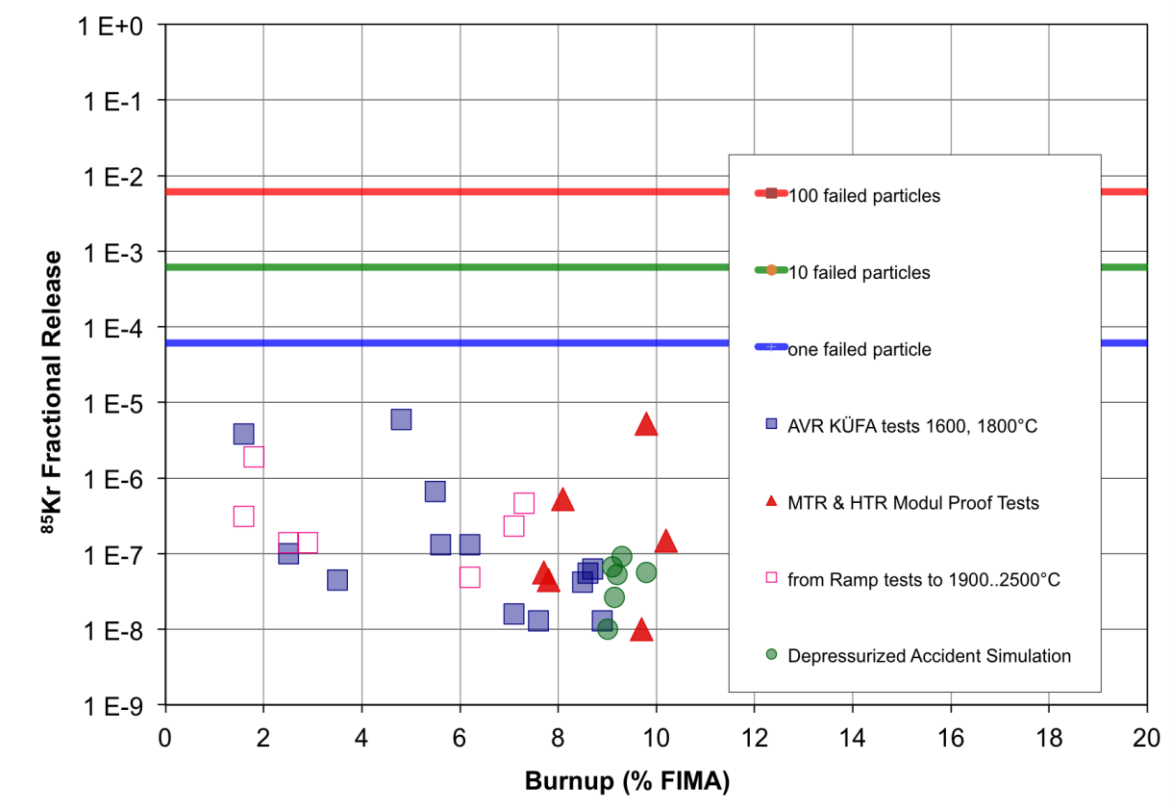

Figure 107: Post-irradiation fission gas release fractions at 1 250 °C measured during heat-up prior to accident simulation tests with GLE-3 fuel elements containing LEU UO_2 TRISO particles of various burnups. The horizontal lines show predicted krypton release fractions

The ^{85}Kr fractional release data in Figure 105 and Figure 106 are indicative of the EOL fuel performance for the GLE-3 elements irradiated in the AVR. For the 11 GLE-3 elements subjected to isothermal accident tests the release data were measured at the 1 250 °C hold period during the ramp-up to test temperature and are directly representative of EOL AVR performance. For those elements subjected to a constant heating ramp to temperatures > 1 900 °C, only release data in the temperature range of 1 250 °C to ~ 1 400 °C were used to estimate EOL AVR performance. And finally, for those elements subjected to a design basis HTR Module depressurisation event temperature profile, only the release data along the temperature curve where the furnace

temperature was between 1 490 °C and 1 500 °C were used as representative of EOL AVR performance.

Based on the ^{85}Kr fractional release data from 24 accident simulation tests, the EOL performance of the GLE-3 fuel elements at the time of discharge from the AVR are excellent. Most of the release fractions, with a few exceptions, are $< 10^{-6}$ in the temperature range of 1 250 °C to well beyond 1 400 °C. The ^{85}Kr release fraction of a single LEU UO_2 TRISO particle at these temperatures is $\sim 6 \times 10^{-5}$ and the release fractions measured from the 24 separate GLE-3 elements are lower by one to three orders of magnitude. The AVR GLE-3 element fractional release data also compare well with ^{85}Kr release data obtained from accident simulation testing of MTR irradiation and HTR Module proof test specimens.

Collectively, the 24 GLE-3 elements represent a population of 393 600 LEU UO_2 TRISO-coated particles and — with no in-reactor failures — their EOL performance is representative of a failure fraction of $\leq 7.6 \times 10^{-6}$ at the one-sided upper 95 % confidence limit. It should be noted that zero in-AVR particle fuel failure has not always been the case. The test and evaluation method described here had previously identified AVR GLE-1 fuel with near 50 % particle failure in the 1970s (Wimmers, 1977).

9. Appendix B

9.1. Experiments regarding self-acting decay heat removal in modular high-temperature gas-cooled reactors

9.1.1. Overview

After the total loss of active cooling in a modular HTR the decay heat is transported solely through processes of conduction, radiation and free convection from the core to the environment. This chain of heat transport includes several steps in the reactor and depends in a complex way on various parameters of the reactor design. Figure 108 shows a simplified overview of the relevant structures and the chain, as well as of parameters, which influence the heat transport and the temperature profile.

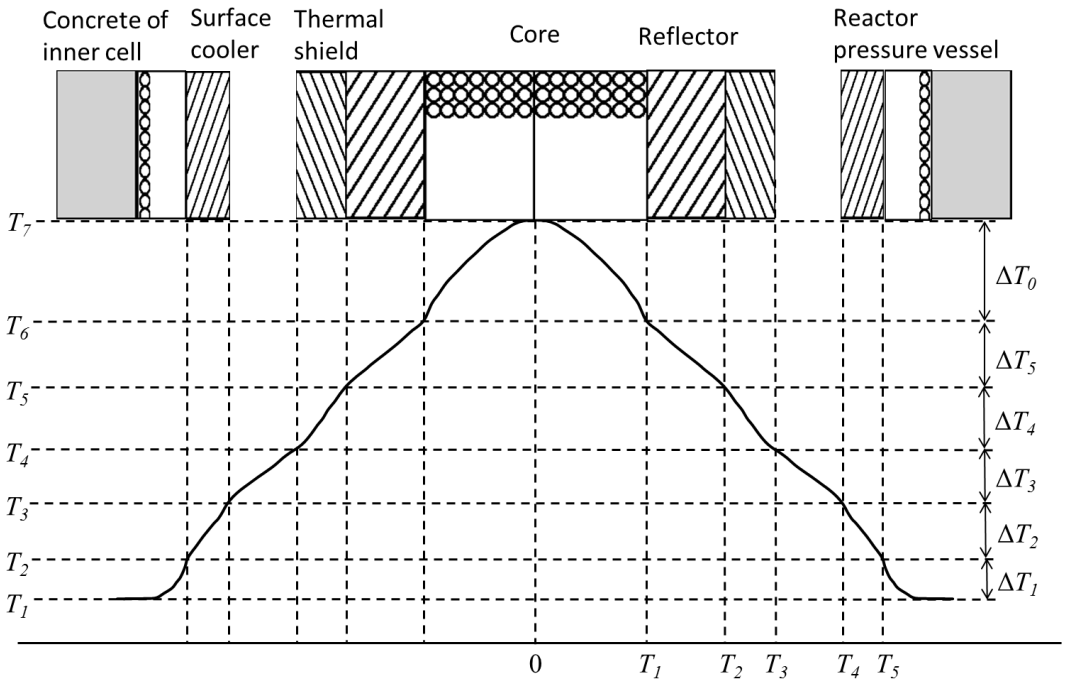

Figure 108: Stationary radial temperature profile in case of self-acting decay heat removal in a modular HTR (Tmax in the hottest part of the core)

The maximum temperature in the hottest fuel elements is given by a dependency of the type:

$$T_{max} = T_{cold} + \bar{\dot{q}}_c''' * \beta * f_n(t^*) * \Phi(r_i, \lambda_i, \varepsilon_i, \alpha_i) \quad (104)$$

where:

T_{max} = maximum temperature in the hottest fuel elements;
Φ = function describing the heat transport through the whole reactor system;
T_{cold} = temperature of the environment (temperature in surface cooling system or in the air outside the inner concrete cell);
$\bar{\dot{q}}_c'''$ = average power density in the core;
β = peak factor of power density;

$f_n(t^*)$ = factor of decay heat function (in a modular JTR of around 200 MWth) around 3.0E-03 after 30 hours.

The function Φ contains a description of the total chain of heat transport which, oriented on the designation in Figure 109, denotes as follows:

$$\Phi = \frac{{r_1}^2}{4\lambda_{eff}} + \frac{r_1}{2} * \frac{(r_2 - r_1)}{\lambda_G} + \frac{r_1}{2} * \frac{r_1}{r_3} * \frac{(r_2 - r_1)}{\lambda_S} + \frac{r_1}{2} * \frac{r_1}{r_4} * \frac{1}{\overline{\alpha_S}} + \frac{r_1}{2} * \frac{r_1}{r_5} * \frac{(r_5 - r_4)}{\lambda_S} + \frac{r_1}{2} * \frac{r_1}{r_5} * \frac{1}{\overline{\alpha_\alpha}} \qquad (105)$$

The relevant parameters of the heat transport chain need experimental validation. The main data influencing the temperature profile is briefly introduced in Figure 109.

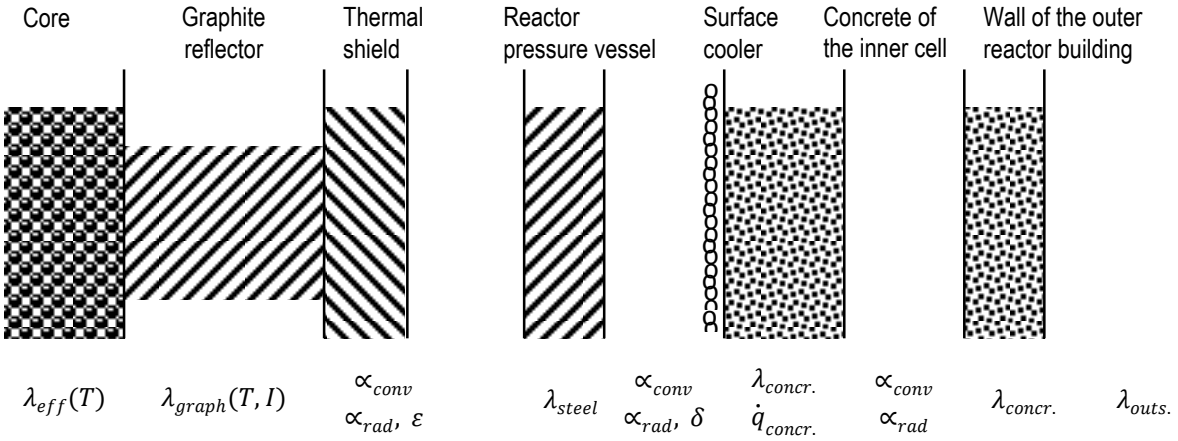

Figure 109: Parameters which influence the chain of the self-acting transport of decay heat in a modular HTGR

The following experiments were carried out to validate data relevant to self-acting decay heat removal in modular HTGRs.

- Measurements of $\lambda_{eff}(T)$ in the pebble bed after total loss of active cooling: this was done in a lot of relatively small laboratory tests and in a large integral test (SANA).
- Transport of the heat through the thick-walled graphite reflector: λ_G depends on temperatures and irradiation doses. Many results are available from the irradiation programmes. Different qualities of graphite have been qualified regarding these characteristic loads.
- The natural convection, which occurs in a reactor under full helium pressure after loss of forced convection, was measured in the LUNA experiment. The dependence of convection in internal gaps and in the core is known for different gases and conditions of temperature and pressure.
- In the gaps between the graphite reflector and the thermal shield, and between the thermal shield and the inner side of the reactor pressure vessel, there is heat transport by conduction, radiation and free convection. Measurements in the large PASCO (passive cooling of containment) test facility and measurements of the emission coefficients ε for various materials are available.
- The heat release from the surface of the reactor pressure vessel mainly by radiation and free convection was measured in various large facilities. Results from the INWA facility, for instance, helped gain broad experience on the release of decay heat from the surface of

reactor pressure vessels and on the function of the concrete (cast-iron) cell surrounding the reactor as an outer heat sink.

- Many results for the release of heat from the surface of the reactor pressure vessel and the function of the outer surface cooler were gained from experiments conducted by the Japanese Atomic Energy Agency (JAERI).
- Measurements on Castor and Mosaik vessels for spent fuel elements enlarged the knowledge of decay heat removal by natural convection and radiation from the surface of the reactor pressure vessel.
- In case of storage of decay heat in the concrete of the inner cell, knowledge of material behaviour and the behaviour of large concrete blocks with load by heat flux is necessary. Large experiments with different types of concrete were carried out.
- In very extreme cases the liner or surface heat exchanger cooling could fail too; the reflooding was tested in connection with the experiments on concrete at very high temperatures.
- Heat transport by free convection inside the reactor building and transport to the outside (environment) were tested in the PACOS facility.
- The total chain of heat transport was tested in the AVR reactor in an integral experiment. This was carried out with a reactor status with pressure and without pressure. Relevant temperatures in the reactor structures were measured.

Figure 110 gives an overview of the experiments and their purposes, as discussed before. It is clear that the main steps of the chain of heat transport have been tested corresponding to the experimental conditions and the specific situation in a modular HTGR. All these experiments provide proof for the validity of the concept of self-acting decay heat removal.

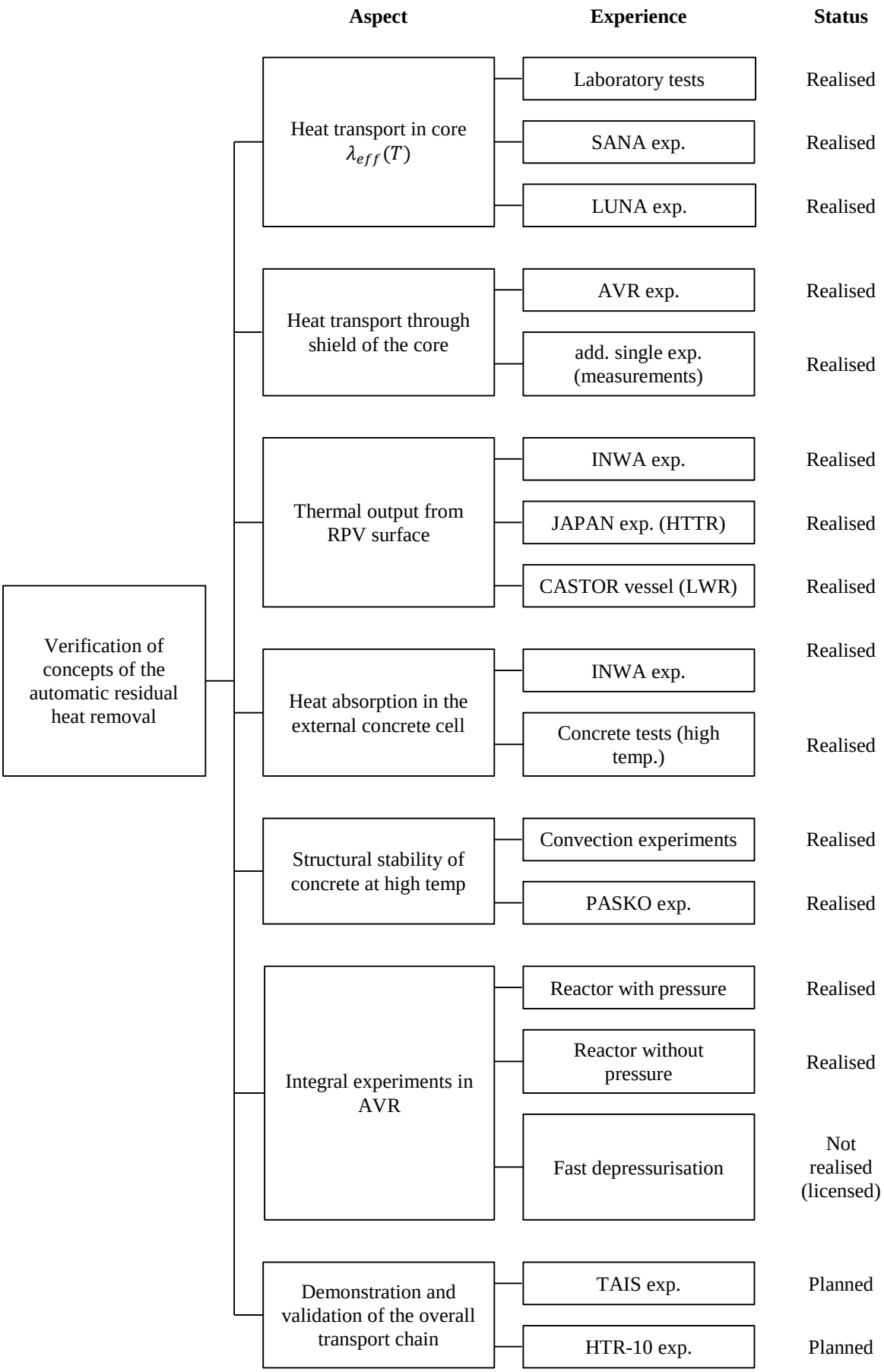
Aspect
Experience
Status
Verification of concepts of the automatic residual heat removal
Heat transport in core $\lambda_{eff}(T)$
Laboratory tests
Realised
SANA exp.
Realised
LUNA exp.
Realised
Heat transport through shield of the core
AVR exp.
Realised
add. single exp. (measurements)
Realised
Thermal output from RPV surface
INWA exp.
Realised
JAPAN exp. (HTTR)
Realised
CASTOR vessel (LWR)
Realised
Heat absorption in the external concrete cell
INWA exp.
Realised
Concrete tests (high temp.)
Realised
Structural stability of concrete at high temp
Convection experiments
Realised
PASKO exp.
Realised
Integral experiments in AVR
Reactor with pressure
Realised
Reactor without pressure
Realised
Fast depressurisation
Not realised (licensed)
Demonstration and validation of the overall transport chain
TAIS exp.
Planned
HTR-10 exp.
Planned

Figure 110: Overview of experiments to evaluate the concept of self-acting decay heat removal of a modular HTR

The experiments delivered enough data to calculate the temperature distribution and to define the temperatures in the fuel elements. Moreover, histograms to describe the time- and space-dependent distribution of temperature loads on all fuel elements can be derived with high accuracy. In addition to the abovementioned experimental evaluations, a value is added to take statistical effects on the maximum fuel temperature into account:

$$T_{max} = T_{max}(nominal) + \Delta T \qquad (106)$$

The value of ΔT in most analyses until now has been approximately 100 °C; some variations of this value are possible corresponding to the requirements of different licensing bodies.

A maximum temperature 100 °C higher than the nominal value causes higher fission-product releases from the fuel. These differences are in the order of approximately 50 % for the relevant isotopes ^{137}Cs and ^{90}Sr. If effective filtering of the helium, leaving the primary system in case of an accident, is possible, this does not change the release from the plant. This is fulfilled in the case of a non-bursting primary enclosure.

It can also be fulfilled by burst protection or by a totally prestressed primary enclosure. The materials for this concept are concrete, cast iron or cast steel.

9.2. Heat transport in the reactor core $\lambda_{eff}(T)$

9.2.1. Laboratory experiments

The temperature dependence of the heat conductivity in the pebble bed is important to calculate the temperature distributions in the core in case of the accidents discussed here. The temperature difference between the centre and the surface of the core is estimated by the following equation:

$$T_{max} - T_{surf} \sim \frac{\overline{\dot{q}_c'''} * \beta * f_n(t^*) * {r_1}^2}{4 * \overline{\lambda_{eff}}} \qquad (107)$$

$\overline{\lambda_{eff}}$ is a suited average value over the radial temperature profile here. $\overline{\lambda_{eff}}$ values at lower temperatures are important for the structure of the histogram of the fuel temperature too. This aspect is important when estimating fission-product releases during the entire time of an accident.

In the course of the development of HTGRs $\overline{\lambda_{eff}}$ has been measured several times (Barthels, et al., 1984) (Breitbach, 1978) (Barthels, et al., 1984) (Robold, 1982) in laboratory experiments. A characteristic example is shown in Figure 111. A heating and a cooling system generates a temperature field, which allows the definition and measurements of heat conductivities in small regions with temperature distributions.

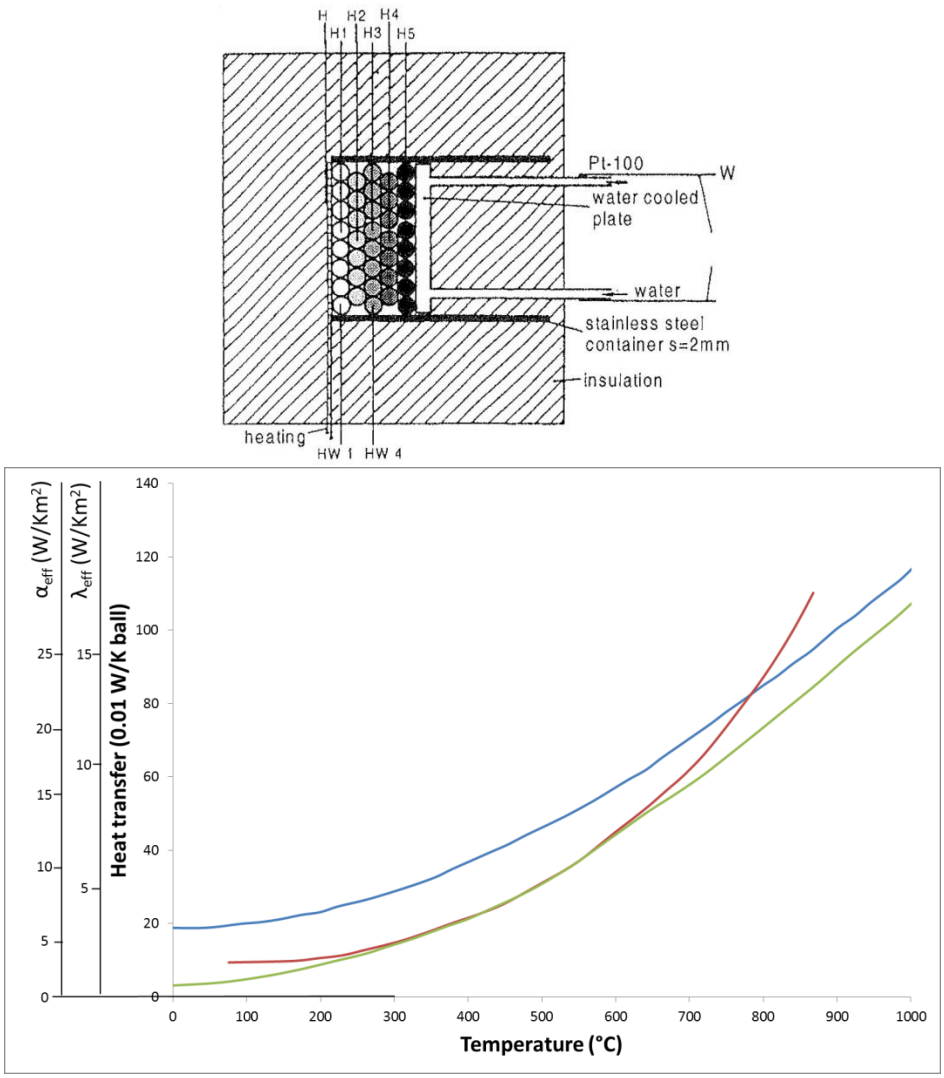

Figure 111: Measurement of ($\overline{\lambda_{eff}(T)}$) in a laboratory experiment with 6 cm graphite balls: (a) arrangement for measurement of ($\overline{\lambda_{eff}(T)}$ in a pebble bed; (b) result for the effective heat conductivity in a pebble bed ($\overline{\lambda_{eff}(T)}$)

The results of this type of experiment are summarised in Figure 111. There are some deviations, which are explained by the specific conditions of different experiments. Furthermore, theoretical models delivered results which fit into the field of available experiments relatively well. An analytical expression of the temperature dependence, which describes the results relatively well, is denoted as:

$$\lambda_{eff}(T) = 2.549 * 10^{-4} * T^{1.545} + 1.5 \quad for\ T \leq 1\,300 \ \ °C \qquad (108)$$

$$\lambda_{eff}(T) = 2 * 10^{-3} * (T - 135)^{1.29} + 0.003 \ \ for\ 1\,300^{0}C \ \leq T \leq 2500 \ \ °C \qquad (109)$$

Here the following dimensions are valid: $\lambda_{eff}\ [W/mK]$ and $T[^{\circ}\ C]$. The uncertainty of these equations is estimated to be as high as ± 10 %, and there are indications that the actual value is even higher (Fricke, 1987).

The value of λ_{eff} is also influenced by natural convection processes in the pebble bed. The influence of irradiation is also included in the equation given above. Figure 112 shows these influences in comparison to irradiated fuel element graphite.

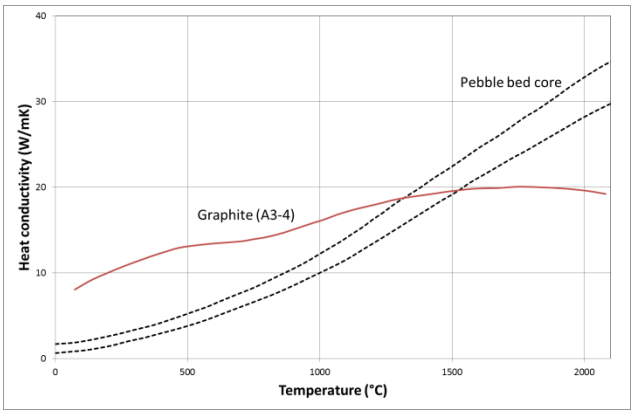

Figure 112: Dependencies of λ_{eff} from temperature and irradiation status

9.2.2. SANA experiment

Since the heat conductivity and the temperatures in the core are so important for the concept of the self-acting decay heat removal, a large-scale experiment was carried out in the SANA-test facility (SANA = Selbsttätige Abfuhr der Nachwärme (self-acting removal of decay heat)). 9 500 graphite balls 6 cm in diameter were heated using electrical heating to simulate the decay heat in a reactor core. Inserted ceramic heating elements in the pebble bed (see channels Figure 113 (left) made it possible to establish radial and axial temperature profiles (Lange, 1995) (Niessen, et al., 1994) (Niessen, et al., 1995) (Niessen, 2001) (Niessen, et al., 2001) (Stöcker, 1997).

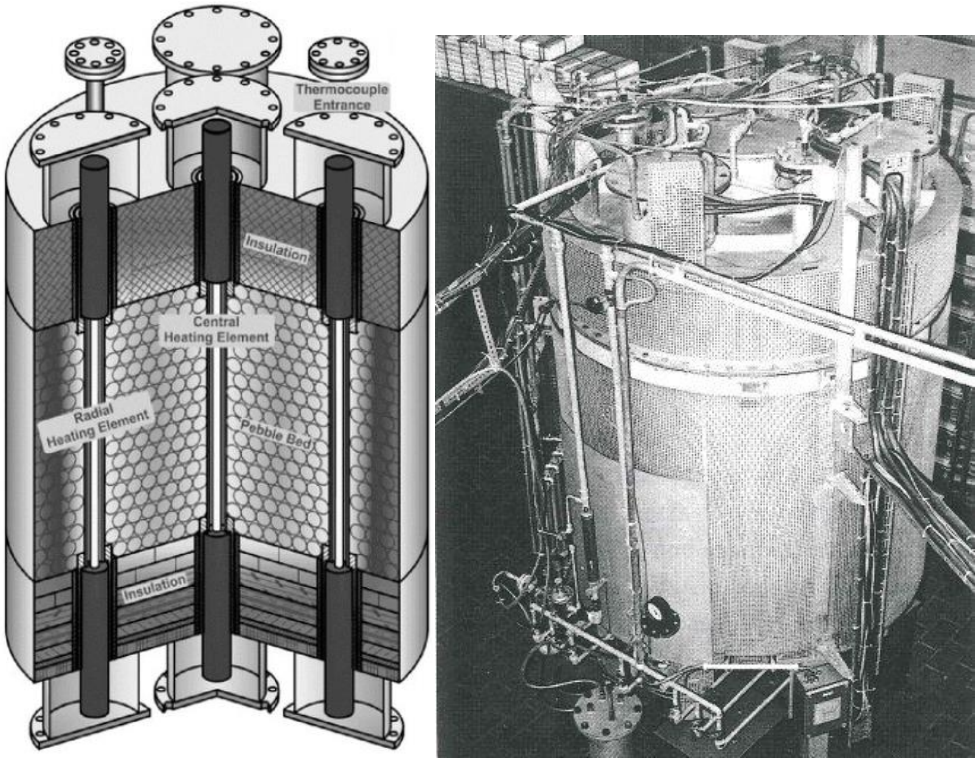

Figure 113: SANA-test facility: (a) cross section; (b) picture

Table 50: Data on the experiment

Parameter	Dimension	Value	Remark
Maximum electric power	KW	50	Different heating elements
Height of furnace	m	1	
Diameter of furnace	m	1.5	
Diameter of graphite balls	mm	60	Smaller balls have been tested too
Number of graphite balls		9 500	
Maximum bed temperature	°C	1 600	Normally max. 1 200 °C
Gas filling		Helium	Nitrogen too

The boundaries were cooled. More than 100 thermocouples in the arrangement of pebbles made it possible to measure the time- and space-dependent temperature profiles. It was possible to reach maximum temperatures of 1 200 °C inside the pebble bed.

The main tasks of the experiments were:

- measurement of time-dependent three-dimensional temperature distribution;
- determination of effective heat conductivity as a function of the temperatures in the core structures;
- evaluation of permitted heat flux densities at different boundary conditions;
- collecting data for programme validations (e.g. Thermix/Direkt, TINTE);
- statements concerning natural convection phenomena.

Many experiments were carried out varying the temperature, heating power and the filling gas in the facility. Helium, nitrogen and mixtures of both gases were used.

Figure 114 shows characteristic stationary temperature profiles in a specific height of the arrangement. On the basis of this type of temperature profile $\lambda_{eff}(T)$ was derived from the experiments.

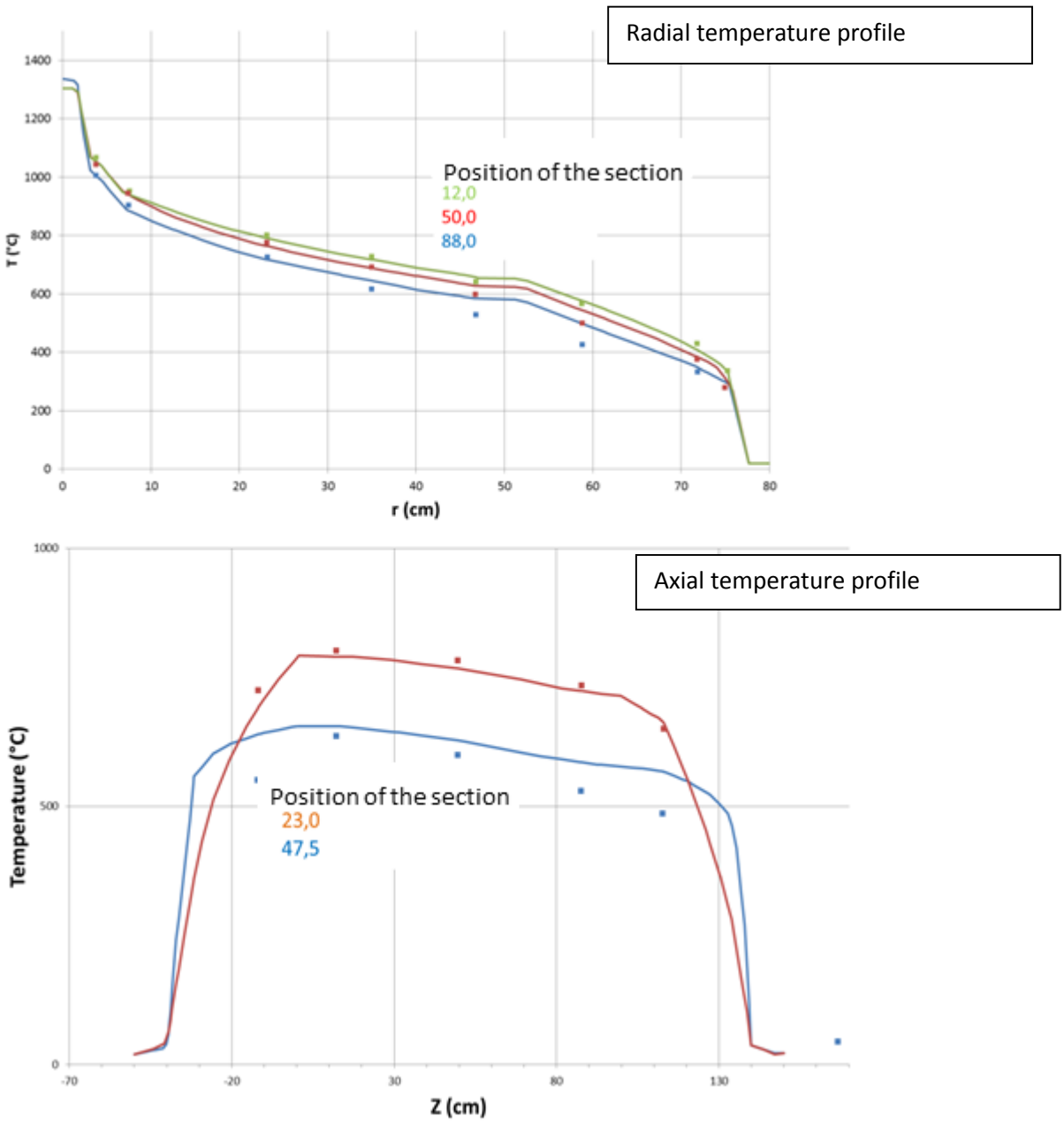

Figure 114: Characteristic results of measurements of stationary temperature profiles in the SANA facility (heating power 50 KW; N2 as filling gas; no radial insulation)

The temperatures close to the heating elements partly reached 1 400 °C in this experiment. From the measured profiles it was possible to get the dependence $\lambda_{eff}(T)$ to temperatures of approximately 1 000 °C.

The comparison between measurements and calculations displays close agreement (Figure 115)

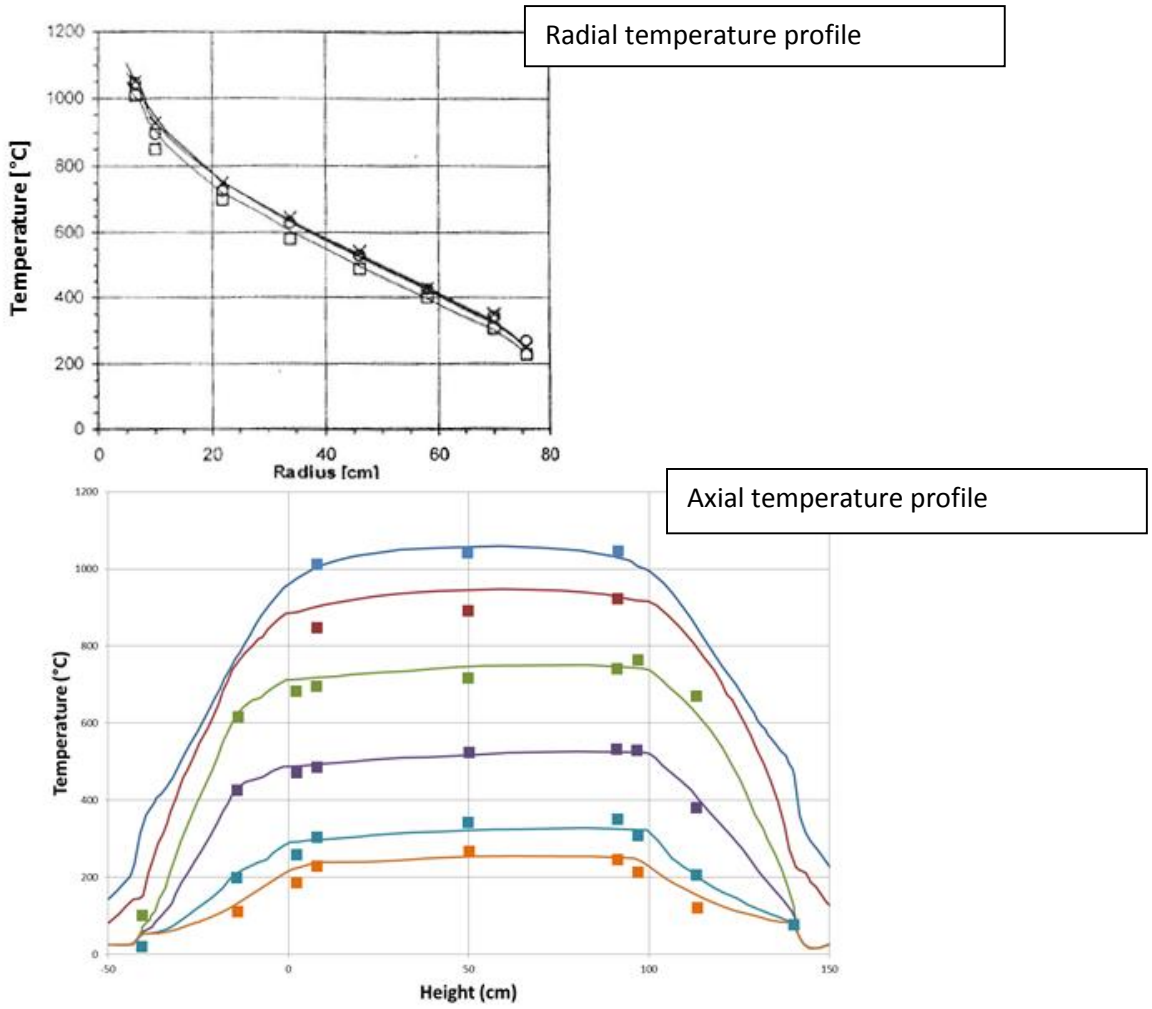

Figure 115: Comparison between measured and calculated values in the SANA facility (power 30 KW; helium as filling gas; without insulation)

An important aspect was the influence of natural convection. There was a remarkable difference between helium and nitrogen. In case of nitrogen or air in the pebble bed the influence of the filling gas has to be taken into account, as Figure 116 may indicate.

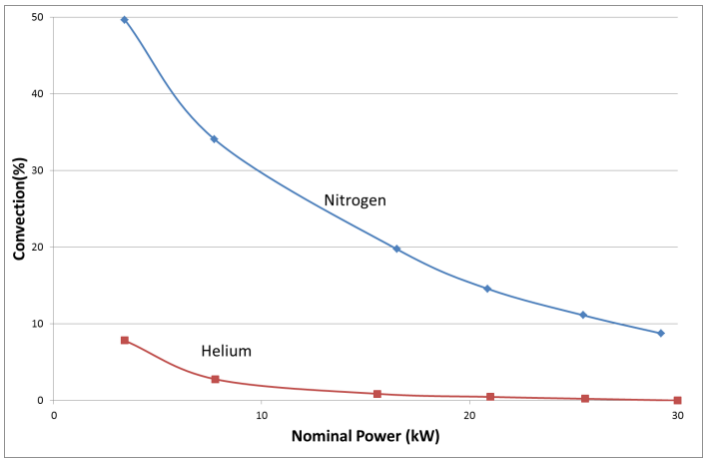

Figure 116: Results of free-convection measurements: transport of heat by natural convection; difference between nitrogen and helium

The total effective heat conductivities in the pebble bed with gas filling are shown in Figure 116. The figure shows the differences for helium and nitrogen. Helium delivers somewhat higher values compared to nitrogen. The resulting measurements are systematically higher compared to the values obtained in the theoretical analysis (Zehner/Schlünder theory).

In summary it can be stated that in the experimental data that are available, the concept of heat transport inside the pebble bed is evaluated and the possibility of calculating the temperature distribution and maximum temperatures in accidents is given. Additionally, a similar large experiment for the self-acting transport of heat is carried out in the PBMW project. The first results are in accordance with the available data.

9.2.3. LUNA experiments

The LUNA (Loop zum Naturkonvektionsumlauf im Primärkreis des HTR = loop to test circulation by natural convection in the primary circuit of HTRs) experimental facility was built and operated with the following goals:

- to gain experience in the field of natural convection;
- to get data for the validation of computer programs;
- to get more information on special effects (influence of the position of the heat sink in the circuit conditions of change of flow through the hot pebble bed, influences of the type of media in the circuit).

The experiment contained an electrical heated pebble bed and a heat exchanger, which could be arranged at different heights relative to the heat source.

The heating furnace had a diameter of 0.7 m and a height of 1.23 m. It was filled with 100 000 pebbles made of steel (diameter 19.5 mm). The porosity of the pebble bed was approximately 60.4 % corresponding to the conditions in the real core of a pebble-bed reactor.

The heater could reach a power output of 200 KW. This power made it possible to reach temperatures of 300 °C at 40 bar. In the pebble bed 80 thermocouples allowed the radial and axial temperature profile to be measured. In the different experiments with variations of the position of the heat sink and the type of gas (air, helium) the relevant temperatures and the mass flow in the circuit were measured. The data then enabled the application of computer programs and the necessary validation of these instruments. Figure 117 provides an overview of the LUNA facility.

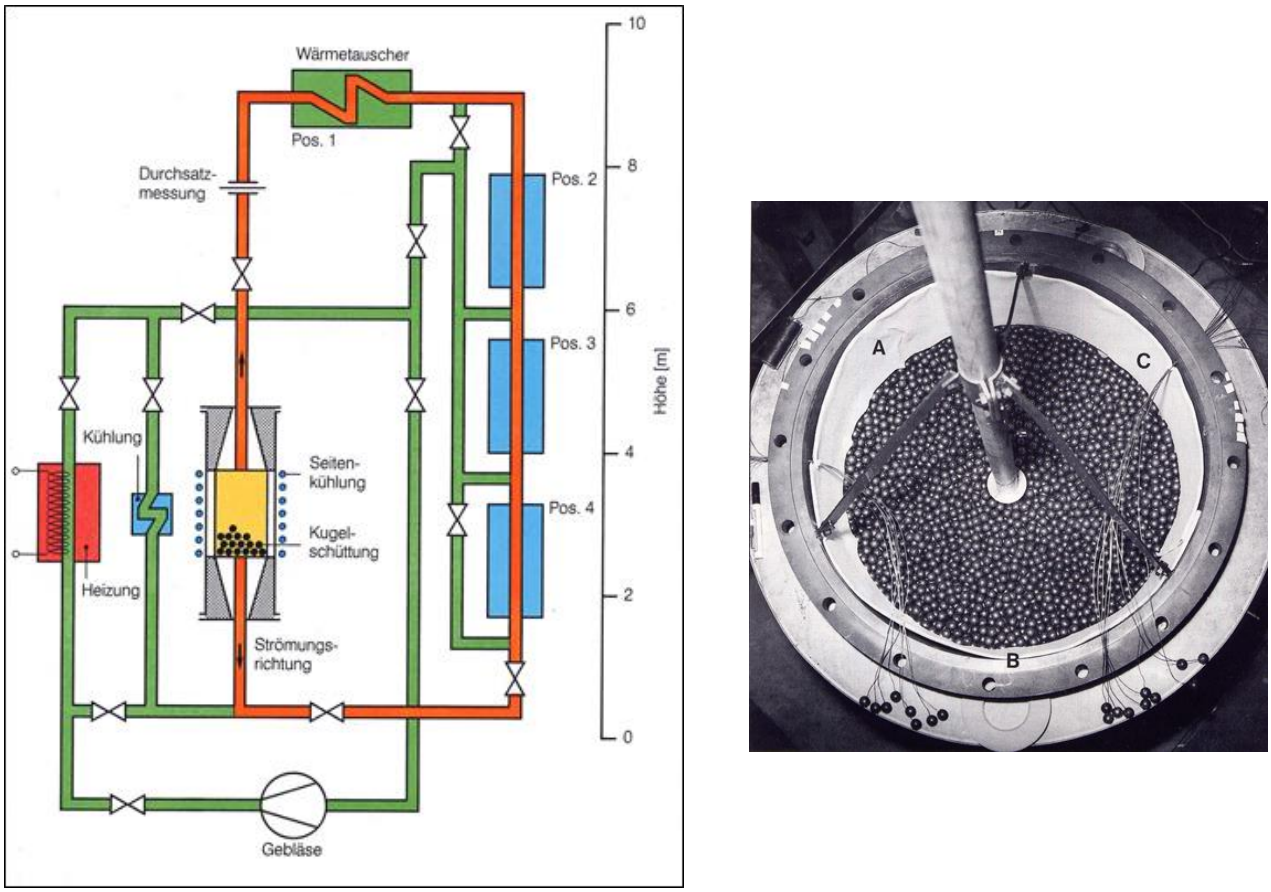

Figure 117: Experimental facility LUNA: (a) overview; (b) view into the pebble bed

Figure 118 shows results that could be obtained.

(a) It could be shown that the mass flow in the cycle is larger in case of air compared to helium.
(b) Measurements and calculations show close agreement. Cooling of the pebble bed by natural circulation was relatively fast, as indicated in Figure 118 (b) and (c).

The position of the heat sink had a major influence on the height of the mass flow and on the direction of the flow (Figure 118 (d)). The position of the heat exchanger below the geodetic height of the heat source was a change of direction from the beginning of the cooling process. This is an important aspect for the design of modular HTRs. The relevant experiences from the LUNA experiments can be summarised as follows:

- mass flow and direction of the flow depend on the medium and the positions of the heat source and the heat exchanger;
- under specific conditions stagnation and change of flow direction are possible;
- a deep arrangement of the heat sink in any case causes an upward flow through the pebble bed;
- the results enabled the validation of existing programmes and the overestimation of measurements, and showed that the pre-calculations could be confirmed by the experiments.

(a)

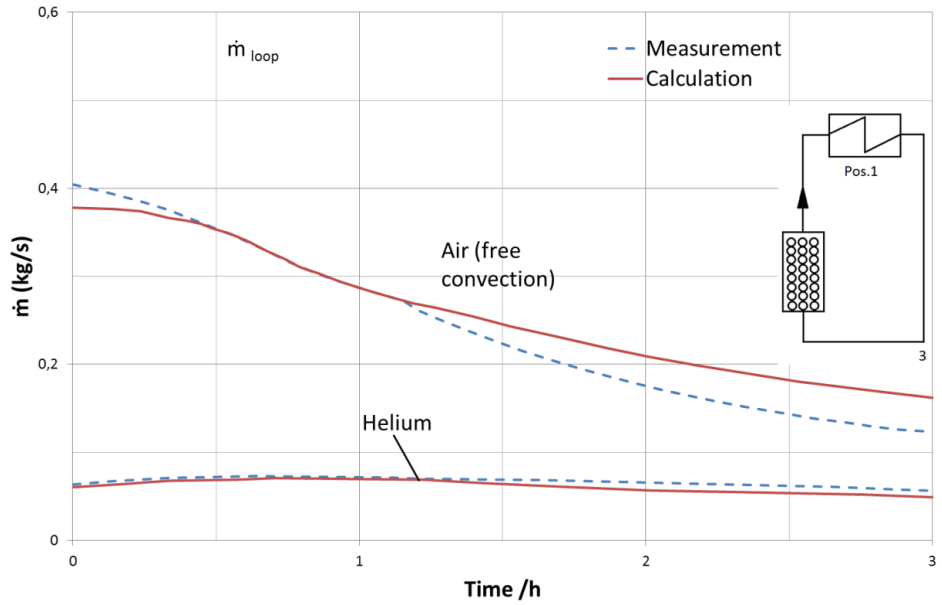
0,6
0,4
0,2
0
ṁ loop
Measurement
Calculation
ṁ (kg/s)
Air (free convection)
Helium
Pos.1
3
0
1
2
3
Time /h

(b)

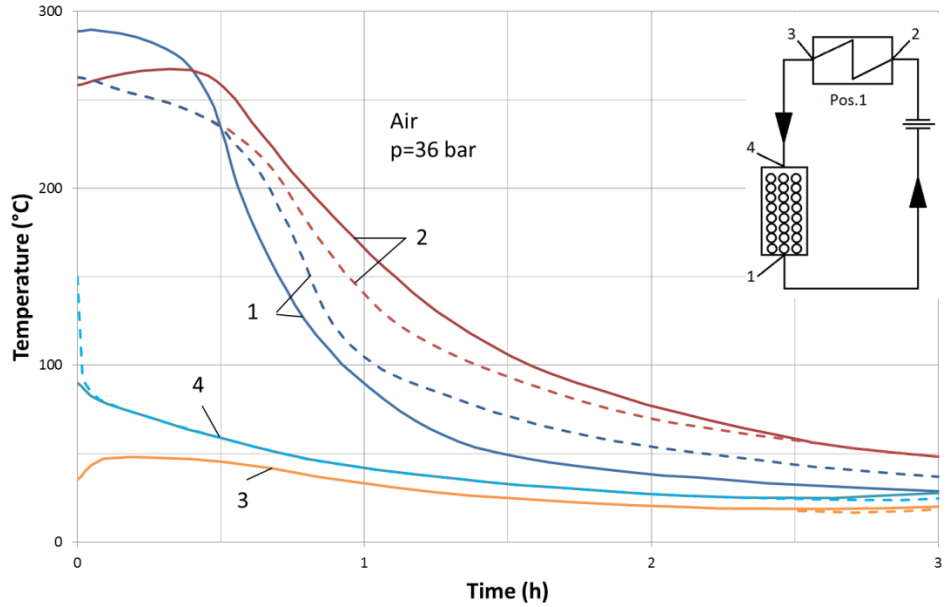
300
200
100
0
Temperature (°C)
Air
p=36 bar
1
2
3
4
Pos.1
0
1
2
3
Time (h)

(c)

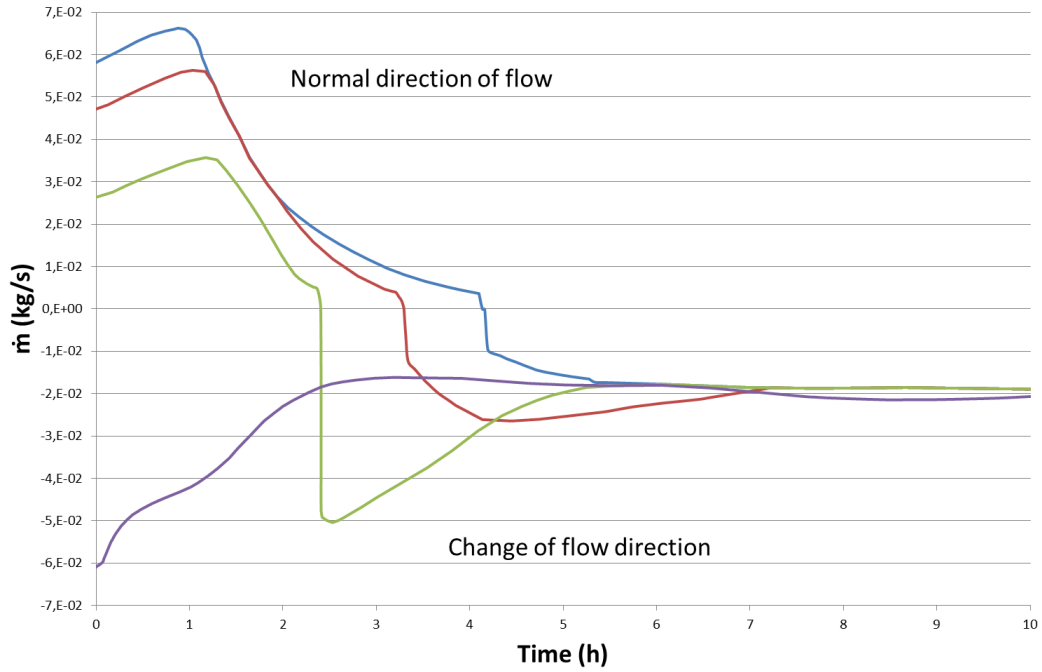

(d)

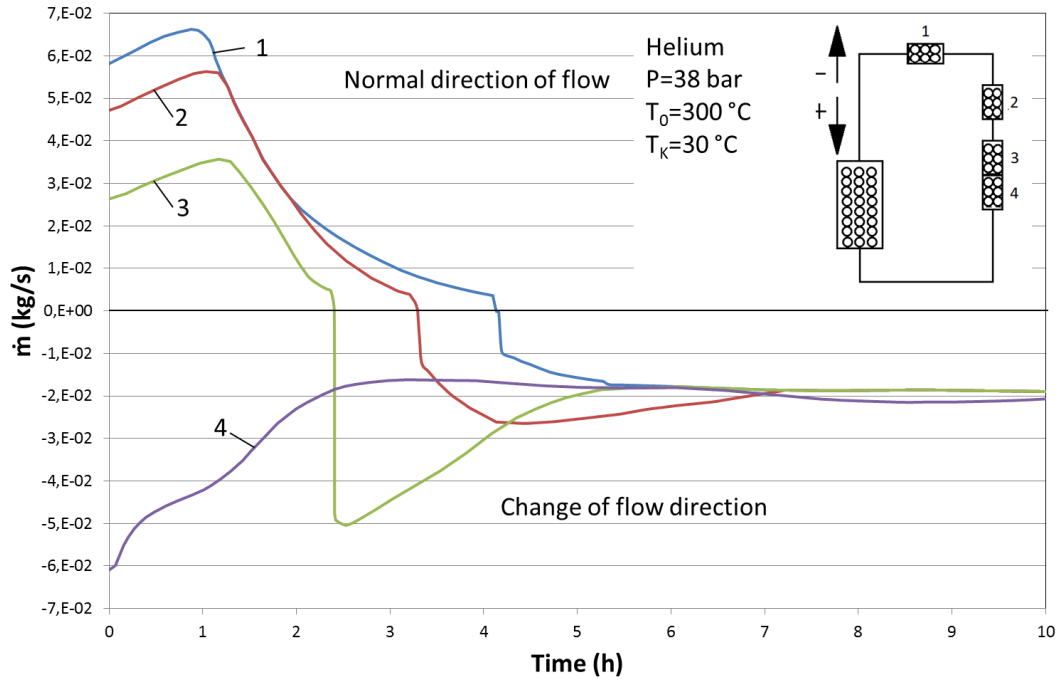

Figure 118: Measurements and calculations — results of the LUNA facility: (a) mass flow dependent on time; (b) temperature dependent on time (air at 36 bar); (c) temperature dependent on time (helium at 37 bar); (d) mass flow in circuit in case of different positions of the heat sink

9.3. Heat transport through the shield of the core

9.3.1. Heat transport of the graphite reflector including the influence of irradiation ($\lambda_G(T, D)$)

The decay heat conducted from the core will be transported through the graphite structures of the reflector surrounding the core (Delle, et al., 1983, 1984).

In the graphite reflector a heat flux corresponding to the following relationship is necessary to remove the decay heat from the core:

$$\overline{\dot{q}(t)} \approx P_{tn} * f_D(t) * 2\pi * D * H \qquad (110)$$

$\mathrm{D} = \text{outer diameter of the core;}$

$\mathrm{H} = \text{height of the core.}$

In case of self-acting decay heat removal, ΔT is the temperature difference in the graphite, ΔS is the thickness of reflector and λ_G is the heat conductivity of the graphite, which is dependent on the temperature and the irradiation dose. For a conservative analysis one has to assume that the graphite has been irradiated over the whole time at full operational power (e.g. 30 years, Figure 119).

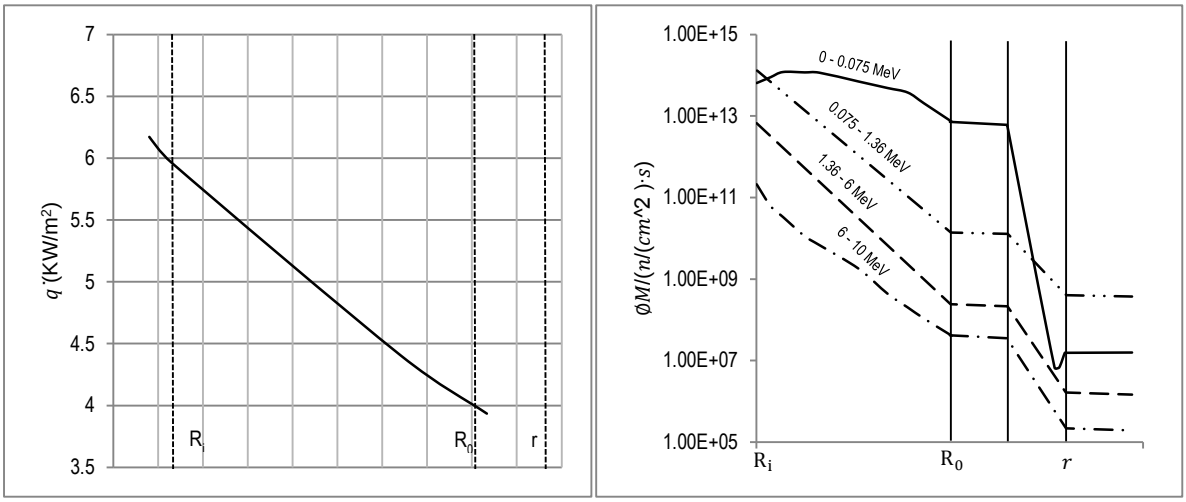

Figure 119: Aspects of heat transport in the side reflector of a modular HTR in case of self-acting decay heat removal

The left side of Figure 119 shows the average heat flux depending on the radial position in the reflector; the right side shows the radial dependence of the fast heat flux in the graphite reflector.

Corresponding to the explanation in Figure 119 a stepwise analysis of the different layers of the reflector and the relevant graphite data is required. Many irradiation experiments have delivered these values and are available in form of data libraries. Figure 120 shows data for a characteristic material with rising neutron influence while the heat conductivity is reduced at high temperature by a factor of 2. In many cases, the temperature distribution in the reactor together with the dependence on the changes by radiation, 30 to 50 years of operation have to be taken into account to evaluate the temperature differences in the graphite reflector as part of the heat transport chain (Haag, et al., 1990). Generally these irradiation effects are important for a relatively thin layer of the

thick-walled graphite reflector (approximately the first 1 m close to the core) and regions relevant to core structure.

The dependence of the heat conductivity can be described by an equation of the following type (Delle, et al., 1990).

$$\lambda(T) = \alpha_0 + {}^{\alpha_1}/_{T^2} + \alpha_2 * exp\left({}^{-1\,250}/_{T}\right) \qquad (111)$$

An example of a suitable reflector graphite is ATR-2E.

The irradiation causes a reduction in the values of heat conductivity as shown in Figure 120. The effect is relatively strong at low temperatures, while at high temperatures annealing effects play a role.

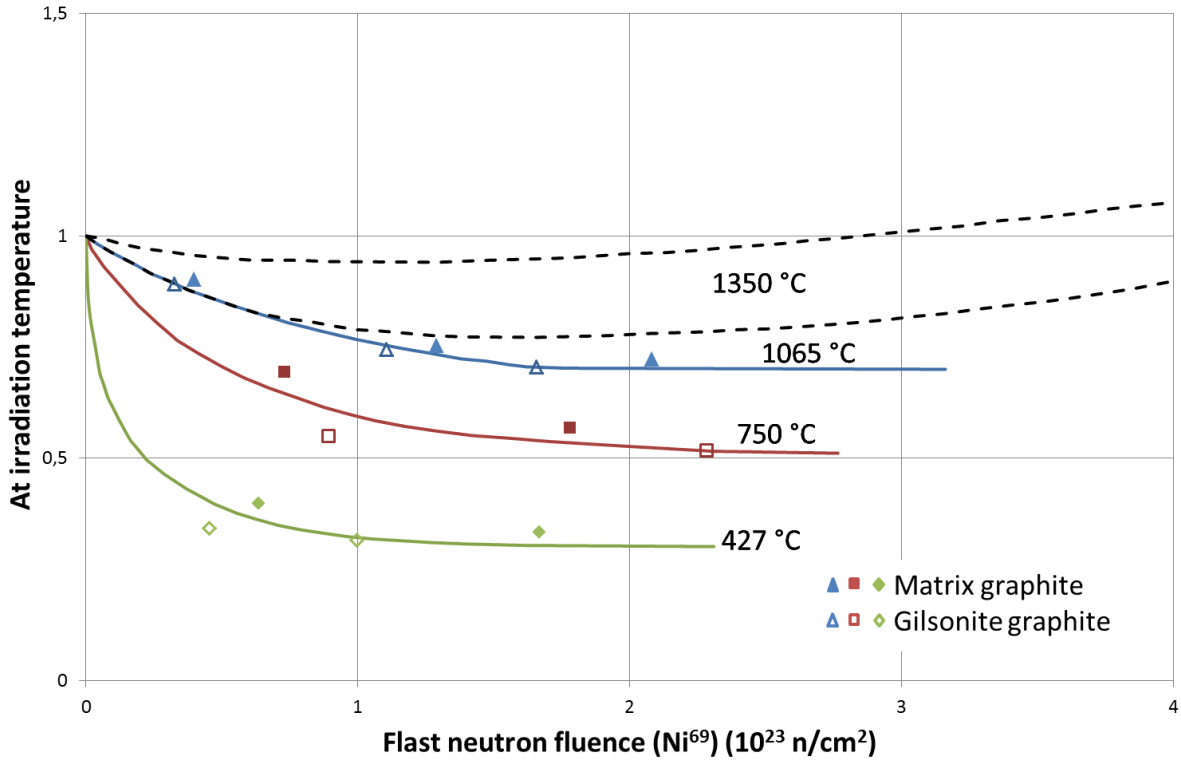

Figure 120: Behaviour of irradiated graphite relevant for the description of 'loss of active cooling' accidents and action of self-acting decay heat removal: heat conductivity dependent on fast neutron dose and temperature (irradiation at 950 °C)

For the decrease in the fast neutron flux in the radial direction the dose is given by the equation:

$$D(r) = D_{max} * exp(-\Sigma * \tau) \qquad (112)$$

$\Sigma \approx 0.011 cm^{-1}$ can be applied for (hands-on) estimates. This results in a reduction in the fast neutron flux by a factor of more than 10^4 at a reflector thickness of 1 m.

Applied to the case of self-acting decay heat removal in a modular reactor, characteristic data for the heat flux entering into the graphite reflector and the temperature difference across this component

can be obtained. With a decay power $\dot{Q}_D$ and core dimensions (radius R and average height H) the average and the maximum heat fluxes are given by:

$$\overline{\dot{q}''} = \dot{Q}D \Big/ (2\pi * R * D);\ \dot{q}''(max) = \overline{\dot{q}''} * \beta, \beta \approx 1.6 \qquad (113)$$

This delivers a value of around 6 KW/m^2 at a time of 1 day after a 'loss of cooling' accident at the boundary of the core as an average value and ~ 10KW/m^2 as the maximum load. However, these values would decrease during an accident as the decay heat decreases.

With a value of 100 W/(mK) for the heat conductivity of unirradiated graphite this results in an average temperature difference of 50 °C across the graphite reflector in the radial direction.

Changes in the heat conductivity after many years of operation and irradiation would make this value increase in case of accidents. Again, the graphite zone near the core especially plays a major role regarding changes of heat conductivities.

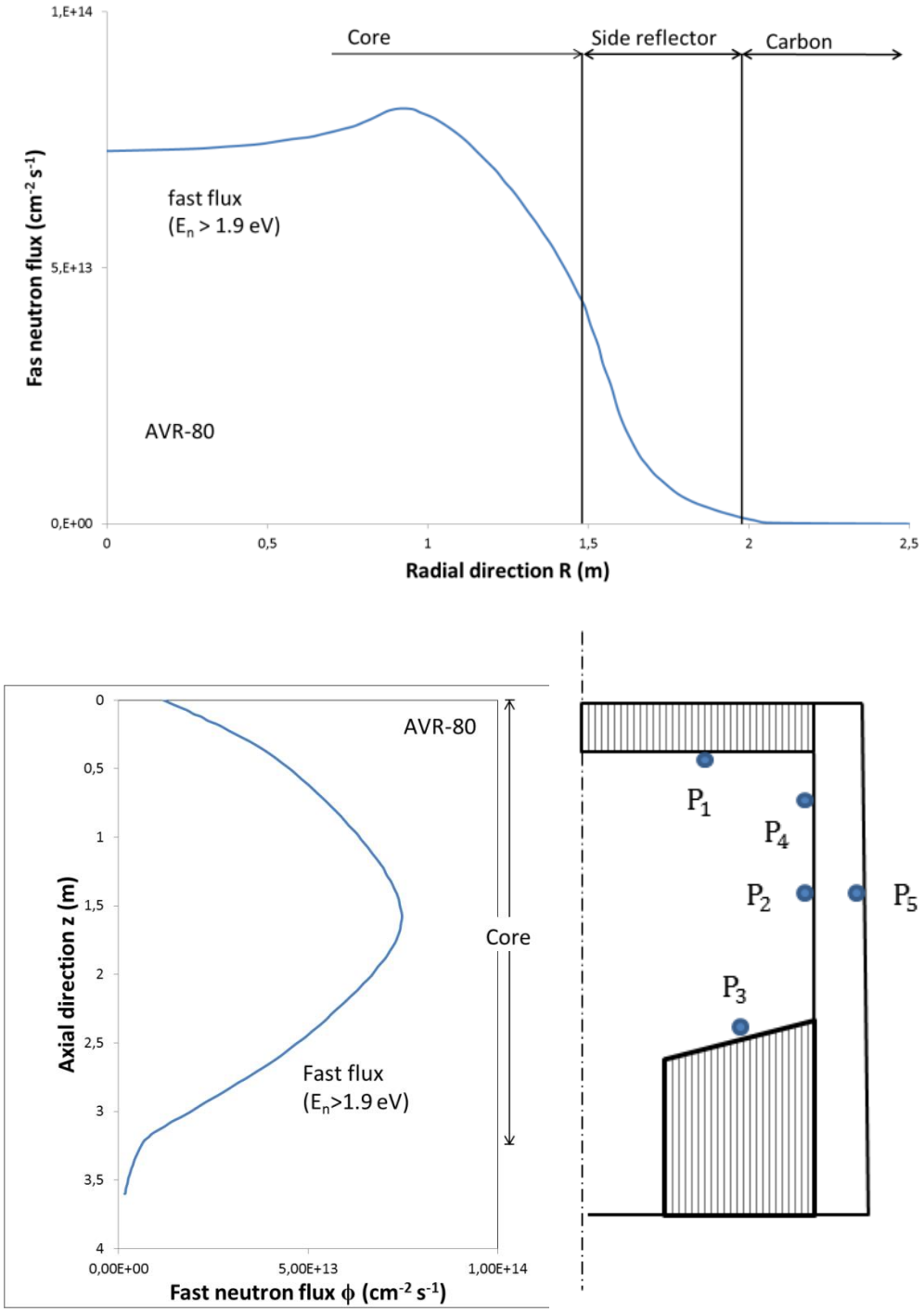

Figure 121: Aspects of heat transport through the graphite reflector in case of 'loss of cooling' accidents: (a) radial dependence of neutron flux (e.g. AVR; 1.85 m under core upper surface); (b) axial dependence of neutron flux (e.g. AVR; on core axis); (c) positions of the reflector

Table 51: Characteristic of fast neutron dose at different positions of reflector (e.g. HTR Module; after 30 years of operation)

Point	Temperature (°C)	Fast flux n/cm^2	Fast dose n/cm^2
P1	250	7×10^{13}	2×10^{22}
P2	500	5×10^{13}	1.5×10^{22}
P3	700	1×10^{13}	3×10^{21}
P4	250	6×10^{13}	2×10^{22}

P5	300	1×10^{10}	1×10^{19}

9.4. Heat transport in gaps between reactor internal structures by radiation and free convection — general experiences from laboratory experiments

9.4.1. General experiences from laboratory experiments

Natural convection of air, helium or mixtures of helium and air play a major role during all processes of decay heat removal in modular HTGRs.

In the chain of heat transport from the core to the environment there are several steps which contain heat transfer mainly by radiation and free convection. This is the case at the following positions (Figure 122):

- in the gap between the graphite reflector and the thermal shield;
- in the gap between the thermal shield and the wall of the reactor pressure vessel;
- in the space between the reactor pressure vessel and the cooling panels of the surface cooler;
- on the outside of the inner concrete cell;
- on the inside of the reactor containment building;
- on the outside of the reactor containment building.

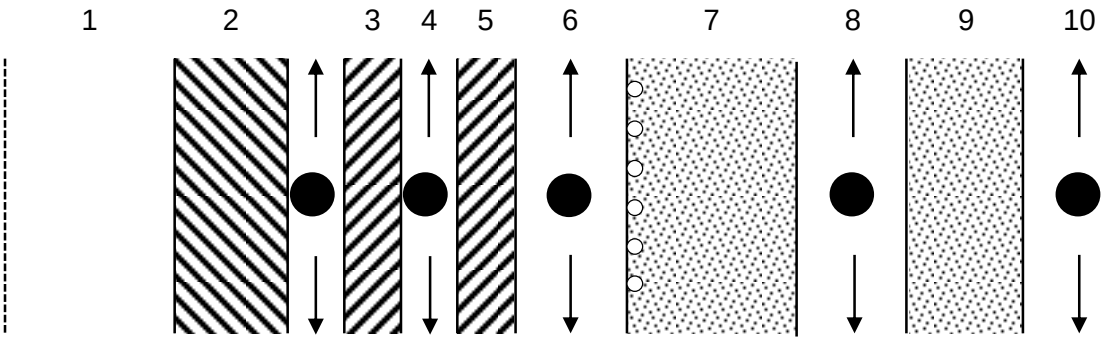

Figure 122: Positions where natural convection plays a role

The numbers used in Figure 122 denotes the different components and structures.

(1) Core.
(2) Graphite reflector.
(3) Thermal shield.
(4) Gap with structures between thermal shield and reactor pressure vessel.
(5) Reactor pressure vessel.

(6) Cavity between reactor pressure vessel and surface cooler.
(7) Inner concrete cell with surface cooler.
(8) Room of the containment building with inner structures.
(9) Concrete wall of the containment building.
(10) Environment.

Corresponding to these heat-transfer requirements, different heat transport mechanisms are relevant here (Figure 123):

- heat transport between two surfaces with different temperatures (and different emissivities) of surfaces;
- heat release from a hot surface to a surrounding medium, such as release to the atmosphere in the building;
- heat penetrating into structures from a hotter atmosphere.

Normally the heat flux in these gaps can be described by equations of the following type (Figure 123(a)).

$$\dot{q} = (\alpha_{conv} + \alpha_{rad}) * (T_1 - T_2)$$

The temperature difference $(T_1 - T_2)$ is responsible for heat transfer by radiation and by internal free convection of helium or helium/air mixtures in case of accidents.

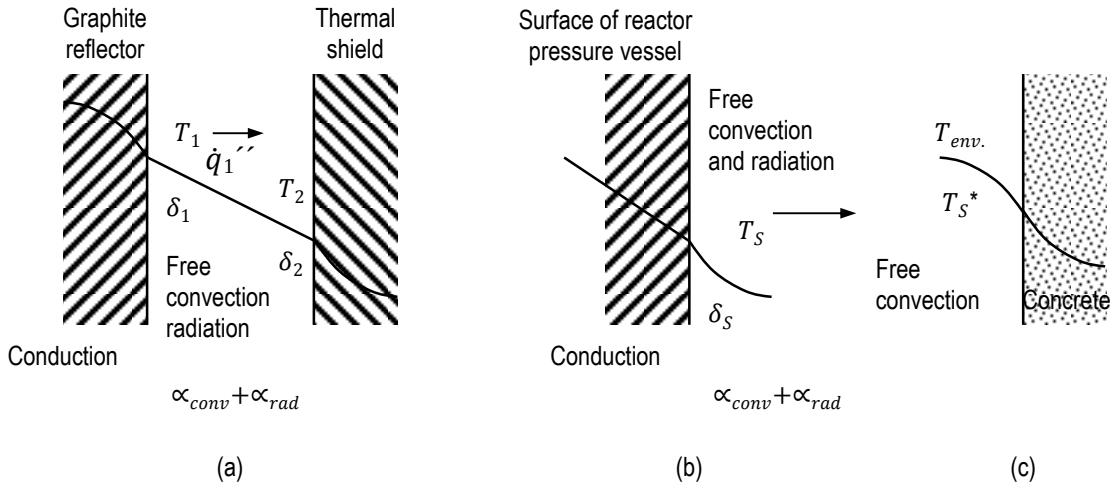

Figure 123: Heat transport mainly by free convection and radiation — three important situations in the chain of heat transport of a modular HTR: (a) between two surfaces in the reactor internals; (b) from hot surfaces to the atmosphere of the reactor containment building to concrete structures

For the heat transfer by radiation, the temperatures of the radiant and of the absorbing surface and the coefficients of environment are relevant (Schürenkremer, et al., 1983) (Schürenkremer, 1984).

$$\alpha_{rad} \approx \varphi(T_1, \varepsilon_1) \approx C_{12} * \frac{C_S(\varepsilon_1 * {T_1}^4 - \varepsilon_2 * {T_2}^4)}{} = C_{12} * C_S * \beta_T(T_1, T_2, \varepsilon_1) \qquad (114)$$

The factor C_{12} covers the emissivity and is, for parallel flat surfaces, defined as:

$$C_{12} = C_s/\left(\frac{1}{\varepsilon_1}+\frac{1}{\varepsilon_2}-1\right) \quad (115)$$

in which C_s is the radiation constant with the value 5.77 W/(m^{2}K^4). The emissivity of graphite has a value of 0.9. For steel one can apply 0.6 to 0.85 for ε depending on the status of surfaces.

The function β_T is shown in Figure 124 depending on the temperatures of the surfaces:

$$\beta_T(T_1, T_2, \varepsilon_1) = \left(\varepsilon_1 * {T_1}^4 - \varepsilon_2 * {T_2}^4\right)/(T_1 - T_2) \quad (116)$$

A temperature difference of 100 °C allows in the region of 460 °C a β_T value of 2, and therefore a heat flux of around 5 KW/m^2 in the core structures (graphite/thermal shield).

For small differences between T_1 and T_2 at elevated temperatures the following approximation can be used:

$$\beta_T \approx \frac{4}{100} * \left(\frac{T_{av}}{100}\right)^4, T_{av} = 0.5 * (T_1 + T_2) \quad (117)$$

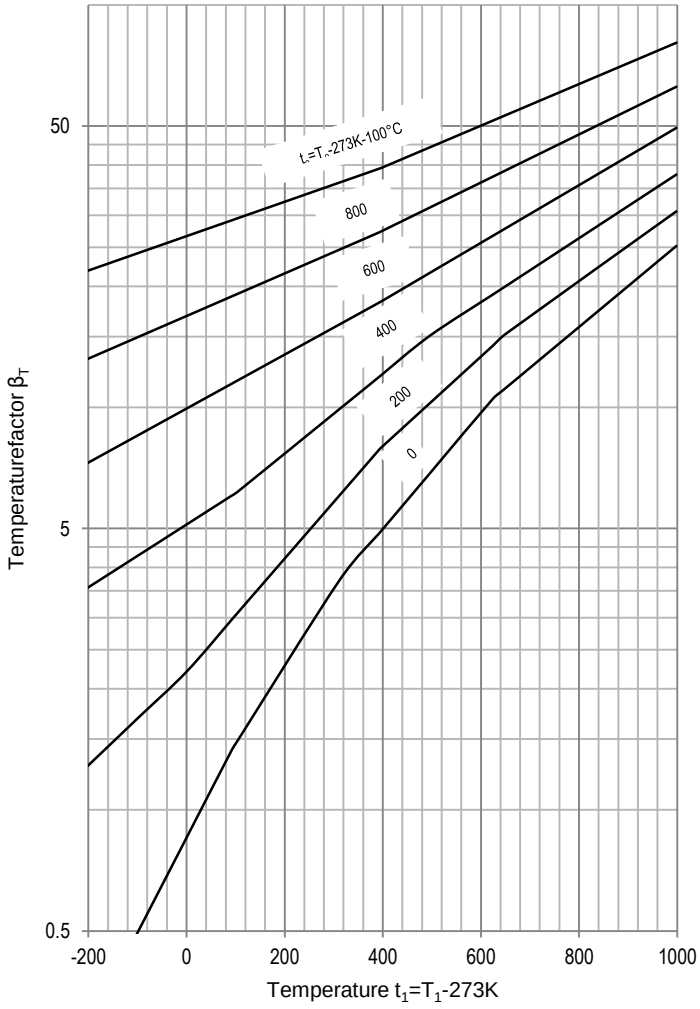

Figure 124: Dependence of the function $\beta_T(T_1, T_2, \varepsilon_1)$ $(\varepsilon_1, \varepsilon_2 = 1)$

For the heat transfer by free convection many empirical equations are available.

The convective heat transfer in the gaps depends mainly on the temperature profile, on the characteristic dimension s_i and on the types of materials used. Additionally, the influence of pressure has to be considered:

$$\alpha_{conv} = f(T_1, H, s_1, p)$$

Some common equations for the convective heat transfer are summarised in Table 52 (Hell, 1979) (Hottel, et al., 1964).

Table 52: Some relations for the natural convection of air

For vertical walls	$\alpha = c_1 * \sqrt[4]{(T_w - T_{env}) * H}, c_1 = 1.39\ at\ 0^0C\ till\ 1.14\ at\ 300^0C$
For horizontal plates	$\alpha = \lambda/4 * 137 * \sqrt[3]{Gr * Pr}, Gr = g * l^3 * \beta * \Delta T/r^2, Pr = r/a$
For horizontal pipes	$\alpha = \lambda/d_a * 0.372 * \sqrt{g * {d_a}^3 * (T_w - T_{env})/r^2 * T_{env}}$

9.4.2. PASCO experiment to measure $\alpha_{conv}(T)$ and $\alpha_{rad}(T)$

For some new reactor concepts specific cooling systems to remove the decay heat from the containment have been proposed. For example, in the PWR AP1000 the heat will be released through a gap between the steel of the containment and the outer thick concrete wall. This heat transport needs effective free convection in the gap.

To get enough information on this type of reactor containment cooling by free convection of air the large PASCO test facility has been in operation in Germany. The major reason to construct the facility was the innovative containment of future pressurised water reactors. The results, however, are relevant for the different steps of heat transfer in a modular HTGR insofar as gaps are considered.

Figure 125 shows the PASCO experimental facility (Cheng, et al., 1996) (Cheng, et al., 1996) (Cheng, 1998) (Hennies, et al., 1990) (Kucerza, et al., 1993) (Neitzerl, 1992).

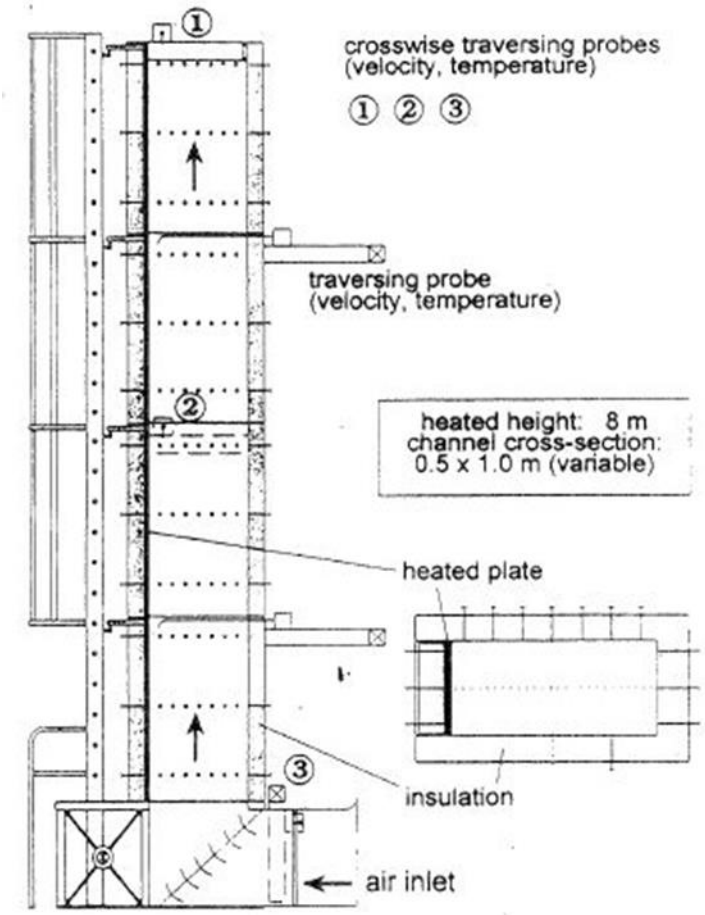

Figure 125: PASCO test facility to measure the release of heat from hot surfaces by radiation and free convection and to determine flow velocities

The principle for cooling the containment, which is part of the AP1000 concept, is that in the gap between a steel shell and a concrete wall a mass flow of air exists, and that this mass flow transports the decay heat, which is transferred through the wall of the steel shell to the environment. Alternatively, water can be added on the top of the containment. In this way the cooling effect would be enhanced. A filter on top of the flow path removes radioactive substances, which could be contained in the air flow due to leakages of the steel shell. The heat transport from the shell between the steel liner and the concrete wall outside was analysed using the large PASCO experiment.

The test facility was operated to obtain further data on the described idea. PASCO consisted of a channel with a height of 8 m. The cross section of the channel was 1 m × 0.5 m.

One side was heated by electrical resistance heating; the other side was insulated. The air inlet was at the bottom of the facility in a channel with a 90° bend. The heat flux was variable in the axial direction. The temperature of the heated wall was between 100 °C and 175 °C corresponding to the conditions in containment. The temperature distribution in the wall, the flow regions and the air velocity were measured.

From many experiments average heat-transfer numbers were derived. Based on the definition one gets a value of around 17 W/m^{2}K for $\bar{\alpha}$, if a heat flux of 1.5 KW/m^2 is applied. In the value for $\bar{\alpha}$ given

above (around) 15 W/m^{2}K is caused by radiation. The value for $\bar{\alpha}$ by free convection fits in very well with results from other experiments. For vertical walls a good approximation, already mentioned as;

$$\alpha_{conv} \approx 1.28 * \sqrt[4]{\Delta T / H} \qquad (118)$$

could be derived. Here α is given in W/m^{2}K, ΔT in °C and H in m.

For the example chosen here (H = 8 m, ΔT = 130 °C), α_{conv} =2.5W/m^{2}K. This corresponds well to the values measured in the PASCO facility.

In total, these types of experiments delivered results such as the one given in Figure 126 for the heat-transfer coefficients and for possible heat fluxes.

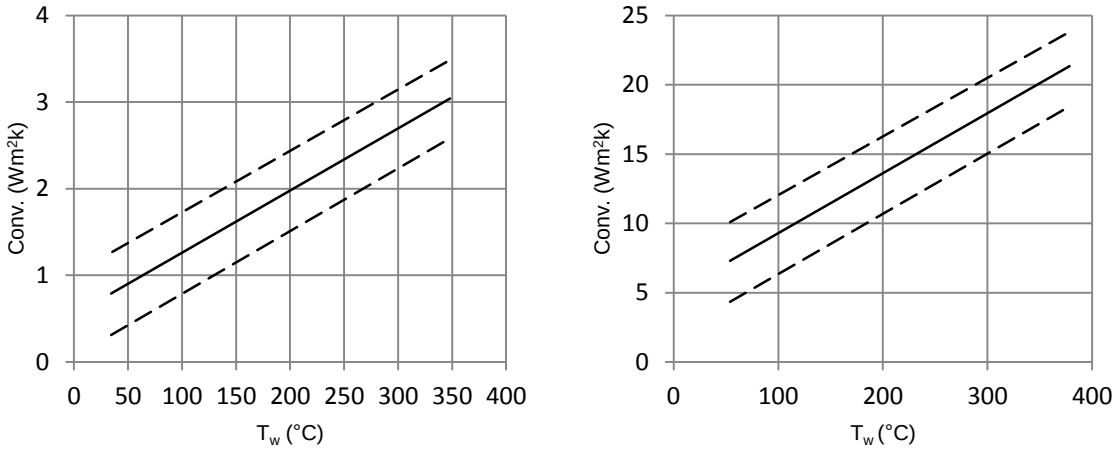

Figure 126: Heat-transfer coefficients and possible heat fluxes

Using total heat-transfer coefficients of around 15 W/m^{2}K at a surface temperature of the reactor pressure vessel of a modular HTR of 350 °C, one gets a heat flux of nearly 4.5 KW/m^2 which sufficiently high to remove the decay heat totally after 30 hours following a 'loss of coolant' accident has happened (given for modular HTR, 200 MWth).

The overall experiences from all these experiments on heat transfer by natural convection and by radiation delivers a clear picture for the application of modular HTRs. In the hot core structures gaps cause temperature differences in case of self-acting transport of decay heat.

For example, between the thermal shield and the inside of the reactor pressure vessel a heat flux of approximately 5 KW/m^2 has to be transferred after a time of 30 hours (after the start of a 'total loss of cooling' accident). With a heat-transfer coefficient of 30 W/m^{2}K at this higher surface temperature this results in a temperature difference of approximately 100 °C between the hot surfaces of the graphite reflector and the thermal shield as one important step.

If the surface cooler fails too, the heat is released from the surface of the inner concrete cell of the environment in the reactor containment building by radiation and free convection.

Assuming a value of around 1 000 m^2 for the surface one gets an average heat flux from there to the containment building atmosphere (after a long time) of around 300 W/m^2. If the heat-transfer

coefficient is in the order of 5 W/m^{2}K the surface temperature of the concrete would in this case be around 80 °C.

9.5. Heat transfer from the surface of the reactor pressure vessel by free convection and radiation

9.5.1. INWA experiment

A very important step in the chain of heat transport is the release of the decay heat from the surface of the reactor pressure vessel to the surrounding concrete cell (including the surface cooler). The 'normal' solution for modular HTRs is the use of a forged-steel vessel for the reactor and a water-cooling system for the outer surface cooler. Alternatively, prestressed vessels made either from cast iron with an inner liner or from cast steel without a liner are attractive solutions. Furthermore, the concrete structures of the inner cell can be modified in such a way that they contain cast-iron blocks with borings. These borings allow natural convection to remove the decay heat. Figure 49 shows this principle with a prestressed cast-iron vessel for a 200 MWth modular HTR. This vessel is prestressed by many axial and radial tendons and can therefore never burst. The 'leak before break' criterion is fulfilled by the design of this vessel, which consists of many cast-iron blocks and a liner for the gas tightness of the system. The surrounding system of cast-iron blocks with borings for air flow allows the removal of approximately 600 KW if the water cooling of an additional surface cooler has failed.

It was necessary to get more information on some important questions and data for simulation calculations:

- temperatures dependent on time in different structures of the pressure vessel and of the outer cell (for different size of applied heat fluxes);
- behaviour of structural elements under thermal loads
- measurement of cooling capacity of outer structures;
- measurement of more dimensional temperature fields to get data for computer programs;
- integral demonstration of the concept of self-acting decay heat removal.

The large INWA (Inaktives Wärmeabfuhrsystem (inactive system for decay heat removal)) test facility has been built and operated to get information on the influence of the main parameters (Beine, 1991) (Geis, et al., 1993) (IAEA, 1994) (IAEA, 2001) (Kugeler, et al., 1991) (Kugeler, et al., 1994) (Wolf, et al., 1994).

Corresponding to Figure 127, a segment of the reactor pressure vessel and of a concrete cell have been tested. For the reactor pressure vessel an inner liner was applied. The concrete cell was modified in such a way that it contained cast-iron blocks and concrete. Additionally, free convection cooling of these blocks was planned.

The figure shows a perspective view of the INWA test facility which corresponds to a 20°-section of a proposed prestressed cast-iron reactor pressure vessel for the 200 MWth Siemens/KWU HTR modular pebble-bed reactor design (HTR Module). The test facility was constructed with all the details of a realistic vessel and with a cast-iron/concrete composite structure with circumferential tendon reinforcement at real scale. The height of the section was chosen to be about 2 m (a fraction

of the total axial systems extension). Therefore, free-circulation conditions in the embedded tubes had to be simulated accordingly by appropriate forced-convection conditions.

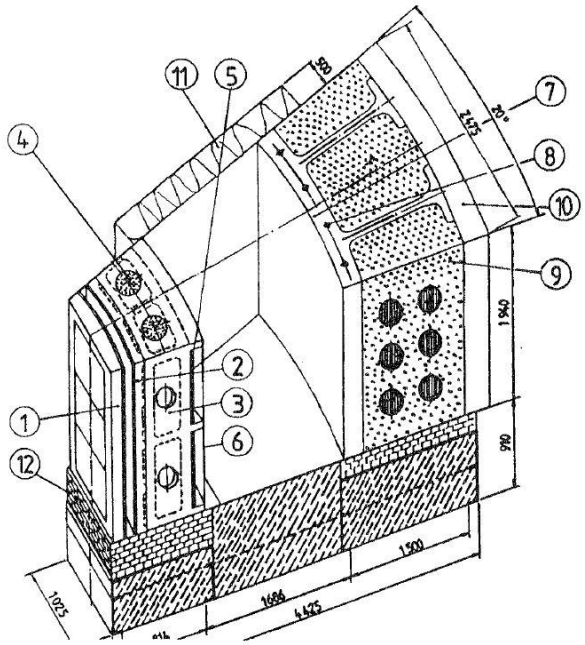

Figure 127: Internals of the INWA-test facility

The numbers shown in Figure 127 (dimensions in mm) with a cast-iron wall are explained below.

(1) Electric heater and core vessel.
(2) Liner with liner-support structure.
(3) Pressure vessel wall.
(4) Axial prestressing cable.
(5) Cover plate for hoop pressurising cable.
(6) Cover plate for hoop pressurising cable.
(7) Cast-iron block of the reactor cell.
(8) Cooling system.
(9) Reinforced concrete.
(10) Box for sprinkler system.
(11) Insulation.
(12) Refractory support.

In order to provide an ultimate heat sink in case of the failure of both redundant and free-circulation piping systems, a film cooling device was installed in order to descend on the outside reactor cell composite surface. The complete INWA facility was embedded within 500 mm-thick thermal insulation. Also, the supporting base structure was carefully designed for its insulating properties. All of these precautionary measures were necessary to keep the heat losses from the INWA facility as low as possible. The thermal power is provided by an electric heater. This heater consists of four independently controlled heating circuits to ensure a surface temperature that is as uniform as possible.

The decay heat was simulated by a flux through the liner. There was a maximum electrical heating power of 10 kW, which allowed heat fluxes up to 10 kW/m^2. The concept included a special outer concrete cell design with a high iron content. This design was chosen to allow effective conduction and storage of heat in the cell. The total arrangement was surrounded by very thick insulation to minimise heat losses. During the experiments heat fluxes oriented on the estimates for 'loss of cooling' accidents were applied. Figure 128 shows the time dependence of the heat fluxes in typical experiments. It partly simulates extreme conditions of heat fluxes. A value of around 3-5 kW/m^2 is characteristic after 30 hours in a modular HTR (200 MWth) Here the depressurisation of the primary system was assumed, and in the first phase of the accident a heat flux value of 5 kW/m^2 would be characteristic. After several hundred hours the value was reduced to 2 kW/m^2.

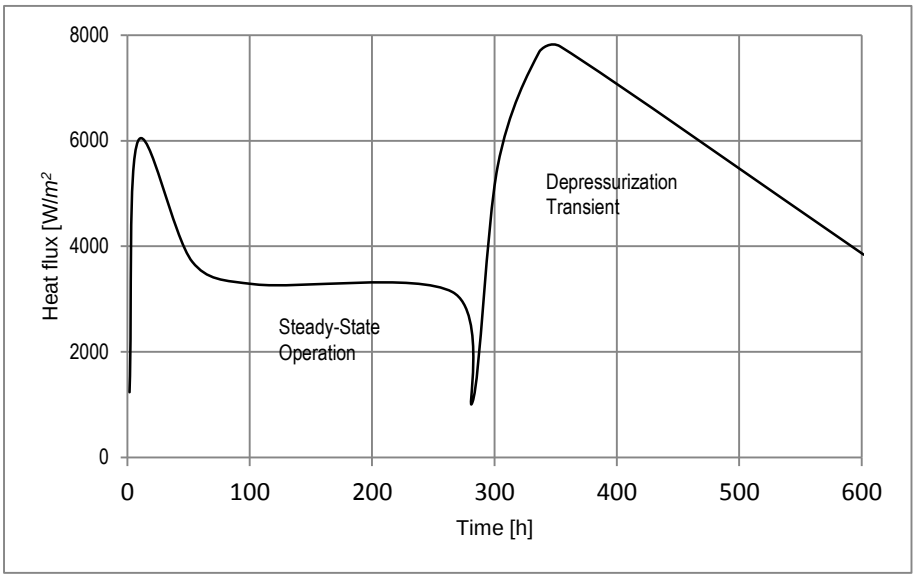

Figure 128: Time dependence of heat flux on the liner surface of the INWA test facility (a power of 4 kW corresponds to a heat flux of/4 kW/m^2)

Figure 129 shows a measured radial temperature profile at different points of the arrangement.

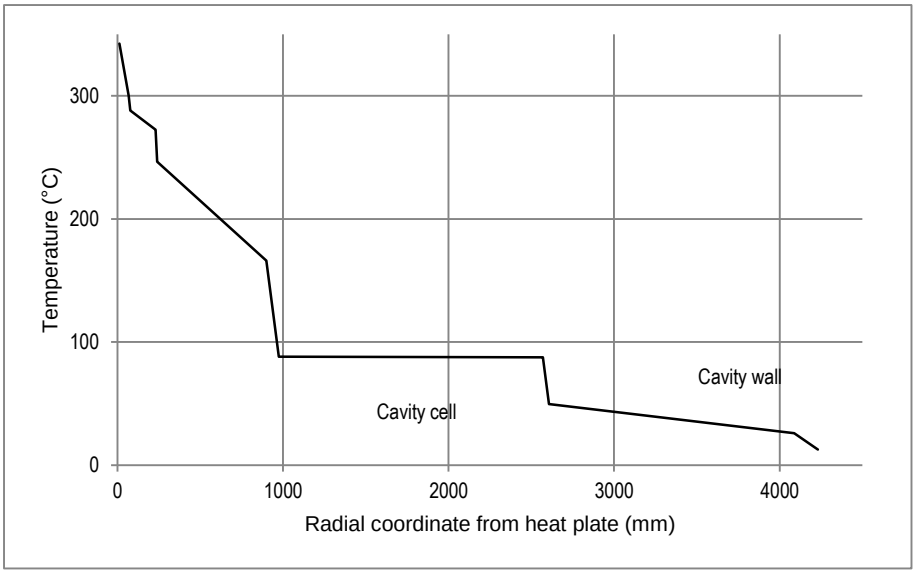

Figure 129: Radial dependence in the reactor pressure vessel and concrete cell structures (at the time when the highest temperature of the vessel occurs)

This was the basic information for 3D calculations of temperature distribution and flow. Measurements and calculations were in close agreement. The calculated temperatures of the liner showed an even higher level of accuracy.

Certain time dependencies of different temperatures in the structures which occurred in a test with a heat flux corresponding to Figure 128 are shown in Figure 130 and Figure 131. The temperature of the liner never reached a temperature higher than 550 °C, even in case of very high heat fluxes.

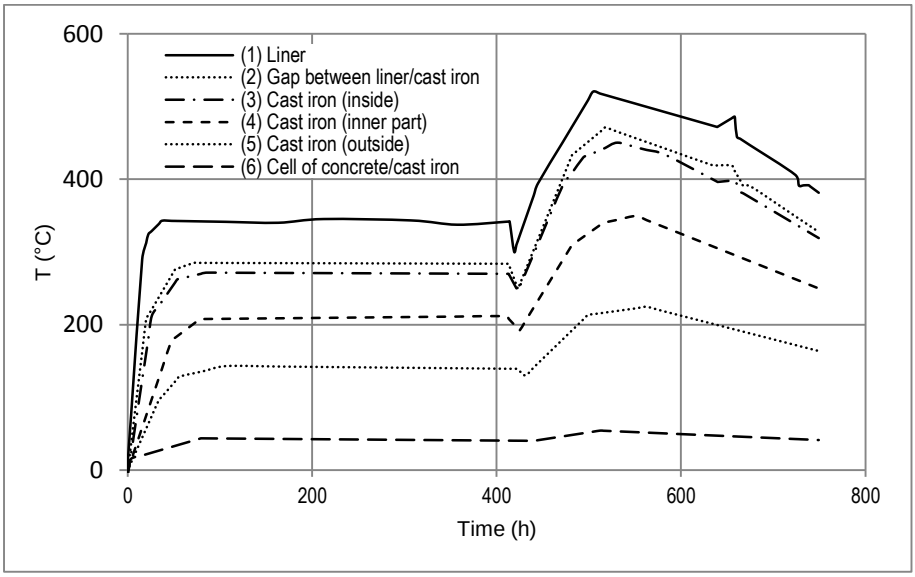

Figure 130: Time dependence of the temperatures during experiments in the liner-surface of the INWA-test facility (a power of 4 kW corresponds to a heat flux of 4 kW/m2).

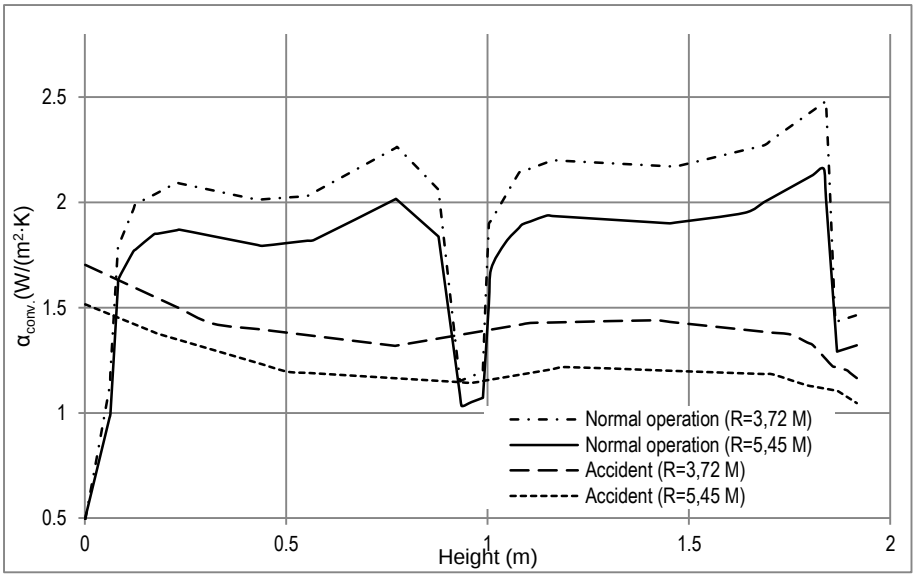

Figure 131: Heat-transfer numbers by natural convection measured in INWA test facility dependent on the height for the cases of normal operation and of 'loss of active cooling' accidents

The heat-transfer coefficients by natural convection on the surface of the cast-iron block which simulated the wall of the reactor pressure vessel are shown in Figure 131. The results were obtained at approximately 2 W/m^{2}K for the case of depressurisation, i.e. a 'loss of active cooling' accident.

Relevant experience gained from the experiments can be summarised as follows.

The maximum temperature on the inside of the reactor pressure vessel would stay below 500 °C, even if the water cooling of the concrete cell is not available. On the outer side of the wall of the vessel the temperatures would stay below 350 °C. The liner system would reach a temperature of less than 500 °C (Figure 130).

The heat transport from the surface of the reactor pressure vessel to the concrete/cast-iron cell consisted of (roughly) 90 % from radiation and 10 % from free convection. This was shown by direct special measurements.

From these experiments an effective heat-transfer coefficient for the heat release from the surface of the reactor pressure vessel of 25 W/m^{2}K was derived. This agrees very well with the available data from other experiments. Heat fluxes of more than 3 KW/m^2 can be tolerated (Figure 131). The computer programs for the heat transport are suitable for describing the processes with sufficient accuracy.

In total the experiment has shown that this concept of a reactor pressure vessel and of the outer concrete cell is very well suited to fulfilling the requirements of the principle of self-acting decay heat removal. It would not need water cooling in the outside concrete structure. Some important conclusions are explained by Figure 132.

This concept of an inner concrete cell with the possibility of cooling by free convection with air can be applied in connection with a forged-steel reactor pressure vessel or a prestressed cast-steel vessel. Additionally, later cooling of the structure by nitrogen injection is possible.

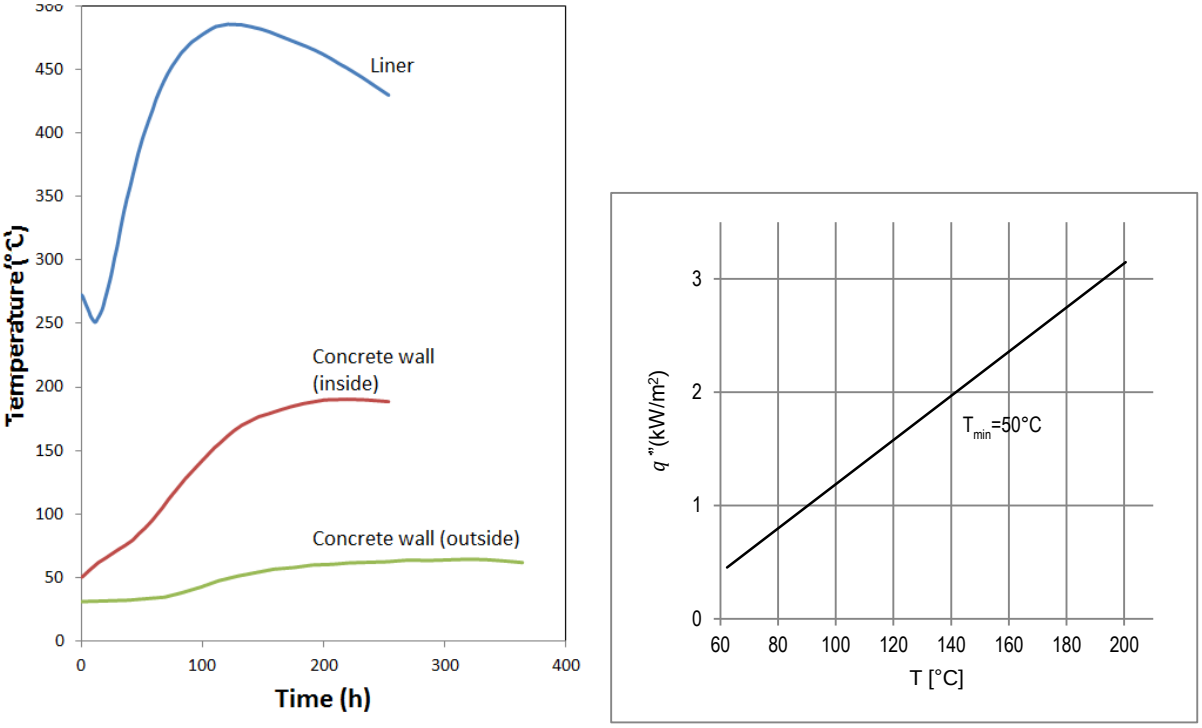

Figure 132: Some important results of tests carried out at the INWA test facility (a) time dependence of temperatures of liner and concrete (heat flux: 4 KW/m^2); (b) heat flux dependent on the temperature of the outer wall (here: 50 °C) and the surface of the cast-iron vessel

9.5.2. JAERI experiment (Japan)

In some modular HTR designs an outer-surface cooling system is provided to remove the decay heat which has been removed from the surface of the reactor pressure vessel by radiation and free convection. The action and efficiency of such a surface cooling system was tested by an experiment carried out by JAERI in Japan. Here different conditions and different heat loads were tested. Figure 133 shows a cross section of the installation. An electrical heating system that generated a specific distribution of the heat flux in the axial direction was installed in the vessel. The temperature distribution which occurred at the surface of the vessel and in the gap between vessel and cooling system was measured (Hishida, et al., 1989) (IAEA, 2001) (Takeda, et al., 1994) (Takeda, et al., 1996).

Furthermore, the flow distributions in the gap and the heat fluxes in different sections of the arrangement were measured dependent on time.

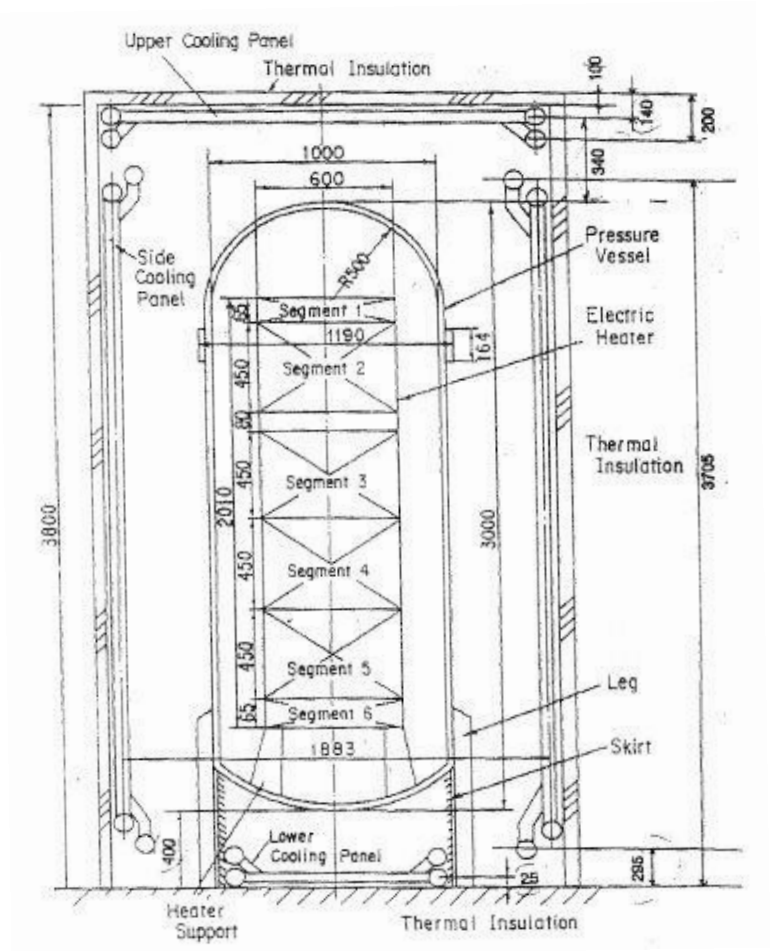

Figure 133: Schematic diagram of the JAERI test facility for the measurement of heat fluxes and temperature distributions

The flow sheet of the cooling system and the arrangement of cooling surfaces are indicated in Figure 134. It was possible to heat the vessel in different sections and to apply cooling in different positions of the surface.

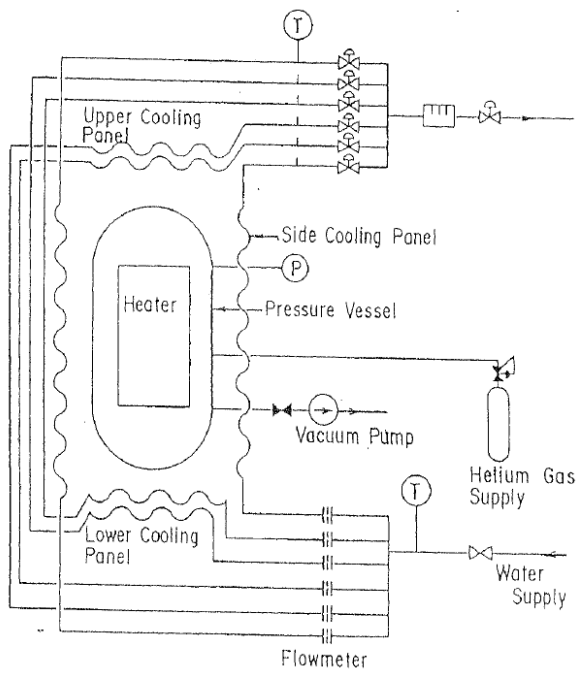

Figure 134: Schematic flow sheet of the JAERI-test facility

Table 53: Important data on the test facility

Parameter	Dimension	Value
Maximum heat input	KW	100
Height of the vessel	M	3
Diameter of the vessel	M	1
Working fluid		Helium, nitrogen
Pressure	Pa	1.3
Maximum temperature of the heater	°C	600
Surface cooling panels	m^2	~ 4
Maximum flow of water	m^3/h	10

Some characteristic results of many experiments are given in Figure 135, Figure 136 and Figure 137. They show the axial distribution of the heat flux and the measured pressure vessel temperatures.

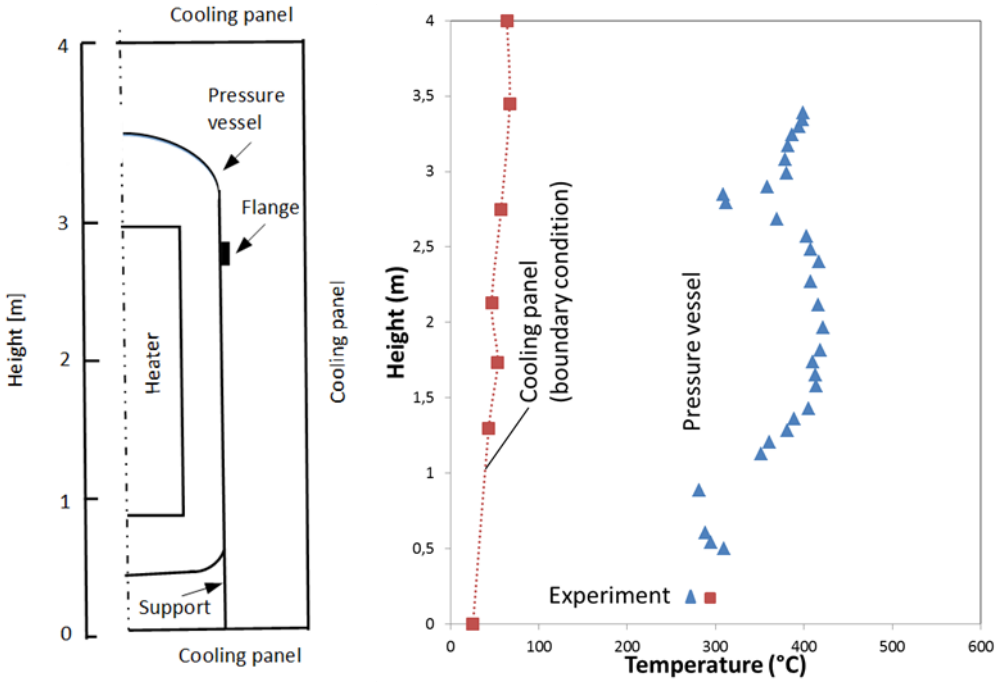

Figure 135: Case A: 94 KW; nitrogen; 1.1 MPa; cooling water in cooling system

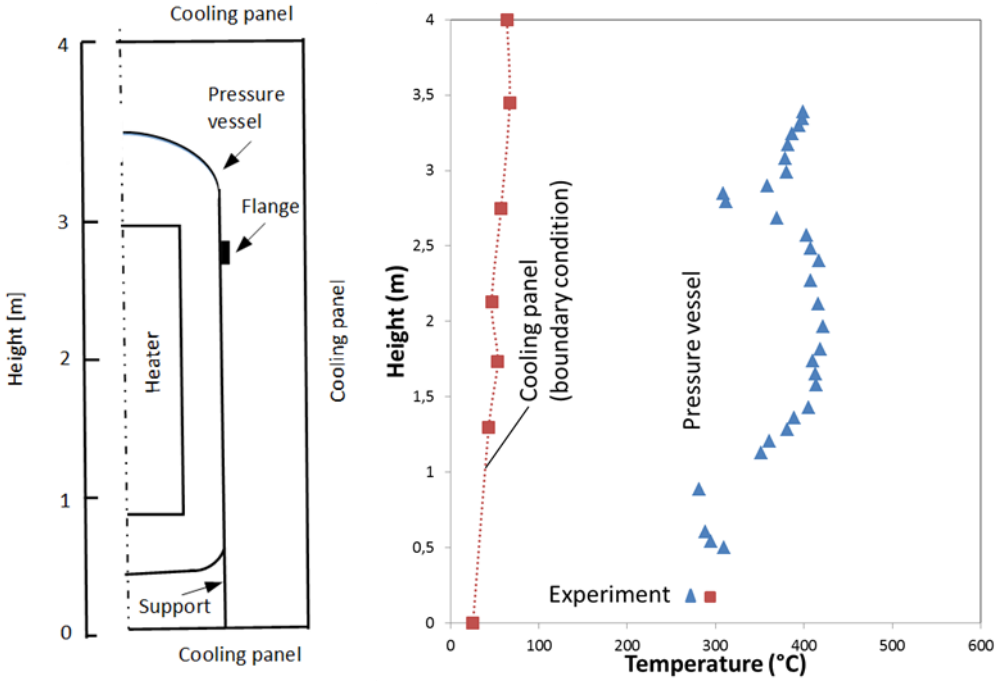

Figure 136: Case B: 77.5 KW; helium; 0.47 MPa; cooling water in cooling system

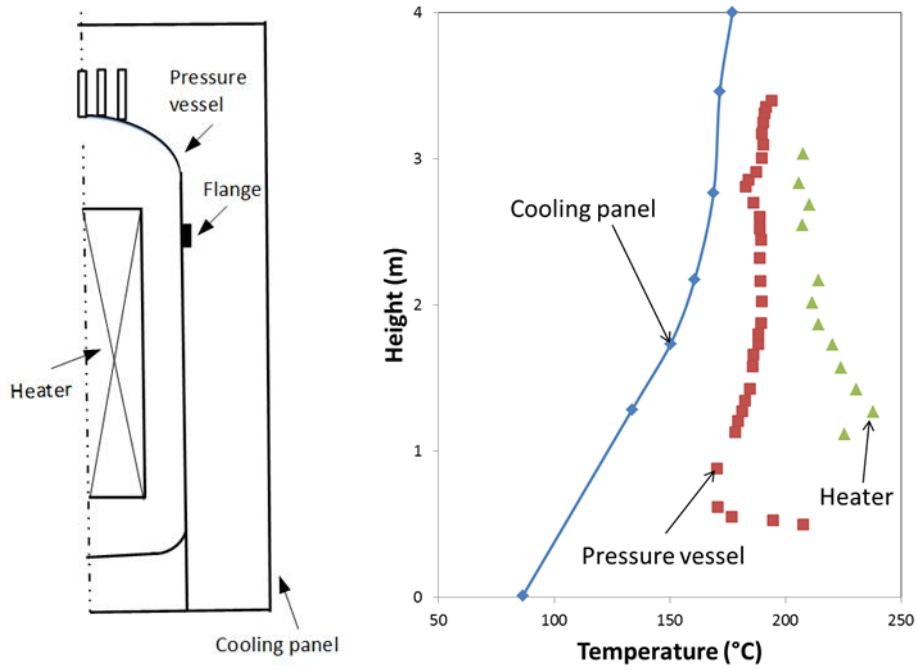

Figure 137: Cooling panel operated with air (8 KW; helium; 1 MPa; air coolant)

The evaluation of the experimental results delivered the following.

Between the surface of the reactor pressure vessel and the cooling panel a temperature difference of around 250 °C is present, corresponding to an effective heat-transfer coefficient α of 25 W/m^{2}K. This value includes radiation with a share of around 85 % to 90 % and free convection with a share of around 10 to 15 %.

It was possible to derive an empirical equation for the free convection of air:

$$\propto_{aff} (T_{wall}) \approx c_1 + c_2 \cdot T_W'' \quad (119)$$

The Nusselt number for the cylindrical arrangement was found to be:

$$Nu = 0.286 \cdot Ra^{0.258} \cdot Pr^{0.06} \cdot H^{-0.238} \cdot K^{0.442} \quad (120)$$

Ra is the Raleigh number, Pr is the Prandtl number, H is the height and K is the ratio of the diameter of the concentric cylinders.

In the course of the work at JAERI a broad experimental programme to evaluate the heat transfer and the flow behaviour in the gap between the reactor pressure vessel and the surface cooling system was carried out.

Simplified equations to describe the experimental results are:

$$Nu = 0.1974 \cdot Ra^{0.25} \; for \; 10^6 \leq Ra \leq 10^8 \quad (121)$$

$$Nu = 0.312 \cdot Ra^{0.33} \; for \; 10^{96} \leq Ra \leq 5.5 \cdot 10^8 \quad (122)$$

The α number for free convection is then given by:

$$\propto_{conv} = Nu \cdot \lambda / D \quad (123)$$

D is a characteristic geometrical parameter; here it is the diameter of the vessel.

A value of from 3 to 4 W/m^{2}K can be derived from the experiments for the conditions of an HTR Module. The share of heat transfer by radiation was estimated from the following equations:

$$Q_{12} = A_1 \cdot \varepsilon \cdot C_s \cdot C_{12} \cdot (T_1^4 - T_2^4) \quad (124)$$

$$\varepsilon = \frac{1}{\frac{1}{\varepsilon_1} + \frac{A_1}{A_2}\left(\frac{1}{\varepsilon_Z} - 1\right)} \quad (125)$$

The factor C_{12} depends in a complex manner on the geometry of the system and on the emissivity ε of the surfaces.

Index 1 characterises the inner and index 2 the outer surface of the cylindrical arrangement.

The values of emissivity ε and the surface depend on the conditions of the components, as previously discussed. Table 54 provides an overview of some values measured and known information from the literature.

Table 54: Values of emissivity of some different materials in the self-acting decay heat removal chain

Material	Value of ε	Temperature (°C)	Remark
Steel	0.88	425	Oxidised, polished
Steel	0.92	800	Oxidised, polished
CrNi steel	0.85	440	Oxidised (25 % Cr, 20 % Ni, 51 %Fe)
CrNi steel	0.90	795	polished
Graphite	0.80	630	
Concrete	< 0.80	20	
Concrete	> 0.80	100	

The results are, for example, suited to optimising the structure of the cooling panels. Hot parts can be identified and modifications of the cooling concept are possible.

9.5.3. Heat release from the surface of the CASTOR vessel

In addition, many experiments have been carried out on heat transfer by radiation and free convection from the surfaces of storage vessels loaded with spent fuel elements. In these cases the characteristic surface temperatures of the cast-iron or cast-steel vessels were below 100 °C. In particular, for heat release from concrete structures (with a relatively high steel content) these results delivered additional helpful information (Deutsches Atomforum eV, Kerntechnische Gesellschaft eV, 2001) (Hauck, 2003) (KLE, Kernkraftwerk Lippe-Ems GmbH, 1998) (RSK, 2002) (Schartmann, 2000) (von Heesen, et al., 1983).

Figure 138 shows the concept of those storage systems and indicates the relevant temperature profiles in the radial and axial directions.

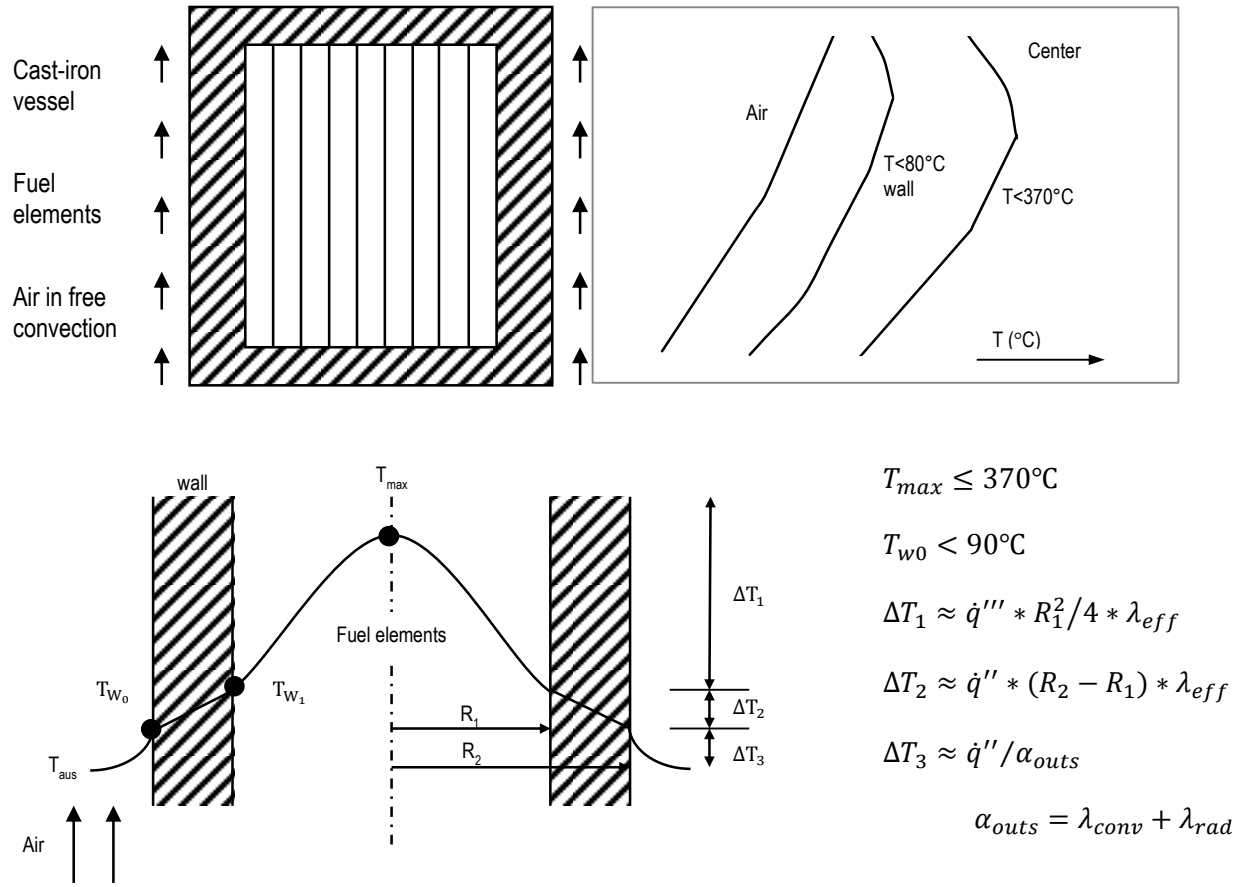

Figure 138:Principle of heat transport in storage vessels for spent fuel elements: (a) the principle of a storage vessel with surface cooling; (b) the radial temperature profile; (c) the axial temperature profile; (d) some data and relations for temperature differences

Some results of measurements of heat transport from the surface are shown in Figure 139. These were carried out during the licensing process for storage vessels and showed as result that there is a dependency between the Nusselt and Rayleigh numbers:

$$Nu = C \cdot Ra''' \quad (126)$$

The Rayleigh number is defined by the product of the Prandtl and Grasshoff numbers:

$$Ra = Pr \cdot Gr \quad (127)$$

The Prandtl and Grasshoff numbers are defined by the equations:

$$\mathrm{Pr} = \eta \cdot C_p/\lambda, Gr = g \cdot \beta \cdot \Delta T/L^3/(v^2) \quad (128)$$

The parameters are given as follows:

g = gravitational constant (m/s^2);
β = isobaric thermal expansion coefficient (1/K);
ΔT = characteristic temperature difference (K);
L = characteristic length (m);
v = kinematic viscosity (m^2/s);
η = dynamic viscosity (kg/ms);

C_p = specific heat capacity (Ws/kg K);
λ = heat conductivity (W/mK).

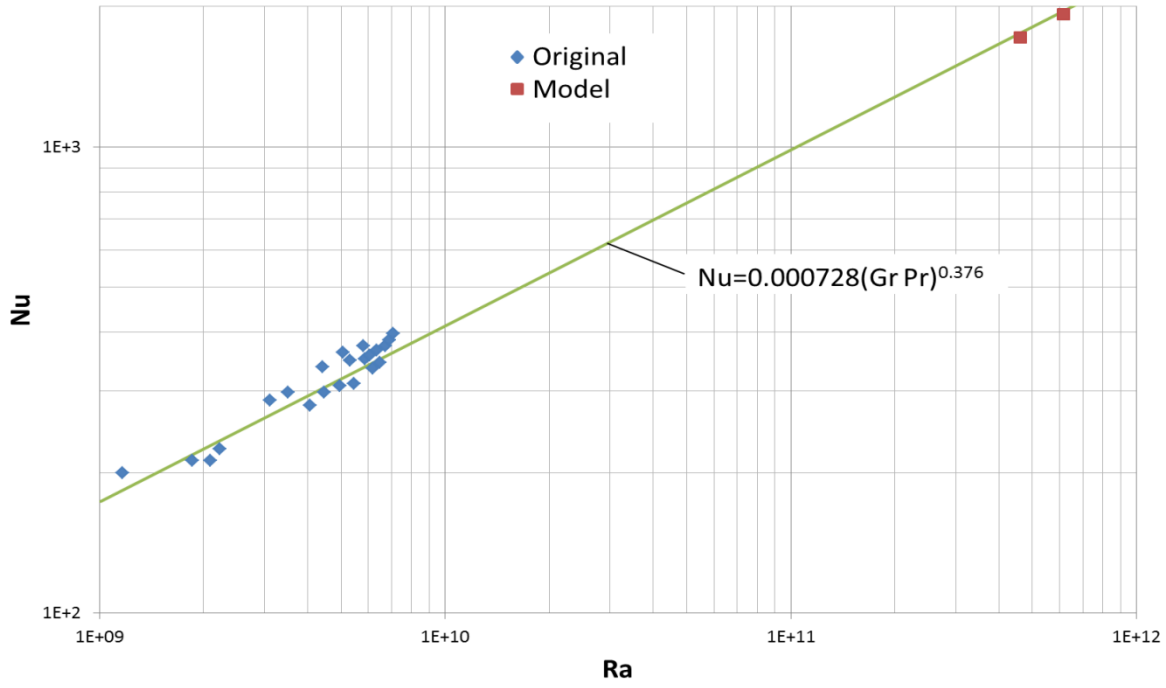

Figure 139: Results of measurement of heat transfer by free convection on the surface of storage vessels

As a practical example, for a surface temperature of 90 °C one gets a value of $c_{conv} \approx 2\,W/m^2K$. The total heat-transfer coefficient including radiation will be in the order of 8 to 10 W/m^{2}K. This will allow a heat flux of approximately 500 W/m^2 from the surface of the vessel. A storage vessel for spent LWR fuel elements, for example, can be designed for a total power of approximately 40 KW.

These results are also consistent with further data obtained for heat transfer on the hot surfaces of storage vessels for the intermediate storage of glass coquilles.

These practical experiences of heat transfer from hot surfaces can be used for heat release from the inner concrete cell and from the outer surface of the reactor containment building.

9.6. Heat transport in the outer structures around the reactor pressure vessel

9.6.1. Overview of different design options

The design of the outer heat sink to remove the decay heat requires some attention. As shown in Figure 140 different possibilities dependent on the type of the reactor pressure vessel and the design of the surrounding inner concrete cell exist. Assuming that the surface cooler may fail the design of the outer cell becomes increasingly important to guarantee transport of the decay heat.

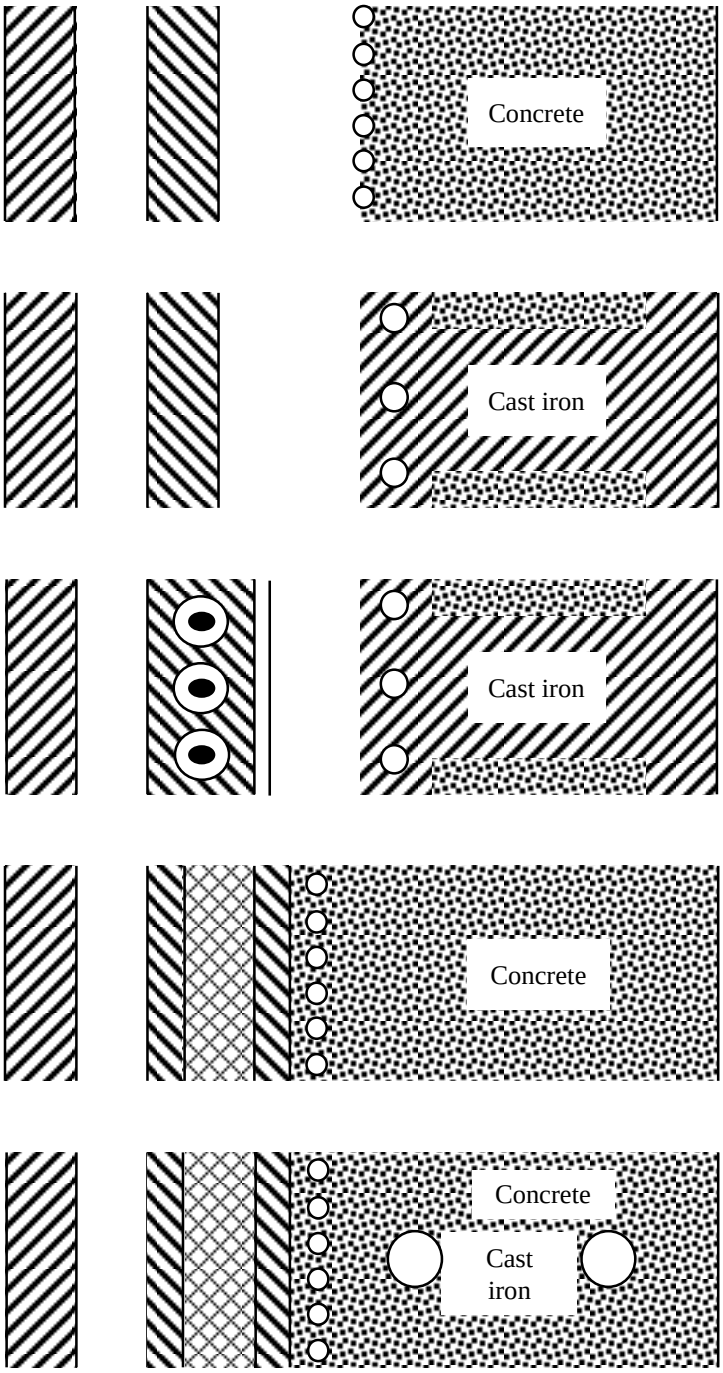

Figure 140: Possibilities to set up reactor vessel and outer cell systems with good heat-transfer and heat-storage capabilities

- Corresponding to the present concepts of modular HTRs the heat is transported from the surface of the RPV (made of steel) to a surface cooler and to the concrete cell behind the cooler (Figure 140(a)). If the surface cooler fails the concrete absorbs the heat directly and stores it. After a relatively long period of time the heat is transferred from the surface of the concrete to the air inside the building. Finally, the heat is transferred through the wall of the building to the environment.
- Cast-iron blocks can be embedded in the concrete cell to store the heat if the cooler fails. Additional holes inside the cast-iron blocks allow air to flow by free convection. Therefore, the temperature of the RPV stays below 400 °C even if the water cooler fails (Figure 140(b)).

- The RPV (made of steel) can be substituted with a prestressed RPV made of cast-iron or cast-steel rings and blocks. The prestressing is done by a lot of axial and radial tension cables. Therefore, this type of vessel cannot burst here. The outer heat sink can be set up as in the case discussed before (Figure 140(c)).
- If the established PCRV (prestressed concrete reactor vessel) is used, the self-acting decay heat removal will also work if the cold helium temperature in the vessel is limited (for example to 250 °C). The insulation of the concrete vessel under these conditions should be thin enough to allow the heat flux to become high enough to cool the core structures. The cooling system of the liner usually removes the heat. If this system also fails the heat penetrates to the concrete structures. As a lot of large-scale experiments have shown, some special types of concrete can even be heated up to 1 000 °C without severe damage (Figure 140(d)).
- If this heating of concrete is to be avoided it is possible to integrate cast-iron blocks into the cylindrical wall of the PCRV. Holes allow air to cool these metallic structures sufficiently by free convection. In this way it is very unlikely that there will be any intolerable temperature rises in the concrete (Figure 140(e)).

For the different design options experimental results are available. The results allow the evaluation of the safety aspects of these solutions in case of a 'total loss of active cooling' accident.

9.6.2. Behaviour of the surface cooling system

The surface cooling system consists of heat exchanger panels that are well known as they have been studied in conventional boilers over long periods of time. Table 55 shows the concept, applied in some modular HTGRs and coal-fired boilers.

The design requirements of a surface cooler are much easier to fulfil than that in large steam generators for the production of hot steam. The capacity of the necessary system is given by

$$Q_D = P_{th} \cdot f_D(t) = \dot{q}'' \cdot A = \bar{k} \cdot (T_{RPV} - T_{cool}) \cdot A = \dot{m}_{H_2O} \cdot C \cdot (T_{out} - T_{in}) \qquad (129)$$

For example $\dot{q}'' \approx 3\,KW/m^2, A \approx 300m^2, Q \approx 900KW$ are characteristic values for the surface cooling system of the HTR Module (200 MWth).

Table 55 provides some data that allow a comparison between the concepts. It shows that the surface cooler can easily be set up as proven solutions in conventional energy technology are available (Spilker, 1989) (Steag, 1988). In these installations the heat fluxes and wall temperatures are much higher than they are in the case of the HTGR surface cooler. Therefore, this component for modular HTGRs can be designed with a very high safety factor.

Table 55: Comparison of some data on the surface cooler of the modular HTR and the surface cooler of a coal-fired boiler

Parameter	Dimension	Surface cooler of HTR Module	Burning chamber of coal-fired boiler
Maximum power	MW	< 1	500
Maximum temperature of the fluid	°C	< 80	~ 360

Maximum pressure	bar	~ 10	180
Average heat flux	KW/m^2	5	100
Area of the cooler	m^2	200	10 000
Maximum wall temperature	°C	< 100	370
Lifetime	hours	3e + 5	3e + 5
Material		13CrMo44	13CrMo44

9.6.3. Heat storage and transport in the concrete structures of the inner reactor cell

If the outer surface cooler fails as well, the decay heat is transported to the concrete structure of the inner cell and is stored there. As a consequence the temperature of the reactor pressure vessel, of the internal structures and the outer parts of the core would increase. However, the maximum temperature in the core and in the control part would undergo only negligible changes. Figure 141 outlines the heat transport in this accident, which is regarded as 'beyond design-basis accidents' (BDBA).

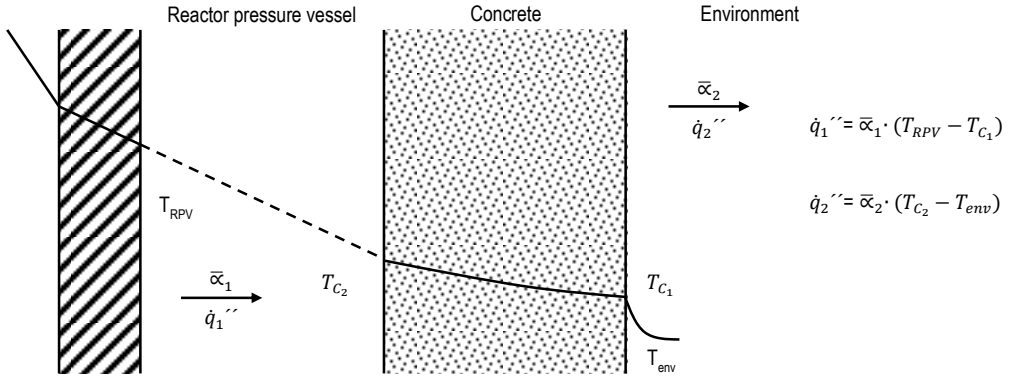

Figure 141: Heat transfer if the surface cooler fails

A major matter for concern is, if the stability of the concrete is given, whether the temperature of the concrete increases, especially in supporting regions. Temperatures of more than 300 °C can occur (Lohnert, 1990) (Siemens/ Interatom, 1988). Figure 142 shows the time dependence of the temperature of the concrete if the surface cooler has failed. A characteristic value for the heat-rate of the concrete in the first phase of the accident would be:

$$\Delta T_c/\Delta t \approx 80°\mathrm{C}/day$$

Subsequently, the temperature increase of the concrete becomes smaller as the decay heat production decreases (Figure 142(e)). Besides using concrete for the inner cell surrounding the reactor pressure vessel there are other possibilities for setting up this structure. The release of heat from this component can be improved by using structures which display better energy storage behaviours. Moreover, the heat could be released via natural convection of air (blocks of cast iron integrated into the concrete, for example, would fulfil both requirements). This would limit the system temperature of the outer heat sink to relatively small values.

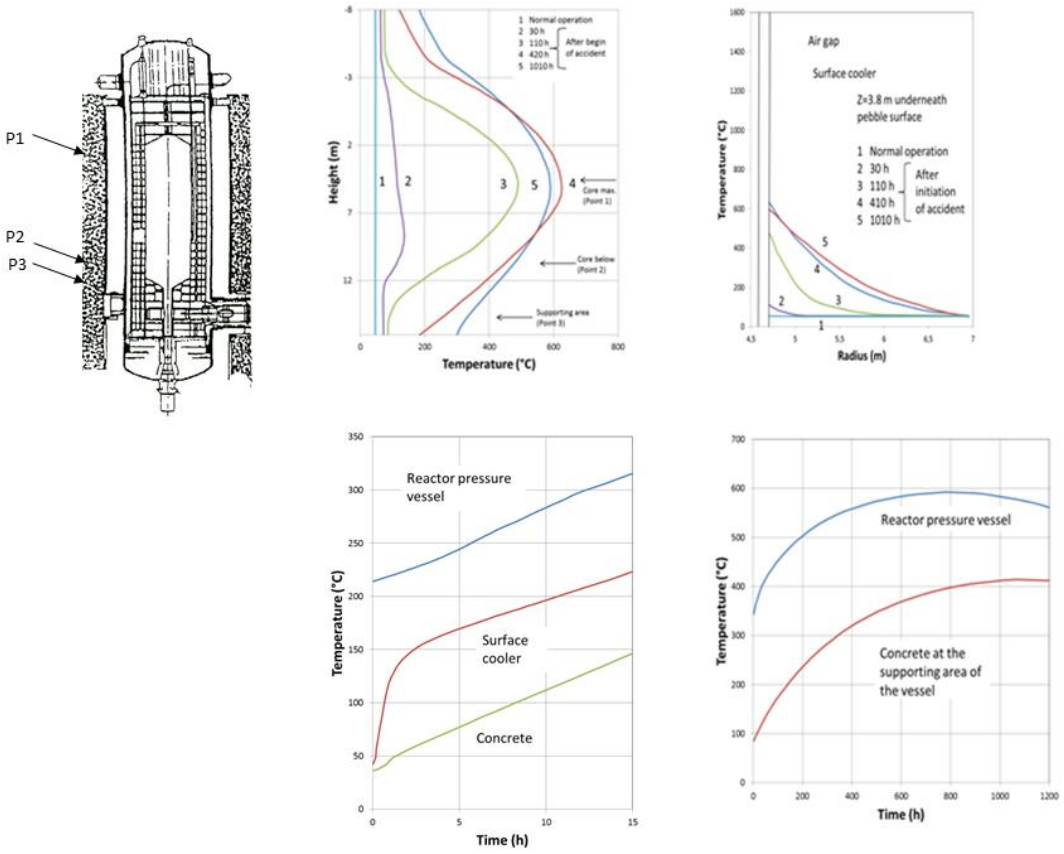

Figure 142: Heating of the inner concrete cell after failure of the surface cooler

The top left figure shows the reactor pressure vessel in the relevant position, top middle the dependency of the temperature in axial direction from time, top right the dependency of the temperature in the radial direction from time, bottom left the rising temperatures in the first 30 hours and bottom right the rising temperatures over a long period of time.

The behaviour of concrete in case of high temperatures has been measured in many experiments, especially on large test specimens in connection with the development of prestressed concrete reactor pressure vessels and the qualification of the liner cooling as an alternative decay heat removal system. The results that can be derived from these experiments are that special qualities of concrete stay intact at temperatures of approximately 600 °C. Even at these high temperatures the samples showed relatively good strength values (Figure 143) (ISF/KFA-Jülich, 1984) (Schneider, et al., 1981).

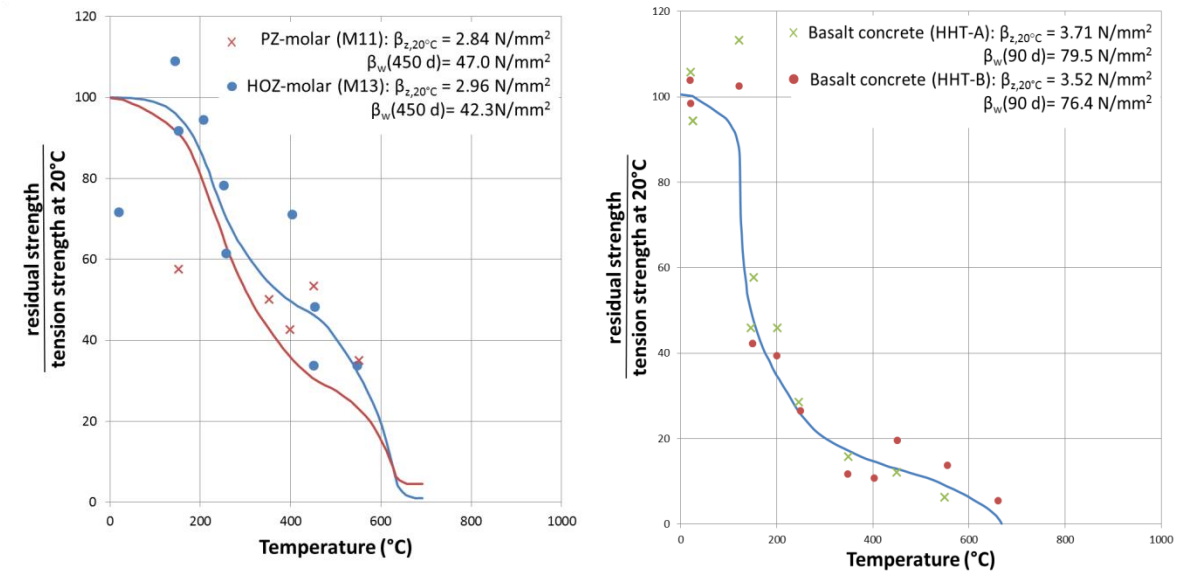

Figure 143: Strength of concrete at higher temperatures

The heat conductivity of concrete and the modulus of elasticity also stay at tolerable values at high temperatures (Figure 144). However, they are reduced by a factor of 2 if the temperature rises to around 300 °C. The values at elevated temperatures are still sufficient to design a structure which can support the RPV.

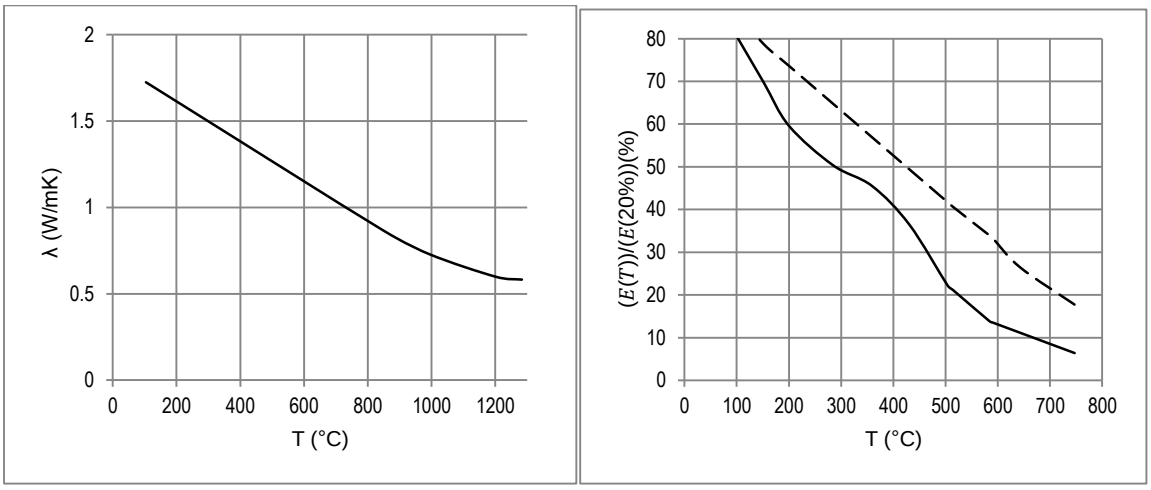

Figure 144: Changes to important parameters of concrete at high temperatures: (a) heat conductivity; (b) modulus of elasticity

9.6.4. Behaviour of large concrete structures at high temperatures

In case of accidents during which the surface cooler also fails, the heat penetrates into the concrete of the inner cell and is stored there for some time. Parts of these structures would gain temperatures of approximately 450 °C, for example in the area where the reactor pressure supports are situated. Figure 145 provides a brief overview of the situation.

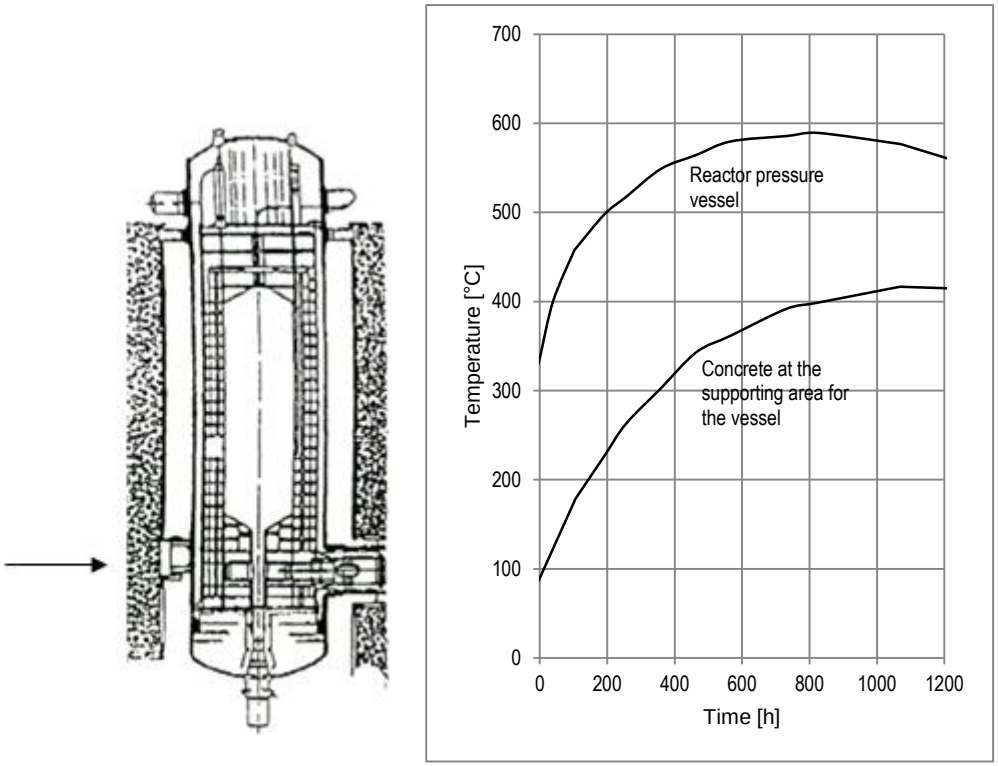

Figure 145: Time dependence of temperatures supporting concrete structures of modular HTRs ('total loss of active cooling' and 'failure of surface cooler' accidents)

In this case the questions of whether the concrete stays stable and the reactor pressure vessel support stays intact are relevant for the safety of the reactor.

Various experiments on the behaviour of concrete in the case of small bodies have been carried out and enable the evaluation of this question. Nevertheless, it was decided to run a large experiment to test the concrete behaviour at very high temperatures in an integral experiment (Altes, et al., 1983) (Altes, et al., 1987) (Altes, et al., 1989) (Altes, et al., 1989).

Large concrete blocks with a volume of roughly 1 m^3 were heated to 1 200 °C (Figure 146). Heat fluxes of around 5 KW/m^2 were applied to reach these temperatures. These heat fluxes are comparable to those which could occur in a modular HTR.

The concrete blocks had a liner, together with liner cooling and insulation on the side where the heat flux was applied. The temperature was measured in many positions to get an exact temperature profile.

Two concepts were tested in detail:

- THTR concrete with basaltic material and metallic fossil insulation;
- HTR 500 concrete with calcinitic material and fibre insulation.

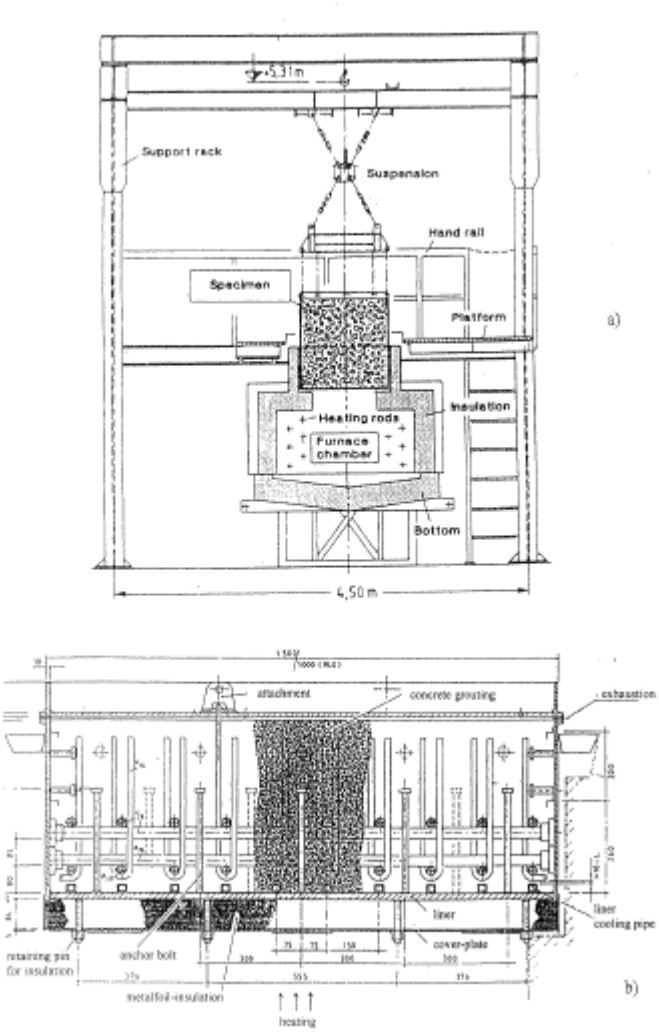

Figure 146: Experimental facility to test large concrete blocks at high temperatures

The upper figure shows the vertical section through the test facility and the lower one the detail of the concrete block (corresponds to THTR concrete with liner, liner cooling and metallic foil insulation).

The samples were heated to high temperatures for more than 1 000 hours. During this time the temperature distribution and the release of gases and steam were measured continuously. After the experiments were finished the material was analysed and information was delivered on the status of the concrete.

Figure 147 shows characteristic time dependencies of the temperature of cover plates of released water. After approximately 400 hours of operation time, all at very high temperatures (1 000 °C), nearly 100 kg of water (relating to m^3 of concrete) was released.

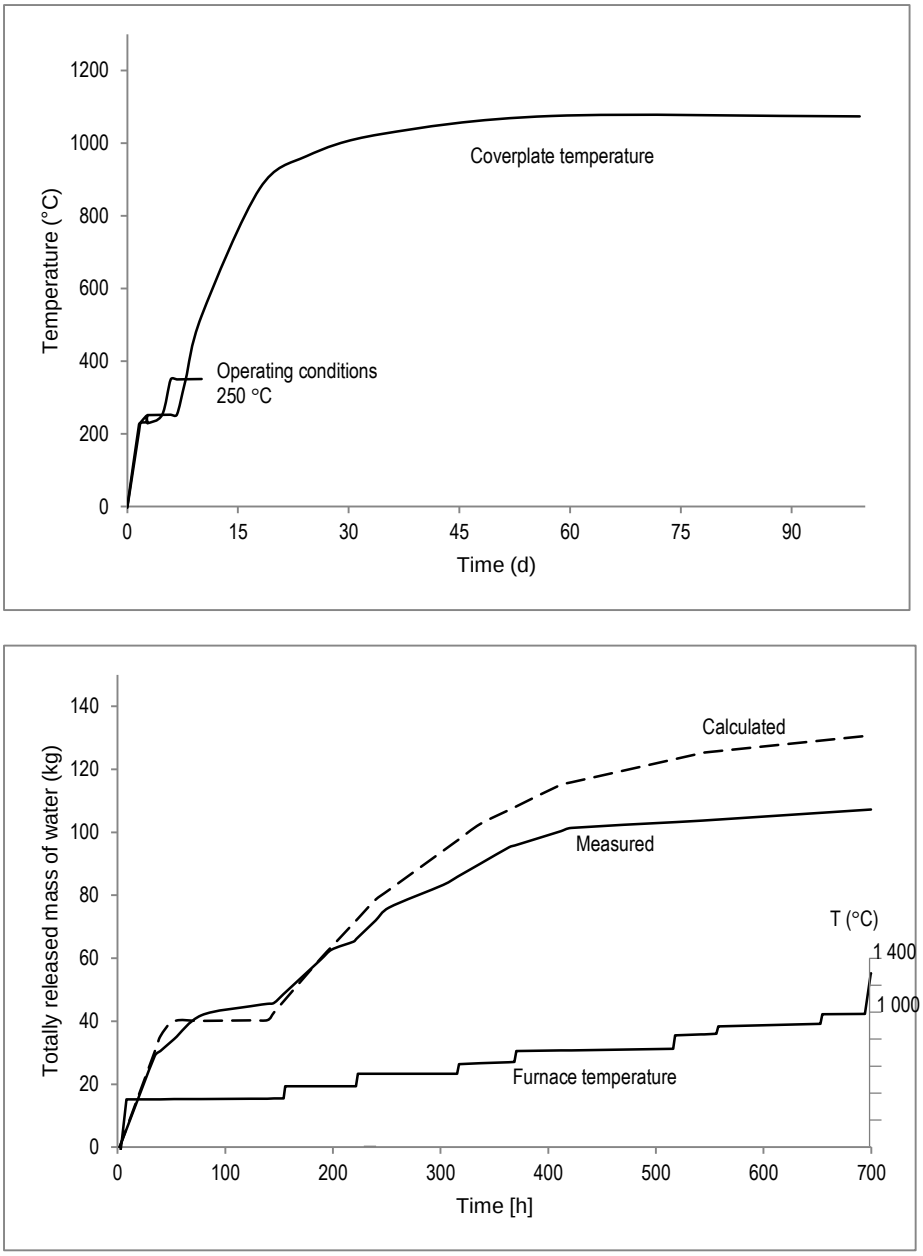

Figure 147: Some results of tests on large concrete blocks

The upper figure shows the time dependence of the cover plates of a test specimen during a heating experiment and the lower one the totally released mass of water from the concrete during heating up; calculated and measured values.

The release of water and gas was relatively small despite the operation at very high temperatures. The state of the concrete block after a long heating time at a maximum temperature of 1 200 °C basically did not change. As the figure indicates, the structural stability of the concrete block was preserved.

The ability of the concrete to absorb the heat and to store it for a long time was demonstrated convincingly by these experiments. It was an important question relevant for the behaviour of prestressed concrete reactor pressure vessels in case of an extreme 'loss of cooling' accident. These results are important to predict the behaviour of modular HTRs during extreme 'loss of cooling' accidents when parts of the inner concrete cell may reach a temperature of approximately 500 °C. A

further question was whether it would be possible to feed water into the liner cooling system after a long delay time. It was shown that this would be possible even after 300 hours.

The re-flooding and re-establishing of the water cooling was possible without any damage to the cooling tubes. Temperature decreases in the cooling process of approximately 10 °C/min were carried out without problems. It would be possible to restart the water cooling of the surface cooler or of the liner cooling of a prestressed concrete reactor pressure vessel even after a long period of time if failures of these components occurred.

9.6.5. Cooling of the surface of the reactor pressure vessel by interventions

As already discussed, the temperature of the reactor pressure vessel could rise up to a large extent in case of accidents with failure of a damaged surface cooler.

The experiments on the liner cooling of large concrete blocks at much higher temperatures have demonstrated this possibility. Figure 148 shows the temperatures and mass flows measured for these experiments. (Kim, 1991) (Rehm, et al., 1984)

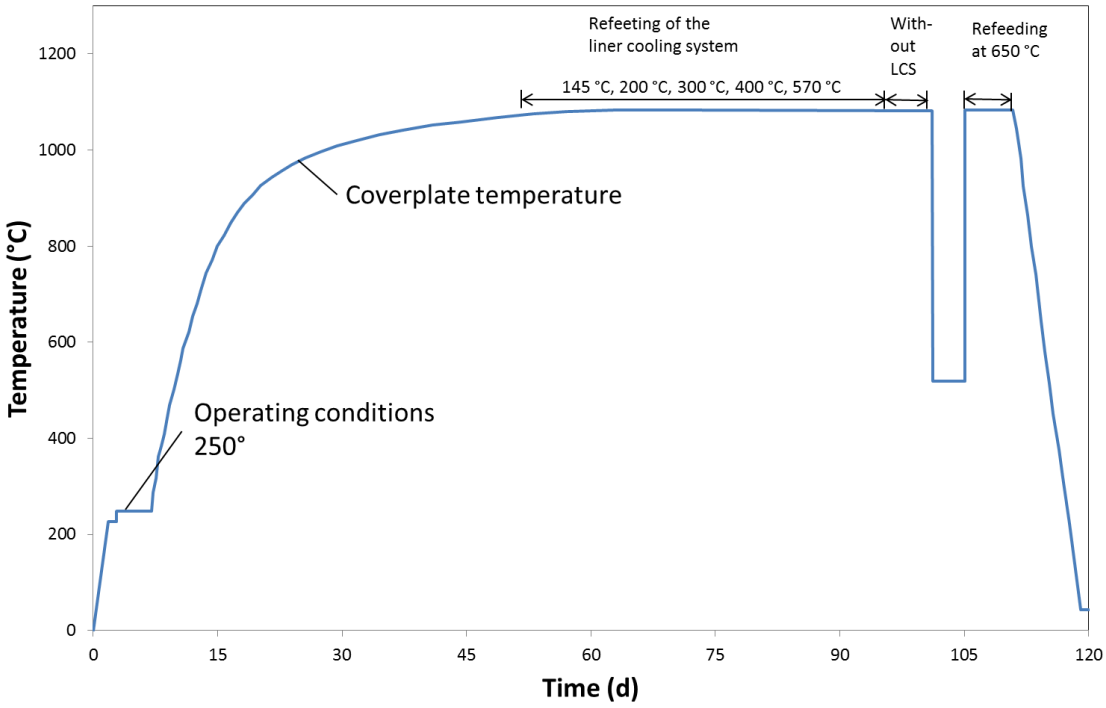

Figure 148: Results of experiments reflooding a liner cooling system

If the surface cooler were out of operation the maximum temperature of the cooling pipes would be around 300 °C after 2 weeks. In this time it should be possible to re-establish the water supply for cooling. If necessary the reactor pressure vessel can be cooled directly with water or nitrogen. The amount of coolant can be estimated as:

$$\dot{Q}_D \approx \dot{m} * r \qquad (130)$$

where r is the evaporation heat.

In the case of water around 0.4 kg/s (~ 1.5 t/h) is needed to remove a decay heat of 600 KW (after 2 days). Using liquid nitrogen the demand is 5 kg/s (~ 20 t/h).

9.7. Heat transport inside the reactor building — integral experiments

If the surface cooler has failed the inner concrete cell will be heated and free convection will be the major process of heat transport (some radiation from surfaces with higher temperatures may play a role too). The heat is removed from the hot surfaces of the inner cell to the atmosphere of the reactor building and from there to the inner side of the walls. Different situations in which free convection occurs have to be considered (Figure 149):

- on vertical walls (a),
- on horizontal walls (b),
- on pipes and components with a cylindrical surface (c).

Mainly the heating of pipes and channels, which contain cables for control and instrumentation equipment requires attention and usually specific precautions for protection.

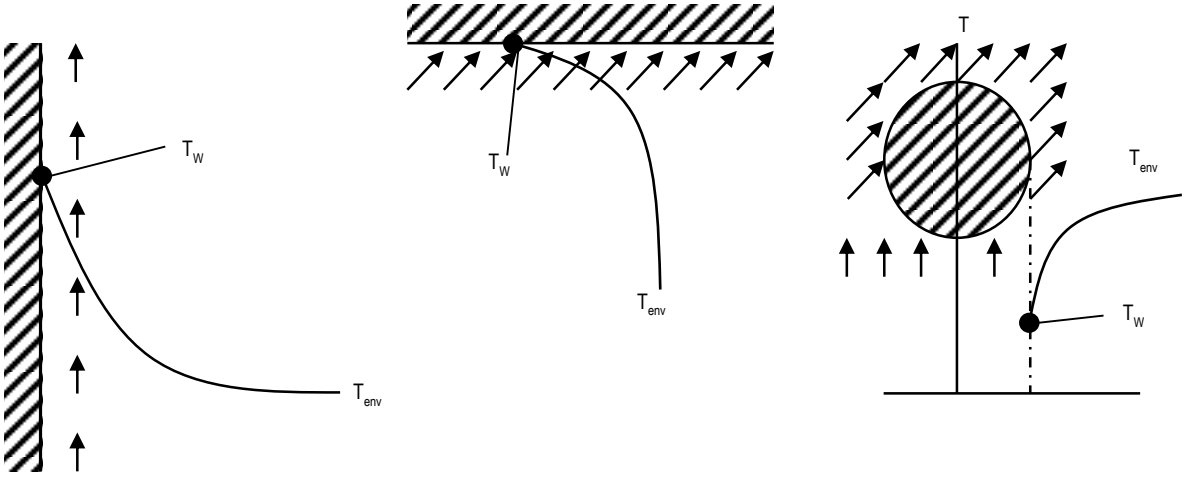

Figure 149: Different situations of heat transfer by free convection in the containment building

Figure 149 shows, from left to right, free convection from a hot vertical wall to the environment, from the environment to colder structures and from the environment to colder pipes or components.

These situations of heat transfer can be described by empirical equations. In the case of vertical walls the following equation can be used:

$$\alpha_{conv} = C * \sqrt[4]{\frac{T_W - T_{env}}{H}} \qquad (131)$$

H is the height of the wall and $T_w - T_{env}$ is the temperature difference between the wall and the environment of the reactor building. As shown in Table 56 the factor C shows little dependence on the applied temperatures in case of free convection.

Table 56: Temperature dependence of factor C

T (°C)	50	100	150	200	250	300
C	1.31	1.26	1.22	1.19	1.16	1.14

For the outside of the concrete cell a value of $\alpha \approx 2.2\ W/m^2K$ is characteristic of a temperature difference of 150 °C and a height of 10 m.

The heat flux for release of decay heat to the atmosphere of the reactor building would then be around 330 W/m^2. Together with a surface area of around 1 500 m^2 for the outside of the inner concrete cell, this corresponds to a heat release of 500 KW. This is the decay heat production after 1 week. Therefore, the storage capacity of the cell chosen must be large enough.

The heat transfer from the reactor containment building atmosphere to the inside of the building wall delivers similar values. Since the surface is much larger than that of the inner concrete cell, the amount of heat which can be transferred is much larger than mentioned before.

If horizontal surfaces are considered, α depends on the angle between vertical and inclined surface (angle ϕ) (Teuchert E., 1992):

$$\alpha_\varphi/\alpha = f(\varphi), f(\varphi) \approx 1 \ldots 0.83 \qquad (132)$$

$\varphi = 90^o$ would for instance result in $f(\varphi) \approx 0.83$.

Cylindrical components or pipes are connected to heat transfer by free convection, corresponding to the following equation:

$$Nu = 0.47 * \sqrt[4]{Gr * Pr = \frac{\alpha * d_a}{\lambda}} \qquad (133)$$

in which:

Gr = the Grasshoff-number

Pr = the Prandtl number

For air the following equation can be used:

$$\alpha = C^* * \sqrt[4]{\frac{T_W - T_{env}}{d_a}} \qquad (134)$$

The factor C^* for horizontal piping is given in Table 57; the average temperature is defined as:

$$(T_W + T_{env})/2. \qquad (135)$$

Table 57: Temperature dependence of the factor C^* in the equation for free convection around a body of diameter d_a

T (°C)	50	100	150	200	250	300
C	1.18	1.16	1.09	1.06	1.04	1.02

A cylindrical structure with a diameter of 1 m, for example, arranged in the building, gets a heat-transfer number of around 3.5 W/m^{2}K for a temperature difference of 150 °C.

These values allow a relatively precise heat balance for the reactor building and all internal structures if the decay heat is transported in case of extreme accident (BDBA case). In any case, for a modular HTGR with a power of 200 MWth the values of α are high enough to remove the total decay heat after a few days. Moreover, further measures could be used to enlarge the heat-transfer area inside the containment building.

9.8. Heat release from the reactor building to the environment

Usually, the transport of heat through the walls of the reactor building to the environment requires the use of cooling loops. As indicated in Figure 150 several possibilities are available:

- cooling loops with pumps are installed at cooling towers outside (Figure 150(a));
- cooling loops can be operated only by natural convection without a pump for circulation (Figure 150(b));
- cooling loops can be used with natural convection, which can be improved by water injection if necessary (Figure 150(c));
- heat pipes can be used to transport the heat directly from the inside of the building to the outside (Figure 150(d)).

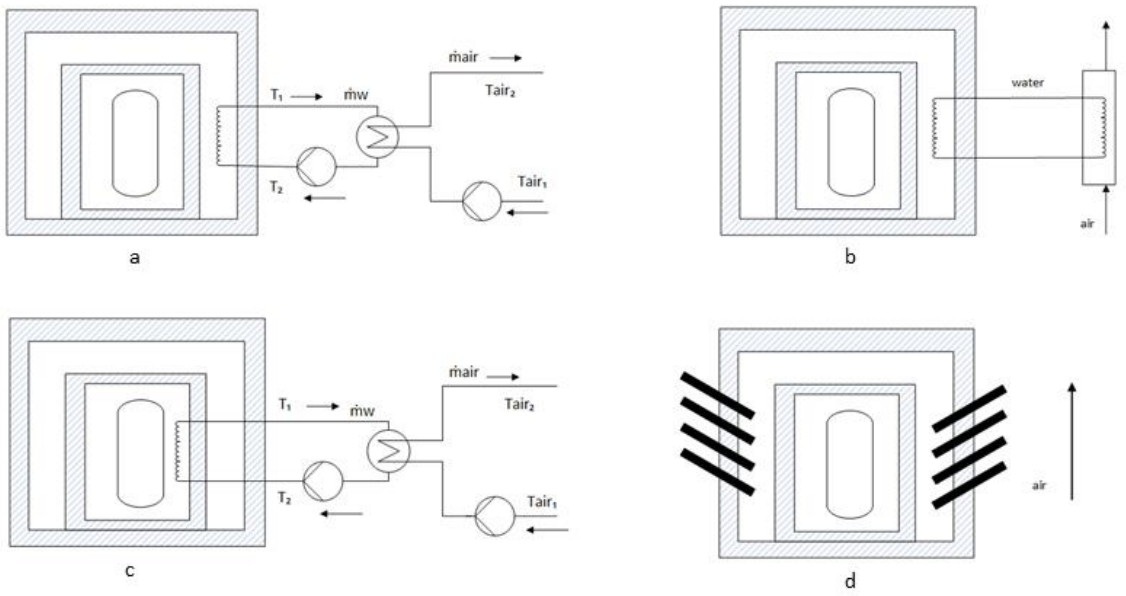

Figure 150: Concepts to remove the decay heat from the reactor containment building

From upper left to lower right the following concepts are shown:

(a) water cooling of the surface cooler using pumps and forced convection;
(b) water cooling of the surface cooler using natural circulation of media;
(c) water cooling of the inner side of the reactor containment building and natural circulation of media;
(d) heat pipes for the transport through the walls of the reactor containment building.

Cooling of the concrete walls using water or nitrogen is another option which is well established in conventional plants. Boiling-water reactors for instance have an injection system to ensure fast insertion into the containment (Rehm, et al., 1984).

In addition, cooling by intervention after a long time period is possible. Reflooding of the surface cooler would be an example of this. It allows fast cooling of the concrete structures and of the reactor pressure vessel.

The chain of heat transport from the RPV to the inner wall of the containment includes heat conduction, thermal radiation and free convection. In the end the wall of the reactor containment building is only slightly heated. Figure 151 briefly illustrates the heat transfer to the wall of the containment building.

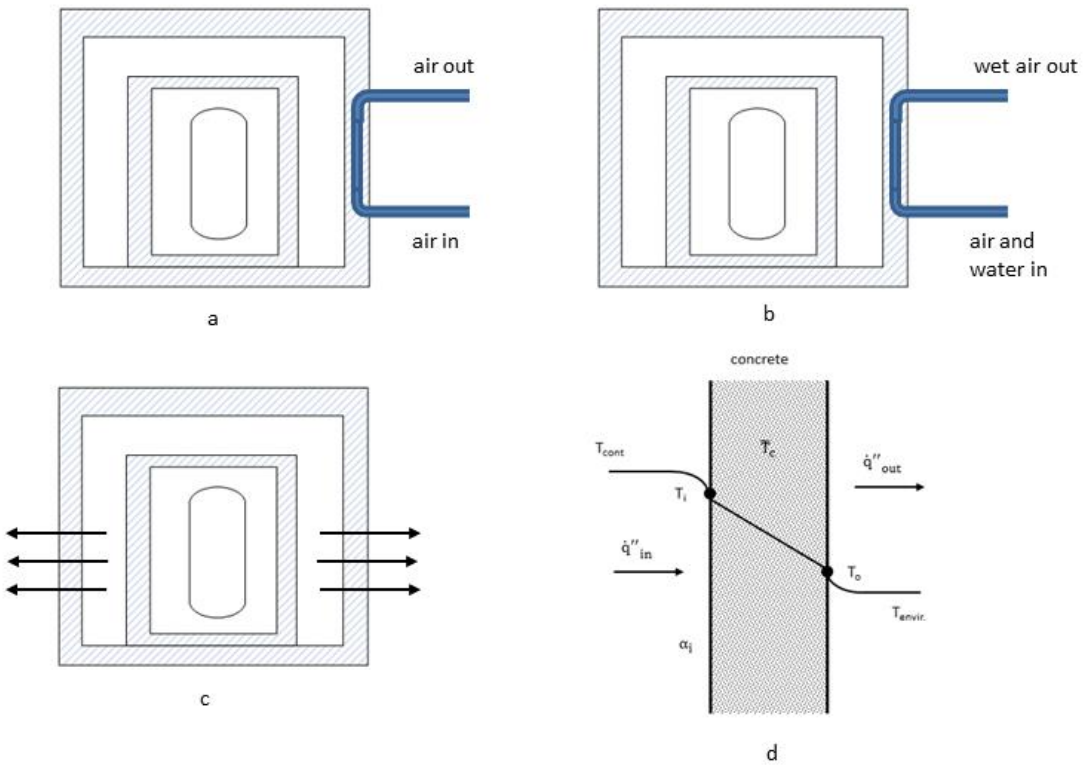

Figure 151: Alternative cooling concepts for reactor containment buildings

From upper left to lower right the following concepts are shown:

(a) free convection of air in borings in the wall of the reactor containment building (with cast-iron blocks);

(b) free convection of air together with water in the wall of the reactor containment building (with cast-iron blocks);
(c) principle of heat transfer to the inner surface of the reactor containment building and release to the environment;
(d) heat flux through the wall of the containment building.

The heat transferred from the inner atmosphere in the building to the inner side of the wall can be estimated as:

$$\dot{Q} = \bar{\alpha}_i * A_{cont} * (T_{cont} - T_i) \quad (136)$$

in which:

T_{cont} = corresponds to the temperature of the inner atmosphere;

A_{cont} = is the inner surface area;

T_i = is the temperature on the inner side of the building.

With characteristic values of $A_{cont} \approx 800m^2$, $\bar{\alpha}_i \approx 2W/m^2K$ and $T_{cont} - T_i \approx 50°C$ a value of approximately 800 KW is received. This is the decay heat of a 200 MWth HTR Module after several days. After that the decay heat is stored in the concrete and later released to the environment.

9.9. Integral experiments on the AVR reactor, demonstration of the concept of self-acting decay heat removal

9.9.1. Loss of active cooling (reactor under full pressure)

In the 1970s the AVR was also used to carry out important experiments regarding the concept of self-acting decay heat removal (ATW, 1968) (Engelhard, 1972) (Krüger, et al., 1988) (Schulten, et al., 1976) (VDI, 1990) (Ziermann, et al., 1997).

Both helium blowers were switched off during normal operation of the reactor at full power. With these measures the active core cooling was totally interrupted. The four shutdown rods were blocked, which also simulated the total loss of the active shutdown capability of the reactor. As a result of these two independent failures, which simulated a very extreme accident, the thermal power of the reactor decreased immediately (Figure 152) and led to a reactor shutdown by physical means.

The reason was the strong negative temperature coefficient of the reactor caused by the temperature-dependent change in the resonance absorption.

The changes of temperature indicated in Figure 152 are mainly caused by internal convection processes. There were some low-level oscillations in the power as the reactor became critical again after 23.5 hours as a result of xenon decay. However, the power then was just 1.8 MW. It was dissipated without any difficulties via the steam generator. This was possible because of natural convection, which took place because of the specific arrangement of the AVR steam generator above the core.

It was shown that the heat balance for the plant was fulfilled in the form:

$$P_D = P_a * f_D(t) = \dot{m}^*_{st} * (h^*_{st} - h_{FW}) + \dot{Q}_{losses} \quad (137)$$

$$\dot{m}_{He} = (h^*_{st} - h_{FW}) \approx \dot{m}^*_{He} * C_{He} * \left(T^*_{He_m} - T_{He_m}\right) \quad (138)$$

$$\dot{Q}_{losses} \approx A * \overline{K} * (\overline{T}_{He} - T_{env}) \quad (139)$$

The asterisk should indicate that this is the status after a time of 23.5 hours (if no shutdown process is carried out and the reactor is 'self-controlled'), $\dot{m}_{He}$ is the mass flow by natural convection and $\dot{m}^*_{st}$ is the necessary flow of feed water. The temperature difference between steam and feed water $(h^*_{st} - h_{FW})$ can be assumed to correspond to the evaporation heat of steam.

The rises in temperature in the reactor structures did not cause any problems. For example, the thermal shield got approximately 50 °C hotter compared to the temperature during normal operation, the temperature of the bottom reflector rose by nearly 100 °C and the temperature in the graphite noses rose by approximately 200 °C for a short time of 5 hours compared to the temperatures during normal operation. After that time the graphite noses cooled down again.

Based on the temperature distributions measured in the structures the temperature distributions in the core have been calculated. Figure 152 shows some results which indicate that the fuel temperatures never exceeded values above 1 100 °C in the case of AVR operation with an average helium outlet temperature of 850 °C.

Generally a temperature span of approximately 100 °C has to be added to cover uncertainties in the data which are important for the heat transport in the core. However, the resulting maximum fuel temperature still stays under the specified maximum temperature for operation. This was 1 250 °C for THTR BISO fuel.

It was estimated that the additional fission-product release from the fuel would be negligible for this accidental situation compared to release during normal operation.

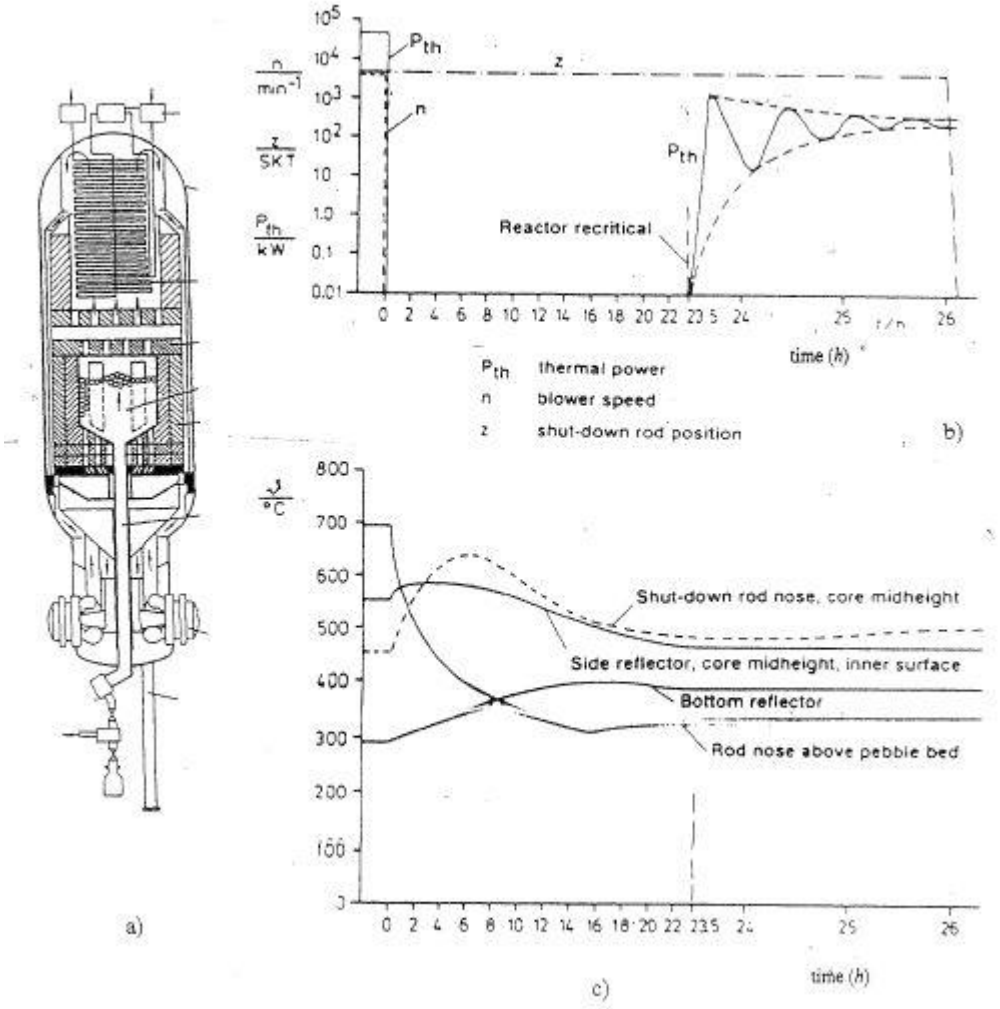

Figure 152: Loss of active cooling + loss of all shutdown rods (blocked

The left figure gives an overview of the reactor system, the top right shows the time dependence of the power and the lower right shows the time dependence of some important temperatures in the reactor structure.

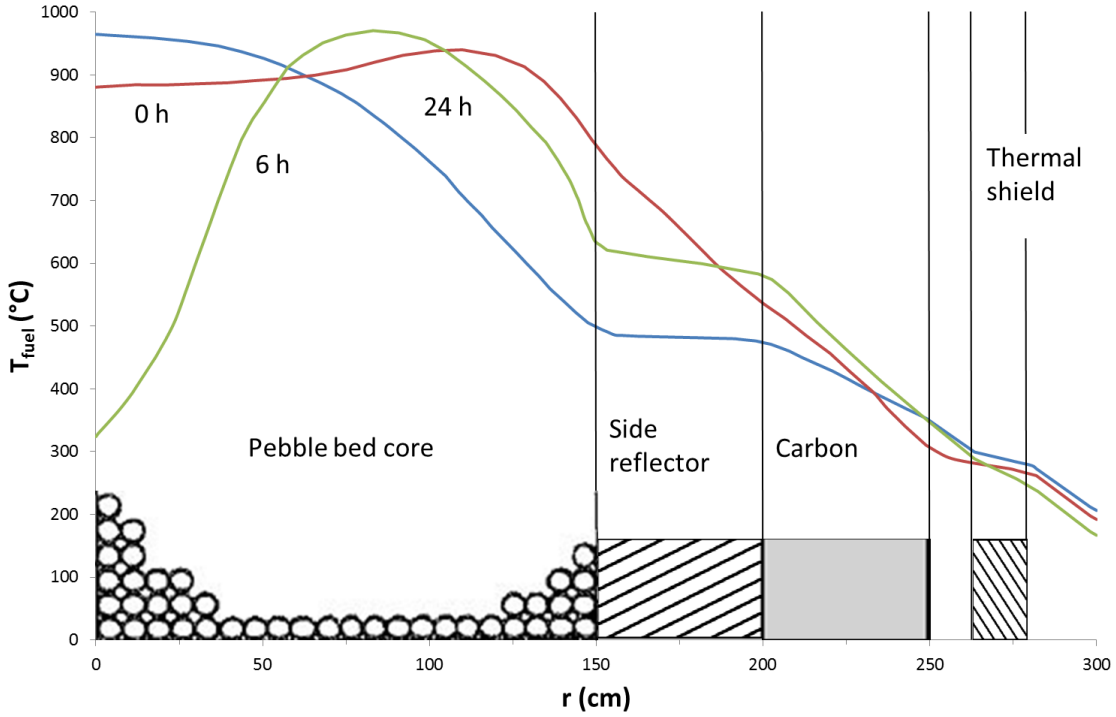

Figure 153: Calculated temperature distribution inside the AVR during loss of decay heat removal accident (calculations for the assumption 'loss of control and loss of active decay heat removal', reactor under full helium pressure)

9.9.2. Loss of active cooling (reactor under normal helium pressure of 1 bar)

One of the most severe accidents in a modular HTR is the total loss of active cooling including the depressurisation of the primary circuit. In this case the explained concept of self-acting decay heat removal acts and removes the decay heat solely by principal physical processes such as heat conduction, heat radiation and free convection of air or an air/helium mixture. The maximum fuel temperatures in this accident stay below 1 600 °C.

An experiment was carried out in the AVR to demonstrate this system behaviour. It was shown that the core and the structures have the capability to store the decay heat, to transport the heat and to release the heat via the surface of the reactor pressure vessel. In 1988 this experiment was performed in the following manner. In the first phase the cooling gas was pumped out of the primary system, because a rapid depressurisation was not licensed at that time. The plant was then operated for some time with a thermal power of 4 MW. In this way a stationary status was reached in the core that showed a temperature profile at full-power operation and an average helium outlet temperature of 950 °C.

After that a reduced power level caused by fission was established to simulate decay heat. In total, accident conditions were set up which corresponded to those of a reactor operating at full power in which an accident would happen.

In Figure 154 the decay heat curve is shown. After 1 hour at a power of approximately 500 kW, 1 % of the nominal power was available as decay heat. After 2 days most of the energy was transported to the steam generator.

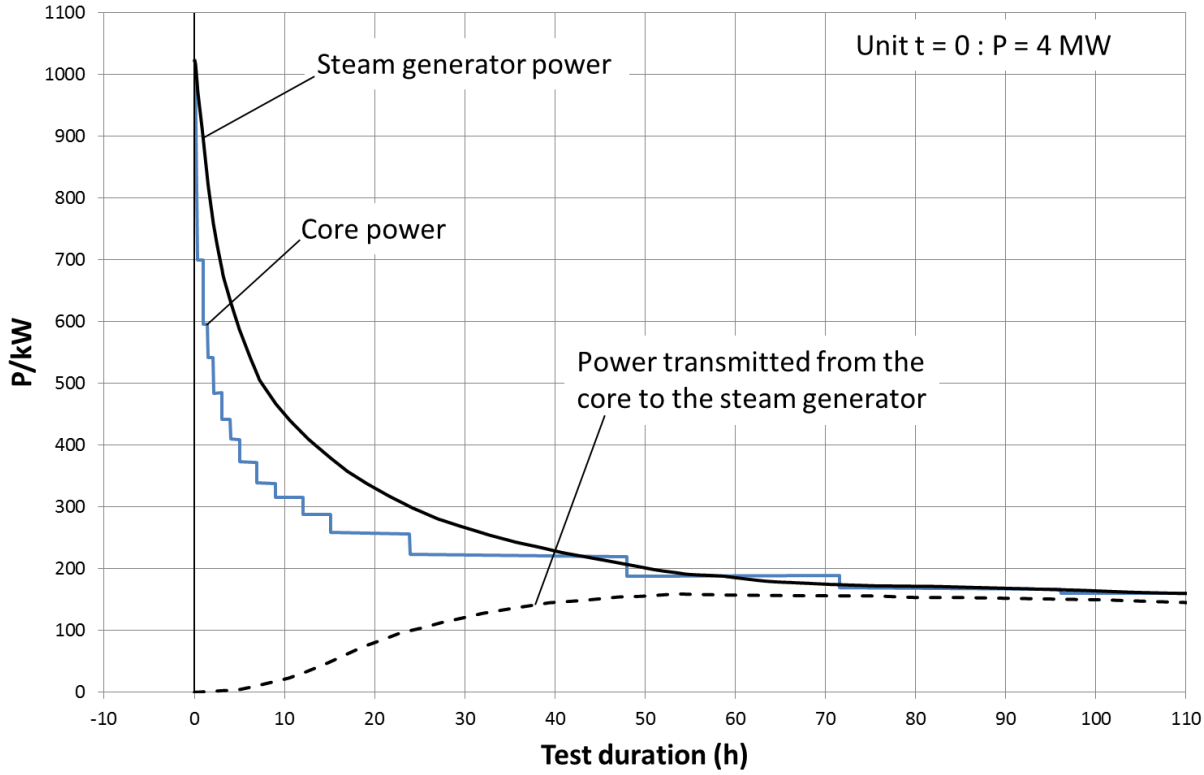

Figure 154: Decay heat production in the AVR during total loss of active cooling with a depressurised core

In the reactor structures the time dependence of temperatures has been measured. Figure 155 shows the position of the thermocouples. They were arranged near the core, for example on the graphite noses. Later some test graphite balls with melt-wires were put into the pebble bed together with the normal fuel elements.

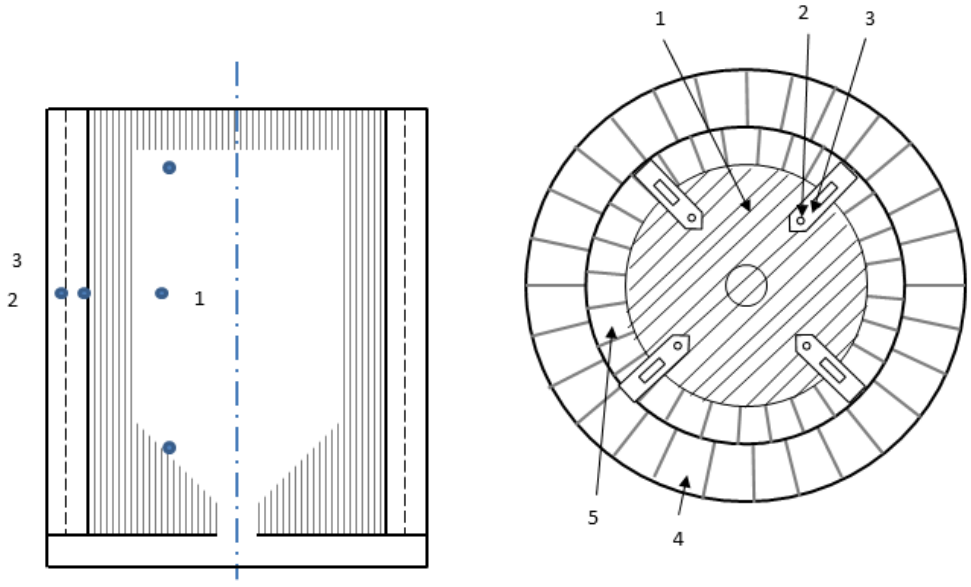

Figure 155: Positions of thermocouples to measure temperatures in the internal structures of the AVR: (a) vertical section; (b) horizontal section

The vertical cross section is shown on the left of Figure 155 and the horizontal cross section on the right. The numbers denote the following.

(1) Pebble bed.
(2) Control rod borehole.
(3) Reflector nose.
(4) Carbon brick layer.
(5) Graphite reflector.

In Figure 156 the results of the measurements are given. The curves show that the hottest parts of structure, the noses for the shutdown rods above the core, became colder. The temperature of the graphite structure in the noses (situated in the middle of the core) increased by approximately 300 °C. The temperature decreased after 100 hours.

Temperature increases in the side reflector were in the order of 150 °C (maximum) and occurred after approximately 25 hours. After that time this temperature also decreased.

The core bottom, which was relatively cold at the beginning of the accident, became hotter and reached a temperature of approximately 500 °C after 100 hours. In total the core bottom structure acted as an efficient heat sink over a long time.

The possible influences of free convection and heat transport to the steam generator were analysed as well. For this purpose the main flaps on the blowers were closed and opened. The difference was negligible. In fact, based on this result it was stated that the contribution of the steam generator as a heat sink was very small in this experiment. The main mechanisms to remove the decay heat from the core were conduction, radiation and free convection in the core internal structures. The results measured were compared with 3D computer calculations and the overall estimate was very good.

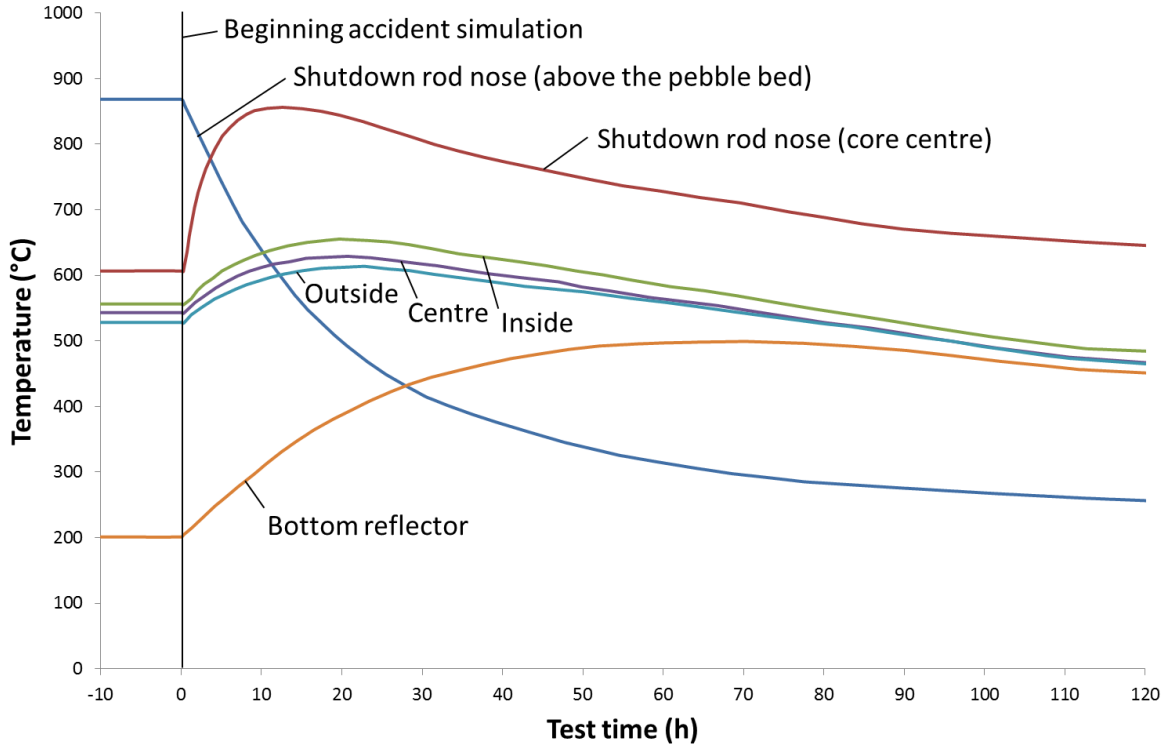

Figure 156: Results of a 'loss of coolant and loss of pressure in primary system' experiment in the AVR (46 MW; T_{He} = 950 °C)

On the basis of the measured temperature distributions in the structures and the power density temperature fields inside the pebble bed have been calculated. Figure 157 shows the radial dependence of the time-dependent profile. It corresponds to the axial position in the middle of the core. Following these calculations no fuel elements were hotter than 1 300 °C in this accident.

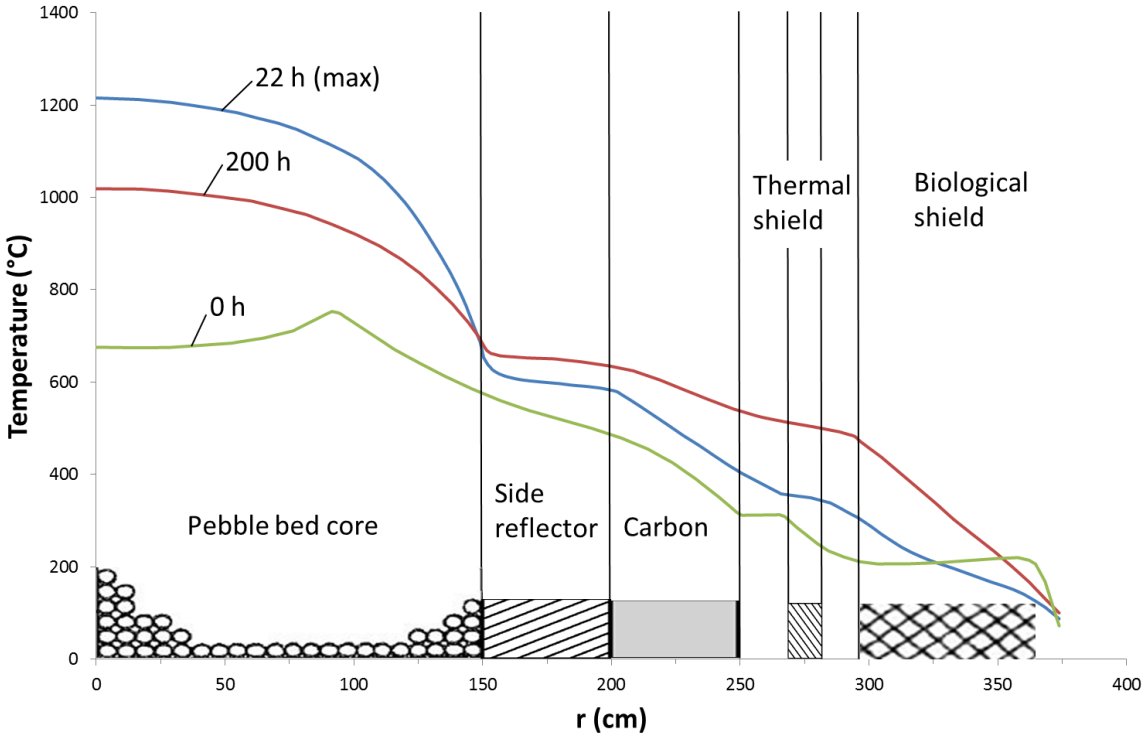

Figure 157: Temperature distribution inside the AVR reactor system in a 'loss of coolant' accident (calculations for the assumption: total loss of coolant and loss of active decay heal removal)

Analysis indicates that only 5 % of the fuel elements stayed at temperatures between 1 250 °C and 1 300 °C for less than 50 hours. All other fuel elements stayed at lower, partly much lower, temperatures. The release of fission products from the fuel elements is therefore relatively small.

The concept of self-acting decay heat removal was demonstrated convincingly by this experiment. The results were a large contribution to the knowledge concerning the accident behaviour of modular HTRs. To successfully transfer this knowledge on newly build HTR, the materials and dimensions of the core structure should be designed similar. The results of these experiments have been used for the validation of different computer programs. Figure 158 shows that the results of the computer programs were in close agreement with the experiments.

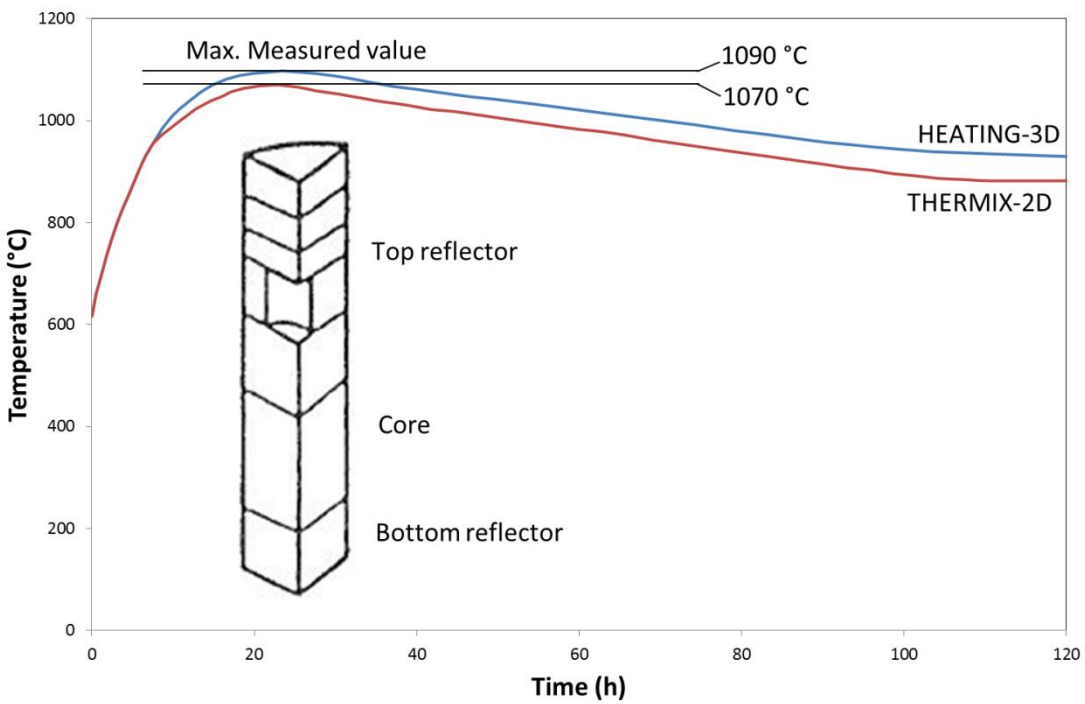

Figure 158: Time-dependent temperature distribution in the AVR during 'total loss of active decay heat removal' accident, depressurisation of primary circuit: temperature (maximum values at centre line) depending on time

10. References

Abramowitz M., Stegun I.A. 1965b. *Handbook of mathematical functions, Eq. 6.6.1.* Dover, New York : s.n., 1965b.

Abramowitz, M und Stegun, I. A. 1965. *Handbook of mathematical functions. Eq. 26.1.20.* Dover, New York : s.n., 1965.

AFCEN. 2012. AFCEN RCC-MRx Code - Design and Construction Rules for mechanical components of nuclear installations. [Online] 2012. http://www.afcen.com.

Altes, J und et al. 1983. *Zum Störfallverhalten des HTR-500. Eine Trendanalyse.* Jülich : KFA Jülich, 1983. JÜL-Spez. 220.

Altes, J, et al. 1989. *Behaviour of the prestressed concrete pressure vessel of the HTR-500 at severe accident temperatures.* Arnheim : SmiRT, 1989. Vol. H.

Altes, J, et al. 1987. *Experimental study of the behaviour of prestressed concrete pressure vessel of High Temperature Reactors at accident temperatures.* Lausanne : Smirt, 1987. Trans 9.

Altes, J, et al. 1989. *Experimental study of the behaviour of the prestressed concrete pressure vessel of the THTR-300 at severe accident temperatures.* Tokyo : SmiRT, 1989. Vol. H.

Archer. *Seventh framework Archer project: Archer website: www.archer-project.eu.*

ATW. 1968. Der AVR Reaktor. *Atomwirtschaft.* 1968, Sonderdruck.

Audebeau, G. 1971. *Statistical aspects of failed particle fraction and free uranium in HTR fuel bodies.* Winfrith : DRAGON Project, 1971.

Barthels, H und Schürenkremer, M. 1984. *Die effektive Wärmeleitfähigkeit in Kugel-Schüttungen unter besonderer Berücksichtigung des Hochtemperaturreaktors.* Jülich : s.n., 1984. JÜL-1893.

Beine, B. 1991. *Large scale test setup for the passive heat removal system and the prestressed cast iron pressure vessel of a 200 MWth modular high temperature reactor.* New Delhi : 3rd Int. seminar on small and medium sized nuclear reactors, 1991.

Boothe, A H. 1957. *A method of calculating fission gas release from UO2 fuel and its implication to the X-2-f loop test.* Chalk River : Atomic Energy of Canada Ltd., 1957. Report 496; CRDC-721.

Brähler, G et al. 2008. *The PBMR fuel plant: proven technology in an advanced safety environment.* Washington : s.n., 2008.

Brähler, G. et al. 2010. *Developments and economical aspects in the fabrication of HTR fuel elements.* Prague : HTR 2010, 2010.

Breitbach, G. 1978. *Wärmetransportvorgänge in Kugelschüttungen unter besonderer Berücksichtigung der Strahlung.* Aachen : RWTH Aachen, 1978. Dissertation.

Buckthorpe, D E. 2014. *ARCHER Project: Progress on Material and component activities for the Advanced High Temperature Reactor.* Weihai : HTR2014 Conference, 2014. paper 41258.

Buckthorpe, D E und Genot, J S. 2010. RAPAHEL: Synthesis of Achievements on materials and components and future direction. *Nuclear Engineering Design.* 2010.

—. 2008. *RAPHAEL: Achievements within the VHTR Materials and Components Programme.* Washington : HTR2008, 2008.

Buckthorpe, D. 2006. *Materials Development for the VHTR; Results from HTR-M and M1 Projects plus future RAPHAEL Programme.* Johannesburg : HTR2006, 2006. paper E00000111.

—. 2004. *Results from EU 5th Framework HTR projects HTR-M & HTR-M1.* Beijing : HTR2004 Conference, 2004. paper E12.

Cheng, X. 1998. *Entwicklung experimentell gestützter analytischer Verfahren zur Auslegung der Containmentkühlung mit Luft durch Naturkonvektion.* Karlsruhe : FZ Karlsruhe, 1998. FZKA 6056.

Cheng, X und Grötzbach, G. 1996. *Stand der Entwicklung von FLUTAN für die Modellierung der Wärmeübertragung in LWR-Systemen.* s.l. : Jahrestagung Kerntechnik, 1996.

Cheng, X, Erbacher, F J und Neitzel, H J. 1996. *Passive Containment Cooling for Next Generation Water Cooled Reactors.* New Orleans : ICONE-4 Conf., 1996.

Delle, W und Nickel, H. 1990. AVR Graphite Structures. *AVR experimental high temperature reactor.* VDI Verlag, 1990.

Delle, W, Koizlick, K und Nickel, H. 1983, 1984. *Grafitische Werkstoffe für den Einsatz in Kernreaktoren, Teile1, 2.* s.l. : Thiemig Verlag, 1983, 1984.

Derz, H, et al. 1990. *Experiment HTA-8: The determination of the maximum coolant temperatures in the AVR core.* Jülich : Research Center Jülich, 1990. Internal report HTA-IB-3/90.

Deutsches Atomforum eV, Kerntechnische Gesellschaft eV. 2001. *VDI Gesellschaft Bautechnik, VDI Gesellschaft Energietechnik.* Bonn : Inforum Verlag, 2001.

Dräger, P. 2001. *Zur Widerstandsfähigkeit von Sicherheitsbehältern für Kernkraftwerke gegen Terrorattacken mit großen Verkehrsflugzeugen.* München : s.n., 2001.

EN13445. 2012. CEN Standard. *"Unfired pressure vessels - Part 3: Design".* 2012.

Engelhard, J. 1972. *Abschlussbericht über die Errichtung und den Anfahrbetrieb des AVR-Atomkraftwerks.* 1972. K72-23.

Freis, D. 2010. *Störfallsimulationen und Nachbestrahlungsuntersuchungen an kugelförmigen Brennelementen für Hochtemperaturreaktoren.* Aachen : Technical University RWTH Aachen, 2010.

Fricke, U. 1987. *Untersuchungen zur Leistungssteigerung von inhärent sicheren Hochtemperaturreaktoren durch Optimierung der Coreauslegung.* Duisburg : Uni GH-Duisburg, 1987. Dissertation.

Fu X., Liang T.X., Tang Y., Xu Z., Tang C.H. 2004. Preparation of UO2 kernel for HTR-10 fuel element. *Journal of Nuclear Science and Technology 41.* 2004, S. 943-948.

Fütterer M., et al. 2008. Results of AVR fuel pebble irradiation at increased temperature and burn-up in the HFR Petten. *Nuclear Engineering and Design.* 2008, Bde. 238:2877-2885.

Fütterer, M und et al. 2008. Results of AVR fuel pebble irradiation at increased temperature and burn-up in the HFR Petten. *Nuclear Engineering and Design.* 2008, Bde. 238:2877-2885.

Geis, M und et al. 1993. *Experimentelle und analytische Arbeiten zur Absicherung von Druckbehältereinheit und Primärzelle des HTR Modul.* Frankfurt : Batelle Institut, 1993. INWA-Projekt, BEF 40045-0.

Gottaut H., Krüger K. 1990. Results of experiments at the AVR reactor. *Nuclear Engineering and Design.* 1990, Bde. 121:143-153.

Groot, Sander de, et al. 2013. *Nuclear Cogeneration with High Temperature Reactors: Overview and Perspectives of European Projects.* s.l. : FISA2013 Conference, 2013.

Haag, G, et al. 1990. Development of reactor graphite. *Journal Nuclear Materials.* 1990, Bd. 171.

Halli, G. 2004. *Microstructural modelling of nuclear grade graphite.* Manchester : University of Manchester, 2004.

Harth, R. und et, al. 1990. Ecperience Gained from the EVA II and KVK Operation. *Nuclear Engineering and Design.* 1990, Bd. 121.

Hauck, M. 2003. *Auslegung und Beanspruchung von Lagerbehältern für radioaktive abfälle unter extremen Störfallbedingungen.* Aachen : Dipl. Arb.: RWTH Aachen, 2003.

Hell, F. 1979. *Grundlagen der Wärmeübertragung.* Düsseldorf : VDI-Verlag, 1979.

Hennies, H H, Kessler, G und Eibel, J. 1990. *Improved Containment Concept for Future Pressurized Water Reactors.* Vienna : IAEA, 1990. TECDOC-550.

Hishida, M, et al. 1989. *Studies on the primary pipe ruptureaccident of a high temperature gas cooled reactor.* s.l. : NURETH-4, 1989. Proc.4, Vol.1.

Holzkamp, K. 1987. *Thermohydraulische Untersuchungenzum Primärkreis des HTR's für die Nachwärmeabfuhrmit Naturumlauf am Beispiel des HTR 500.* Aachen : Diss: RWTH Aachen, 1987.

Hottel, H C und Sarofim, A F. 1964. *Radiative Transfer.* New York : MacGraw-Hill, 1964.

How to obtain an inherently safe power reactor. **Lohnert, Günter. 2007.** Stuttgart : Uni Stuttgart, 2007.

Hrovat, M, et al. 1988. Spherical Fuel Elements for Small and Medium Sized HTRs. *Nuclear Engineering and Design.* 1988, Bd. 109:253.

Hunt, R.D., et al.,. 2010. The addition of silicon carbide to surrogate nuclear fuel kernels made by the internal gelation process. *Journal of Nuclear Materials.* 2010, S. 55-59.

Huschka H., Vygen P. 1977. Coated fuel particles: requirements and status of fabrication technology. *Nuclear Technology.* 1977, Bde. 35:238-245.

IAEA. 1994. *Decay heat removal and heat transfer under normal and accident conditions in gas cooled reactors.* Vienna : IAEA, 1994. TECDOC-757.

—. 1997. *Fuel performance and fission product behavior in gas cooled reactors.* Vienna : International Atomic Energy Agency, 1997.

—. 2001. *Heat transport and after heat removal for gas cooled reactors under accident conditions.* Vienna : IAEA, 2001. TECDOC-1163.

ISF/KFA-Jülich. 1984. *Spannbetonbehälter unter hypothetischen Störfallbelastungen.* Jülich : s.n., 1984. Förd. Vorhaben RS 447, 3Bd..

Kadner, M., Baier, J. 1977. Production of Fuel Kernels for High-Temperature Reactor Fuel Elements. *Kerntechnik 18.* 1977, S. 413-420.

Kania M.J., Nickel H. 1980. *Performance assessment of the (Th,U)O2 HTI-BISO coated particle under PNP/HHT irradiation conditions.* Jülich : Research Center Jülich, 1980.

Kim, D. 1991. *Wiederinbetriebnahme der Linerkühlung eines mittelgroßen HTR-Spann-Betondruckbehältersbei einem Kernaufheizstörfallmit Ausfall der Linerkühlung.* Jülich : FZ Jülich, 1991. JÜL-2543.

KLE, Kernkraftwerk Lippe-Ems GmbH. 1998. *Kurzbeschreibung des Standortzwischenlagers Lingen am Kernkraftwerk Emsland.* 1998.

Krohn, H. 1982. *Freisetzung von Spaltprodukten aus dem Core eines Kugelhaufenreaktors bei Störfällen mit Core-Aufheizung.* Jülich : Research Center Jülich, 1982. Report Jül-1791.

Krüger, K, Ivens, G und Kirch, N. 1988. Operation experiments and safety experiments with the AVR power station. *Nuclear Engineering and Design.* 1988, Bd. 109.

KTA3201. 2015. *"Komponenten des Primärkreises von Leichtwasserreaktoren" Parts 1 to 5.* s.l. : Der Kerntechnische Ausschuss (KTA), 2015.

KTA3221. 2015. *"Metallische HTR Komponenten" Parts 1 to 3, Draft Standard. KTA Standards.* s.l. : Der Kerntechnische Ausschuss (KTA), 2015.

Kucerza, B, Erbacher, F J und Scholtyssek, W. 1993. *Investigation on Ex-Vessel Core Melt Cooling in a future PWR-Containment.* Villingen, Switzerland : IAEA, 1993.

Kugeler, K, et al. 1994. *Development of an inactive heat removal system for high temperature reactors.* Vienna : IAEA, 1994. TECDOC-757.

Kugeler, K, Sappock, M und Wolf, L. 1991. *Development of an inactive heat removal system for high temperature reactors.* s.l. : Jahrestagung Kerntechnik, 1991.

Kuhn, K, Hinssen, H_K und Moormann, R. 2003. *Behaviour of C-based materials in contact with oxidizing gases.* Cordoba : Proceedings of ICAPP '03, 2003. paper 3031.

Lange, M. 1995. *Experimente zur selbsttätigen Abfuhr der Nachwärme bei Hochtemperaturreaktoren-Planung, Vorbereitung und Ergebnisse.* Jülich : s.n., 1995. JÜL-3012.

Laurie M, et al. 2010. *Results of the HFR-EU1 fuel irradiation of INET and AVR pebbles in the HFR Petten.* Prague : HTR 2010, 2010.

Laurie, M und et al. 2010. *Results of the HFR-EU1 fuel irradiation of INET and AVR pebbles in the HFR Petten.* Prague : HTR2010, 2010.

Lohnert, G. 1990. Technical Design Features and Essential Safety Related Properties of the HTR-Module. *Nuclear Engineering ans Design.* 1990, Bd. 121.

Martin-Bermejo, J, Hugon, M und van Goethem, G. 2001. *Research activities on High Temperature Gas-cooled Reactors (HTRs) in the 5th EURATOM RTD.* Washington : 16th SMiRT Conference, 2001.

Mehner, A W, et al. 1990. Spherical fuel elements for HTR manufacture and qualification by irradiation testing. *Journal of Nuclear Materials.* 1990, Bde. 171:9-18.

Melese, G und Katz, R. 1984. *Thermal and flow design of helium cooled reactors.* Illinois : American Nuclear Society, 1984.

Mertens, J und et al. 1985. *Sicherheitstechnische Untersuchungen zum Störfallverhalten des HTR-Modul.* Jülich : s.n., 1985. LÜL-SPEZ.-335.

Merwe, J J van der. 2004b. *Development and validation of fission product release models and software at PBMR.* Beijing : HTR2004, 2004b.

Merwe, J J van der und Coetzee, P P. 2007. Development of a model to predict fission product behavior in spherical fuel elements during water ingress events. *Nuclear Engineering and Design.* 2007, Bde. 237:47-53.

Merwe, J J van der. 2004. *Verification and validation of the PBMR models and codes used to predict gaseous fission product releases from spherical fuel elements.* Johannesburg : MSc Thesis, Rand Afrikaans University, 2004.

Mueller, A. 2006. Establishment of the technology to manufacture uranium dioxide kernels for PBMR fuel. 2006.

N.N. 1981. *Häufigkeit schwerer Erdbeben, charakteristische Daten in: Sicherheitsstudie für HTR-Konzepte unter deutschen Störfallbedingungen.* Jülich : s.n., 1981.

Nabielek, H et al. 1984. Fuel for pebble-bed HTRs. *Nuclear Engineering and Design.* 1984, Bde. 78: 155-166.

Nabielek, H und et al. 1990. Development of advanced HTR fuel elements. *Nuclear Engineering and Design.* 1990, Bde. 121:199-210.

Nabielek, H, et al. 1974. *Performance limits of coated particle fuel. Part III: Fission product migration in HTR fuel.* Winfrith : Dragon Project, 1974. Report 828/III.

Nabielek, H, Tang, C H und Mueller, A. 2010. *Recent advances in HTR fuel Manufacture.* Prague : HTR 2010, 2010.

Nabielek, H, Verfondern, K und Kania, M J. 2008. *Fuel and fission products in the Jülich AVR pebble-bed reactor.* Washington, D.C. : HTR 2008, 2008.

Neitzerl, H J. 1992. *Abschätzung der Wärmeabfuhr durch Naturkonvektion bei einem alternativen Containmentkonzept.* Karlsruhe : Kernforschungszentrum Karlsruhe, 1992. KfK-5005.

Nickel, H, et al. 2002. Long time experience with the development of HTR fuel elements in Germany. *Nuclear Engineering and Design.* 2002, Bde. 217:141-151.

Niessen, H F. 2001. *The SANA 1-experiments for self-acting removal of the afterheat from a pebble bed.* Vienna : IAEA, 2001. TEC-DOC-1163.

Niessen, H F und Lange, M. 1994. *SANA experiments related to self-operating removal of decay heat.* Vienna : IAEA, 1994. TEC-DOC-757.

Niessen, H F und Stöcker, B. 1995. *SANA 1 Code-to-experiment summary description of benchmark,3rd IAEA Research Coordination Meeting on Heat Transport and Afterheat Removal for Gas-cooled Reactors under Accident Conditions.* Vienna : IAEA, 1995.

Niessen, H F, Gerwin, H und Scheuer, W. 2001. *Numerical simulation of the SANA 1-experiments with the TINTE code in: Heat transport and afterheat removal for gas cooled reactors under accident conditions.* Vienna : IAEA, 2001. TECDOC-1163.

Nuclear Energy for Hydrogen Production. **Verfondern, Karl.** Jülich : Verfondern, Karl. 9783893364688.

Pohl, P. 2009. *Experimental evaluation of the AVR melt-wire test.* Düsseldorf : Arbeitsgemeinschaft Versuchsreaktor GmbH, 2009.

Raphael. *ReActor for Process heat, Hydrogen And ELectricity generation sixth Framework Project: www.raphael-project.org.*

Ratton, Burchall T. R. 2005. Graphite Irradiation Creep Capsule AGC-1Experimental Plan. 2005.

Rehm, W und et al. 1985. *Sicherheitsanlage der Kernkühlungsstörfälle kleiner und mittlerer HTR.* 1985. BWK Bd. 37.

Rehm, W, Jahn, W und Verfondern, K. 1984. *Zur passiven Nachwärmeabfuhr beim HTR mit dem Linerkühlsystem als Wärmesenke.* Jülich : s.n., 1984. JÜL-1951.

Reutler, H und Lohnert, G. 1984. Advantages of going modular in HTR. *Nuclear Engineering and Design.* 1984, Bde. 78:129-136.

Robold, K. 1982. *Wärmetransport im Inneren und in der Randzone von Kugelschüttungen.* Jülich : s.n., 1982. JÜL-1796.

Röllig, K. 1993. Anlagenspezifische Referenztests. *Abschlussbericht zum Fördervorhaben Brennelemente unter Normal- und Störfallbedingungen.* 1993, Bde. Report HTR-M-0210-BA-GHRA 006910.

—. 1977. Release of rare fission gases from spherical elements with coated fuel particles. *Nuclear Technology.* 1977, Bde. 35:516-523.

RSK. 2002. *Längerfristige Zwischenlagerung von Abfällen.* Jülich : FZ Jülich, 2002.

Rütten, H. 2007. Temperaturentwicklungen im HTR-Modul bei extremer Störung der Nachwärmeabfuhr durch Überdeckung. *Private Mitteilung.* 2007.

Schartmann, F. 2000. *Wärmeabfuhr von Transport- und Zwischenlagerbehältern für hochradioaktive wärmeerzeugende Stoffe im Normalbetrieb und bei Störfällen.* Aachen : RWTH Aachen, 2000. Dissertation.

Schenk, W. 1977. *Nachbestrahlungsausheizverfahren für Kugelbrennelemente und andere Brennstoffproben.* Jülich : Research Center Jülich, 1977. Report Jül-1454.

—. 1983. *Störfallsimulation an bestrahlten Kugelbrennelementen bei Temperaturen von 1400 bis 2500°C.* Jülich : Research Center Jülich, 1983. Report Jül-1883.

Schenk, W und et al. 1993. *Simulation der maximalen MODUL-Störfallaufheizkurve und deren Extrapolation auf 1700°C.* Jülich : Research Center Jülich, 1993. Technical Note FZJ-IWE-TN-17/93.

Schenk, W und Nabielek, H. 1989. *Kugelbrennelemente mit TRISO-Partikeln bei Störfalltemperatur.* Jülich : s.n., 1989. JÜL-SPEZ-487.

Schenk, W. 1978. *Untersuchungen zum Verhalten von beschichteten Brennstoffteilchen und Kugelbrennelementen bei Störfalltemperaturen.* Jülich : Research Center Jülich, 1978. Report Jül-1490.

Schenk, W, et al. 1991. *Jod- und Xenonfreisetzung aus kurz bestrahlten Brennelementen bei 1000° bis 1600°C (FRJ2-A2).* Jülich : Research Center Jülich, 1991.

Schenk, W, Pitzer, D und Nabielek, H. 1988. *Fission product release profiles from spherical HTR fuel elements at accident temperatures.* Jülich : Research Center Jülich, 1988. Report Jül-2234.

—. 1986. *Spaltproduktfreisetzungsverlauf von Kugelbrennelementen bei Störfalltemperaturen.* Jülich : s.n., 1986. JÜL-2091.

Schenk, W, Pott, G und Nabielek, H. 1990. Fuel accident performance testing for small HTRs. *Journal of Nuclear Materials.* 1990, Bde. 171:19-30.

Schneider, U und Diederichs, U. 1981. Physikalische Eigenschaften von Beton von 20° Celsius bis zum Schmelzen Teil 1 und 2. *Betonwerk + Fertigteil-Technik, Hefte 3 und 4 .* 1981, Bd. 3 und 4.

Schulten, R und Tranger, D. 1976. Gas Cooled Reactors. *Trans Amer. Nucl. Society.* 1976, Bd. 24.

Schulze, R., Schulze H.A., Rind W. 1982. *Graphitic matrix materials for spherical HTR fuel elements.* Jülich : Research Center Jülich, 1982.

Schürenkremer, M. 1984. *Theoretische und experimentelle Untersuchungen der Naturkonvektion im Kern des Kugelhaufen-Hochtemperaturreaktors.* Jülich : s.n., 1984. JÜL-1912.

Schürenkremer, M und Barthels, H. 1983. *Experimentelle Untersuchungen zur Thermohydraulik in Kugelschüttungen im Vergleich mit dem Rechenprogramm THERMIX-20. Die Untersuchung des dispersiven Wärmetransportes am Beispiel einer Kaltgassträhne.* Jülich : s.n., 1983. JÜL-1839.

Seeger. 2012. *Simulated accident testing of a fuel element from the HFR-EU1bis irradiation campaign.* Tokyo : HTR 2012, 2012. HTR2012-3-036.

Siemens/ Interatom. 1988. *Hochtemperaturreaktor-Modul-Kraftwerksanlage; Safety Report Vol. 1-3.* Bensberg : Siemens, 1988.

Siemens/Interatom. 1988. *Safety Report: Hochtemperaturreaktor-Modul-Kraftwerksanlage.* Bensberg : Siemens Interatom, 1988. Bd. 1-3.

Stöcker, B. 1997. *Untersuchungen zur Selbsttätigen Nachwärmeabfuhr bei Hochtemperaturreaktoren unter besonderer Berücksichtigung der Naturkonvektion.* Aachen : RWTH Aachen, 1997. Dissertation.

Stoker, C C, et al. 2010. PBMR radionuclide source term analysis validation based on AVR operating experience. *Nuclear Engineering and Design.* 2010, Bde. 240:2466-2484.

Takeda, S und et al. 1996. *Mockup experiment of vessel cooling system.* Oarai : KFA-JAERI, 1996.

Takeda, S und et, al. 1994. *Test apparatus of cooling panel system for MGHR.* Vienna : IAEA, 1994. TECDOC-757.

Tang C.H., et al. 2002. Design and manufacture of the fuel element for the 10 MWth HTGR. *Nuclear Engineering and Design.* 2002, Bde. 216:91-102.

Tang C.H., Fu X., Zhu J., Zhao H., Tang Y. 2010. *Comparison of two irradiation testing results of HTR-10 spheres.* Prague : HTR 2010, 2010.

Tang, C H, et al. 2010. *Comparison of two irradiation testing results of HTR-10 spheres.* Prague : HTR2010, 2010.

Technical and Safety Aspects of Processes of Hydrogen Production using Nuclear Energy. **Kugeler, K. 2005.** Seoul : Int. Congress on Advances in Nulear Power PlantsICAPP 05, 2005. Paper 5729.

U.S. DOE Nuclear Energy Research Advisory Committee and the Gen. IV International Forum. 2002. *A Technological Roadmap for Generation IV Nuclear Energy Systems.* s.l. : U.S. DOE Nuclear Energy Research Advisory Committee and the Gen. IV International Forum, 2002. 03-GA50034.

Vaidya, V.N. 2008. Status of sol–gel process for nuclear fuels. *Journal of Sol-Gel Science and Technology 46.* 2008, S. 369-381.

VDI. 1990. *AVR-Experimental High-Temperature Reactor; 21 years of succesful operation for a future technology.* s.l. : VDI-Verlag, 1990.

—. 2001. *Stellungnahme: Die sicherheitstechnische Auslegung von kerntechnischen Anlagen in Deutschland gegen Terrorismus.* Düsseldorf : VDI, 2001.

Venter, St. 2004. The PBMR Fuel Development Laboratories at NECSA. *Current Status and Future Prospects of Gas Cooled Reactor Fuels.* 2004.

Verfondern, K. 1983. *Numerische Untersuchung der 3-dimensionalen stationären Temperatur- und Strömungsverteilung im Core eines Hochtemperaturreaktors.* Jülich : s.n., 1983. JÜL 1826.

—. 2007. *Status of German spent HTGR fuel research.* Beijing : Proc. IAEA Technical Meeting on Safety Aspects of Modular HTGRs, 2007.

Verfondern, K und Petersen, K. 1979. *Untersuchung der Temperatur- und Strömungsfelderfür den Corebereich des THTRim 5-Stundenfall.* s.l. : KFA, 1979. IRE/IB 29/79.

von Heesen, W und et, al. 1983. Heat transfer from transport cask storage facilities for spent fuel elements. *Nuclear technology.* 1983, Bd. 62.

Wimmers, M. 1977. *Das Verhalten kugelförmiger Brennelemente bei der Massenerprobung im AVR-Reaktor.* Düsseldorf : Arbeitsgemeinschaft Versuchsreaktor GmbH, 1977. PhD Thesis.

Wolf, L, et al. 1994. *Passive heat removal experiments for an advanced HTR-Module reactor pressure vessel and cavity design.* Vienna : IAEA, 1994. TECDOC-757.

Ziermann, E und Ivens, G. 1997. *Abschlussbericht über den Leistungsbetrieb des AVR-Versuchskernkraftwerks.* Jülich : s.n., 1997. JÜL-3448.

GETTING IN TOUCH WITH THE EU

In person

All over the European Union there are hundreds of Europe Direct information centres. You can find the address of the centre nearest you at: http://europea.eu/contact

On the phone or by email

Europe Direct is a service that answers your questions about the European Union. You can contact this service:
- by freephone: 00 800 6 7 8 9 10 11 (certain operators may charge for these calls),
- at the following standard number: +32 22999696, or
- by electronic mail via: http://europa.eu/contact

FINDING INFORMATION ABOUT THE EU

Online

Information about the European Union in all the official languages of the EU is available on the Europa website at: http://europa.eu

EU publications

You can download or order free and priced EU publications from EU Bookshop at: http://bookshop.europa.eu. Multiple copies of free publications may be obtained by contacting Europe Direct or your local information centre (see http://europa.eu/contact).

KJ-NA-28712-EN-N

JRC Mission

As the science and knowledge service of the European Commission, the Joint Research Centre's mission is to support EU policies with independent evidence throughout the whole policy cycle.

EU Science Hub
ec.europa.eu/jrc

@EU_ScienceHub

EU Science Hub - Joint Research Centre

Joint Research Centre

EU Science Hub

Publications Office

doi:10.2760/270321

ISBN 978-92-79-71311-8